105-01865/

REPRODUCTION QUALITY NOTICE

This document is the best quality available. The copy furnished to DRDCIM contained pages that may have the following quality problems:

: Pages smaller or Larger than normal

: Pages with background colour or light coloured printing

: Pages with small type or poor printing; and or

: Pages with continuous tone material or colour photographs

Due to various output media available these conditions may or may not cause poor legibility in the hardcopy output you receive.

☐ If this block is checked, the copy furnished to DRDCIM contained pages with colour printing, that when reproduced in Black and White, may change detail of the original copy.

DEFENCE RESEARCH ESTABLISHMENT
CENTRE DE RECHERCHES POUR LA DÉFENSE
VALCARTIER, QUÉBEC

DREV – TN – 2001-116
Unlimited Distribution / Distribution illimitée

WIND TUNNEL TESTS WITH A SPINNING MODEL OF A 5-CALIBRE ARMY-NAVY SPINNER AT MACH 0.5 TO 3.0

by

Bertrand Girard and Gédéon Drouin

September/septembre 2001

Approved by/approuvé par

Head, Precision Weapons Section
Chef, Section armes de precision

16 August 2001
Date

WARNING NOTICE

The information contained herein is proprietary to Her Majesty and is provided to the recipient on the understanding that it will be used for information and evaluation purposes only. Any commercial use, including use for manufacture, is prohibited. Release to third parties of this publication or of information contained herein is prohibited without the prior written consent of DND Canada.

© Her Majesty the Queen in Right of Canada as represented by the Minister of National Defence, 2001

ABSTRACT

Wind tunnel tests were performed in the DREV 0.6 m x 0.6 m trisonic facility with a spinning model of an ARMY-NAVY SPINNER 5-calibre. This is a standard model configuration used to qualify and normalize wind tunnel test results. Tests were carried out from Mach 0.5 to 3.0 and at angles of attacks from -15 deg to +15 deg. primordially to measure the spin damping and the Magnus force, in order to evaluate the results that can be obtained with a spin rig apparatus and its controller developped at DREV. Comparisons of test results were made with those from free flight tests of various sources and showed that measurements from DREV tunnel facility averaged the scatter of those other results when superposed.

RESUME

Des essais en soufflerie ont été effectués dans la soufflerie trisonique de 0.6 m x 0.6 m du CRDV avec un modèle tournant de Army-Navy Spinner 5 calibres. Il s'agit d'une configuration standard de modèle utilisée à des fins de qualification et de normalisation d'essais en souffleries. Des essais ont été faits à des nombres de mach variant de 0.5 à 3.0 et à des angles d'attaques de –15 deg à +15 deg primordialement pour mesurer l'amortissement en roulis et la force de magnus, afin d'évaluer les résultats qui peuvent être obtenus avec un système de support tournant ainsi que son contrôleur développés au CRDV. Les comparaisons des résultats obtenus avec ceux provenant d'essais en vol libre faits dans d'autres laboratoires montrent que les mesures provenant de la soufflerie du CRDV et de cet appareillage se situent dans la moyenne de la plage de dispersion de ces autres résultats lorsque superposés.

TABLE OF CONTENT

ABSTRACT/RÉSUMÉ i

EXECUTIVE SUMMARY vii

NOMENCLATURE ix

1.0 INTRODUCTION 1

2.0 MODEL, CALIBRATION HARDWARE AND SUPPORT CONFIGURATIONS 6

  2.1 Electrical Spin Rig Concept and Rationale 6

  2.2 Mechanical Design 9

  2.3 Calibration Hardware 17

  2.4 Model and Support Configuration 21

3.0 DREV TRISONIC FACILITY - DESCRIPTION 28

4.0 SPIN RIG CONTROLLER - DESCRIPTION 36

5.0 CALIBRATION TESTS 42

  5.1 Determination of Model Inertia Moment 42

  5.2 Measurement of Rolling Moment vs Motor Current 43

6.0 SPIN TESTS - MEASUREMENT APPARATUS, TEST CONDITIONS AND PROCEDURE, SPIN DAMPING DATA REDUCTION 45

7.0 DATA ACQUISITION SYSTEM 63

  7.1 Static and Dynamic Force tests 63

7.2 Calibration Tests.......... 69

8.0 TREATMENT OF DATA - AERODYNAMIC COEFFICIENT MEASUREMENTS WITH SPINNING MODELS.......... 70

9.0 RESULTS.......... 75

9.1 Spin Tests.......... 75

9.2 Recorded Motor Data Results During Wind Tunnel and Calibration Tests.......... 96

10.0 AERODYNAMIC COEFFICIENT MEASUREMENT ERRORS...... 101

11.0 DISCUSSIONS.......... 106

11.1 Measurement of Magnus Effects and Spin Damping 106

11.2 Influence of the Sting Interference on Model Base Pressure.......... 110

11.3 Rationale of Testing Spinning Models and Future Prospects.......... 116

12.0 CONCLUSIONS.......... 134

13.0 ACKNOWLEDGEMENTS.......... 138

14.0 REFERENCES.......... 139

FIGURES 1 to 79

TABLES I to IX

APPENDIX A - Summary of Runs

APPENDIX B - Summary of Results

APPENDIX C - Balance Overloads

APPENDIX D - Measurement Errors

EXECUTIVE SUMMARY

Most of shells and bullets that are fired from a gun barrel have to be gyroscopically stabilized during flight by a high spin rate (axial) and this must be made in conjunction with a proper ratio of their axial and lateral inertia moments.

During the development and research of these vehicles, wind tunnel and aeroballistics range tests must be made in order to perform comparative studies and determine the best configurations to be retained. Afterwards, from this aerodynamic data, it will be possible to calculate the flights characteristics, performances and expected ranges and firing tables. An aspect of interest will be to calculate, with flight simulation programs, the range where the projectiles become unstable. This instability is used with certain types of small calibre training ammunitions, in order to increase the drag and decelerate them quickly to limit their effective range.

For the wind tunnel tests related to such research programs, it is very desirable to be able to spin the model which makes possible to evaluate the aerodynamic effects induced by the spinning motion as the Magnus forces and moments, the spin/roll damping and also to study the influence of the spin rate on other aerodynamic coefficients (lift, drag, pitching moment, etc...)

Unfortunately, it is very rarely that wind tunnel facilities are equipped with spin rigs and relevant equipment to perform spin tests. Usually this kind of equipment will be found in large wind tunnel facilities and where air turbines are used to spin models. The first objective was to enable DREV to perform spin damping and Magnus effects measurements in its trisonic wind tunnel facility and it was found that a small electrical spin rig would be more desirable than an air turbine system, when considering the relatively small size of the test section. The technology of using an electrical motor is a departure from the more current air turbine state-of-the-art but has proven to be efficient with the DREV facility.

This memorandum describes wind tunnel tests made in the DREV 0.6 m x 0.6 m trisonic wind tunnel with a spinning model of an ARMY-NAVY SPINNER 5-calibre. This is a standard model configuration used to qualify and normalize wind tunnel test results. These tests were primordially intended to measure the spin damping and the Magnus force and also the influence of the spin rate on other standard aerodynamic coefficients, in order to evaluate the results that can be obtained with a spin rig apparatus and its controller developed at DREV. The benefits are the facility to perform spin tests in the DREV wind tunnel to achieve more in-depth aerodynamic studies for flight vehicles stabilized with a spin/roll motion. Also, the qualification of a patented electrical spin rig apparatus has its own interest in itself. All the necessary details are included to enable a pursuit of subsequent experiments. Results then obtained compare well with data from literature for similar models tested in aeroballistic range facilities. These wind tunnel tests have increased the knowledge on experimental aerodynamics technics for spinning projectiles configured with a flat base. The database then obtained will be useful for present and further projects in research and development of spin decelerated limited range training ammunitions.

NOMENCLATURE

A	Axial Force
a	Distance between BRC and the point of application of N_1, balance forward normal force, a = 26.65 mm for both models of 0.50-in Able balances used for the test series
BRC	Balance Reference Centre, forward of model base
b	Distance between BRC and the point of application of N_2, balance aft normal force, b = 26.65 mm for both models of 0.50-in Able balances used for the test series
CA = C_A	Axial force coefficient
CAB = C_{AB}	Base drag coefficient induced by the difference between base pressure and $P_\infty = P_v$
CAO = C_{A_0}	Axial force coefficient at $\alpha = 0$
CD = CDF	Forebody drag coefficient
CDT = C_{DT}	Total drag coefficient
C_ℓ = CRM	Rolling moment coefficient (uncorrected)
C_{ℓ_c} = CRMC	Rolling moment coefficient (corrected)
CL = C_L	Lift coefficient
CLP = C_{ℓ_p}	Spin deceleration coefficient (uncorrected)
CLPC = $C_{\ell_{pc}}$	Spin deceleration coefficient (corrected)

$CLA = C_{L_\alpha}$	Lift coefficient slope at $\alpha = 0$ (deg^{-1})
$C_m = CM$	Pitching moment coefficient about MRC
$CMA = C_{m_\alpha}$	Pitching moment coefficient slope about MRC at $\alpha = 0$ (deg^{-1})
CMNB	Pitching moment coefficient about BRC
$CN = C_N$	Normal force coefficient
$CNA = C_{N_\alpha}$	Normal force coefficient slope at $\alpha = 0$ (deg^{-1})
$CNP = C_{n_p}$	Magnus moment coefficient
C_p	Specific heat at constant pressure
C_v	Specific heat at constant volume
$CY = C_y$	Side force coefficient
CYMB	Yawing moment coefficient with respect to BRC
$CYM = C_n$	Yawing moment coefficient with respect to MRC
$CYP = C_{y_p}$	Magnus force coefficient
$C_{y_{p\alpha}} = \frac{d\,C_{y_p}}{d\,\alpha}$	CYP derivative with respect to α
c	Distance of BRC aft of MRC =-1.28 in = -32.51 mm
d	Body diameter (or calibre) = 1.596 in = 40.54 mm

d^1	Base diameter = 1.596 in = 40.54 mm
e	Distance between BRC and the point of application of S_1 (= Y_1), balance forward side force, e = 21.59 mm for both models of 0.50-in Able balances used for the test series
f	Distance between BRC and the point of application of S_2 (= Y_2), balance aft side force, f = 21.59 mm for both models of 0.50-in Able balances used for the test series
$IX = I_x$	Inertia moment of model about X axis and all moving parts (determined experimentally), units: kg • m^2
L	Model total length
ℓ_{roll}	Rolling moment (uncorrected)
$\ell_{balance}$	Rolling moment measured by the balance
$\ell_{bearing\ friction}$	Torque produced by all friction forces
$\ell\ell$	Rolling moment (corrected for inertial effects)
ℓ_{rotor}	Torque supplied by the motor stator
M_i	Measured Mach number at the time of the i^{th} reading (balance or pressure distribution)
$M = M_\infty$	Average Mach number during data acquisition run time = M (mean)
$\overline{M} = \frac{1}{n}\sum_{i=1}^{n} M_i$	Average Mach number between 3.5 to 6.0 sec. run time (pressure tests)
$M_{\ell_p} = \ell\,\ell$	Torque from aerodynamic spin damping

MRC	Moment Reference Centre, located at the base of model for this test run series
N_1	Forward normal force with respect to balance reference system
N_2	Aft normal force with respect to balance reference system
PSPIN = p	Spin rate in rad/s
PSPIND = $\dot{p}$	Spin rate time derivative in rad/s^2 d PSPIN / dt = $\dot{\text{PSPIN}} = \frac{dp}{dt}$
P_{base}	Model base flow static pressure as measured by the pressure transducer, reference is P_s , see note for P_s
PCV = $P_{base} - P_\infty$	Base pressure with respect to pressure at wall (from wall tap no. 8 corresponding to flow conditions just ahead of the model)
PD/2V	Streamline helix angle around the model
$P_s = P_\infty$	Measured test section static pressure at wall (from wall tap no. 8 corresponding to flow conditions just ahead of the model)
P_{s_i}	Test section static pressure measured at the time of the ith balance reading
P_t	Average air pressure in bag during data acquisition run time
P_{t_i}	Measured air pressure in bag at the ith balance reading

P_v	Calculated static pressure in test section from average Mach number M (mean)
$P_\infty \approx P_v \approx P_S$	Real static pressure in test section
Q	Average dynamic pressure in test section during balance readings run time
QA	Dynamic pressure force used for data reduction
Q_i	Dynamic pressure in test section at the i^{th} balance reading
R	Gas constant for air
$R_{\infty_D} = RE(D)$	$\frac{V \bullet \rho \bullet d}{\mu}$ = Reynolds number based on diameter
$R_{\infty_L} = RE(L)$	$\frac{V \bullet \rho \bullet L}{\mu}$ = Reynolds number based on total length
$R_{CF} = RE(CF)$	$\frac{V_{CF} \bullet \rho \bullet d}{\mu}$ = Cross-flow Reynolds number
REY/M	Reynolds number per meter of model characteristic length
S	Model reference cross-sectionnal area,
S^1	Model base area, $S = S^1$ for the model of present test series
SPIN	Spin rate in RPM
$S_1 (= Y_1)$	Forward side force

S_2 (= Y_2)	Aft side force
t_i	Time reference (s) at the time of the i^{th} balance reading
T_a	Air temperature in bag, °K (Indraft wind tunnel)
T_c	Air temperature in bag, °C (Indraft wind tunnel)
T_v	Air temperature in test section, °K
V	Air velocity in test section
V_{CF}	Cross-flow component of velocity when the model is at angle of attack = $V \bullet \sin\alpha$
XCP	Position of centre of pressure aft of MRC, diameters i.e. longitudinal position of the aerodynamic center
XCP0	Position of centre of pressure aft of MRC at $\alpha = 0°$, (diameters) i.e longitudinal position of the mean aerodynamic center
α	Angle of attack, degrees
$\gamma = C_p/C_v$	Ratio of specific heat, = 1.4 for air
μ	Coefficient of viscosity of air in test section
ρ	Air density in test section

NOTE : Equations used for treatment of data were programmed for SI units and input data and parameters were converted into SI units when necessary to perform the analysis calculations. Results were thereafter reconverted into U. S. units when appropriate for data print-out

1.0 INTRODUCTION

The first wind tunnel tests with spinning model were made by DREV in 1970 with a model of the 120 mm Hotchkiss-Brandt mortar shell in the 5 ft x 5 ft (1.5 m x 1.5 m) trisonic wind tunnel at the National Aeronautical Establishment (NAE) Ottawa (Ref. 5). The model was accelerated by an air turbine and driven by its own spin inertia during measurements. It featured elaborated engineering and has been designed and built by NAE for DREV (Figs. 1 and 3). Aerodynamic coefficient measurements were used as input data for trajectory simulation programmes. The experience was successful but very costly.

In the same period, DREV was beginning to built its own 0.6m x 0.6m trisonic wind tunnel facility which was comparatively very modest for the purposes to make certain types of wind tunnel tests at much lower costs. The facility was operational by early 1977. Later on, in 1984, arose the need to complement some lacking data on the spin damping and other spin induced aerodynamic coefficients of the 105 mm HESH L43 and its training ammunition the C-60. The purpose was an improvement of the firing tables. Also, much work requests were under the field of ballistic table methodology, aerodynamic prediction, experimental and computational techniques.

It appeared that the logical continuation of what had been initiated in NAE wind tunnel with the Hotchkiss-Brandt model would be to develop a low cost system for the testing of spinning models of various configurations in the DREV 0.6m x 0.6m trisonic wind tunnel facility. Measurements of the influence of the spin motion on aerodynamic coefficients would be performed, with an emphasis on getting reliable data on spin damping coefficients. One potential reason was the optimization of the aerodynamic configurations of spin decelerated range limited training ammunitions.

In order to measure unsteady spin induced aerodynamic coefficients of projectiles in a wind tunnel, an instrumented motorized rig system was developed. It was intended to be used in conjunction with an internal sting-mounted 6-component strain-gage balance installed inside a spinning model outer shell. The model being spun at a desired rate during a run, provided a simulation of flow-conditions representative of free-flight.

It must be mentioned that preliminary calculations were performed in order to estimate the magnitude of the rolling moment measurements necessary to obtain spin damping coefficients. Data results available from literature on spinning projectiles were used for that purpose (Refs. 2 to 4). It was found that in order to measure spin damping coefficients in a satisfactory manner, balances with high accuracy and resolution should be available.

It was then decided to proceed for a preliminary wind tunnel feasibility study with the prototype version and to use the DREV facility standard balances for that purpose. The primordial emphasis was the measurement of spin damping coefficients. If results were encouraging, a new concept of balances specially adapted for that kind of experiment would have to be developed, in a second step. Finally, from obtained results it was concluded that measurements with spinning models were feasible but the use of stiff and high accuracy balances was highly desirable.

In a second time, appropriate balances were developed and shall be available in a near future. Their main characteristics are an increased resistance to overloads and vibrations while having more accuracy and resolution (Refs. 7 to 9). Also, a new balance calibrator was designed and constructed. Its innovative properties are 6-DOF simultaneous balance loading and increase accuracy and resolution. This instrumentation has not yet been tested in the DREV wind tunnel facility nor in conjunction with the electrical spin rig either.

As the development of the spin rig was concerned, a survey of the technologies used to spin wind tunnel models in other facilities had shown that an air turbine was generally used to provide the driving force. There were several counterparts of using such an arrangement. A primordial one was the impossibility to keep the spin rate constant during the period of time where measurements are made. A second one was the alterations to the base flow because the model base had to be left opened (because of the air-turbine exhaust).

When using air turbine, it is generally necessary to make large models which consequently can only be tested in relatively large wind tunnel facilities. The reason is that intrinsic physics of air turbine makes their output torque to decrease more rapidly with respect to a reduction of the model diameter than needed power to spin a wind tunnel model do vary with its nominal diameter. By then, the use of a gear train being also forbidden because of consequent induced friction during the shut-off bleed air part of operation cycle, there exists a minimal size to build a successful direct drive air turbine spinning model. Another constraint was that ideally the model cross-sectional area in the DREV (0.6 m x 0.6 m) wind tunnel at transonic Mach numbers, should not exceed 0.4 % of the test section area in order to avoid interference problems. It was consequently impossible to use a conventional air-turbine driven model.

A DREV research program was carried out in conjunction with Laval University (Ref. 1) to develop an alternative solution and build a compact spin rig to perform wind tunnel tests of artillery or bullet projectile models (Fig. 2). The final solution came out under the form of an electrical spin rig.

It was followed up by wind tunnel tests series where the main objective was to investigate the possibility of measuring spin effects on projectile aerodynamics, notably Magnus and roll-damping terms and compare the results against free-flight test data from the literature. Commissioning test run series were made with a 5-Calibre Army-Navy Spinner model. Results then obtained from the DREV spin rig were encouraging. They showed a rather good agreement with data from other facilities (Refs. 2 to 4), having a large scatter but of a similar magnitude.

In addition to spin damping coefficient, other standard aerodynamic stability coefficients were measured, and those affected by spin effects were reduced with respect to spin rate (PD / 2 V), i.e. streamline helix angle around the model.

This memorandum presents a model description, experimental procedures, test instrumentation and conditions, data reduction algorithms and a summary of measurement results.

For this project a total of 209 runs (tunnel log no. 2790 to 2999) were made between May 1988 and December 1988 and related work was performed between June 1985 to April 1999 under W. V. 2nj13 Flight Mechanics of Munitions.

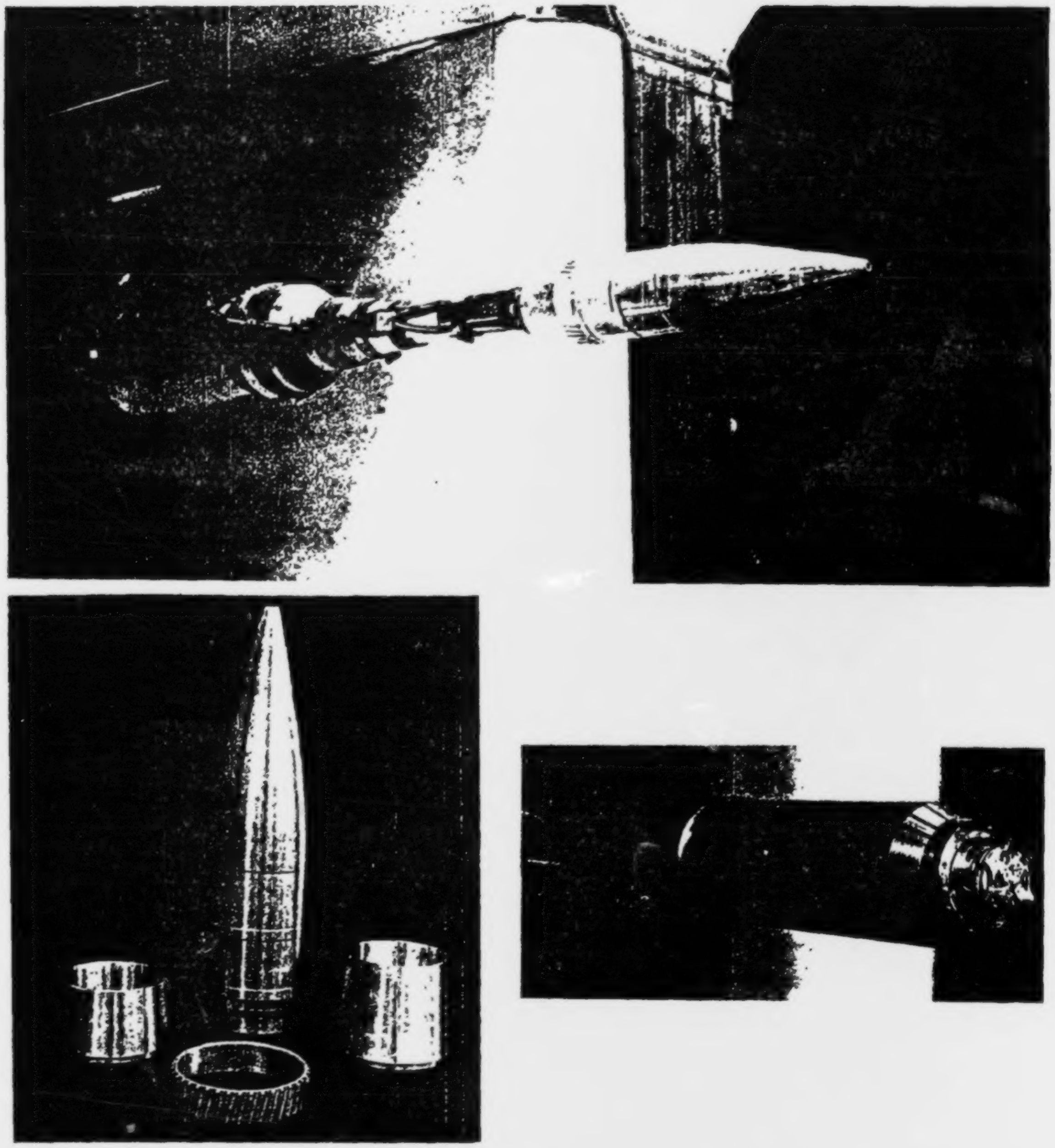

FIGURE 1- First DREV wind tunnel test with a spinning model, 120 mm Hotchkiss-Brandt mortar shell in the NAE 5 ft x 5 ft trisonic facility (top), model spinning outer shell (bottom left), center-core turbine unit (enclosed) with fore end spin rate detection system (bottom right)

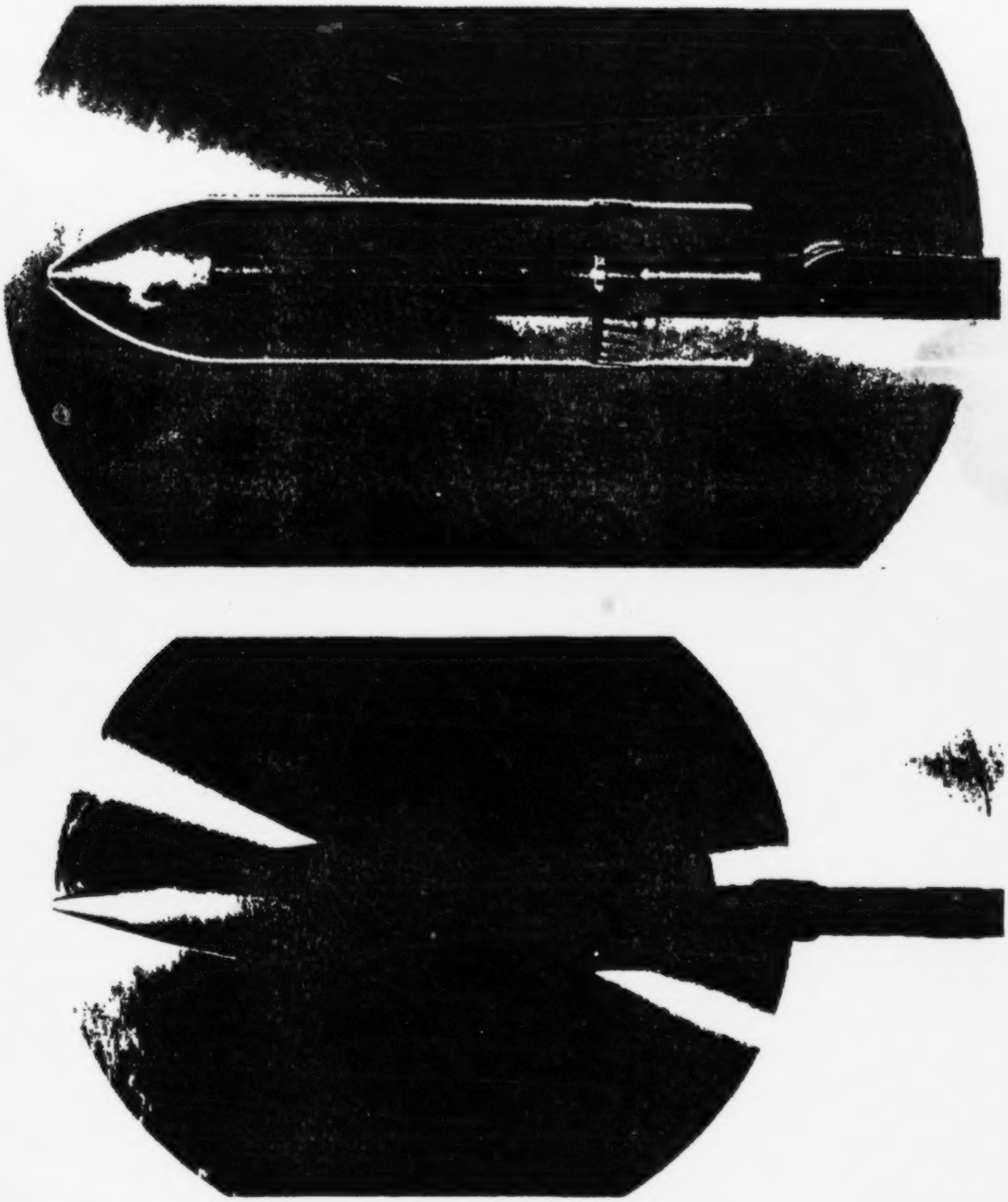

FIGURE 2- Electrical spin rig fitted with outer shell configured to HESH L43A2 artillery projectile (top) and 5D- Army/ Navy Spinner model spinning at 40,000 rpm (bottom), in DREV tunnel test section

2.0 MODEL, CALIBRATION HARDWARE AND SUPPORT CONFIGURATION

The testing of a spinning model implies that several choices had to be made in the planning of the test because of the various approaches that were considered. This chapter presents the design process that was followed. The primordial decisions that were taken could be listed as follows:

a- Was the model to be tested at a constant angle of attack or with a pitching motion?

b- Was the spin rate to be maintained constant, or just an acceleration followed by a slow deceleration was sufficient?

c- Which motor/drive system was to be used?

d- Which size the model could have due to constraints of the mechanical spin device and the tunnel test section interactions?

e- Which amount of alteration to the model base configuration was acceptable?

f- Was a direct measurement of the spin damping a feasible approach or the indirect method of measuring the model spin rate deceleration was a unique solution?

2.1 Electrical Spin Rig Concept and Rationale

In the case of large model sizes (90 mm or 3.5 in in diameter and above) as used in larger wind tunnel facilities an air turbine can be used to spin the models. Figure 3 presents a typical arrangement of this type in the 5 ft x 5 ft (1.5 m x 1.5 m) trisonic wind tunnel at NAE Ottawa, (Ref. 5).

Because of the intrinsic physics of air turbines, it is difficult to fit a suitable direct-drive air turbine into a spinning model with the diameter and length constraint of the DREV

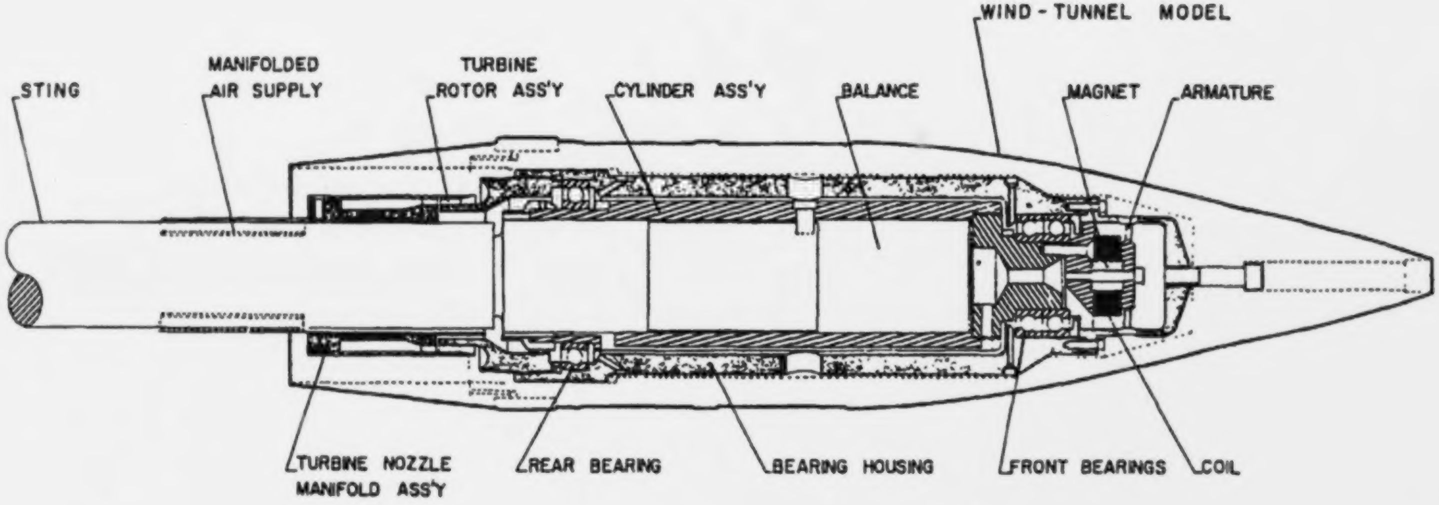
WIND - TUNNEL MODEL
STING
MANIFOLDED AIR SUPPLY
TURBINE ROTOR ASS'Y
CYLINDER ASS'Y
BALANCE
MAGNET
ARMATURE
TURBINE NOZZLE MANIFOLD ASS'Y
REAR BEARING
BEARING HOUSING
FRONT BEARINGS
COIL

National Aeronautical Establishment

FIGURE 3 - Typical arrangement of a spinning model fitted with an air turbine

supersonic tunnel (1.6 in or 40.6 mm diameter and 6.0 in or 153 mm long ideally) for the transonic testing requirements envisaged in the future.

Since the pressure in the line that feeds the turbine acts as an external force on the model system, errors in the balance measurements are generated. For this reason, the air turbine is used only to accelerate the model to the spin-rate required and power must be removed when making measurements. This has a disadvantage for testing with continuously varying angle of attack. The gyroscopic moments induced by the pitching motion of the spinning model cannot be calibrated or measured during the pretest tare-run. In addition, it would be very difficult to incorporate an air turbine into a servo system in order to control the spin-rate.

The presence of an air turbine requires some modification to the model base (in fact, in that case there is no base any more, the model aft end being left completely open. This arrangement results into important base flow interactions and consequent measurement errors. In addition, the air supply could not be maintained during measurements because the turbine air exhaust would modify the base flow which would cause errors in the aerodynamic measurements.

It resulted that aerodynamical, mechanical and frictional constraints made it impractical to use a scale-down version of the NAE air turbine for the DREV wind tunnel facility.

Experience in the wind tunnel testing has demonstrated the following advantages of using an electrical spin rig over the air turbine system:

1 - Spin-rate can be kept constant during measurements.

2 - Model base is closed.

3 - No air exhaust through model base that could modify the flow.

4 - No external force caused by air supply.

5 - Improved servo-control spin-rate for a D.C. motor over an air turbine: no lag, possibility to reverse polarity for a braking effect.

6 - Direct reading of spin damping from balance is possible if a precise servo-controller is used.

7 - Lower cost.

8 - A very small spinning model may be utilized.

9 - With appropriate calibration, measurement of spin damping can be made without the use of a balance fitted with a roll element.

In the past ten years very powerful small D.C. motors have been developed. They use a high-coercive-force permanent magnet stator made of ferrite (or samarium-cobalt which is a lot better). The power-to-volume ratio of these small D.C. motors led to consider the use of this technology to power small-scale spinning wind tunnel models.

2.2 Mechanical Design

The mechanical configuration is very compact (Figs. 4 and 5). A more complete description is given in Ref. 6. The interchangeable outer shell houses the following items:

1. A 6-component strain-gage balance (ABLE 0.50 in balances were used in present test series)

2. A ferrite permanent magnet D.C. motor which can develop 280 watts output for 400 watts input during the time of a wind tunnel run.

3. One or two proximity detectors / photomagnetic or infrared detectors which are used to monitor the spin-rate and to provide velocity feedback information to the motor excitation controller.

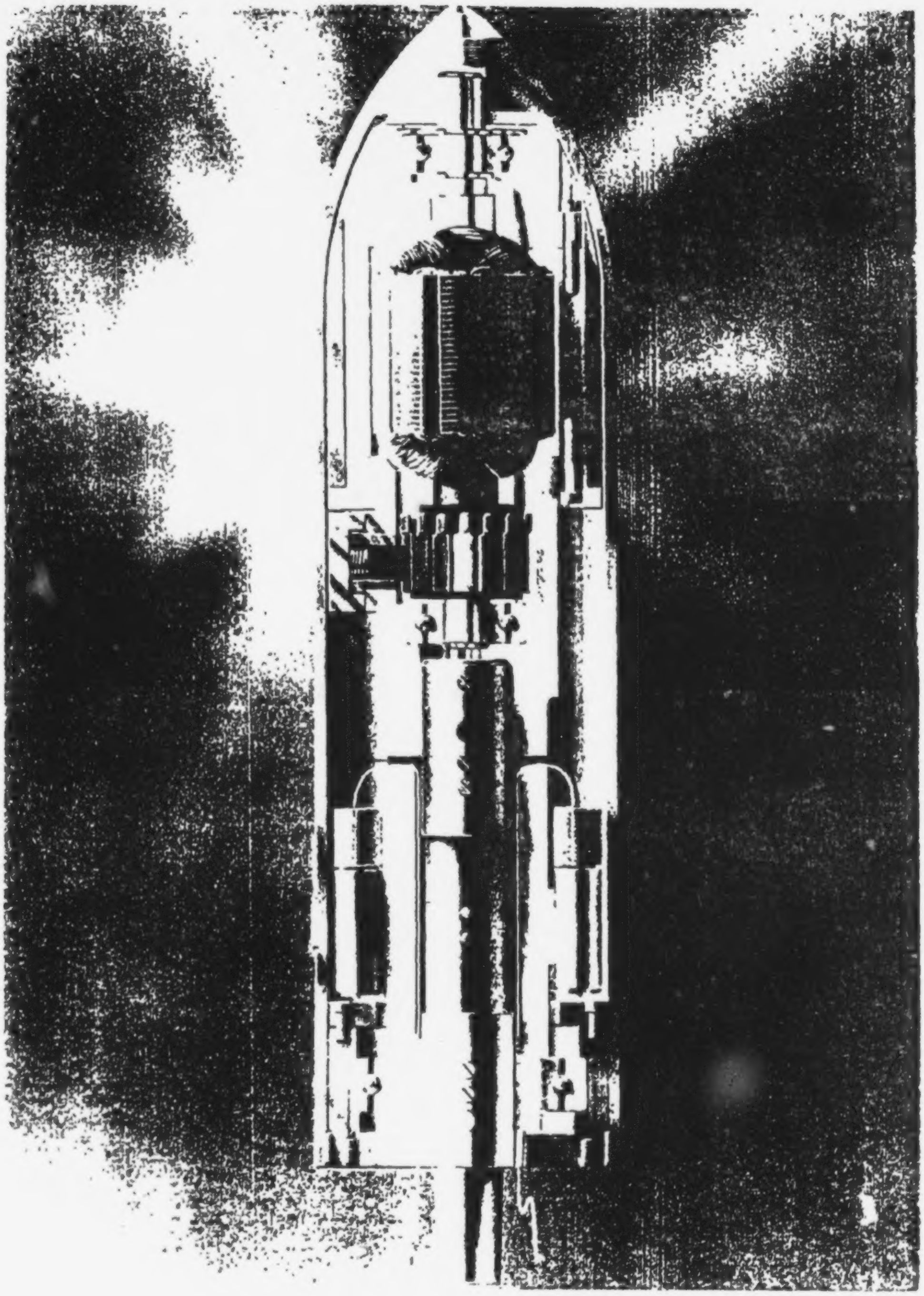

FIGURE 4 - Artist's representation of DREV electrical spin rig for projectile wind tunnel testing

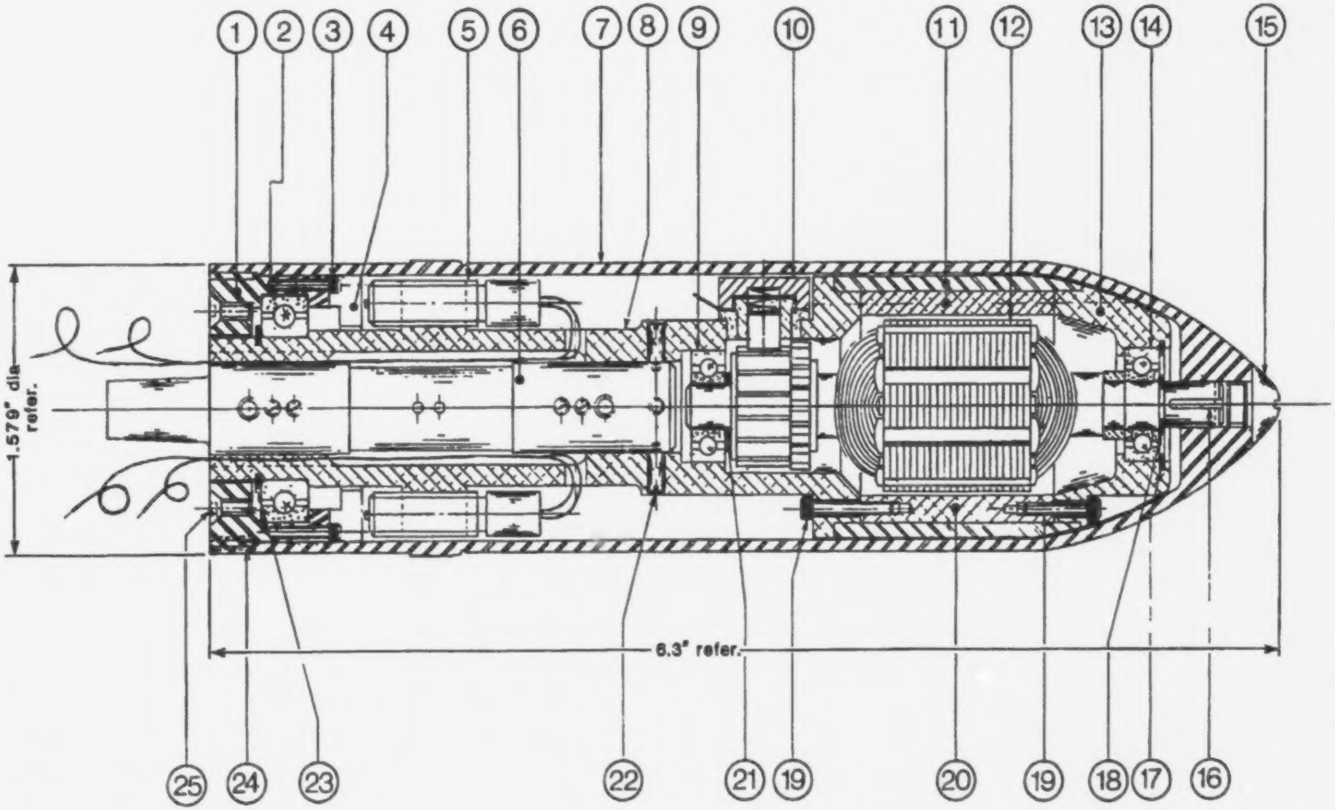

1 - Spinning model base
2 - Ball bearing retention piece and aft end ball bearing
3 - Holding screws
4 - Index poles
5 - Proximity detectors
6 - 6 DOF Strain gauges balance
7 - Spinning projectile outer shell interchangeable to match a particular model
8 - Balance housing
9 - Rotor ball bearing
10 - Motor brushes cap
11 - Motor housing and ferrite permanent magnet stator in two pieces
12 - 8 poles D.C. rotor
13 - Motor end forward
14 - Rotor ball bearing
15 - Nose cap
16 - Driving shaft key slot
17 - Retaining ring
18 - Retaining ring (symmetrical type)
19 - Connecting screws
20 - Cross pieces
21 - Spacer
22 - Balance retention pins
23 - Retaining ring
24 - Assembly screws
25 - Dummy screws

FIGURE 5 - Description of the DREV electrical spinning rig

The principal characteristics are presented in TABLE I. It is worth to mention that simultaneous measurements of the spin rate and D.C. motor current can provide a second mean of measuring the rolling moment if a consequent calibration is made.

TABLE I

Characteristics of the DREV Electrical Spin Rig

Rig dimensions : 1.37 in (34.8 mm) in diameter, mounted in a spinning shell of at least 1.58 in (40 mm) in diameter and 6.3 in (160 mm) long,

Motor: 200 VDC, 2.0 A, 280 W output, 400 W input,

Spin Rate: 15,000 - 45,000 rpm,

Maximum Run Time of the Rig: 30 s,

Cooling Time between runs: 10 mins,

Typical temperature rise for the balance during a wind tunnel run is 1.5 C°.

The interchangeable model outer shell (7) (Fig. 6), its base (1) (Fig. 7), the nose cap (15) and index poles (4) (Fig. 7) are spinning and supported at:

a) the aft end by a large inside diameter ball bearing (2) (Fig. 7),

b) the fore end by the motor rotor driving shaft where spinning movement is transmitted by two keys (16).

The rotor (12) (Fig. 8) is supported by two ball bearings (9 and 14). The motor aft end is an integral part of the balance housing (8) (Fig. 9) and contains the motor brushes (10) and the aft end rotor ball bearing (9) (Fig. 8).

The eight-pole D.C. rotor (12) (Fig. 8) is balanced

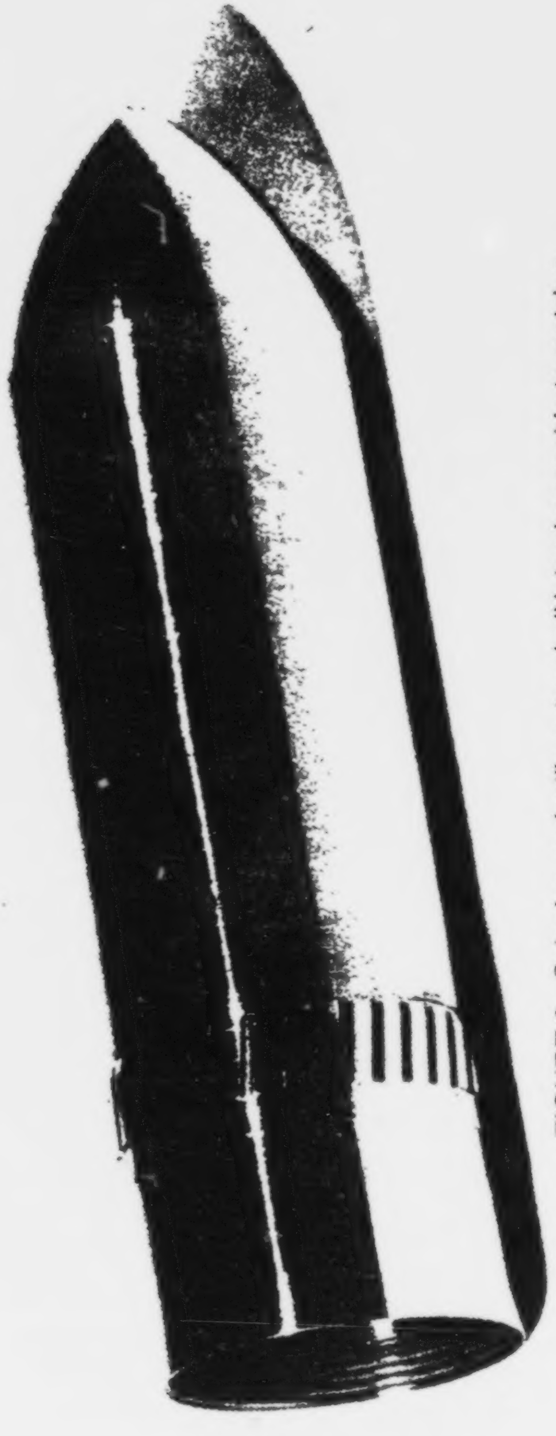

FIGURE 6 - Spinning projectile outer shell interchangeable to match a particular model configuration (HESH 105 mm L43A2 shown)

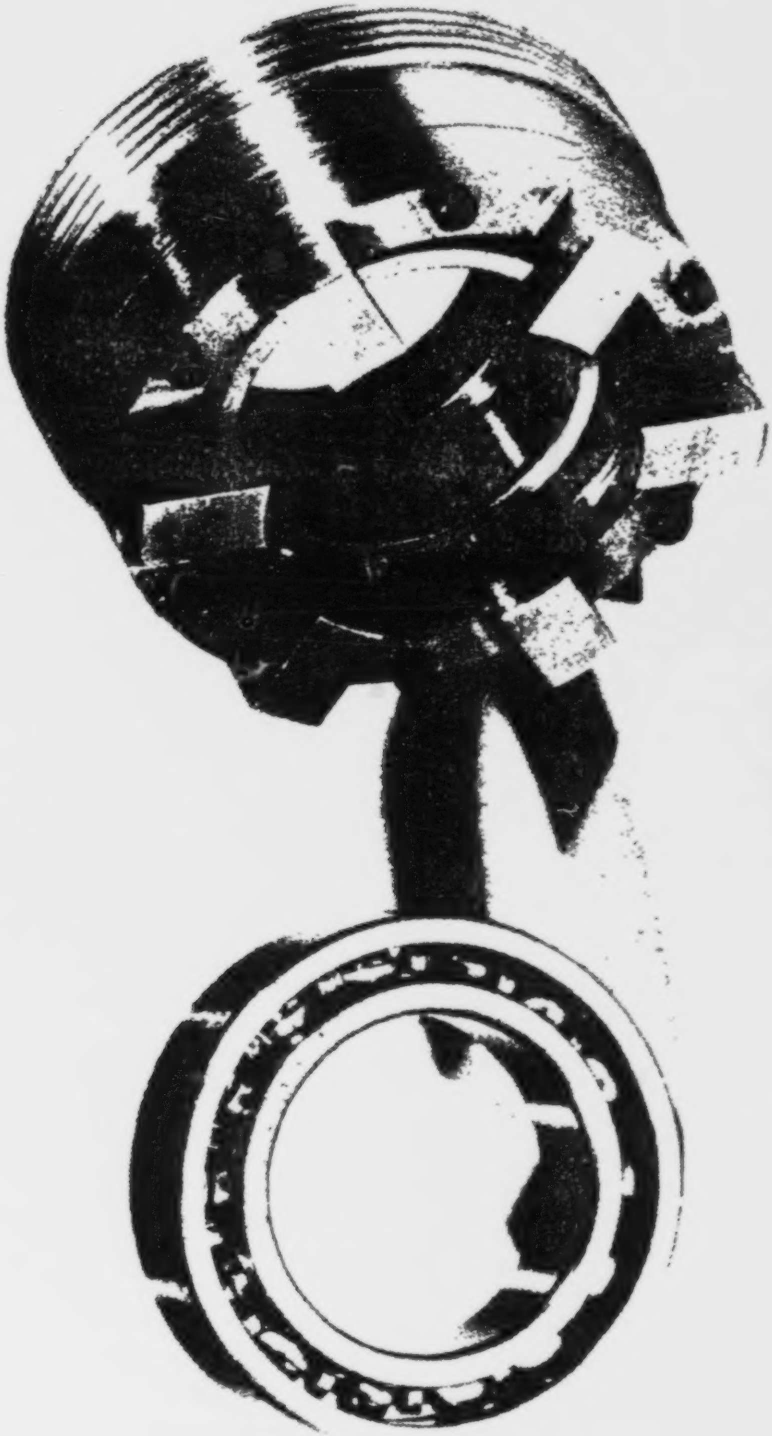

FIGURE 7 - Spinning model base, index poles and large aft end ball bearing

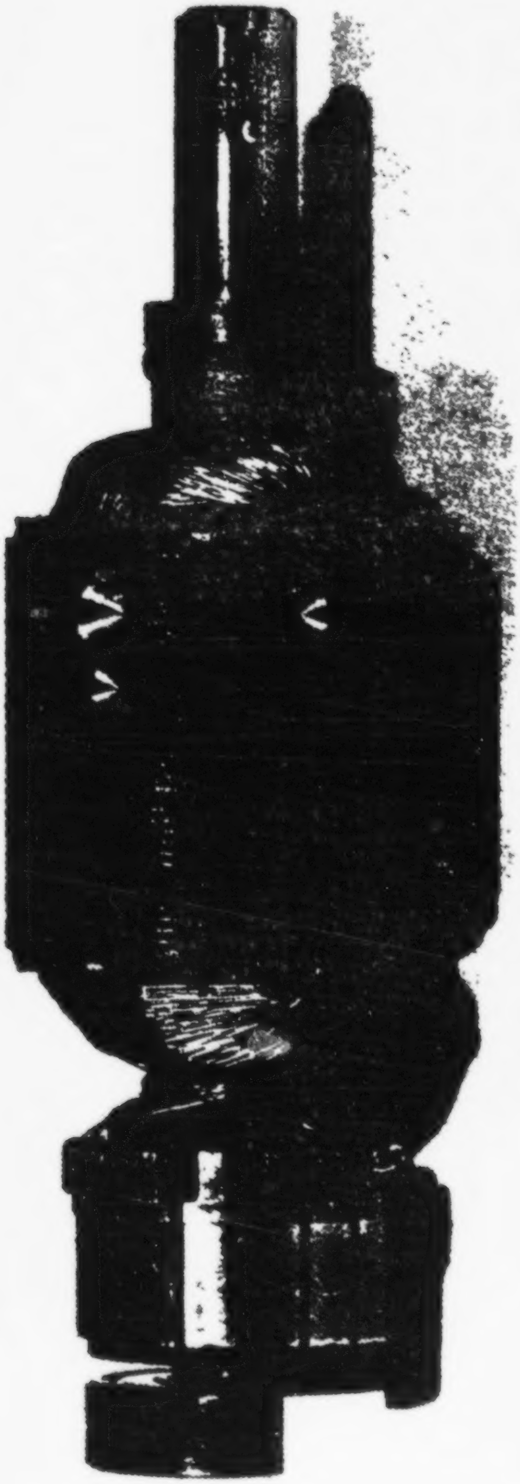

FIGURE 8 - 8 poles D.C. rotor and aft rotor ball bearing

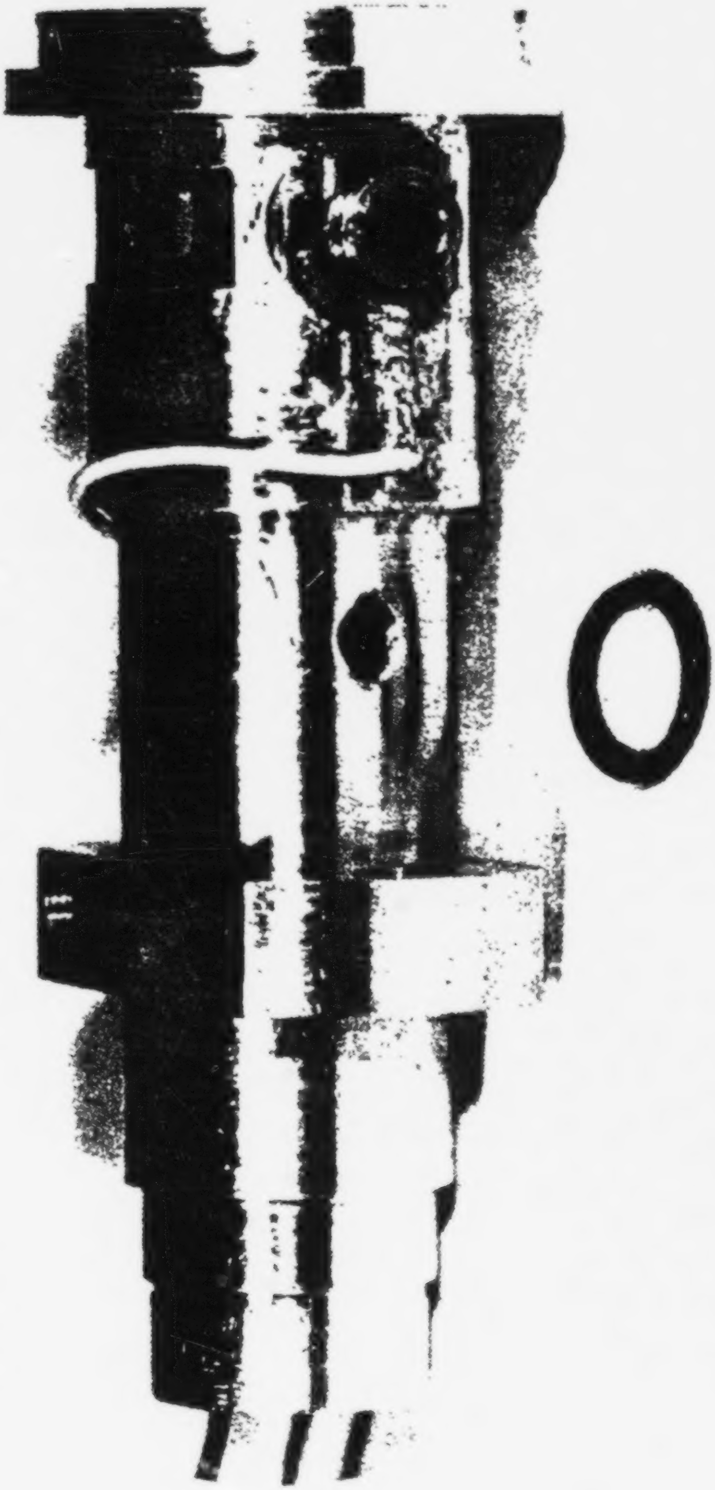

FIGURE 9 - Balance housing and balance retention friction O-ring

dynamically with high precision. The motor fore end (13) (Fig. 10), the ferrite permanent magnet (Fig. 11) and the motor housing (11) (Fig. 11) are held together to the balance housing (8) by two cross-pieces (10) (Fig. 11) and four connecting screws (19) which are located between the two permanent magnet pieces.

The balance housing cavity is grounded with precision (+.0005 in) in order to get a precise hand-slide of the balance which is maintained by an arrangement of three friction O-rings. In the advent of an accidental motor seizing or alike malfunctioning, the sudden torque increment caused by inertial forces of all spinning hardware would make the balance housing to slide for 1/4 to 1/2 turn around the balance without damaging its roll element. The friction force of the O-rings was experimentally calibrated for that purpose.

In the space between the balance housing (8) and the spinning outer shell (7) two proximity detectors (5) (Fig. 12) used in conjunction with six index poles (6) allow to measure the spin rate and the possibility to control it when connected to an appropriate interface, computer and servo system.

2.3 Calibration Hardware

Although the spin rate was likely to stay constant during the usable time of a test run, it still varied slightly due to some small response delays of the motor controller to raise the voltage in order to compensate for the load variations on the motor. It was necessary to compensate for the influence of the inertial effects on the measured values of the aerodynamic rolling moment (spin damping) induced by these spin rate variations.

In order to perform this type of correction on the measured rolling moment, the data reduction algorithm used the model axial moment of inertia (IX), which comprises the outer shell and of all the spinning hardware, i.e spinning components of ball bearings etc... For that purpose, the outer shell was accelerated gradually while the spin rate and the rolling moment felt by the balance were measured simultaneously. In order to avoid that friction moments induced by surrounding atmospheric air could have caused measurements errors, these tests were performed by

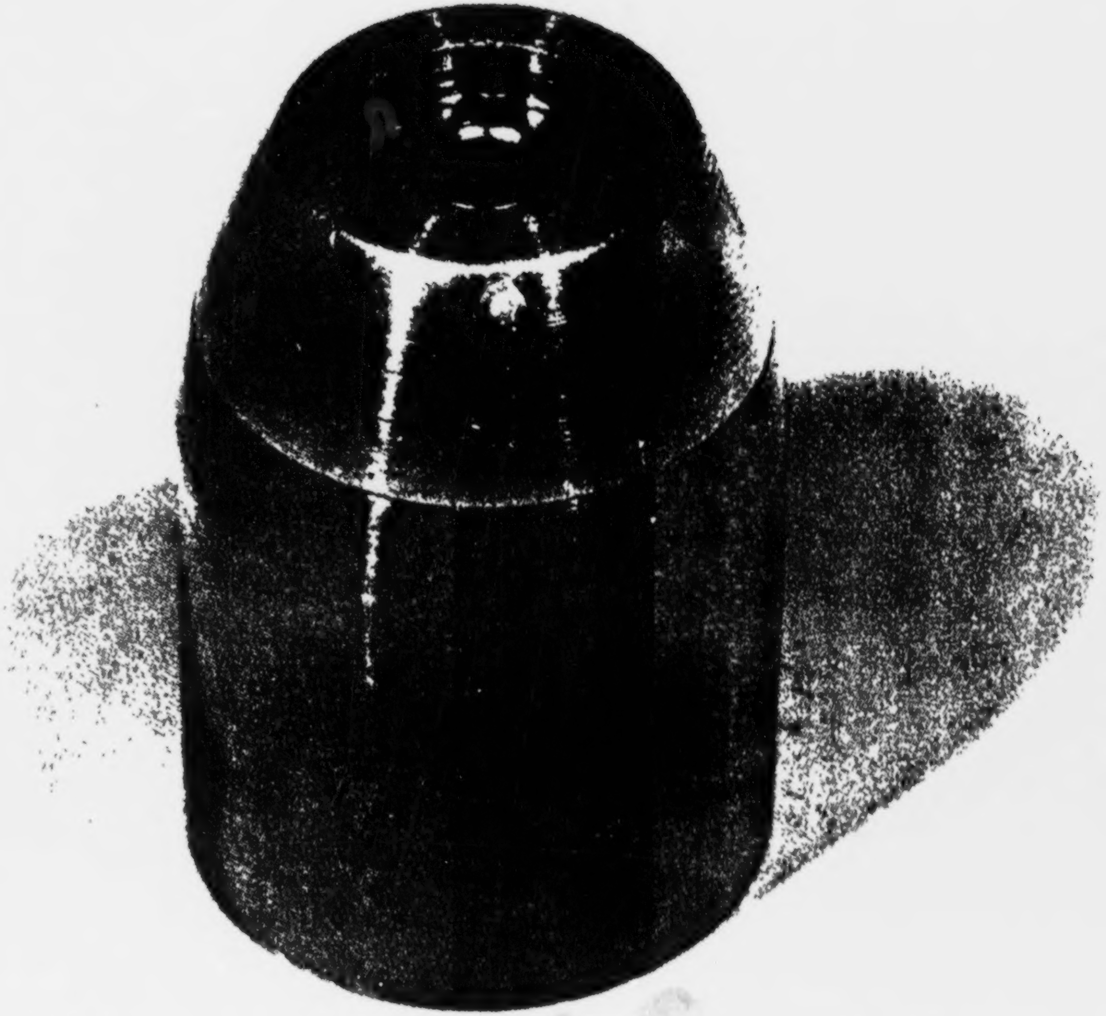

FIGURE 10 - Motor housing, motor forward end, forward rotor ball bearing and retaining ring

FIGURE 11 - Motor housing, ferrite permanent magnet stator in two pieces (dark), cross pieces (clear) and motor forward end at the back; the motor housing is also a conductor for the return of the magnetic field from magnet

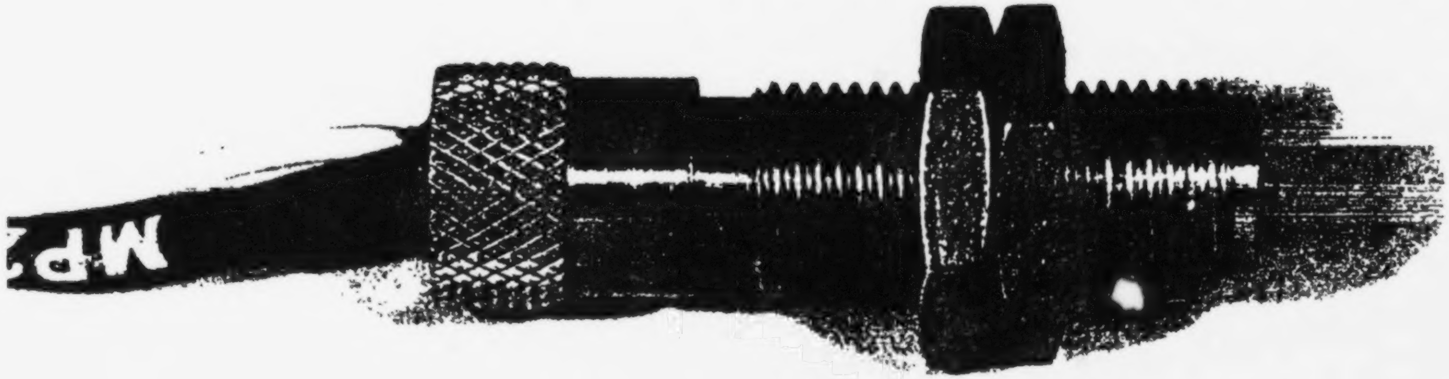

FIGURE 12 - One of the two magnetic proximity detectors used for spin rate measurement

running the spin rig in a vacuum environment. This was achieved by using a special air-tight Plexiglass reservoir (Fig. 13).

Another application for the special air-tight Plexiglass reservoir was to generate the calibration table needed to calculate the aerodynamic spin damping by using the data on the motor current obtained during a wind tunnel test run. It provides a very practical alternative if the balance available for a projected test would not be fitted with a rolling moment element. To perform that sort of measurements, it shall be necessary to calibrate the torque or rolling moment applied to the model outer shell versus motor current. This can be achieved by using the Plexiglass vacuum reservoir mentioned earlier in conjunction with a braking system to simulate aerodynamic spin damping forces on the model.

This braking system, which consists of an electrical Foucault Braking device, can be described as follows. A brass disc (material without inductance) is attached to the base of the model by four screws (Fig. 14). Figure 15 shows the same spin rig while the outer shell of the spinning model has been removed. This disc spins close to two electromagnetic coils which produce a braking effect by inducing Eddy currents in the disc.

In order to get the most from the electrical spin rig system, an optimized 0.50 in balance was patented by DREV and design finalized under contract (Refs. 7, 8 and 9). This balance was not available for present test run series, its construction being not completed. By then, a suitable balance was used, but with less accuracy and resolution than desirable for intended measurements.

2.4 Model and Support Configuration

The configuration of the 5-Calibre Army-Navy Spinner model was adopted for commissioning tests of the electrical spin rig. The resulting outer shell, which was configured to comply with specifications given in Ref. 3, was made of brass and featured 1.596 in (40.5 mm) diameter and 7.980 in (202.7 mm) total length (see Fig. 16). As indicated in Fig. 5, it comprised a nose cap (15) and two driving shaft key slots to receive two keys (16) for transmission of spinning motion. Dimensions of the sting support are given in Figs. 17 and 18.

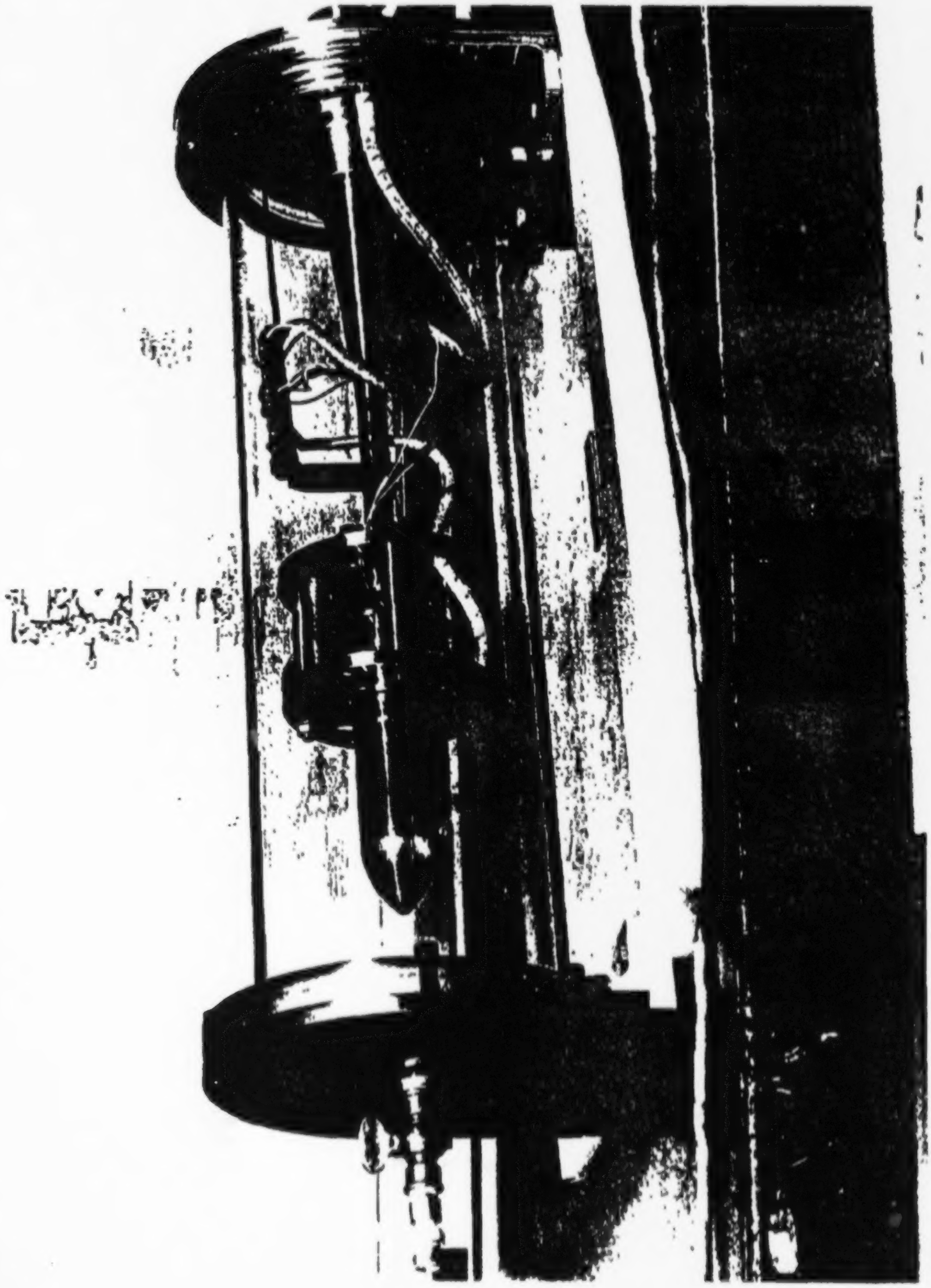

FIGURE 13 - Model in vacuum calibration chamber fitted with electrical Foucault brakes

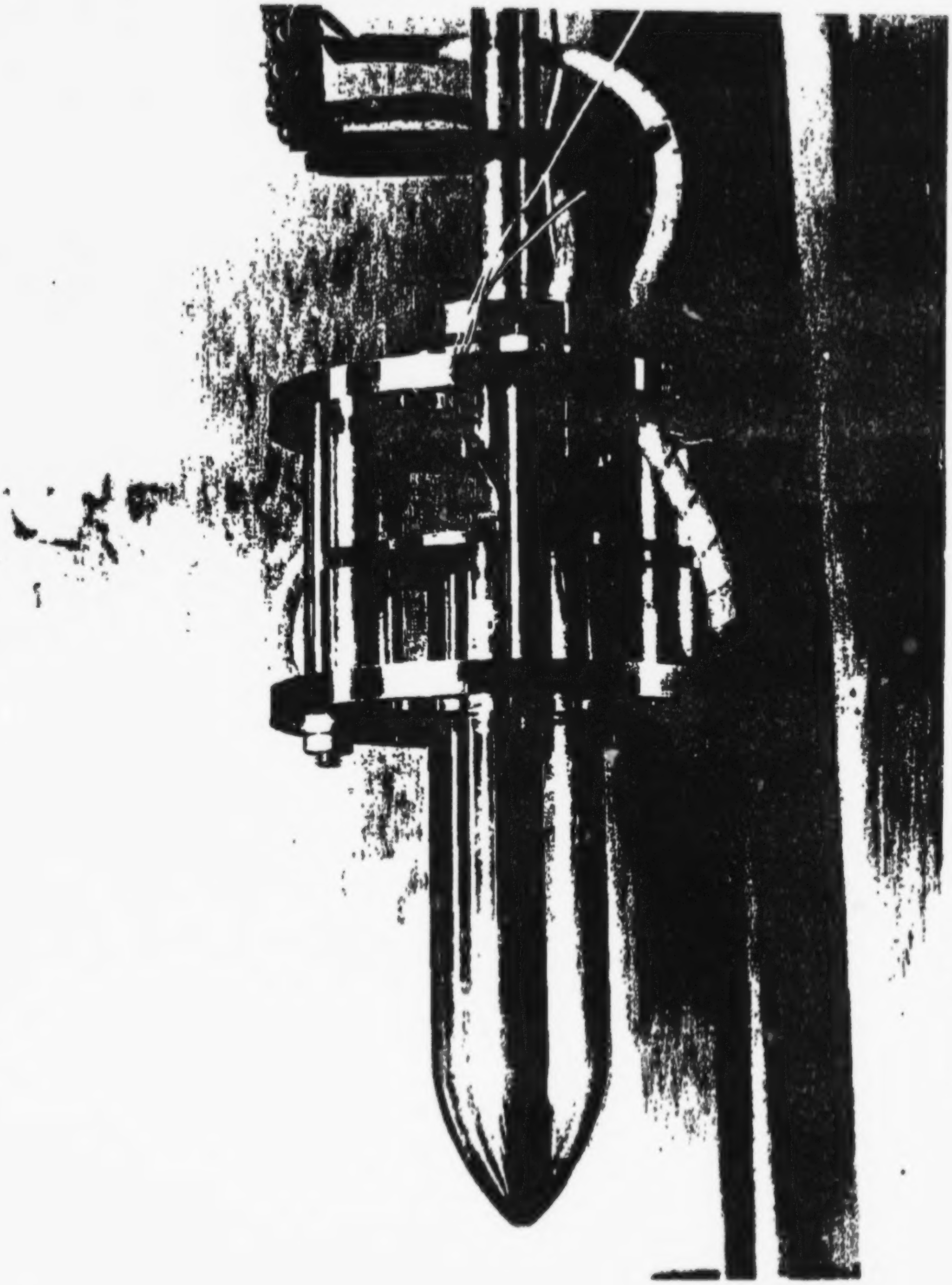

FIGURE 14 - Electrical Foucault brakes rig used in vacuum calibration chamber

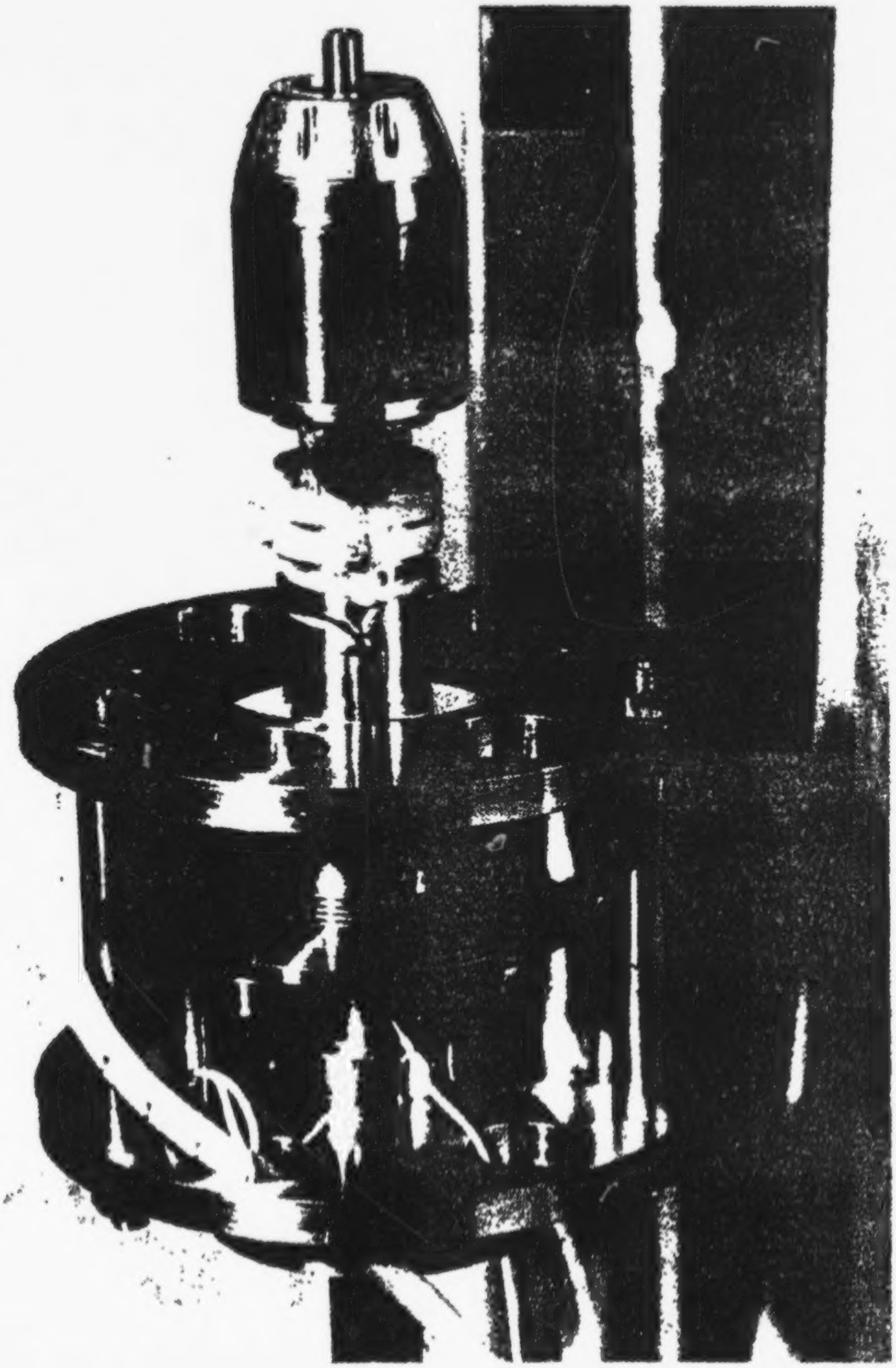

FIGURE 15 - Electrical spin rig with Foucault brakes and spinning outer shell removed

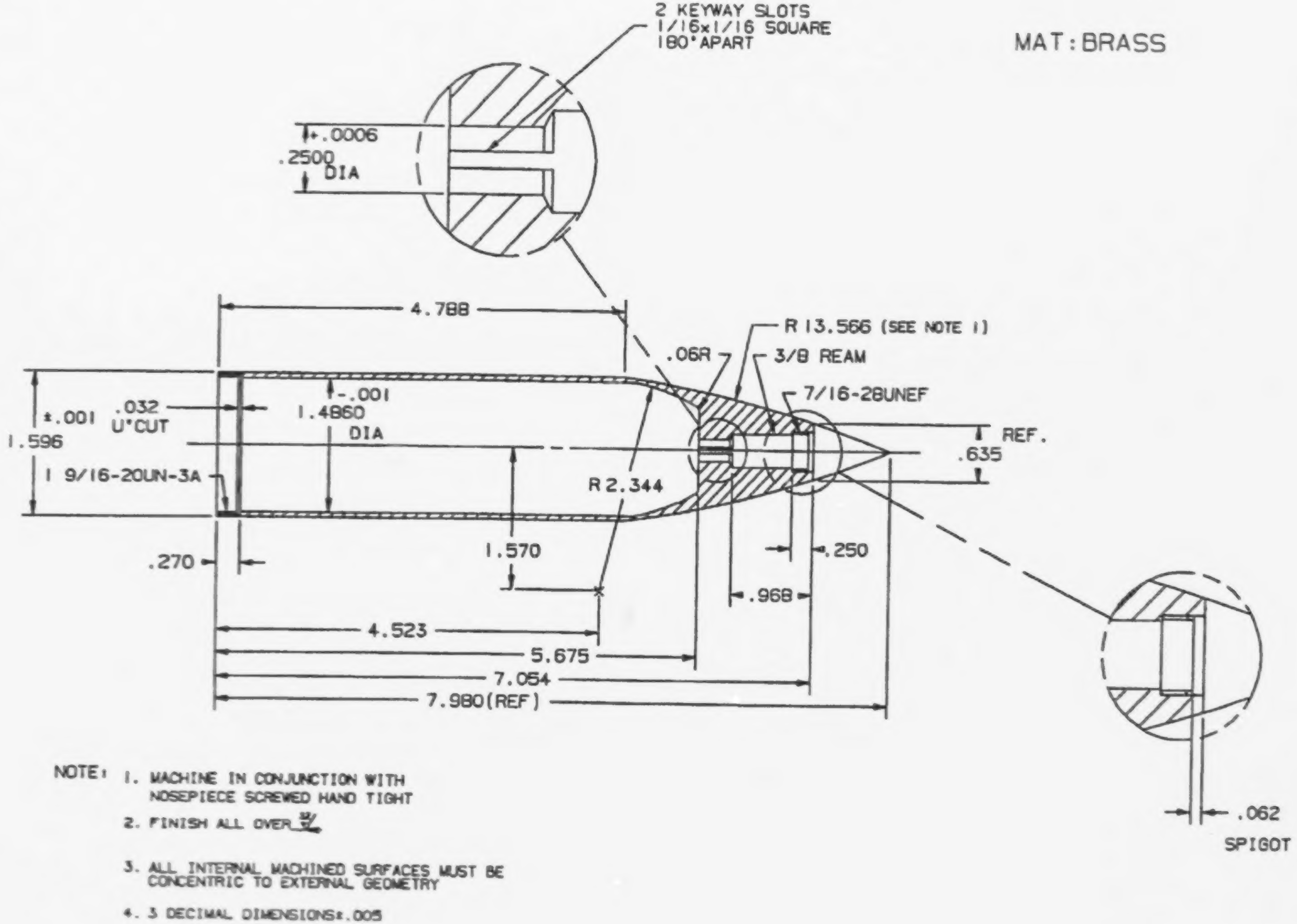
MAT : BRASS
2 KEYWAY SLOTS
1/16×1/16 SQUARE
180° APART
+.0006
.2500
DIA
4.788
.06R
R 13.566 (SEE NOTE 1)
3/8 REAM
7/16-28UNEF
REF.
.635
±.001
1.596
.032
U'CUT
1 9/16-20UN-3A
-.001
1.4860
DIA
R 2.344
.270
1.570
.250
.968
4.523
5.675
7.054
7.980 (REF)
.062
SPIGOT

NOTE: 1. MACHINE IN CONJUNCTION WITH NOSEPIECE SCREWED HAND TIGHT
2. FINISH ALL OVER $\sqrt{32}$
3. ALL INTERNAL MACHINED SURFACES MUST BE CONCENTRIC TO EXTERNAL GEOMETRY
4. 3 DECIMAL DIMENSIONS ±.005

FIGURE 16 - Spin rig outer shell configured to represent the 5-D Army-Navy Spinner model, dimensions in in

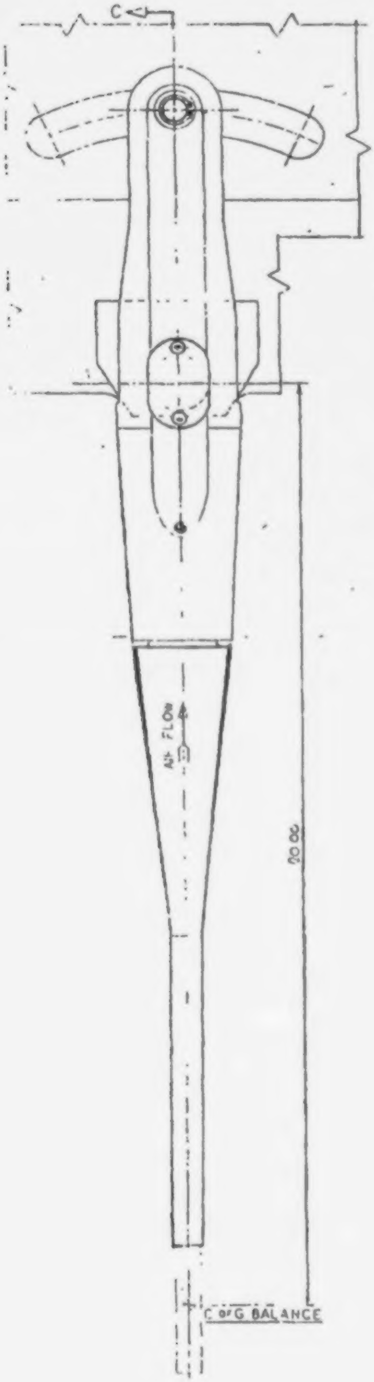
C
AIR FLOW
20.00
C of G BALANCE

FIGURE 17 - Junction configuration between 0.50 in sting and test section strut hub

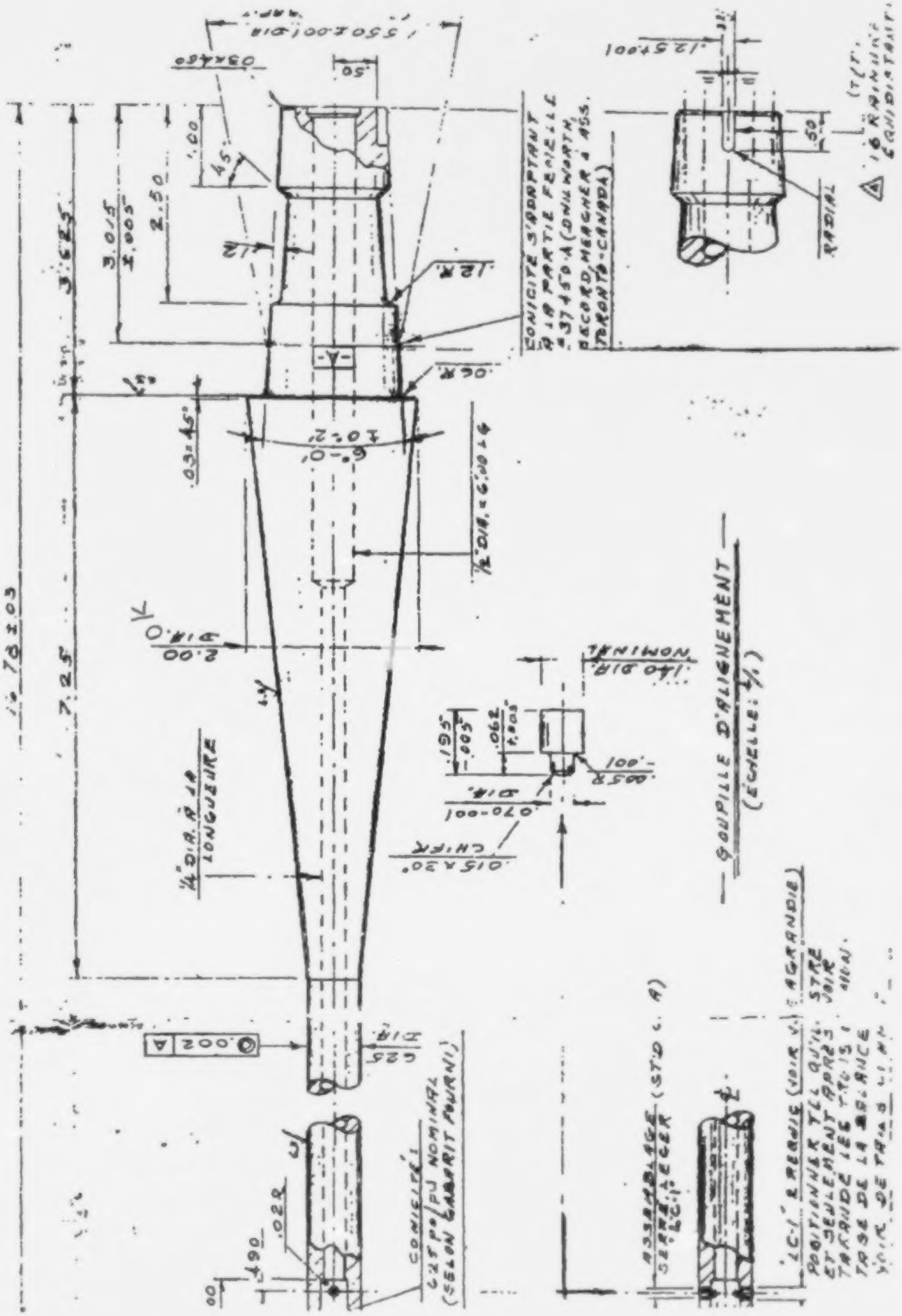
CONICITE S'ADAPTANT A LA PARTIE FEMELLE #37450-A (DONWORTH, ACORD, MEAGHER & ASS. TORONTO-CANADA)
GOUPILLE D'ALIGNEMENT
(ECHELLE: 4/1)
RADIAL
16 RAINURES EQUIDISTANTES
1/4" DIA. A LA LONGUEURE
2.00 DIA.
7.25
3.625
2.50
1.00
.12 R.
.06 R.
.03x45°
.03x45°
.50
1.550±.001 DIA.
.625 DIA.
.002 A
-A-
.125±.001
1.40 DIA. NOMINAL
.015x30° CHFR.
.070-.001 DIA.
.195 -.005
.062
.100 -.005 R.
CONICITE 1:25 po/pi NOMINAL (SELON GABARIT FOURNI)
ASSEMBLAGE (STD A)

FIGURE 18 - Sting No. 0.50.2 (0.625 in), dimensions in in

3.0 DREV TRISONIC FACILITY - DESCRIPTION

The DREV trisonic facility (Figs. 19 to 23), is an intermittent indraft type with a 0.6 m x 0.6 m working test section. During a run, the air flows from a flexible air reservoir (air bag 935 m^3), which has been previously inflated with dry air to slightly above atmospheric pressure, through a manifold section, a settling chamber fitted with proper honey-combs and screens (56% open area over total area), a convergent, nozzles section, the test section, the diffuser and butterfly valve used to initiate and shut-down the flow. Finally air flow exhausts into a vacuum vessel (889 m^3).

The use of such dry air reservoir is necessary because humid atmospheric air would otherwise result into dense fog, water drops and ice pellets in test section at high Mach numbers, making it impossible to watch the model during a run and introducing important errors in measurements. The inlet air, which is normally at ambient temperature in the air bag, has been previously dried to a nominal dew point of -40 C deg through the use of an electrically heated Celica-Gel air dryer and fan system.

Supersonic flow, which has a duration of approximately 7 s (about 5 s are usable), is obtained by separate sets of nozzles (two dimensional) that are used for each of the supersonic test Mach numbers, (1.5 and 2.0 as the present test series is concerned).

The operation of the wind tunnel is controlled by means of an HP-375 data system processor that performs the following duties:

- opening of the butterfly valve to start the flow,
- pitching of the model through the chosen incidence angles (usually -5 deg to +15 deg with standard sting),
- shut-down butterfly valve at the end of a run,
- automatic shut-down of tunnel flow in case of emergency (for example if the balance is overloaded),
- automatic sting return to zero incidence in case of balance overloads and before to flow shut-down in order to avoid stopping shock waves and associated loads to damage the balance,
- and finally acquisition and treatment of data.

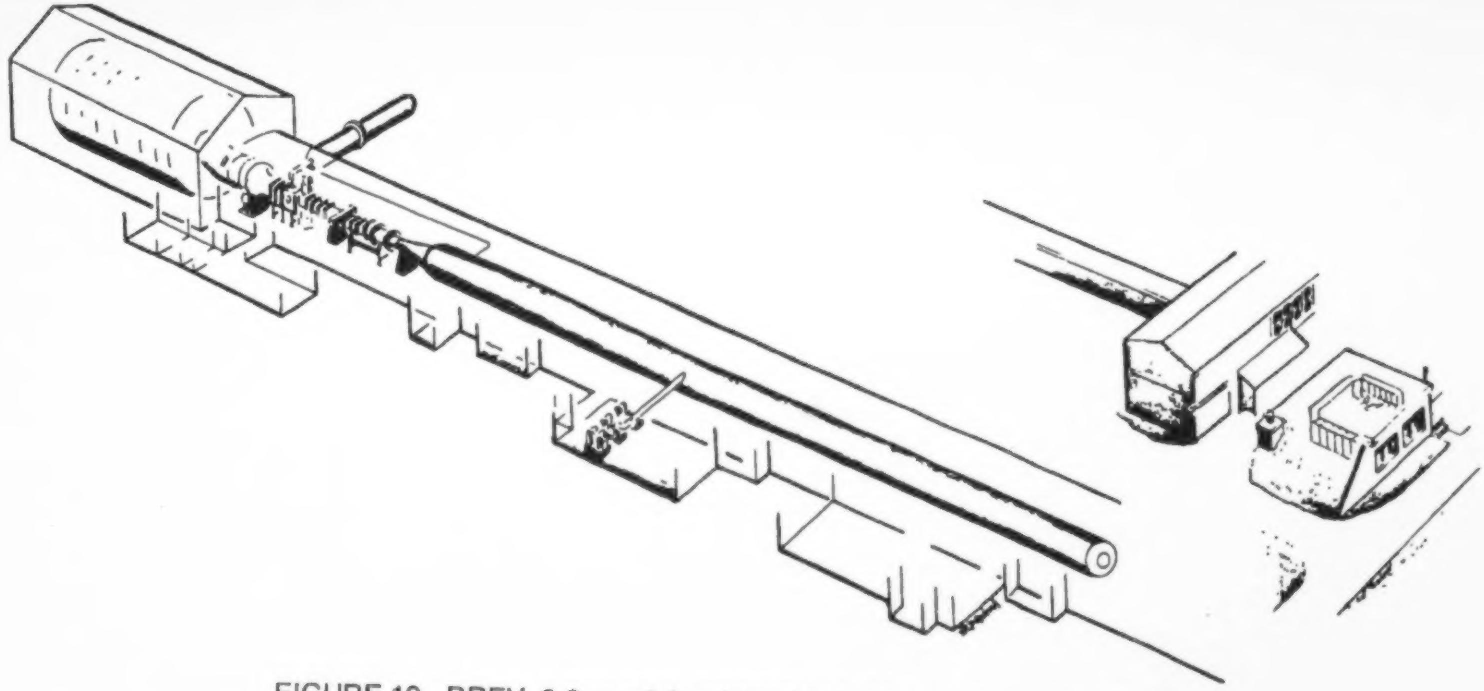

FIGURE 19 - DREV 0.6-m x 0.6-m trisonic wind tunnel, general arrangement

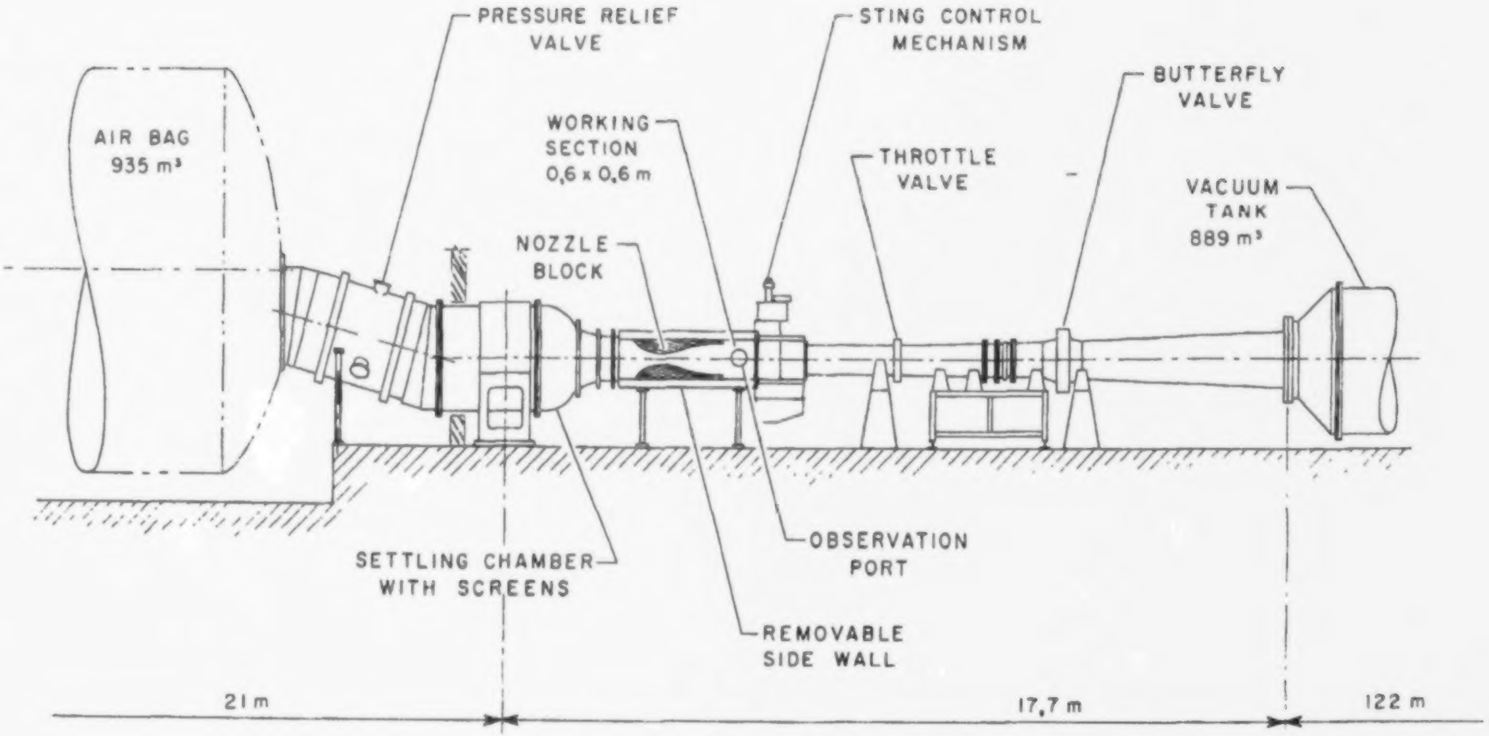

PRESSURE RELIEF VALVE
STING CONTROL MECHANISM
BUTTERFLY VALVE
AIR BAG 935 m³
WORKING SECTION 0,6 x 0,6 m
THROTTLE VALVE
VACUUM TANK 889 m³
NOZZLE BLOCK
SETTLING CHAMBER WITH SCREENS
OBSERVATION PORT
REMOVABLE SIDE WALL
21 m
17,7 m
122 m

FIGURE 20 - DREV 0.6-m x 0.6-m trisonic wind tunnel, principal components and dimensions

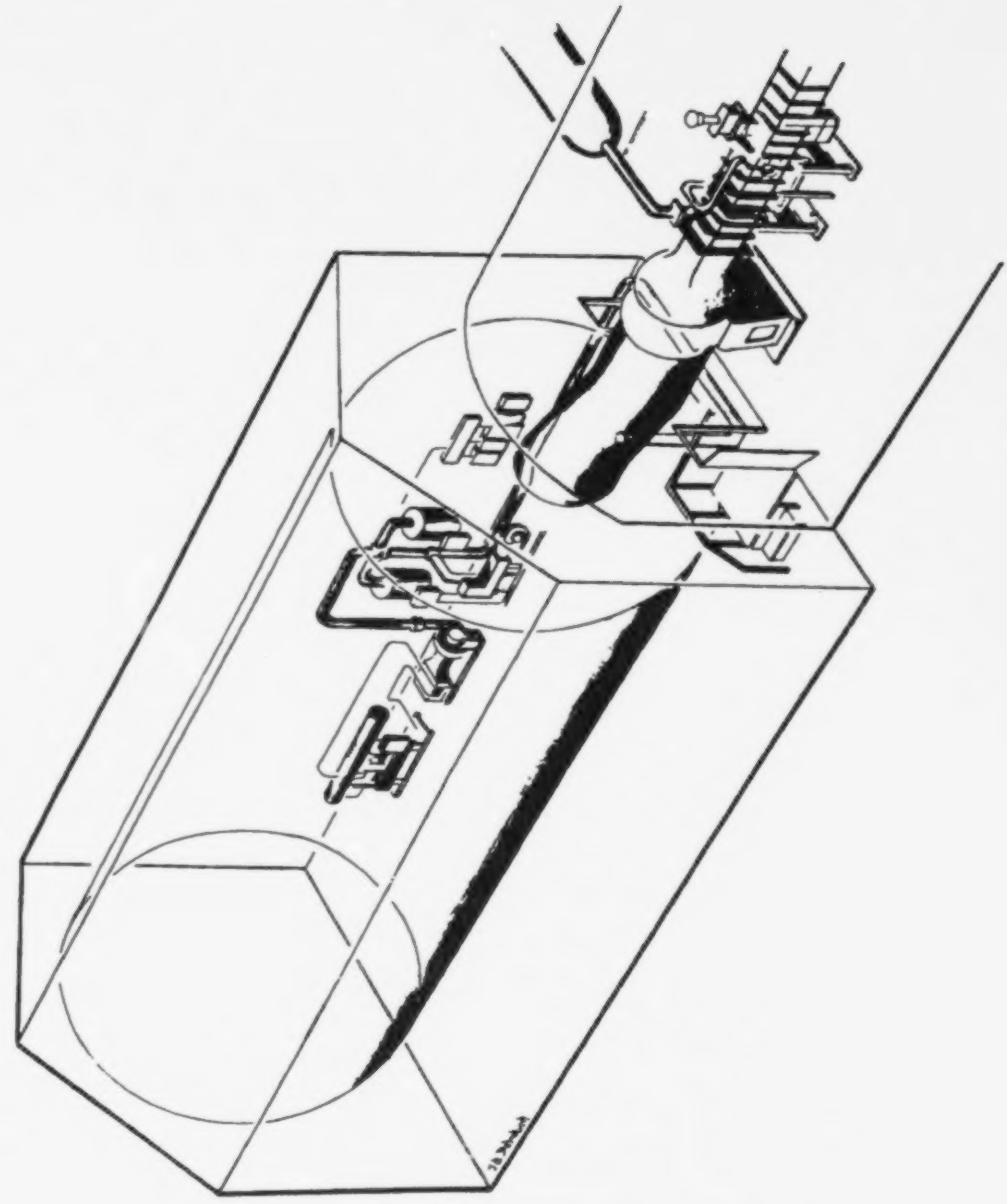

FIGURE 21 - Flexible air reservoir, electrically heated Celica-Cel air dryer and settling chamber

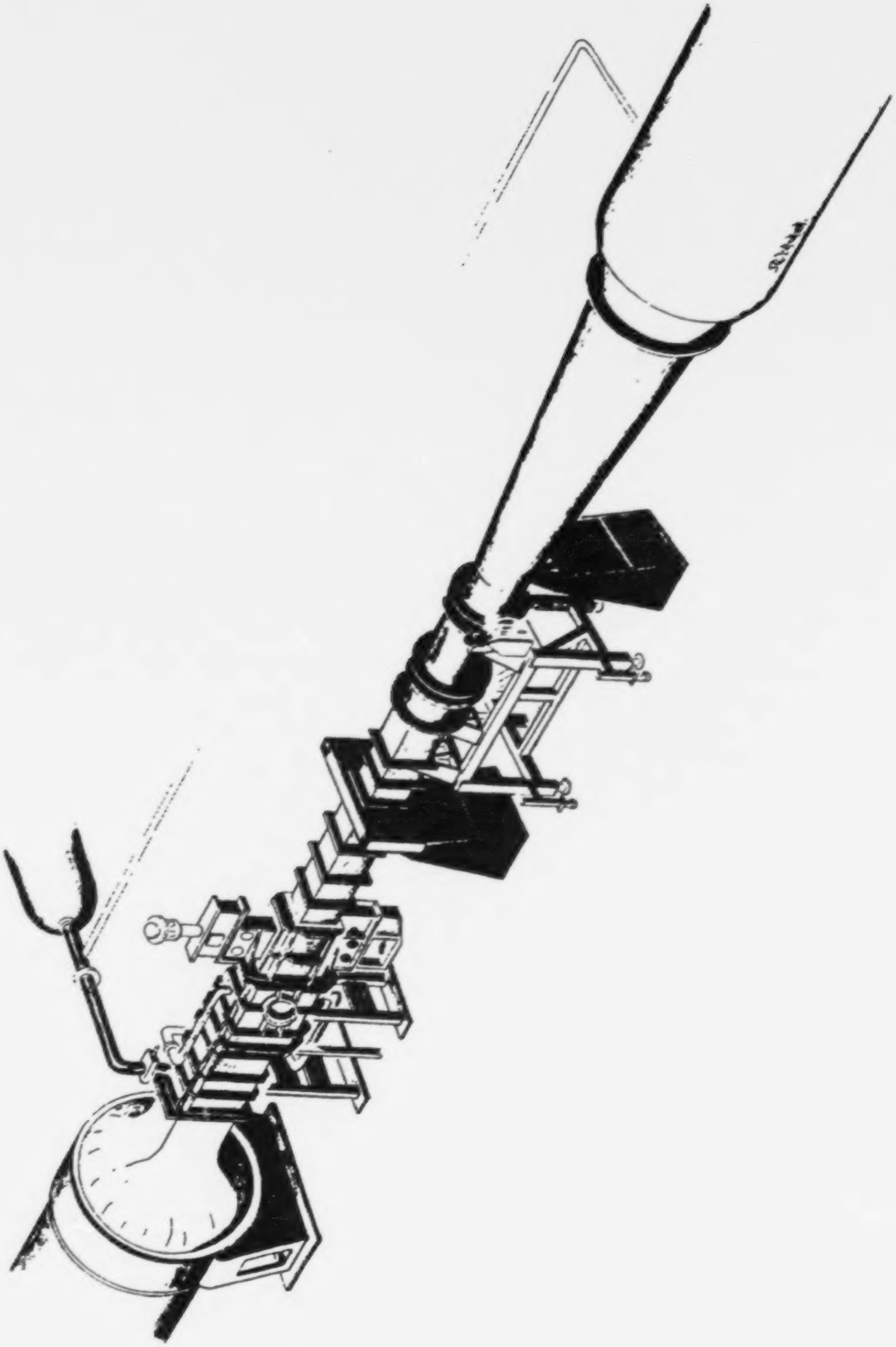

FIGURE 22 - Settling chamber, convergent, test section, throttle valve, diffuser and butterfly valve

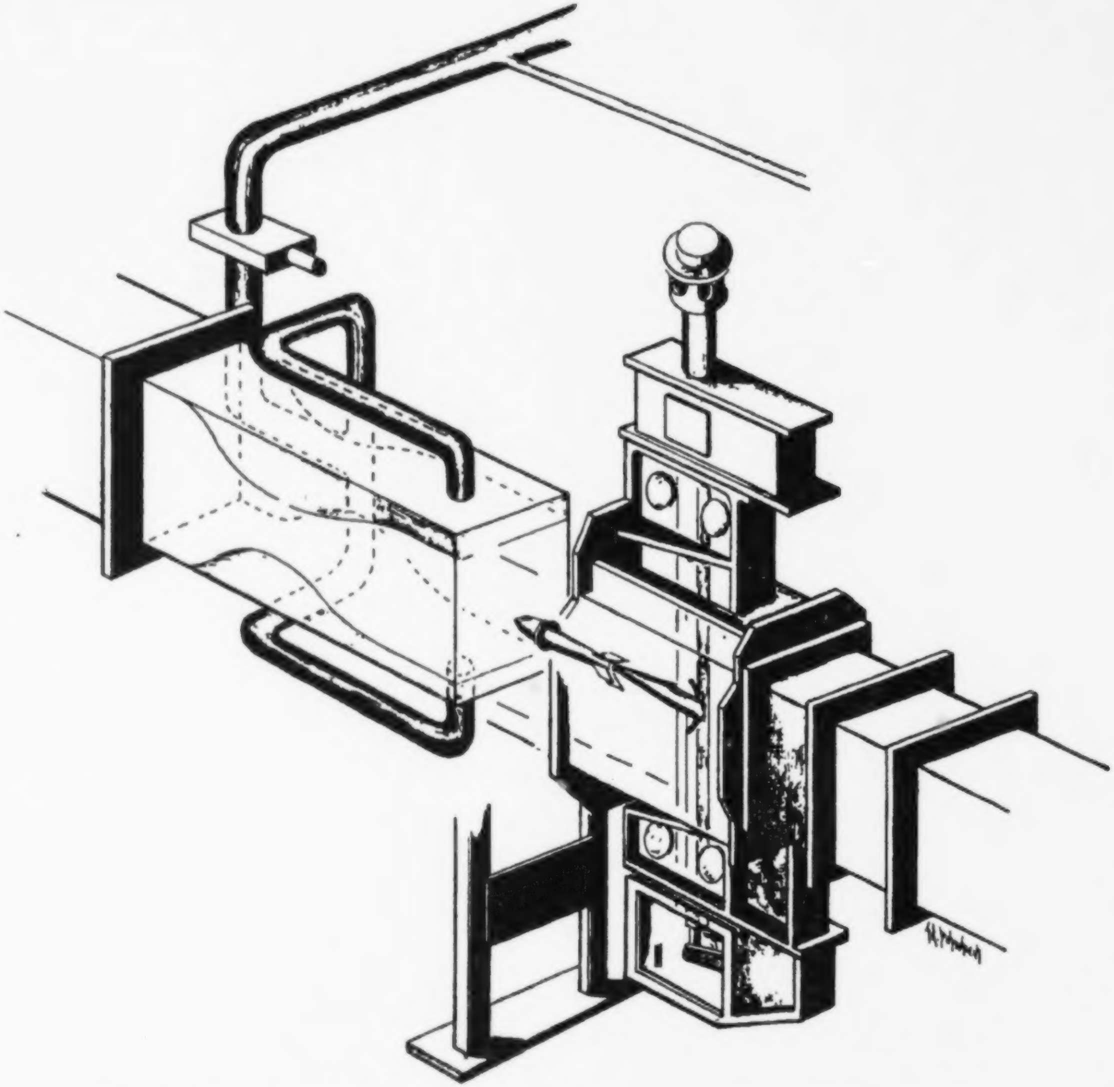

FIGURE 23 - Exploded view of DREV trisonic wind tunnel test section

When desirable, subsonic flow, which has a duration of about 5 s (about 4 s are usable), is produced and controlled with the combined use of a special set of two dimensional nozzles (which are much flatter than supersonic ones) and a variable throttle valve which is located downstream of the working section. When transonic flow conditions are desirable, a dedicated section can be installed in replacement to the standard ones used for supersonic and subsonic tests. The transonic section, which bears hundreds of aspiration holes drilled at angle against flow direction, is utilized in conjunction with proper manifold system and valves in order to obtain a suction through the surfaces that is uniform but variable in intensity. This system, by allowing the aspiration of the lateral flow components that occur after oblique shock waves, avoids shock reflection on test section walls. Otherwise, shock waves, which are almost normal at transonic regime, would have reflected back on the model and introduce measurements errors.

Because the DREV facility is an indraft tunnel drawing air into an evacuated tank from an atmospheric pressure reservoir, the Reynolds number drops to very low values at high Mach numbers. The effect of Reynolds number is often not very well known for most of projected experiments. Reynolds number (per metre of model length) for each Mach number in the test section and Reynolds number that would be obtained in flight at these Mach numbers under standard sea level conditions are listed in Table II. If the flow is not purposely tripped in order to produce a realistic boundary layer velocity profile and no means are available to characterize it, induced errors in aerodynamics coefficients could supervene. It can be observed that test conditions would often correspond more to laminar boundary layer for the model in tunnel and would be favorable to a predominantly turbulent boundary layer for the case of a similar projectile in flight at sea level (which means a farther back transition zone in the tunnel than in atmospheric flight conditions). This data is also presented in graphical form in Fig. 24.

TABLE II

Comparison between tunnel and free-flight unit Reynolds numbers

* Standard Sea Level Conditions in Reservoir

** Standard Sea Level Conditions

Mach No.	Re/x (Tunnel)*	Re/x (Free Flight)**
0.23	5.1 x 10^6/metre	5.3 x 10^6/metre
0.50	10.2	11.4
0.70	13.0	16.0
0.80	14.0	18.3
1.03	15.3	23.6
1.17	15.6	26.8
1.28	15.6	29.3
1.35	15.5	30.9
1.50	15.2	34.3
2.0	12.8	45.7
2.5	10.1	57.2
3.0	7.8	68.6
3.5	6.0	80.0
4.0	4.7	91.5

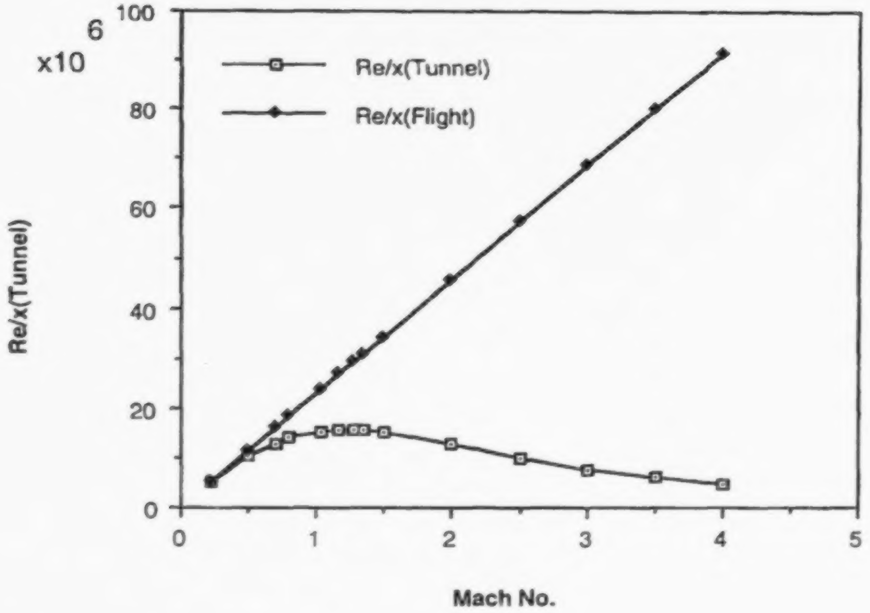

FIGURE 24 - DREV tunnel Reynolds number (per metre) as a function of Mach number

4.0 SPIN RIG CONTROLLER - DESCRIPTION

The motor controller (Fig. 25) working principles are shown diagrammatically in Fig. 26. The purpose of the controller is to supply the motor with the electrical energy necessary to run it at a predetermined spin rate up to a possible maximum of 40,000 rpm, while minimizing variations due to the bearings friction and the aerodynamic forces. Care must be taken to ensure the safe operation of the motor mounted on the balance and to provide outputs proportional to the motor operational parameters.

The energy is supplied to the motor by a servo amplifier which is fed by a voltage proportional to the desired spin-rate. This voltage is compared with a signal proportional to the actual spin-rate and the difference is amplified and used to increase or decrease the energy delivered to the motor. The feedback voltage proportional to the motor spin-rate is derived from the revolution period detected by a magnetic pick-up (which was used in the present experiment) or a photoelectric-infrared sensor and converted to an analog signal.

Since the motor is driven at a much higher voltage (200 VDC) than its rated value (120 VDC), the duty cycle must be kept short and its temperature must be monitored. This function is accomplished by a waveform generator which controls the energy provided by the power amplifier. The latter is turned on by the controlling equipment and turned off automatically after running more than 30 sec. The run time of the rig is longer than the wind tunnel run time because it is needed to accelerate the model to the desired spin rate before initiating a test run. The waveform can also be turned off by the motor temperature monitor which prevents its operation when its temperature gets higher than the set limit value (127 F°). The motor controller box chart circuit is presented in Fig. 27. Table III summarizes the controller characteristics.

Figure 28 shows the spin-rate response with respect to time for various initial settings on the controller. As it can be seen in Fig. 26 under the label " RUN TIME ", during motor acceleration cycle, voltage is increased gradually as per a preset ramp with respect to time (in order to keep current just below 2.0 A). All spin-rate response tests vs time shown in Fig. 28 were made with the same acceleration ramp than used in this wind tunnel test run series.

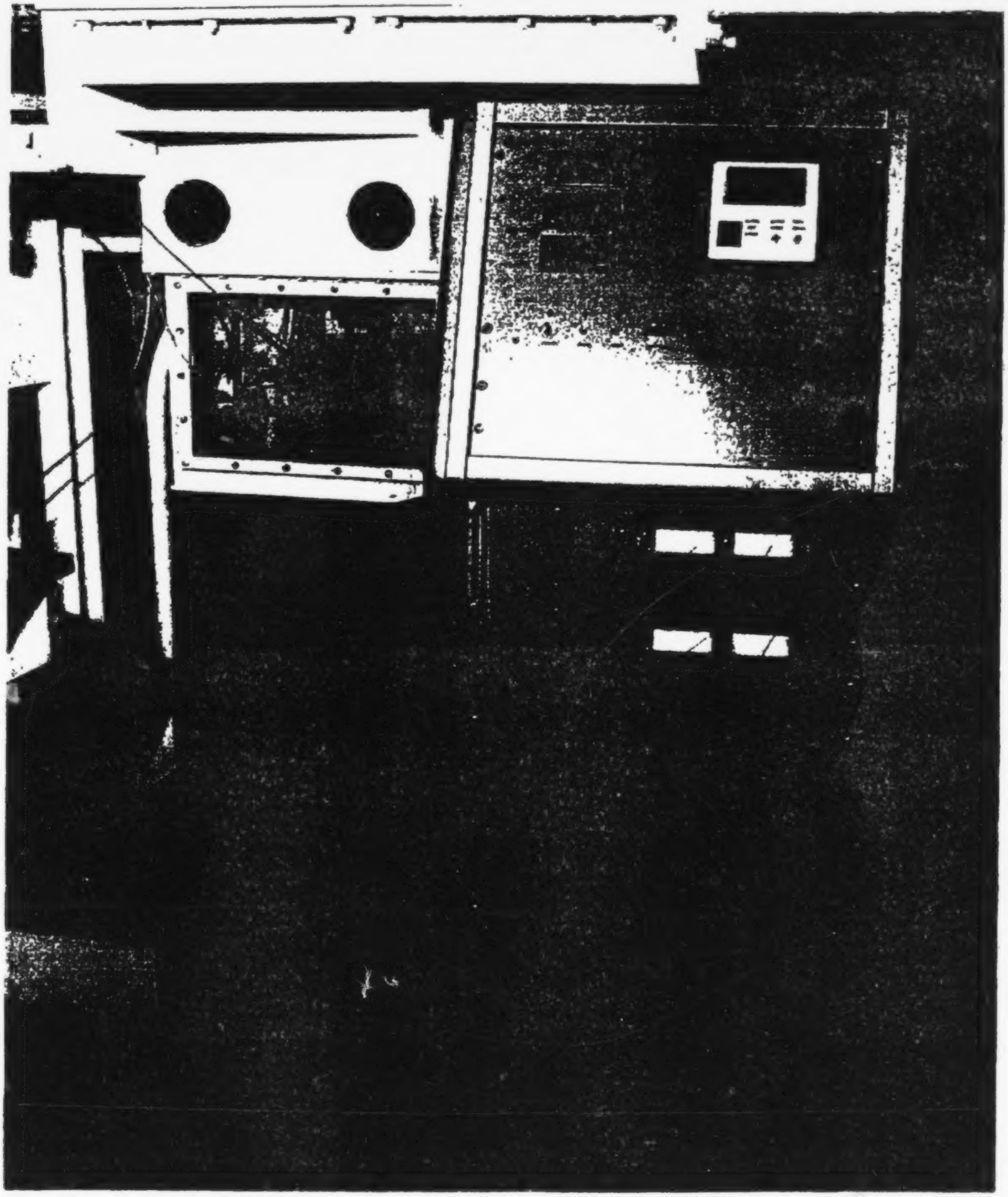

FIGURE 25 - Controller for DREV Electrical Spin Rig

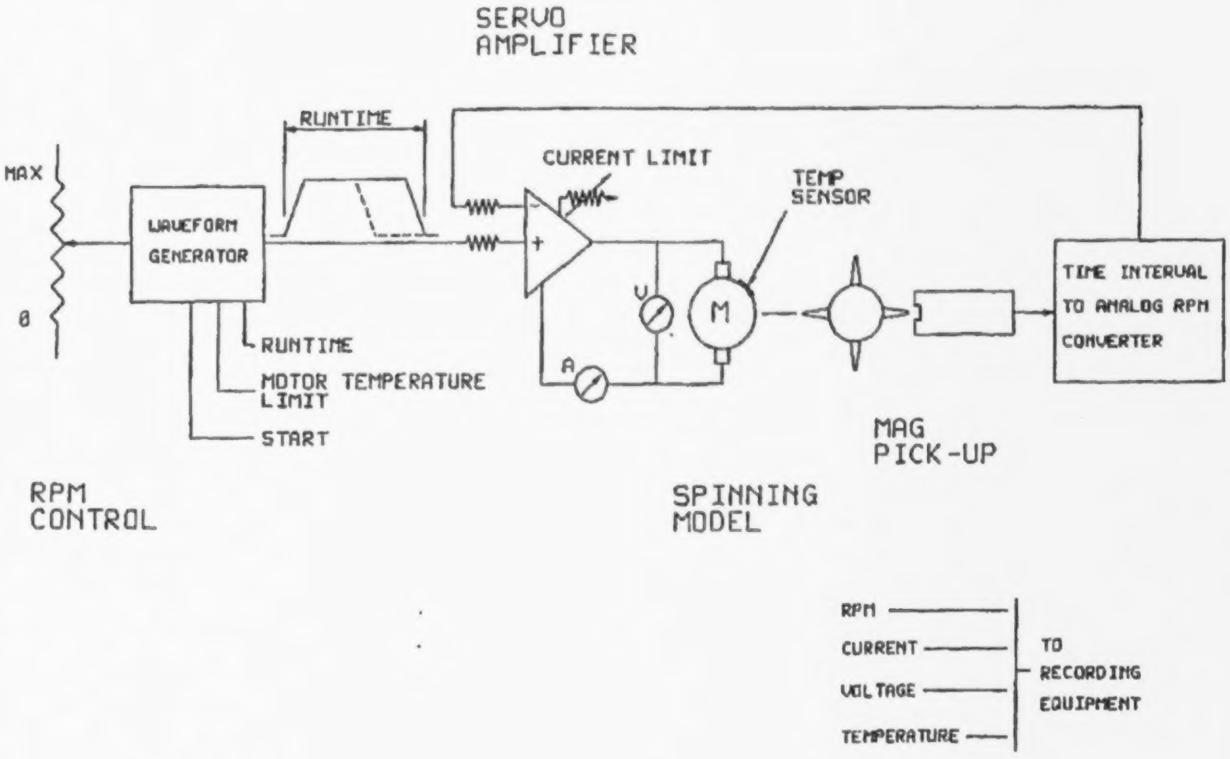
SERVO AMPLIFIER
RUNTIME
MAX
0
WAVEFORM GENERATOR
CURRENT LIMIT
TEMP SENSOR
-
+
V
A
M
TIME INTERVAL TO ANALOG RPM CONVERTER
RUNTIME
MOTOR TEMPERATURE LIMIT
START
MAG PICK-UP
RPM CONTROL
SPINNING MODEL
RPM
CURRENT
VOLTAGE
TEMPERATURE
TO RECORDING EQUIPMENT

FIGURE 26 - Controller schematic principle of work

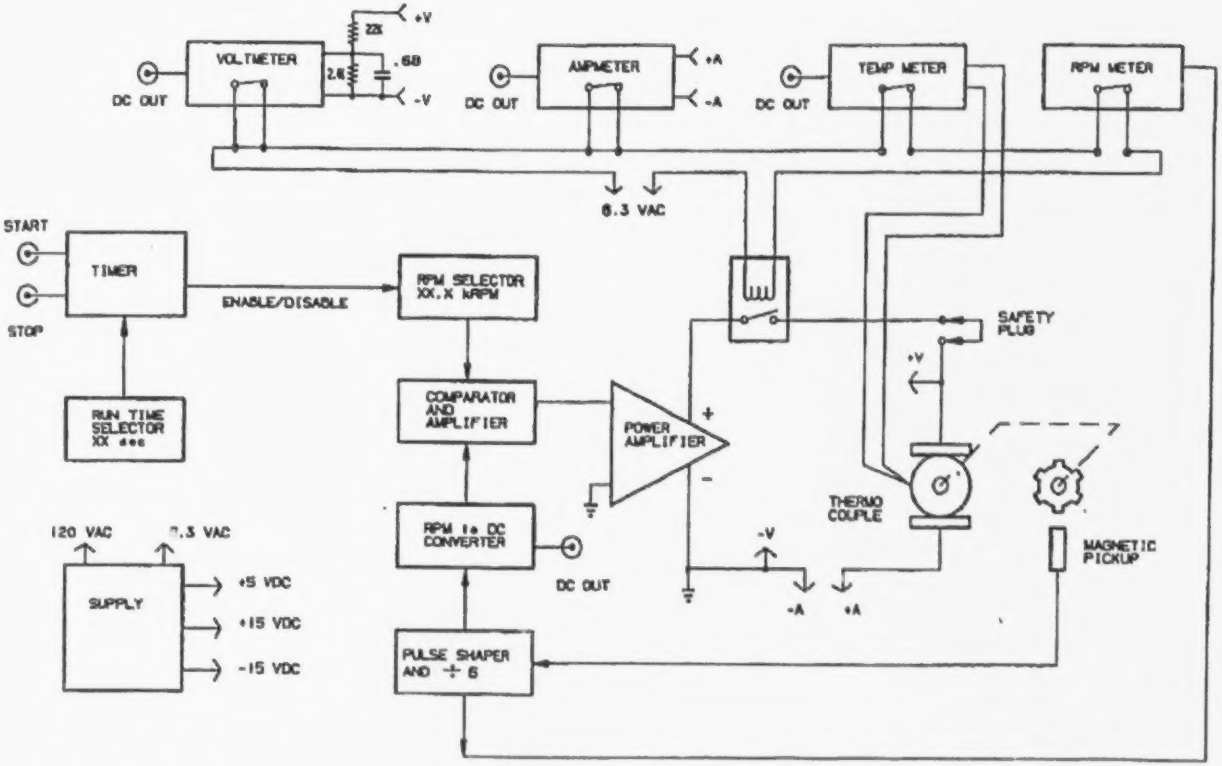
VOLTMETER
DC OUT
22K
2.6
.68
+V
-V
AMPMETER
+A
-A
DC OUT
TEMP METER
DC OUT
RPM METER
6.3 VAC
START
STOP
TIMER
ENABLE/DISABLE
RPM SELECTOR XX.X kRPM
RUN TIME SELECTOR XX sec
COMPARATOR AND AMPLIFIER
POWER AMPLIFIER
+
-
SAFETY PLUG
+V
THERMO COUPLE
MAGNETIC PICKUP
RPM to DC CONVERTER
DC OUT
-V
-A
+A
120 VAC
6.3 VAC
SUPPLY
+5 VDC
+15 VDC
-15 VDC
PULSE SHAPER AND ÷ 6

FIGURE 27 - Spin rig controller box chart

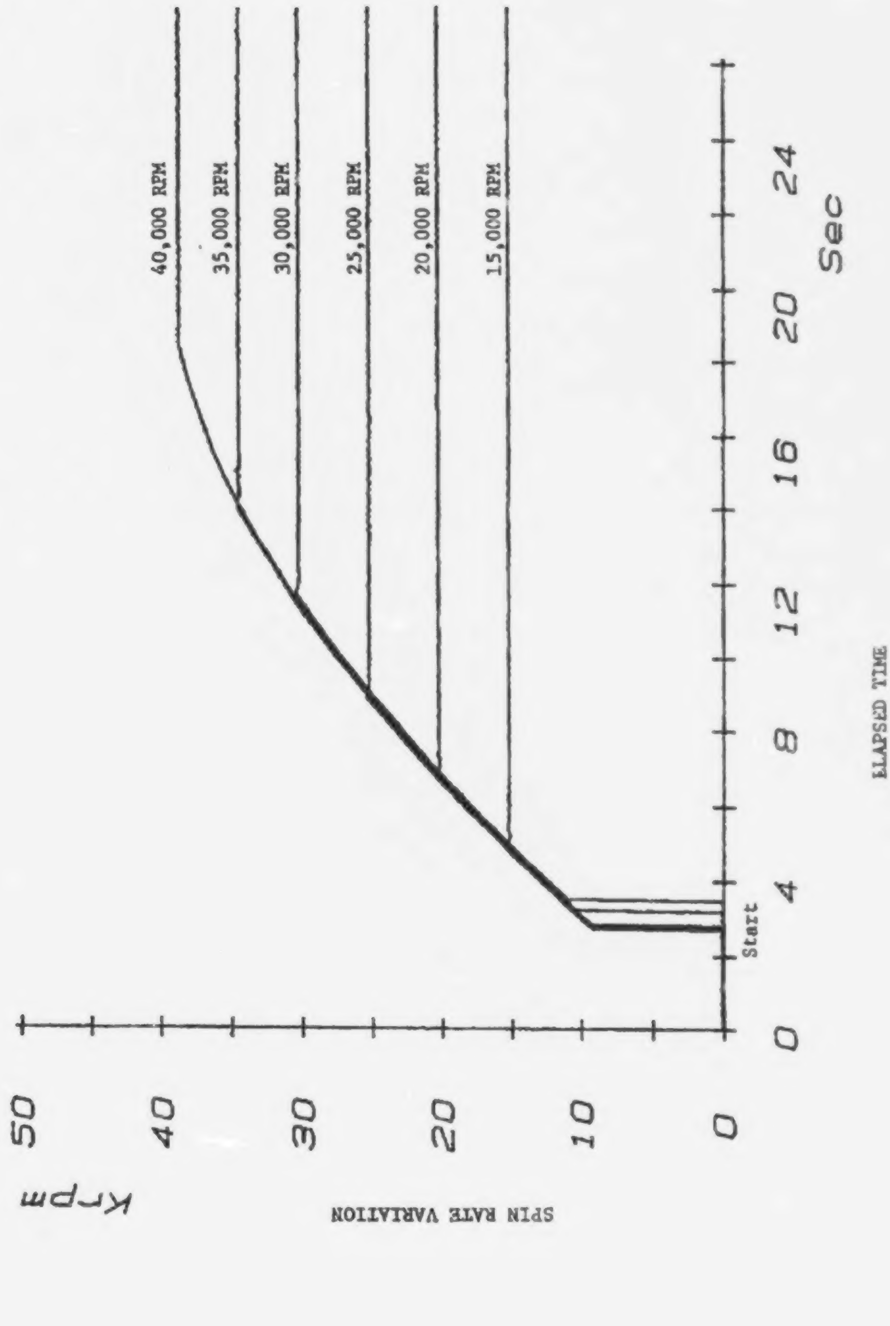

FIGURE 28 - Spin rate response for various initial settings on the controller (no wind)

TABLE III

Electronic Spin Rig Controller Characteristics

Purpose:

This apparatus is used to drive and precisely control the spin rate of a spin test model D.C. motor during a wind tunnel run. It also measures the model spin rate, the voltage applied to the motor, the current delivered to the motor and its temperature in the region of the brushes. The controller shall turn off the motor if its spin rate, applied voltage, current and temperature overpass preset values.

Specifications:

Test duration:	selectable 1 to 99 sec.
Controllable spin rate envelope	15,000 to 40,000 rpm
Voltage applied to the motor	0 to ±200 VDC
Current delivered to the motor	0 to ±2.0 A

Input Circuit:

Start control: Manual, Push Button
Level 1 to 0, Transistor-Transistor Logic Signal
Logic 0 ≡ 0.0 Volt, Logic 1 ≡ 5.0 Volt

Stop control: Manual, Push Button
Level 1 to 0, Transistor-Transistor Logic Signal

Test duration: Selectable 1 to 99 sec.

Note: The stop control command or the one from a TTL signal override the test duration control selectable command.

Output Circuit:

Spin rate: Calibrated 1 volt/10k rpm
Accuracy: 15,000 rpm ± 4 rpm
20,000 rpm ± 7 rpm
25,000 rpm ± 10 rpm
30,000 rpm ± 15 rpm
35,000 rpm ± 20 rpm

Voltage: Calibrated 1 Volt/40 Volts, Accuracy ± 1.0 Volt

Current: Calibrated 1 Volt/400 mA, Accuracy ± 1.0 mA

Motor temperature: Calibrated 5.0 mVolt / F° , accuracy ± 1.0 F°

5.0 CALIBRATION TESTS

The primordial reason for which the the spin rig system was devised at DREV, was to acquire the means to measure the aerodynamic spin damping of projectiles models. During a wind tunnel test run, among other variables, the spin rate, the motor current and the rolling moment felt by the balance were measured simultaneously versus time.

This data provided two methods to determine the spin damping. The most precise one utilized the rolling moment results obtained from the balance in conjunction with the polar inertia moment of the spinning model outer shell versus a time reference scale. Because of the very complicated geometry of the spinning outer shell internal surface, the moving parts like ball bearings and the model base with its spin rate detection system, it was more practical to determine experimentally the value of IX instead to process by calculation.

The second method, which was much less precise, used the motor current data. Data results obtained from a wind tunnel run were interpreted by using a calibration table giving the rolling moment applied on the model outer shell as a function of the motor current. Because the mechanical condition of the system's three ball bearings could not have been monitored accurately, inadvertent changes in their internal friction could have affected the calibration table of the rolling moment versus the motor current.

5.1 Determination of Model Inertia Moment

The polar inertia moment of the model spinning outer shell plus the spinning hardware (like the motor rotor, commutator, inner rings of ball bearings, spinning balls, ball cages, etc...) was measured by using the vacuum calibration chamber (Fig. 13) in conjunction with the motor controller (described in Chapter 4.0) and the 0.50 in balance used for wind tunnel test runs.

It consisted in measuring the model rpm acceleration slope after to have preset the controller for a constant ramp, together with the rolling moment then induced on the balance. The whole system being in a vacuum environment, in order to eliminate any aerodynamic interaction, the rolling moment then measured by the balance was only a function of inertial effects due to the model spin rate acceleration. It was possible to calculate the polar inertia moment, i.e. the value of IX. The following equation was used:

$$IX = \ell \,/\, PSPIND \; (kg \cdot m^2) = 0.000123109 \;\; Kg \cdot m^2$$

$$\text{where: } PSPIND = \frac{d\ PSPIN}{d\ t}$$

In practice, the spin rate data obtained from the motor controller spin detection system was expressed in rpm. The methodology and equations then used to measured experimentally the inertia moment are schematically explained in Fig. 29. It presents an example of the measurement data that was obtained under the form of " VISICORDER " traces of the model spin rate with respect to time and while under a constant acceleration. The rolling moment signal from the balance was also graphically recorded. These curves were used to calculate the polar moment of inertia of all spinning hardware. The motor current with respect to time had also its own trace although not used in the calculations.

5.2 Measurement of Rolling Moment vs Motor Current

In order to calculate the aerodynamic spin damping by measuring the motor current, it was necessary to calibrate the axial torque (or the rolling moment) applied to the model outer shell versus motor current. This is achieved by using the plexiglass vacuum reservoir (Fig. 13) in conjunction with the electrical Foucault Braking braking system (Figs. 14 and 15) to simulate the aerodynamic spin damping forces on the model.

The rolling moment measurements were then taken from the 6-component sting balance and used to generate a calibration table giving the external rolling moment applied to the model versus the spin rate and D.C. motor current. Results are under the form of a family of curves.

In order to compensate for possible non-linearities in the internal friction versus spin rate of the motor brushes and in the ball bearings, a single curve must be generated for each spin rate (rpm).

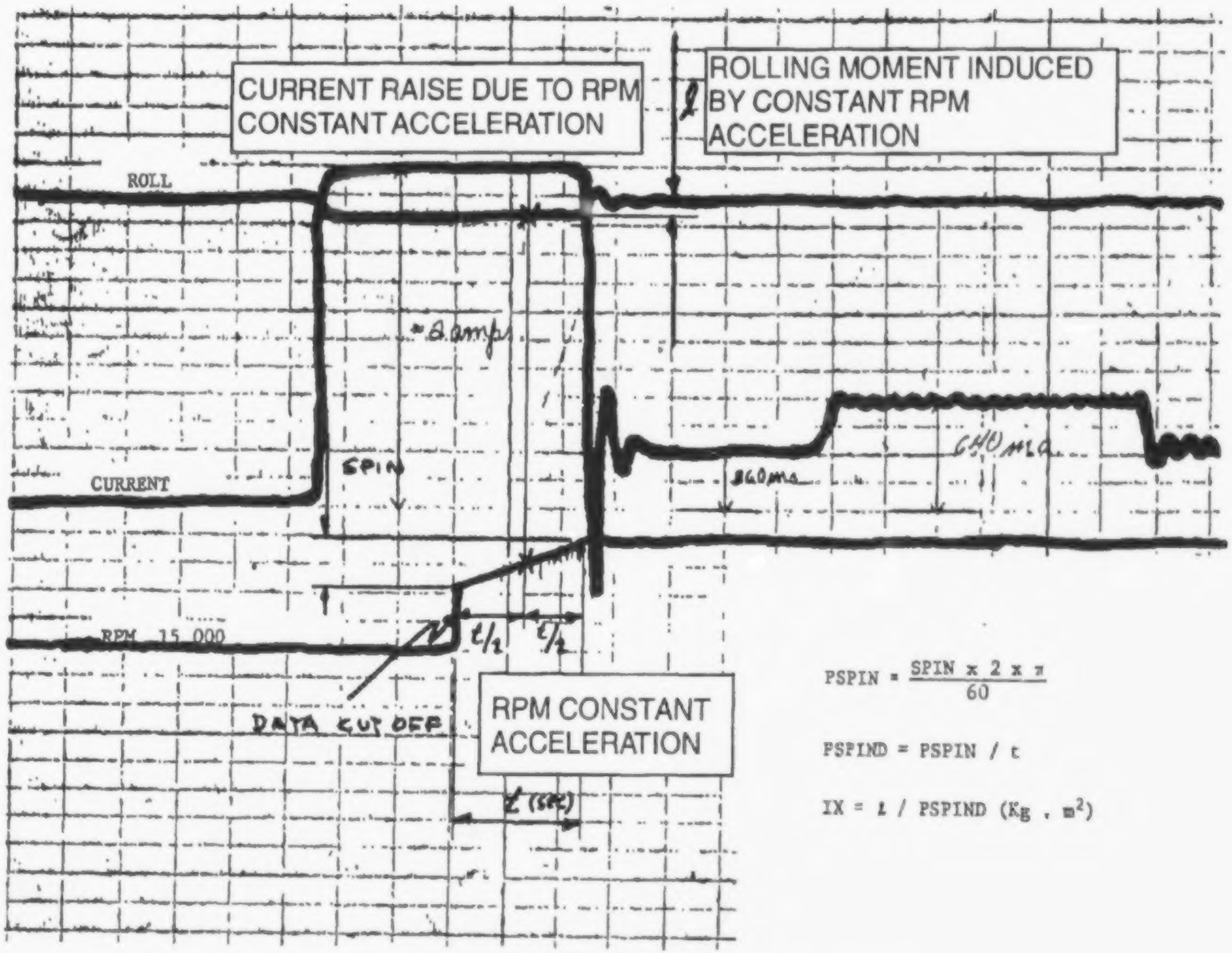

$$PSPIN = \frac{SPIN \times 2 \times \pi}{60}$$

$$PSPIND = PSPIN / t$$

$$IX = \ell / PSPIND \ (Kg \cdot m^2)$$

SPINNING HARDWARE POLAR INERTIA MOMENT

FIGURE 29 - Schematic of the methodology used to measure spinning hardware polar inertia moment

The calibration table then generated has the form of a family of curves where the specific data needed for a particular wind tunnel test must be derived by an interpolation process, (when the test spin rate fell in between those of two calibration curves). This calibration data can be incorporated in the standard wind tunnel data reduction routine. Figure 30 shows a typical variation of motor current while electromagnetic braking was applied for a test made in the Plexiglass vacuum reservoir at 30,000 rpm.

Although some calibrations were made, this method was not used in the data reduction of most wind tunnel test runs of the present series.

6.0 SPIN TESTS - MEASUREMENT APPARATUS, TEST CONDITIONS AND PROCEDURE, SPIN DAMPING DATA REDUCTION

The models aerodynamic coefficients were derived from forces and moments that were measured with two types of 6-component strain gage sting mounted balances. The first five runs were made with an Able MK-VI-A 0.50 in balance. This balance failed due to a roll element strain gage problem so the remaining of the runs were conducted with an Able MK-X-A 0.50 in balance. The dimensions and characteristics of these balances are given in Figs. 31 and 32.

During the run, the sting-strut mechanism pitched the model through a range of angles of attack. The sting-strut mechanism was adjusted to sweep the model around a pivot point (defined as the intersection between model longitudinal axis and tunnel centreline) located at 368.3 mm (14.50 in) from strut hub shoulder. With a 0.5 in balance in use, this arrangement was keeping the Balance Resolving Centre (BRC) on the tunnel centreline. Also, the sting-strut mechanism can be adjusted to get pivot points located at 16.5 in, 18.5 in and 20.5 in from strut hub shoulder (Fig. 33).

The model was attached to the balance so that the Balance Resolving Center (BRC) was located 32.51 mm (1.28 in) ahead of model base plane (to locate the balance aft end flush with model base). The Moment Resolving Centre (MRC) was defined as the model

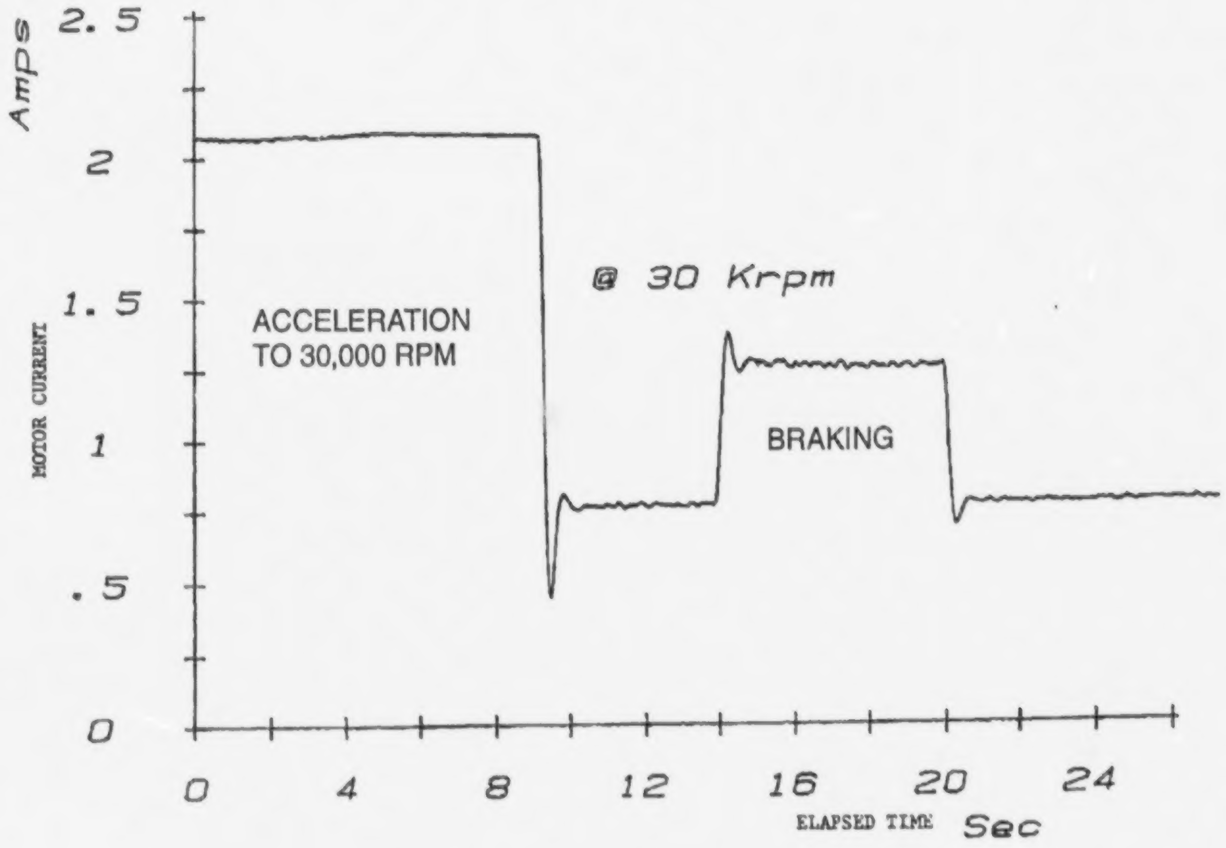

FIGURE 30 - Typical variation of motor current when electromagnetic braking is applied at 30,000 RPM

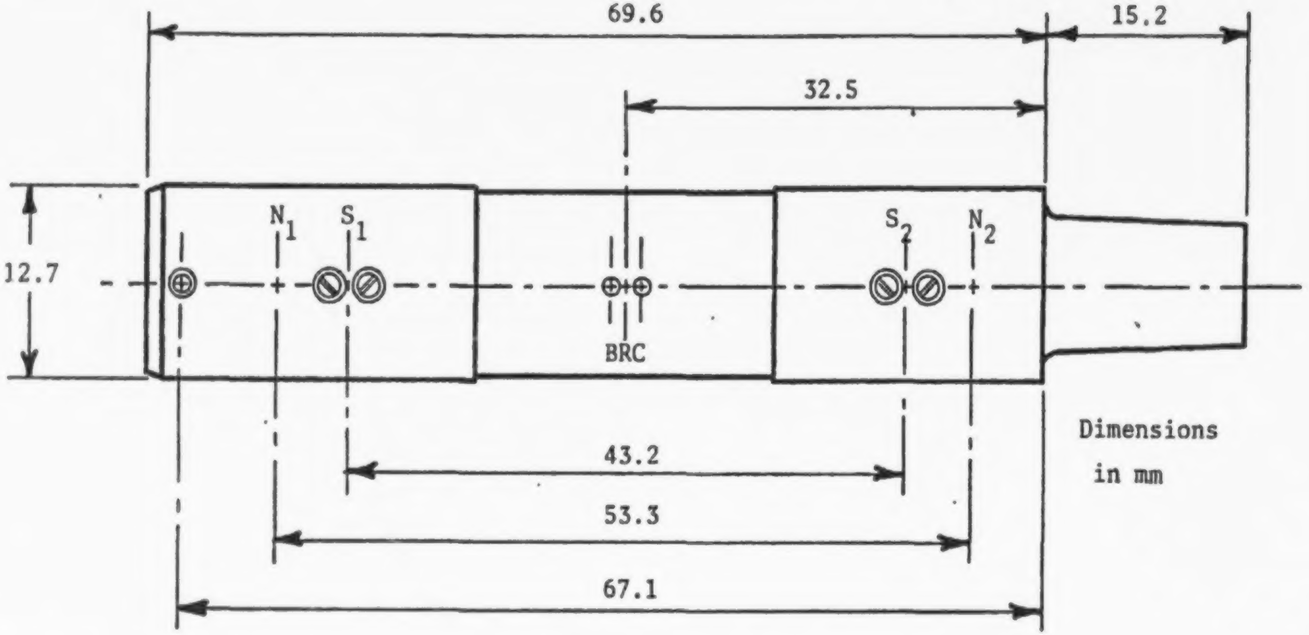
69.6
15.2
32.5
12.7
N_1
S_1
BRC
S_2
N_2
43.2
53.3
67.1
Dimensions in mm

Rated loads:	Total Normal Force (Pitching Moment = 0)	220 N
	Total Side Force (Yawing Moment = 0)	130 N
	Total Axial Force	130 N
	Rolling Moment	1.70 N-m
	Pitching Moment (Normal Force = 0)	5.9 N-m
	Yawing Moment (Side Force = 0)	2.9 N-m

Manufacturer: ABLE Corporation, Anaheim, California

Model: 0.50 MK-VI-A

FIGURE 31 - Dimensions and characteristics of the 0.50 in balance used at the beginning, It was damaged but very accurate and gave very precise results on Magnus effects

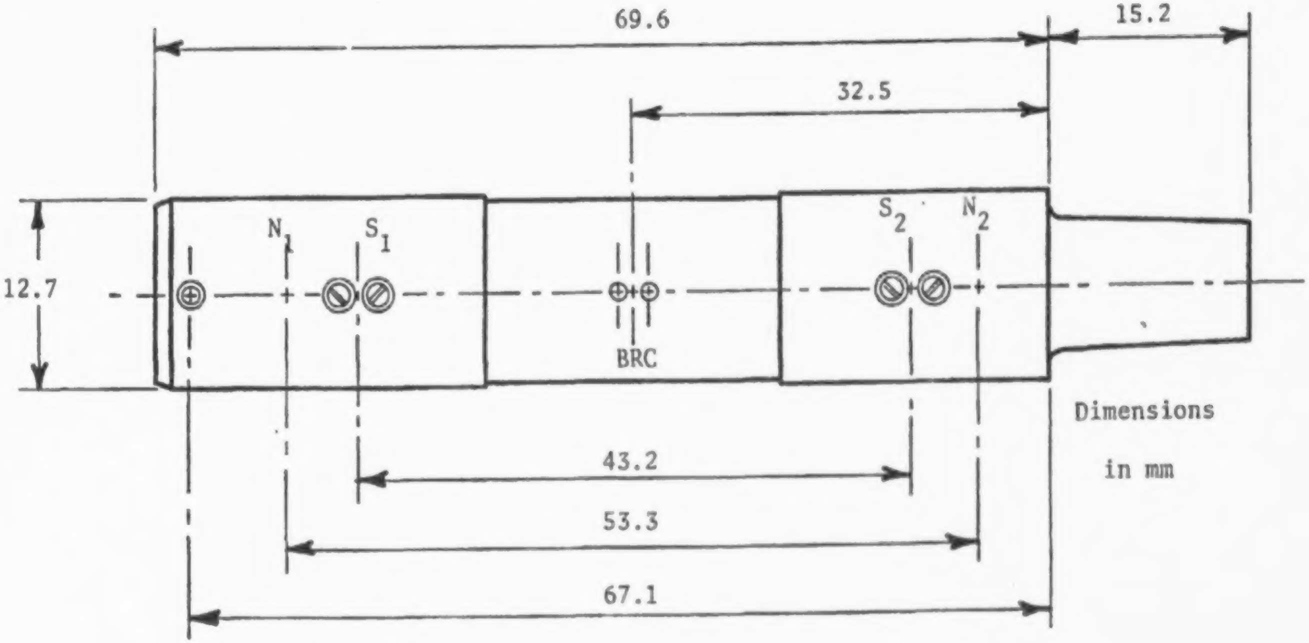
69.6
15.2
32.5
12.7
N1
S1
BRC
S2
N2
43.2
53.3
67.1
Dimensions
in mm

Rated loads:	Total Normal Force (Pitching Moment = 0)	445 N
	Total Side Force (Yawing Moment = 0)	445 N
	Total Axial Force	220 N
	Rolling Moment	1.7 N-m
	Pitching Moment (Normal Force = 0)	11.9 N-m
	Yawing Moment (Side Force = 0)	9.6 N-m

Manufacturer: ABLE Corporation, Anaheim, California

Model: 0.50 MK-X-A

FIGURE 32 - Dimensions and characteristics of the 0.50 in balance used for most of test runs, roll element had an offset but can be calibrated

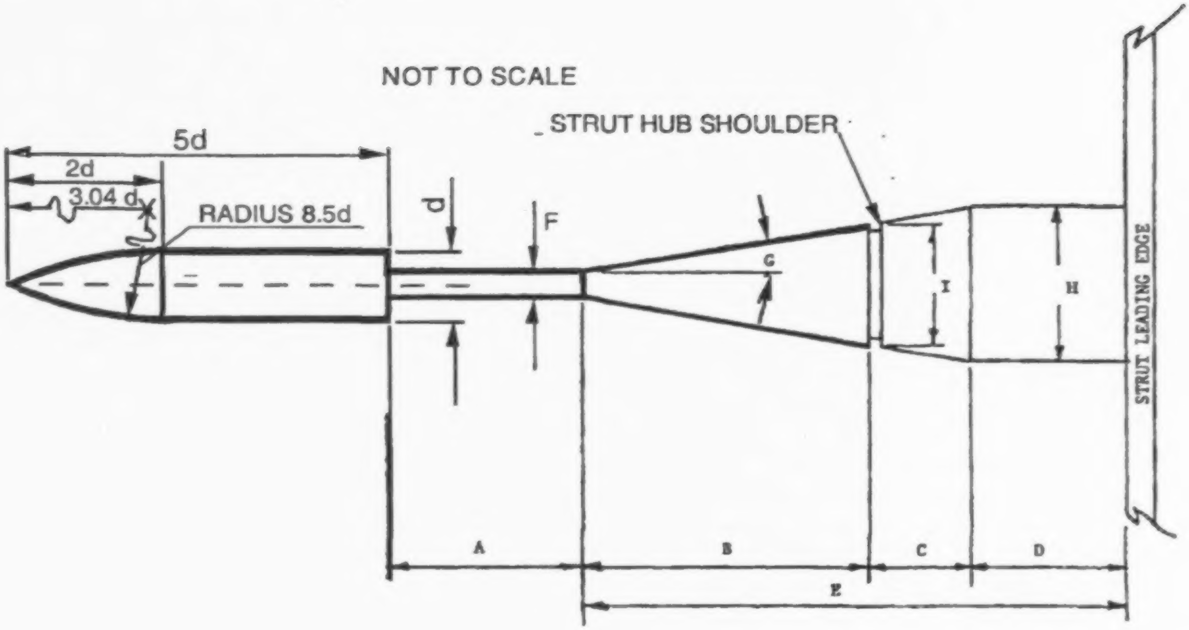
NOT TO SCALE
STRUT HUB SHOULDER
5d
2d
3.04 d
RADIUS 8.5d
d
F
G
I
H
STRUT LEADING EDGE
A
B
C
D
E

5-D ARMY-NAVY SPINNER MODEL/STING/STRUT COMBINATION
RELATIVE DIMENSIONS IN CALIBRES WITH RESPECT TO
MODEL MAIN BODY REFERENCE DIAMETER
TESTS WITH 0.50 IN BALANCE AND STING

A = 3.70
B = 4.54
C = 2.89
D = 0.63
E = 8.06

F = 0.39
G = 10.2 deg.
H = 1.88
I = 1.25

FIGURE 33 - Dimensions of 5-D ARMY-NAVY SPINNER model/sting 0.50 in/strut combination system in model calibres

base plane, so all pitching moments (and related coefficients) were expressed with respect to this point. The model base diameter d^1 was equal to d. The data reduction reference diameter was d= 40.54 mm. Input parameters that were used for treatment of data are summarized in table form at the beginning of Appendix A.

Test runs were done at Mach numbers 0.5, 0.7, 0.8, 0.9, 1.0, 1.15, 1.28, 1.38, 1.50, 1.75, 2.00, 2.50 and 3.00 for constant model spin rates of 20,000, 25,000, 30,000, 35,000 and 40,000 rpm. For most tests, sweeps of angle of attack ranged from -2 to +2 deg. Few runs were made with an angle of attack sweep from -5 to +15 deg.

During the continuous model sweep, the spin rate, the time reference and the three forces and three moments on the balance were recorded at each 0.15 deg increment for -2 to +2 deg tests and 0.50 deg increment for -5 to +15 deg tests. This was achieved by converting recorded voltage signals from the balance into forces and moments by using equations and calibration data in Section 7.1. These forces and moments were thereafter reduced into aerodynamic coefficients with equations presented in Chapter 8.0. The test section static pressure was obtained from the wall tap no. 8 which measured conditions at wall just ahead of the model nose (see Section 7.1 under " TEST SECTION ABSOLUTE PRESSURE TRANSDUCER ").

Appendix A gives a complete summary of test runs performed (see Table AI), run identification, test conditions and values of CNA, CMA, XCP0 and CA0 obtained for each test run. In Appendix B, Table BIV presents the average values of CNA, CMA, XCP0 and CA0 versus Mach number from the whole test series. These results were plotted in Figs. B5 to B8.

The base pressure was measured by installing a base pressure measurement tube (Atlas Inox 304, .049 in diam. .008 in wall) over sting and at a distance of 0.035 in from model base. The base drag (reduced with respect to models reference diameter) was subtracted from the total drag to obtain the forebody drag coefficient. To find a realistic value for the total drag (to be used for trajectory simulation) an appropriate method for estimating base drag corresponding to interference-free conditions must be used. The base drag contribution to the total drag varies with the configuration and Mach number. It is discussed in Chapter 11.0.

As the balance outer shell was vented at its aft end in order to allow a relative mechanical play or movement with respect to its floating frame, there was no loss of effective model base area subject to base flow static pressure, if compared to a real projectile in flight. In fact, to be thorough, there was a very thin loss of model effective base area corresponding to the cross-section of balance axial force element. It is common to consider it as a negligible effect.

The configuration of 0.50 in sting junction with test section strut hub can be seen in Fig. 29 and sting principal dimensions are presented in Fig. 30. The sting was 15.9 mm (0.625 in) in diameter and projected 3.70 model-calibres behind the base before the conical expansion began (10.2 deg). The model being 40.5 mm (1.596 in) in diameter, the sting-to-model base diameter ratio was 0.39. Figure 33 gives dimensions in model calibre of the model/sting support/strut hub combination system.

Aerodynamic variables such as lift and pitching moment coefficients and centre-of-pressure position should not have been influenced by the sting interference. The reason is the base drag that had no vectorial contribution to the normal force (then no influence on pitching moment), and the vectorial component of the base drag on total lift was very low due to test angles of attack less than 15 deg.

The spin damping was measured by direct reading of the rolling moment from the balance, plus a correction for the inertial effects due to the small spin rate variations happening during the time of measurement data acquisition. To do so, a reference timing was used in conjunction with the spin rate data and the equations of Chapter 8.0, in order to derive spin rate acceleration or deceleration. By then, knowing the polar inertia moment of all moving (spinning) parts (including the outer shell of the particular test model configuration), it was possible to compensate the balance rolling moment data for the inertial effects.

The rolling moment from the bearings and commutator friction, aerodynamic spin damping, spin rate variation and sting balance are related together in the following way:

$$\ell_{\text{motor}} = \ell_{\text{rotor}}$$

$$\ell_{\text{motor}} = \dot{p} \bullet IX + \ell_{\text{bearing friction}} + \ell_{\substack{\text{aerodynamic} \\ \text{spin damping}}}$$

$$\ell_{\text{balance}} = \ell_{\text{motor}} - \ell_{\text{bearing friction}}$$

$$M_{\ell_p} = \ell\,\ell = \ell_{\text{balance}} - \dot{p} \bullet IX$$

where $IX = 0.000123109 \ \text{Kg} \bullet \text{m}^2$

The physical meaning of these equations is made more explicit in Fig. 34.

Most of test runs were made using the Able MK-X-A 0.50 in balance that had its rolling element partly damaged and it appeared that an apparent measurement shift was observed in rolling moment data results. It resulted that measurements of positive and negative rolling moments were shifted in such a way that positive rolling moments data results were consistently larger in value than negative rolling moments. As spin tests were concerned, positive rolling moments were to be measured while the model was spinning with a left rotation, and negative rolling moments to be measured for a right rotation (see Fig. B2).

This measurement shift corresponded to a difference between the balance roll element offsets related to positive and negative rolling moments. A part of the measurement shift was due to non-linearities of the output signals that (normally) can be encountered when a balance is being utilized at less than 0.2% of its rated or nominal capacity. Few tests conditions were in that region.

It was then decided to develop a testing-procedure/data-reduction-methodology in order to compensate for this measurement shift as much as possible. Appendix B explains this methodology as data reduction is concerned and the related balance instrumentation

The two only physical forces that act directly on the balance are the torque from the permanent magnet and mechanical friction forces.

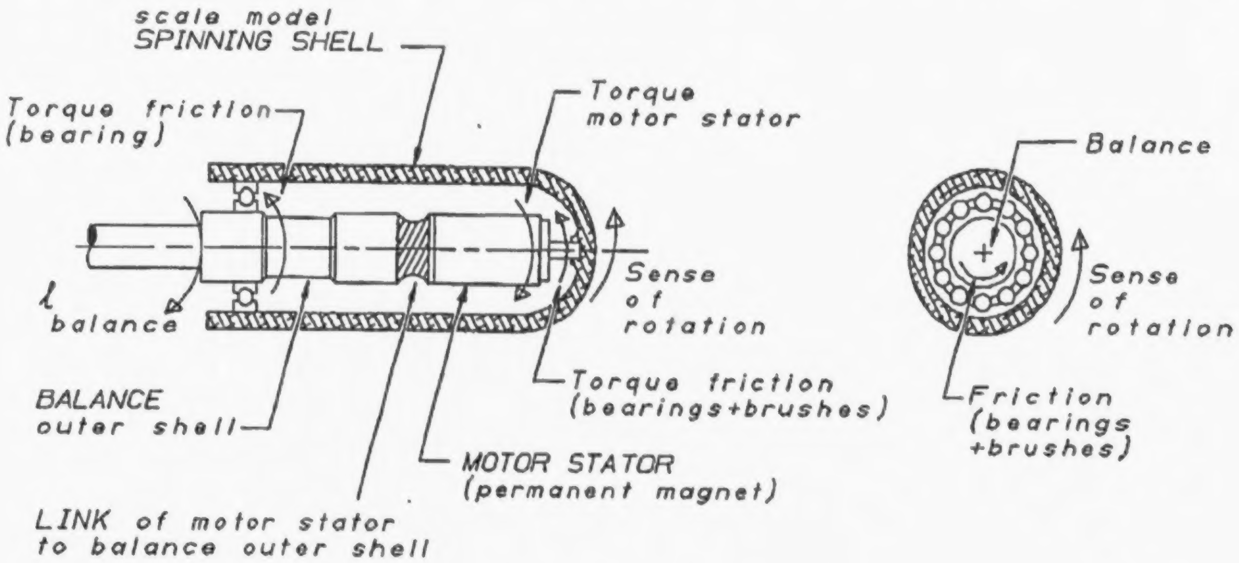
scale model
SPINNING SHELL
Torque friction
(bearing)
Torque
motor stator
Balance
ℓ balance
Sense
of
rotation
Sense
of
rotation
BALANCE
outer shell
Torque friction
(bearings+brushes)
Friction
(bearings
+brushes)
MOTOR STATOR
(permanent magnet)
LINK of motor stator
to balance outer shell

$$\text{Torque of motor rotor} = -\text{Torque of motor stator}$$

$$\text{Torque of motor rotor} = -\ell_{aerodynamic} - \ell_{friction} - I_x \dot{p}$$

$$\ell_{balance} = \text{Torque of motor stator} - \ell_{friction}$$

$$\ell_{balance} = \ell_{aerodynamic} + \cancel{\ell_{friction}} + I_x \dot{p} - \cancel{\ell_{friction}}$$

$$\ell_{balance} = \ell_{aerodynamic} + I_x \dot{p}$$

FIGURE 34 - Schematic description of aerodynamic torque, friction torque and motor torque interrelation

rationale is demonstrated in Appendix D. The resulting measurement errors are also discussed.

In summary, it consisted in repeating each run for each set of test conditions, one with right and one with left rotation. The final spin damping coefficient was thereafter calculated from the average value of both runs (right and left rotation). As explained in Appendix B, it was then possible to compensate for the roll measurement shift. But since the absolute values of the balance roll element shifts related to positive and negative rolling moments were not known, a residual error was left uncorrected. Since that time, a highly precise simultaneous-multiple-loads calibrator has been developped and is in a final stage of testing at present time. This apparatus was deviced to calibrate balance output signal non-linearities.

As demonstrated in Appendix B (see Fig. B3), the measurement shift corresponded to 0.0332% of the balance nominal capacity. Calculations of the observed roll measurement shifts are summarized in Table BIII. In Appendix D, the approximated value of the balance roll element offset was probably around 0.050% of the balance nominal capacity (see Fig. D3).

The magnitude of the roll damping on the Spinner model spread between 0.8% to 0.06% of the balance nominal capacity, depending on the Mach number and spin rate. Figures D2 and D4 give a relation between the test Mach number and the magnitude of the damping. The rolling moment measurements made at a level of 0.06% approached the hysterisis of the balance. This was unavoidable during these feasibility tests, and results must be interpreted accordingly. For future tests, models are expected to have large spin damping moments (range limited spin decelarated training ammunitions) and a suitable balance to be used if not the new balance being developped specially for that purpose (Refs. 7 to 9).

A summary of the aerodynamic data for the spin damping coefficient at zero angle of attack is presented in Table BII where also are given identifications of test runs used to calculate each data point plotted in Figs. 38 and B4. Values of spin damping coefficients obtained for each run can be retrieved in Table AI.

To verify the symmetry of flow conditions in the test section and the capability to reproduce Magnus effects with right and left rotation, side forces and spin damping were measured while the model was swept through a range of angle of attack (Figs 35 and 36). These tests were also repeated for various spin rates at the same Mach number (Fig. 37). Because in Figs. 35 to 37 a distinction is made between right and left rotation, the test run numbers corresponding to plotted data are summarized in Table IV.

TABLE IV

Origin of Data Plotted in Figs. 35 to 37

SPINWT-1

Figure 35	CY (MAGNUS FORCE)		
	- LEFT ROTATION	R2830	
	- RIGHT ROTATION	R2832	
Figure 36	CLP		
	- LEFT ROTATION	R2830	
	- RIGHT ROTATION	R2831	
Figure 37	CY (MAGNUS FORCE)		
	- 0 rpm	R2829	N/A
	- 26,000 rpm	R2835	LEFT
	- 31,000 rpm	R2836	LEFT
	- 35,500 rpm	R2834	LEFT

As mentioned in Chapter 3.0, the wind tunnel Reynolds number had low values at high Mach numbers. While the flow was predominantly laminar over the model in tunnel test section, it would have been almost all turbulent for a projectile in free flight. Due to that, it is possible that separation zones were not well simulated at maximum angle of attack (15 deg). Also, the skin friction drag (which is included in measured total drag), the base drag coefficient, the spin damping coefficient and the Magnus effects coefficients were probably slightly affected by those differences in boundary layer characteristics.

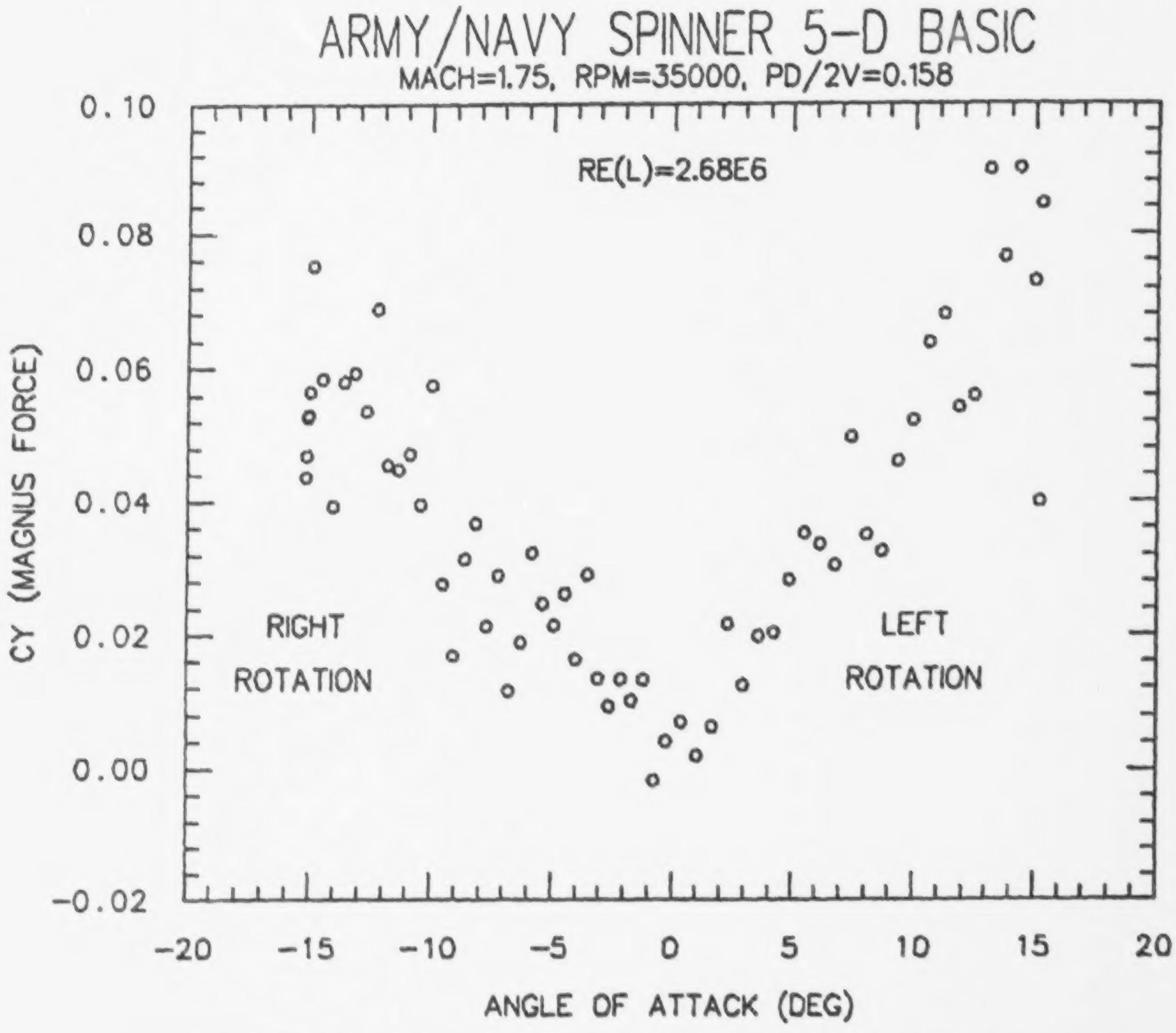

FIGURE 35 - Side force coefficient induced by Magnus effects (right and left rotation)

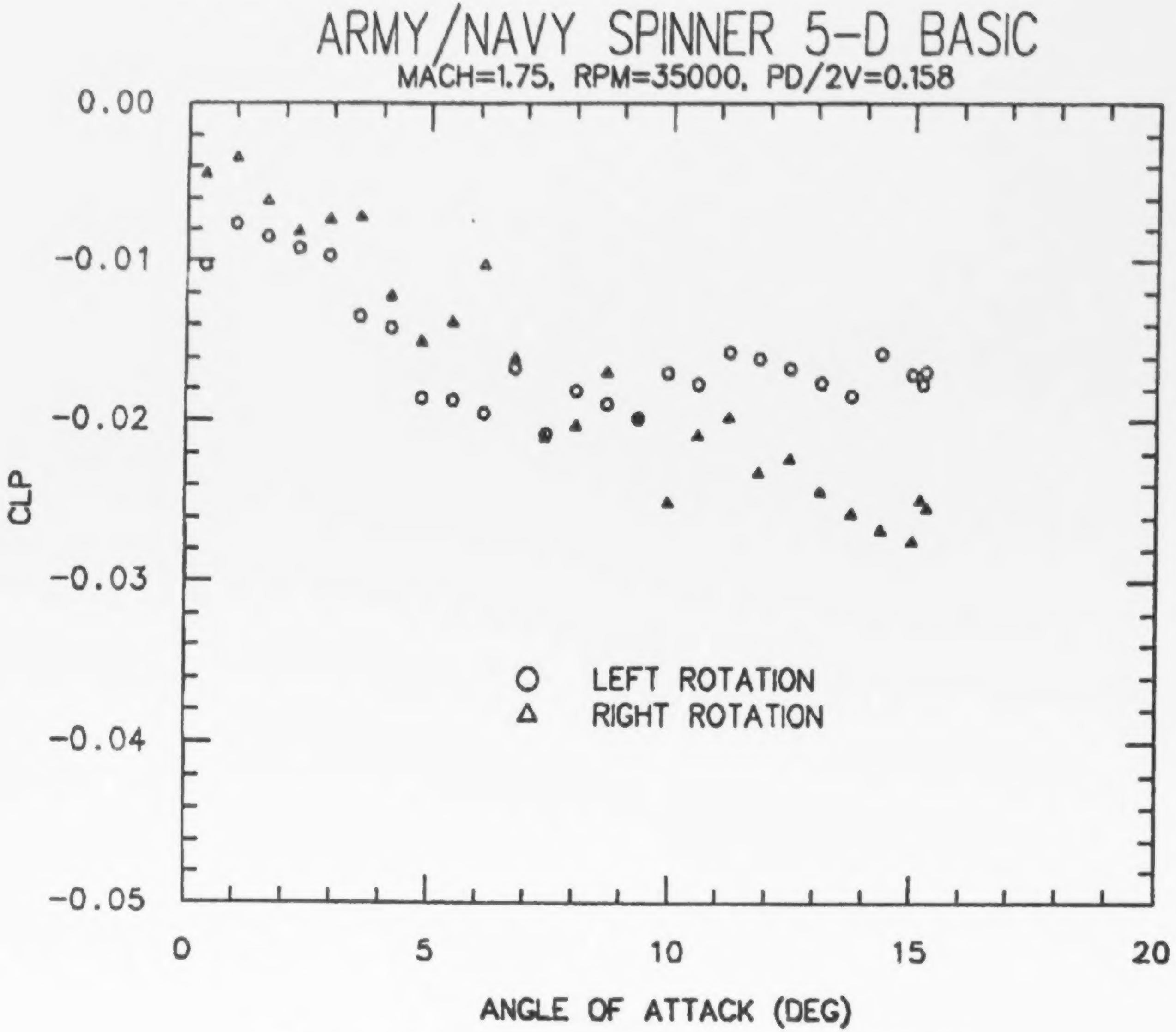

FIGURE 36 - Spin damping coefficient (right and left rotation)

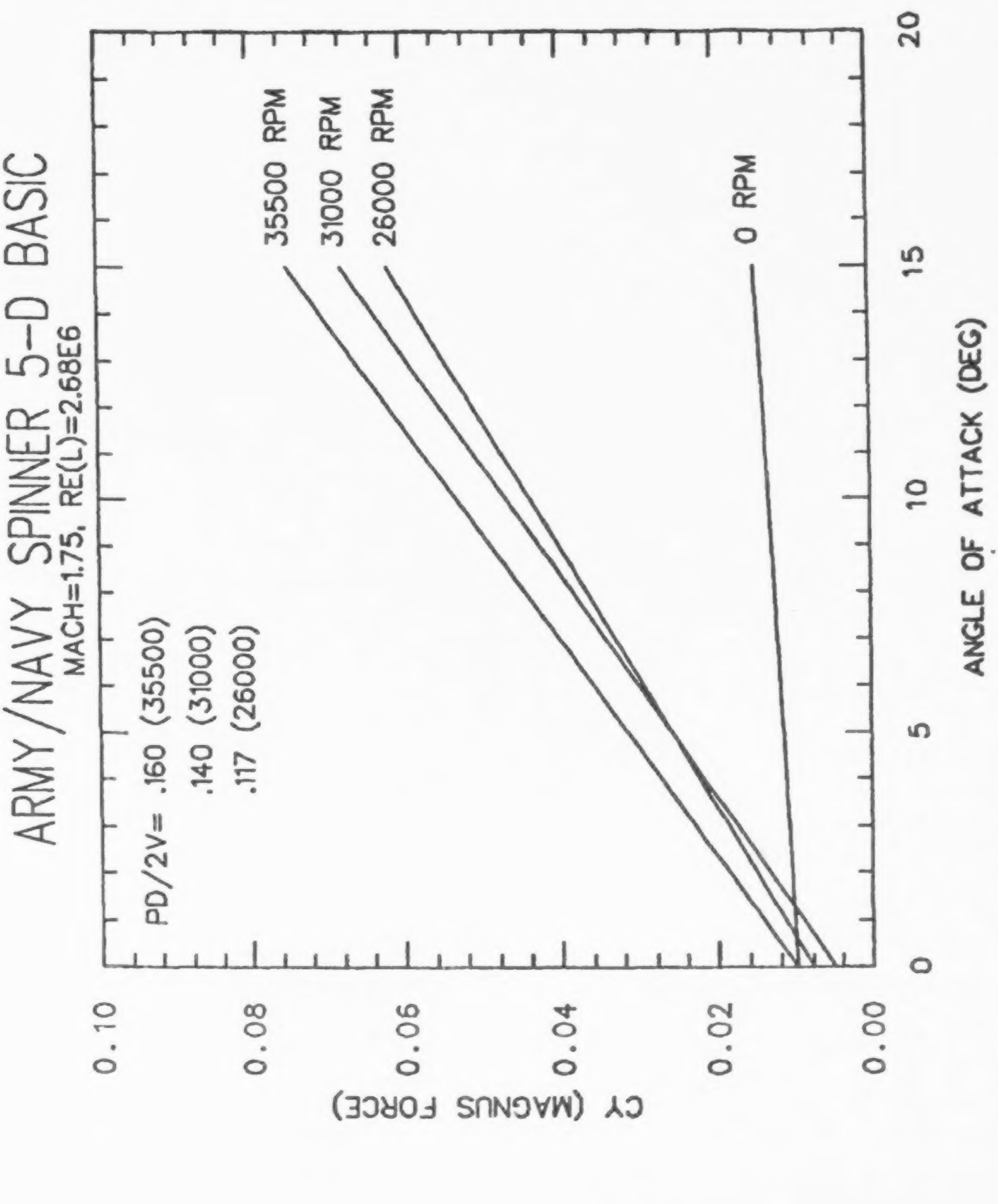

FIGURE 37 - Variation with angle of attack and spin rate of side force coefficient induced by Magnus effects

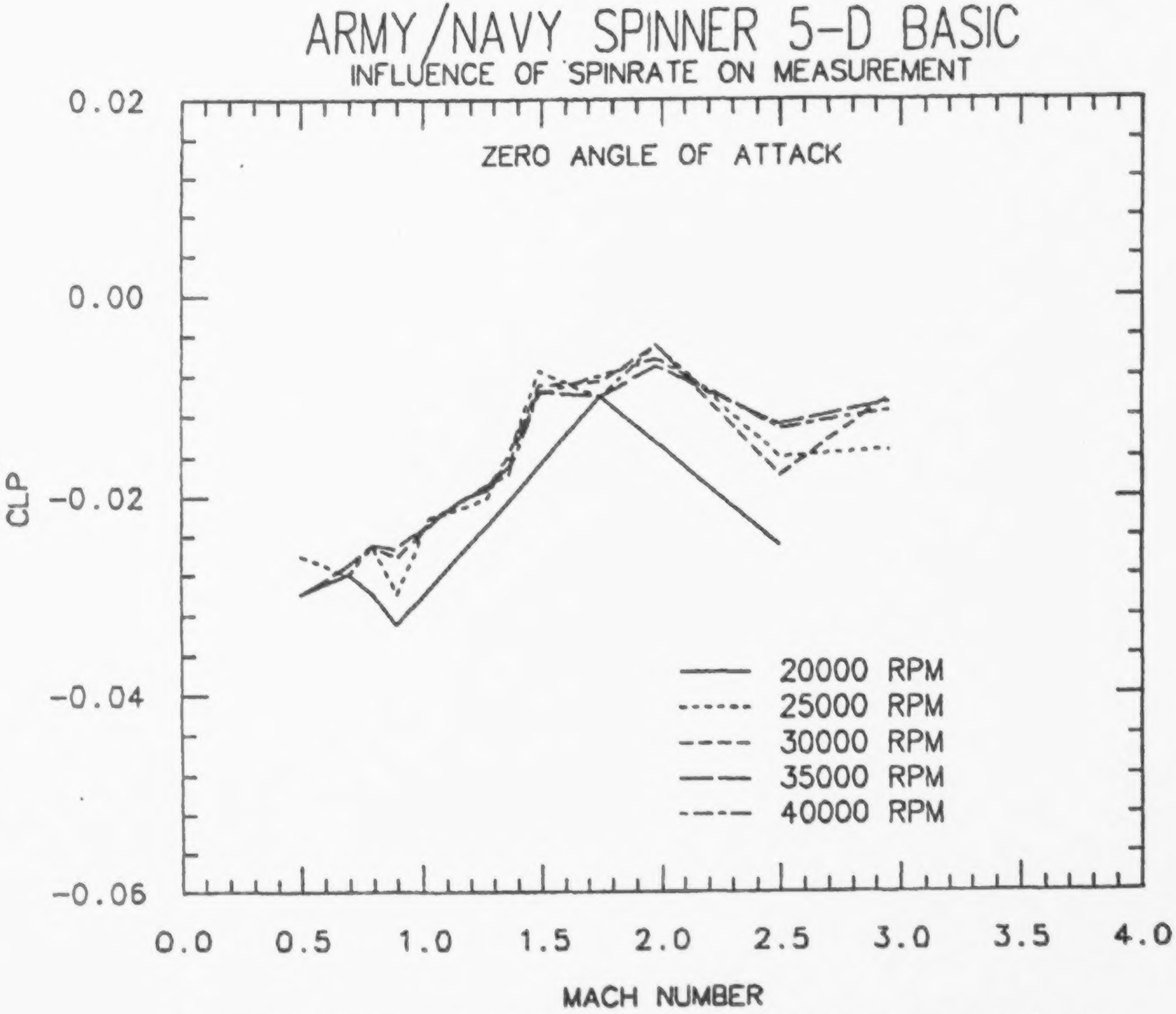

FIGURE 38 - Variation of spin damping coefficient with Mach number and spin rate

Aerodynamics effects induced by the spinning motion of a projectile being viscous phenomena, it is highly desirable to simulate the Mach number together with the Reynolds number when performing wind tunnel tests with a spinning model. If not possible, the Reynolds number (based on total length) should be such that at least fields of turbulent or laminar flow regimes are reproduced. As an indication, Fig. 39 (Ref. 11) gives laminar to turbulent transition Reynolds numbers as a function of the Mach number and configurations of reference.

The Reynolds numbers for the particular flow conditions encountered in the DREV 0.6 m x 0.6 m indraft wind tunnel and at test Mach numbers are given in Table V, and assuming same size projectile in free flight would have been as in Table VI:

TABLE V

5-D Army-Navy Spinner in DREV Wind Tunnel

MACH NUMBER	R_{∞_D}	R_{∞_L}	R_{CF}
NOMINAL			$\alpha = 10$ deg
0.5	$4.13x10^5$	$2.07x10^6$	$7.17x10^4$
0.7	$5.27x10^5$	$2.63x10^6$	$9.15x10^4$
0.8	$5.68x10^5$	$2.84x10^6$	$9.86x10^4$
0.9	$5.90x10^5$	$2.95x10^6$	$10.3x10^4$
1.0	$6.20x10^5$	$3.10x10^6$	$10.8x10^4$
1.15	$6.32x10^5$	$3.16x10^6$	$11.0x10^4$
1.28	$6.32x10^5$	$3.16x10^6$	$11.0x10^4$
1.38	$6.28x10^5$	$3.14x10^6$	$10.9x10^4$
1.50	$6.16x10^5$	$3.08x10^6$	$10.7x10^4$
1.75	$5.39x10^5$	$2.70x10^6$	$9.36x10^4$
2.00	$5.18x10^5$	$2.59x10^6$	$8.99x10^4$
2.50	$4.09x10^5$	$2.05x10^6$	$7.10x10^4$
3.00	$3.16x10^5$	$1.58x10^6$	$5.49x10^4$

TABLE VI

5-D Army-Navy Spinner in Free Flight

MACH NUMBER NOMINAL	R_{∞_D}	R_{∞_L}	R_{CF} $\alpha = 10$ deg
0.5	$4.62\text{x}10^5$	$2.31\text{x}10^6$	$8.02\text{x}10^4$
0.7	$6.49\text{x}10^5$	$3.24\text{x}10^6$	$11.3\text{x}10^4$
0.8	$7.42\text{x}10^5$	$3.71\text{x}10^6$	$12.9\text{x}10^4$
0.9	$8.35\text{x}10^5$	$4.18\text{x}10^6$	$14.5\text{x}10^4$
1.0	$9.57\text{x}10^5$	$4.78\text{x}10^6$	$16.6\text{x}10^4$
1.15	$10.9\text{x}10^5$	$5.43\text{x}10^6$	$18.9\text{x}10^4$
1.28	$11.9\text{x}10^5$	$5.94\text{x}10^6$	$20.7\text{x}10^4$
1.38	$12.5\text{x}10^5$	$6.26\text{x}10^6$	$21.7\text{x}10^4$
1.50	$13.9\text{x}10^5$	$6.95\text{x}10^6$	$24.1\text{x}10^4$
1.75	$16.2\text{x}10^5$	$8.11\text{x}10^6$	$28.1\text{x}10^4$
2.00	$18.5\text{x}10^5$	$9.26\text{x}10^6$	$32.1\text{x}10^4$
2.50	$23.2\text{x}10^5$	$11.6\text{x}10^6$	$40.3\text{x}10^4$
3.00	$27.8\text{x}10^5$	$13.9\text{x}10^6$	$48.3\text{x}10^4$

These figures are given as an indication only and based on results of Ref. 10, it could be concluded that in present test series, runs made at Mach 0.5, 0.7 and 0.8 and at 35,000 and 40,000 rpm were possibly under conditions of supercritical Reynolds number. Figure 39 (Ref. 11) gives laminar to turbulent transition Reynolds numbers as a function of Mach number for a few configurations of reference and in accordance with these figures, tunnel Reynolds numbers would have been subcritical. As a first approximation, these figures (Fig. 39) could be considered as applicable to static as well as spinning projectiles because barrel rifle angles used to be rather small. The lateral tangential velocity component due to spin represents a little contribution relatively to the total air flow velocity due to projectile forward movement.

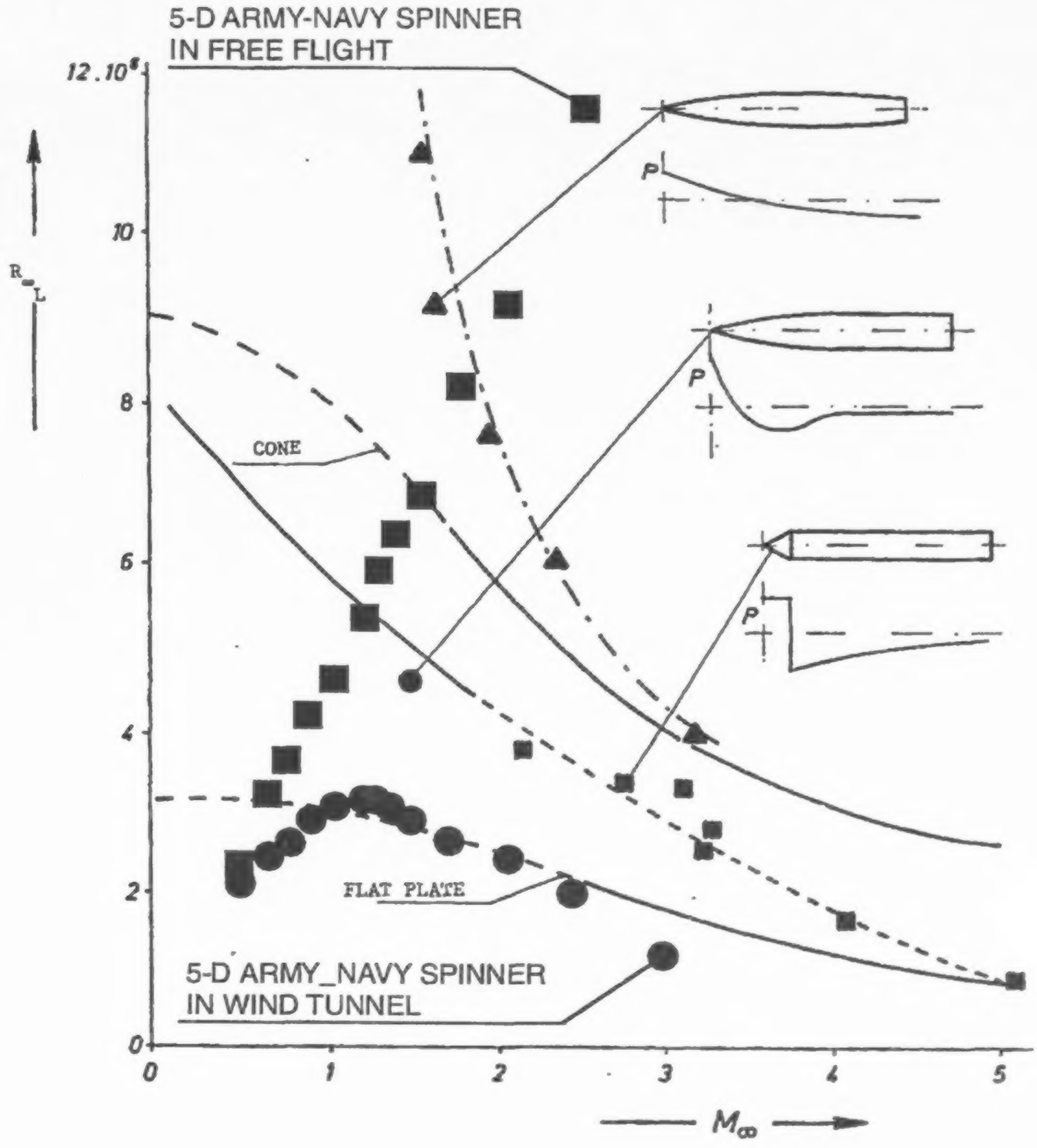

FIGURE 39 - Laminar to turbulent Reynolds number as a function of Mach number and configurations of reference

7.0 DATA ACQUISITION SYSTEM

While performing wind tunnel tests there are three aspects that can become subject to argumentation:

a- Firstly, the aerodynamic physics of model in test section, that can be thought to be or not to be representative of the phenomena intended to be observed and measured experimentally. To counter such possible speculations, Chapters 2.0 to 6.0 and Appendices A and D describe model design, instrumentation and test aerodynamic conditions.

b- Secondly, calibration of the various instruments used for the test can be a matter of questioning. It has not been rare in the past to reprocess recorded digitized analogic signals from a wind tunnel test run series while using different values of calibration parameters or matrices. The present section gives pertinent instrumentation calibration references that were used to reduce measurement signals and produce test data in its original form at the time of tunnel tests.

c- Thirdly, equations utilized to transform the reduced instrumentation readings into aerodynamic coefficients or parameters can also become matter of argumentation. If so, questioning should be, for most of the time, on their pertinency or suitability for the aerodynamic phenomena under experimental study. Chapter 8.0 present these equations. Although rather rarely, it already happened that instrumentation output results were reprocessed afterwards with another set of equations in order to study different aerodynamic aspects that had not been considered originally.

7.1 Static and Dynamic Force Tests

As mentioned in Chapter 6.0 two types of balances were used: one Able MK-VI-A 0.50 in for few tests, and one Able MK-X-A 0.50 in for most of the tests. Appendix A indicates the type of balance utilized for each test run.

During each run, the analog electrical outputs from both the balance elements and the pressure gauges (those connected to side wall pressure taps and also to model base pressure measurement sting tubing) were digitized and fed to an HP-375 data system processor for storage and analysis. A separate tare run was made with no wind (and with the model spinning) to allow for correction of the balance outputs due to model weight, balance offsets, interactions between elements, etc... As rolling moment was concerned, tare data were recorded with no spin and no wind. Otherwise, even still air around a spinning model would have induced rolling moments erroneously included in tare data. This data (balance normal, axial and side forces, pitching, yawing and rolling moments) was thereafter used to calculate various aerodynamic coefficients vs angles of attack (and as specified in Section 9.1) by using the set of equations presented in Chapter 8.0. P_∞, Mach and Q were based on test section wall tap no.8 measurements from Rosemount1301A/317.

Because the balance and " Rosemount " pressure gauges (side wall, model base) rely entirely on a calibration process (that has to be made manually) to convert analog electrical outputs into forces and pressure, the remaining of this section presents transducer characteristics utilized for data reduction. Balance calibration checks that were performed during test series demonstrated evidence of its mechanical and electronic stability.

BALANCE

The balance transfer function is as follows:
e = M•F where:

$$e = \begin{bmatrix} e_1 \\ e_2 \\ e_3 \\ e_4 \\ e_5 \\ e_6 \end{bmatrix} \quad e_i = \text{electrical output " i " of the balance}$$

in mV/volt of excitation

$$F = \begin{bmatrix} N_1 \\ N_2 \\ S_1 \\ S_2 \\ A \\ l_{\text{roll balance}} \end{bmatrix}$$

N_1 = normal force forward of BRC, lb
N_2 = normal force aft of BRC, lb
S_1 = side force forward of BRC, lb
S_2 = side force aft of BRC, lb
A = axial force, lb
ℓ_{balance} = rolling moment, lb-in
BRC = Balance Reference Centre

$$M = \begin{bmatrix} M_{11} & M_{12}\text{--------}M_{16} \\ M_{21} & M_{22}\text{--------}M_{26} \\ - & \\ - & \\ M_{61} & M_{62}\text{--------}M_{66} \end{bmatrix}$$

The balance calibration yielded a sensitivity matrix C for positive forces and moments and a second matrix NC for negative forces and moments. Data processing software selected elements of C or NC according to the polarity of the F components to form the matrix M. Matrix M was then inverted to determine forces and moments.

As the Able MK-VI-A 0.50 in balance is concerned (Fig. 31), calibration, dated 13/06/88, produced the following C and NC matrices. Units of the elements are mV per lb or mV per lb-in per volt of excitation. (Reference weights available for calibration are in pounds). The axial force element was damaged and coefficients set to zero in C and NC matrices.

POSITIVE MATRIX C =

0.061700	-.000560	-.000690	0.000120	0.000000	-.000130
-.002050	0.069000	-.000080	-.000660	0.000000	0.000140
0.000220	0.000070	0.112070	-.001110	0.000000	-.000660
0.000050	-.000600	-.001570	0.117000	0.000000	-.000380
0.000000	0.000000	0.000000	0.000000	0.000000	0.000000
0.000260	0.000130	0.000170	0.000170	0.000000	0.082300

NEGATIVE MATRIX NC =

0.061230	-.000560	-.000580	0.000120	0.000000	0.000050
-.001930	0.068300	-.000070	-.000500	0.000000	0.000580
0.000600	0.000190	0.111900	-.001270	0.000000	-.000520
0.000140	-.000170	-.001600	0.116130	0.000000	0.000010
0.000000	0.000000	0.000000	0.000000	0.000000	0.000000
0.000030	-.000040	-.000090	-.000050	0.000000	0.082060

This balance was damaged at the beginning of the test series rendering it unserviceable. The Able MK-X-A 0.50 in balance (Fig. 32) was then mostly used in this wind tunnel test run series. Although the rolling element of this balance was also damaged at the beginning of the test series, it was still possible to perform a calibration. The consequence of damage to the Able MK-X-A 0.50 in rolling element was a severe shift of the bridge offset (natural offset).

While performing rolling moment calibration as per current DREV methodology, only single slope coefficients were derived for positive and negative rolling moment and an additive constant calculated to compensate for the bridge zero offset. Otherwise there were no means to take account for non-linearities occurring when the balance is used within 1% of its nominal capacity. Calibration, dated 09/08/88, produced the following C and NC matrices utilized for signals interpretation. Units of the elements are mV per lb or mV per lb-in per volt of excitation. (Reference weights available for calibration are in pounds).

POSITIVE MATRIX C =

0.024780	-.000160	0.000110	-.000010	0.000340	0.000520
-.001130	0.026760	0.000130	0.000080	-.000070	0.000210
0.000350	0.000060	0.025970	-.000090	-.000280	0.000400
0.000140	0.000060	-.000350	0.026130	0.000110	0.000180
0.000030	0.000030	0.000000	-.000040	0.025320	0.000780
-.000260	0.000090	0.000290	0.000460	-.000230	0.106740

NEGATIVE MATRIX NC =

0.024490	-.000220	0.000100	-.000010	0.000040	0.000520
-.001100	0.026390	0.000090	0.000010	0.000080	0.000260
0.000370	0.000080	0.025670	-.000120	0.000110	0.000250
0.000110	0.000140	-.000370	0.025740	-.000030	-.000080
0.000020	0.000020	-.000030	-.000020	0.025100	0.000800
-.000620	-.000100	-.000180	-.000230	-.000270	0.106720

TEST SECTION ABSOLUTE PRESSURE TRANSDUCER

used to determine test Mach number

Pressure transducer outputs were converted to the actual pressure through second degree polynomials. Coefficients of all polynomials are grouped under the matrix SB:

$$SB = \begin{bmatrix} A_{10} & A_{11} & A_{12} \\ A_{20} & A_{21} & A_{22} \\ A_{30} & A_{31} & A_{32} \\ A_{40} & A_{41} & A_{42} \\ A_{50} & A_{51} & A_{52} \end{bmatrix}$$

where the parameters were defined as follows:

A_{1i} = Model base pressure,
Kulite SVQH-500-10, SN 2978-3-20, calibrated 25/05/88

A_{2i} = Settling chamber,
(Rosemount 1201F1/587), calibrated 30/05/88

A_{3i} = Test section, tap no. 8,
(Rosemount 1301A/317), calibrated 30/05/88, only this one is used for test section pressure measurement

A_{4i} = Test section, tap no. 9,
(Rosemount 1301 A/318), calibrated 30/05/88

A_{5i} = Blow-off valve position (transonic only).

$$SB = \begin{bmatrix} 0.00000 & 10.58600 & 0.00000 \\ -0.71300 & 0.10321 & -3.54E-8 \\ -10.973 & 0.10261 & 3.38E-8 \\ 27.784 & 0.10074 & 3.52E-8 \\ -13.246 & 15.92657 & 0.00000 \end{bmatrix}$$

For example, pressure (in mbar) read by transducer no. 2 is given by:

$P_2 = A_{20} + A_{21}\, e_2 + A_{22}\, e_2^2$ where

e_2 = Settling chamber transducer output in mV

ANGLE TRANSDUCER

The angle of attack was sensed by a digital shaft encoder tied to the angular displacement mechanism. From the calibration, a third degree polynomial was generated to relate encoder output in bits to angle of attack in degrees as follows:

$$\alpha_{\text{as read by the encoder}} = A_0 + A_1\, x + A_2\, x^2 + A_3\, x^3$$

where x = angle in bits from encoder

A_0 ----- A_3 are constants grouped in vector CDB, and

$$CDB = \begin{bmatrix} 4.072E-03 & 7.990E-03 & 1.232E-08 & -3.531E-11 \end{bmatrix}$$

The angle of attack read on the encoder was corrected for sting and balance deflection. The true angle, α, in degrees, then becomes:

$$\alpha = \alpha_{\text{as read by the encoder}} + C\alpha \quad \text{where}$$

$$C\alpha = K_1 (N_1 + N_2) + K_2 (N_1 a - N_2 b)$$

K_1 and K_2, respectively, are in degrees/lb and degrees/lb-in and were obtained through calibration.

Values for K_1 and K_2 were grouped in vector CDS which was as follows:

(1) for the balance Able MK-X-A 0.50 in mounted on the sting 0.50-2,

$$CDS = [0.01582 \quad 0.00731]$$

(2) for the balance Able MK-VI-A 0.50 in mounted on the sting 0.50-2,

$$CDS = [0.01694 \quad 0.00837]$$

7.2 Calibration Tests

To determine the model inertia moment, several variables had to be measured. For this test, the balance Able MK-VI-A 0.50 in was used to measure the rolling moment with the same data reduction algorithm described in Section 7.1 and that was utilized for the force test. The model spin rate was measured by utilizing the output provided by the motor controller. This data was recorded simultaneously vs a time scale. Although calculations were based on output printed data, a VISICORDER analog graphic recorder was also utilized to verify the synchronization of measurements. The motor current was also traced by the VISICORDER although not needed for the calculations. The calibration tests of the rolling moment vs motor current was made with the same instrumentation than model inertia moment tests. The voltage and current used to activate the electrical Foucault braking system were recorded although not needed for data reduction.

8.0 TREATMENT OF DATA - AERODYNAMIC COEFFICIENT MEASUREMENTS WITH SPINNING MODELS

The following equations were used to process wind tunnel aerodynamic coefficients (the symbol " * " preceding a variable indicates that this variable is displayed in tabulated data) :

P_t = Average air bag pressure (total pressure)

$$= \frac{1}{n} \sum_{i=1}^{n} P_{t_i}$$ during data acquisition run time

P_s = Measured test section static pressure at wall (from wall tap no. 8)

P_{s_i} = Test section static pressure measured at the time of the ith balance reading

$$* \, M_i = \left[\left(\left(\frac{P_{t_i}}{P_{s_i}} \right)^{\frac{\gamma-1}{\gamma}} -1 \right) \frac{2}{\gamma-1} \right]^{1/2}$$

* M = Average Mach number

$$= \frac{1}{n} \sum_{i=1}^{n} M_i$$ during data acquisition run time

γ = Ratio $\frac{C_p}{C_v}$, for air = 1.4

$$P_v = P_t \left(1 + \frac{\gamma-1}{2} M^2 \right)^{\frac{\gamma}{1-\gamma}}$$

$* \; Q = \frac{1}{n}\sum_{i=1}^{n} Q_i$ during data acquisition run time

$$= \frac{\gamma}{2} \bullet M^2 \bullet P_v$$

$QA = Q \bullet S$ Where $S = \frac{\pi d^2}{4}$,

$$* \; CA = \frac{A}{QA}$$

$$* \; CN = \frac{N_1 + N_2}{QA}$$

$$* \; CDT = (CA \bullet COS\alpha) + (CN \bullet SIN\alpha)$$

$$S^1 = \frac{\pi {d^1}^2}{4}$$

$CAB = -\frac{PCV \bullet S^1}{QA}$ Where PCV = base pressure measured with respect to pressure at wall = $P_{base} - P_\infty$

$* \; CDF = CDT - (CAB \bullet COS\alpha)$ is identified as CD in output tables

$PSPIN = \frac{SPIN \bullet 2 \bullet \pi}{60}$ (RPM to rad/s)

$$PSPIND = A_1 + 2 \, A_2 \, t_i + 3 \, A_3 \, t_i^2 = \dot{p}$$

where $PSPIN = A_0 + A_1 t_i + A_2 t_i^2 + A_3 t_i^3 + A_4 t_i^4$ best fit polynomial

$$\ell_{roll} = \ell_{balance}$$

$M_{\ell_p} = \ell\ell = \ell_{roll} - PSPIND \bullet IX$ where IX is measured experimentally

$$* \ \mathrm{CRM} = C_\ell = \frac{\ell_{roll}}{QA \cdot d}$$

$$* \ \mathrm{CRMC} = C_{\ell c} = \frac{\ell\ell}{QA \cdot d}$$

$$* \ \mathrm{CL} = (\mathrm{CN} \cdot \mathrm{COS}\alpha) - (\mathrm{CA} \cdot \mathrm{SIN}\alpha$$

$$\mathrm{CMNB} = \frac{(N_1 \cdot a) - (N_2 \cdot b)}{QA \cdot d}$$

$$* \ \mathrm{CM} = C_m = \mathrm{CMNB} - \mathrm{CN} \cdot \frac{c}{d}$$

$$* \ \mathrm{XCP} = - \frac{\mathrm{CM}}{\mathrm{CN}}$$

$$* \ \mathrm{CY} = \frac{S_1 + S_2}{QA}$$

$$\mathrm{CYMB} = \frac{S_1 \cdot e - S_2 \cdot f}{QA \cdot d}$$

$$* \ \mathrm{CYM} = C_n = \mathrm{CYMB} - \mathrm{CY} \frac{c}{d}$$

$$T_a = 273.15 + t_c$$

$$T_v = T_a \left(1 + \frac{\gamma - 1}{2} \cdot M^2\right)^{-1}$$

$$V = 20.05 \ M \ (T_v)^{1/2}$$

$$* \ \mathrm{CLP} = C_{\ell_p} = \frac{\mathrm{CRM} \cdot 2 \cdot V}{d \cdot \mathrm{PSPIN}}$$

* CLPC = $C_{\ell_{pc}} = \dfrac{\text{CRMC} \cdot 2 \cdot \text{V}}{\text{d} \cdot \text{PSPIN}}$

* CYP = $C_{y_p} = \dfrac{\text{CY} \cdot 2 \cdot \text{V}}{\text{PSPIN} \cdot \text{d}}$

* CNP= $C_{n_p} = \dfrac{\text{CYM} \cdot 2 \cdot \text{V}}{\text{PSPIN} \cdot \text{d}}$

* Pd/2V $= \dfrac{\text{d} \cdot \text{PSPIN}}{2 \cdot \text{V}}$

* CMA = $C_{m\alpha}$ = A_1 of polynomial $A_0 + A_1\alpha$ fitted on CM data between -3 to +3 deg, non dimensional (per rad)

* CNA = $C_{N\alpha}$ = A_1 of polynomial $A_0 + A_1\alpha$ fitted on CN data between -3 to +3 deg, non dimensional (per rad)

$C_{y_{p\alpha}} = \dfrac{d\, C_{y_p}}{d\, \alpha}$ was derived graphically from plotted results

* XCP0 = $X_{cp_0} = -\dfrac{\text{CMA}}{\text{CNA}}$ centre of pressure with respect to MRC ($\alpha = 0°$)

* CA0 = C_{A_0} = A_0 of polynomial $A_0 + A_2\alpha^2 + A_4\alpha^4 + A_6\alpha^6 + \ldots$

... $+A_8\alpha^8$, (deg) fitted on CA data

$$* \ \text{REY/M} = \text{Rey/metre} = \frac{\rho \bullet V}{\mu}$$

$$\text{Where } \rho = \frac{P_t}{R \bullet T_a}\left(\frac{T_v}{T_a}\right)^{\frac{1}{\gamma - 1}} = \frac{P_t}{287.05\ T_a} \times \left(\frac{T_v}{T_a}\right)^{2.5}$$

$$\mu = 1.458 \times 10^{-6} \times \frac{T_v^{1.5}}{T_v + 110.4}\ \text{N} \bullet \text{s/m}^2$$

9.0 RESULTS

Typical result output formats are presented in this section. Complete data can be made available through the author upon request. A list of wind tunnel runs is presented in Appendix A that also gives the correspondence between test series run numbers and tunnel run numbers (i.e. 2207.08 ≡ R2791).

9.1 Aerodynamic Coefficients Measurements

As far as aerodynamic coefficient tests were concerned, the following data has been presented in a table form: α, M, CN, CM, CA, CL, CDT, XCP, CD, CY, CYM, CRM, CRMC, CLP, CLPC, CYP, CNP, RPM, TIME. One table was produced for each individual run as per examples given in Figs. 40, 46, 47, 53 and 54 that bear appropriate headings. These examples give typical test results for Mach numbers of 0.80 (with the Able MK-VI-A 0.50 in balance) and 1.16, 1.73 (with the Able MK-X-A 0.50 in balance).

M(mean) stands for Mean Mach number calculated between time interval during which the measurements were made. The dynamic pressure was based on Mean Mach to reduce values of aerodynamic coefficients printed in a table form. The aerodynamic derivatives CNA, CMA are per radiant. The following aerodynamic coefficients were plotted vs the angle of attack: CN, CM, CL, XCP, CY, CYM, CYP, CNP, CRM, CRMC, CLP, CLPC. An example of reduced data graphical layout is presented in Figs. 41 to 45, 47 to 52 and 55 to 59. The experimental data points are represented by symbols and some together with corresponding best fit curves (represented by lines) based on polynomial of various degrees. Depending on tests conditions (i.e. angle of attack sweep angle, Mach number, spin rate) and particular aerodynamic coefficients, results were more or less scattered and degrees of best fit polynomials were chosen consequently. This was because when the results scatter was important, polynomials of high degrees can become unstable (wavy).

Summaries of aerodynamic coefficient data from this test series are given in Appendix A and Appendix B where also results are presented in graphical form.

```
RUN NO.:R2791 (SPINWT-1-2207.00)      RDATE: 07/07/88 14:30

NOZZLE BLOCKS= 0.80     CHOKE SETTING= 7720     RPM=  35721

M(MEAN)= 0.80     TEMP= 27.0C        Q(PA)=28597     REYN/M= 1.30E7

CNA=2.102      CMA=7.483      XCPO= -3.56

     •      CN      CM      CY      CL     CYM     CRM    CRMC     XCP     CLP    CLPC     CYP     CNP     M   RPM TEMPS
------ ------- ------- ------- ------- ------- ------- ------- ------- ------- ------- ------- ------- ----- ----- -----
 -4.71 -0.2020 -0.7016  0.0120 -0.1811  0.0227 -0.0079 -0.0075 -3.4727 -0.0271 -0.0259  0.0412  0.0781 0.798 35742   0.0
 -4.24 -0.1789 -0.6196  0.0410 -0.1602  0.1042 -0.0082 -0.0079 -3.4643 -0.0281 -0.0271  0.1411  0.3583 0.798 35718   0.1
 -3.78 -0.1581 -0.5517  0.0374 -0.1415  0.1074 -0.0078 -0.0076 -3.4896 -0.0269 -0.0260  0.1286  0.3694 0.798 35742   0.2
 -3.30 -0.1397 -0.4774  0.0407 -0.1253  0.1032 -0.0076 -0.0073 -3.4179 -0.0260 -0.0253  0.1401  0.3549 0.798 35718   0.3
 -2.81 -0.1030 -0.3486 -0.0153 -0.0908 -0.0787 -0.0073 -0.0071 -3.3835 -0.0252 -0.0245 -0.0526 -0.2432 0.798 35742   0.4
 -2.34 -0.1057 -0.3740  0.0113 -0.0955  0.0281 -0.0078 -0.0076 -3.5472 -0.0267 -0.0262  0.0390  0.0692 0.799 35742   0.5
 -1.85 -0.0682 -0.2391 -0.0830 -0.0602 -0.0141 -0.0076 -0.0074 -3.5044 -0.0260 -0.0256 -0.0104 -0.0485 0.798 35693   0.6
 -1.36 -0.0591 -0.2119  0.0188 -0.0532  0.0369 -0.0072 -0.0071 -3.5881 -0.0247 -0.0244  0.0646  0.1271 0.798 35742   0.7
 -0.87 -0.0306 -0.1217  0.0100 -0.0269  0.0388 -0.0075 -0.0074 -3.9758 -0.0258 -0.0255  0.0618  0.1336 0.798 35718   0.8
 -0.38 -0.0272 -0.0996 -0.0009 -0.0255 -0.0255 -0.0072 -0.0071 -3.6628 -0.0247 -0.0245 -0.0031 -0.0877 0.799 35693   0.9
  0.12  0.0289  0.0985  0.0512  0.0283  0.1503 -0.0078 -0.0077 -3.4127 -0.0267 -0.0266  0.1762  0.5170 0.799 35693   1.0
  0.60  0.0129  0.0496  0.0058  0.0103  0.0021 -0.0067 -0.0067 -3.8510 -0.0230 -0.0230  0.0200  0.0073 0.797 35718   1.1
  1.08  0.0405  0.1300 -0.0023  0.0358 -0.0231 -0.0073 -0.0073 -3.2321 -0.0253 -0.0253 -0.0080 -0.0795 0.797 35742   1.2
  1.57  0.0474  0.1761  0.0135  0.0406  0.0420 -0.0078 -0.0079 -3.7164 -0.0270 -0.0270  0.0463  0.1446 0.798 35718   1.3
  2.04  0.0663  0.2347  0.0200  0.0575  0.0570 -0.0077 -0.0077 -3.5382 -0.0266 -0.0267  0.0687  0.1960 0.799 35718   1.4
  2.53  0.0901  0.3406 -0.0090  0.0791 -0.0443 -0.0076 -0.0076 -3.7816 -0.0261 -0.0262 -0.0309 -0.1523 0.797 35718   1.5
  2.99  0.1012  0.3609  0.0074  0.0882 -0.0810 -0.0081 -0.0081 -3.5660 -0.0278 -0.0279  0.0255 -0.0034 0.797 35718   1.6
  3.48  0.1127  0.4107  0.0111  0.0975  0.0122 -0.0076 -0.0076 -3.6460 -0.0262 -0.0263  0.0382  0.0419 0.799 35718   1.7
  3.96  0.1460  0.5191  0.0104  0.1286  0.0080 -0.0078 -0.0078 -3.5563 -0.0267 -0.0268  0.0358  0.0277 0.797 35742   1.8
  4.44  0.1601  0.5687  0.0211  0.1406  0.0464 -0.0083 -0.0084 -3.5518 -0.0287 -0.0288  0.0725  0.1598 0.797 35718   1.9
  4.93  0.1909  0.6634  0.0077  0.1690  0.0089 -0.0080 -0.0080 -3.4757 -0.0275 -0.0276  0.0264  0.0307 0.798 35718   2.0
  5.41  0.1989  0.7804  0.0013  0.1749 -0.0199 -0.0080 -0.0081 -3.5210 -0.0276 -0.0277  0.0044 -0.0684 0.797 35742   2.1
  5.88  0.2109  0.7740 -0.0105  0.1925 -0.0786 -0.0085 -0.0086 -3.5403 -0.0294 -0.0295 -0.0636 -0.2703 0.797 35718   2.2
  6.38  0.2407  0.8471 -0.0251  0.2118 -0.0986 -0.0078 -0.0078 -3.5201 -0.0267 -0.0268 -0.0863 -0.3392 0.796 35718   2.3
  6.87  0.2965  1.0317  0.0202  0.2650  0.0880 -0.0088 -0.0088 -3.4793 -0.0303 -0.0304  0.0694  0.3029 0.799 35718   2.4
  7.36  0.3278  1.1273  0.0228  0.2935  0.0862 -0.0086 -0.0086 -3.4395 -0.0296 -0.0297  0.0783  0.2964 0.798 35693   2.5
  7.83  0.3023  1.0441  0.0042  0.2659  0.0232 -0.0087 -0.0088 -3.4544 -0.0301 -0.0301  0.0145  0.0797 0.797 35742   2.6
  8.31  0.3107  1.1151 -0.0267  0.2798 -0.0722 -0.0086 -0.0086 -3.4986 -0.0296 -0.0296 -0.0919 -0.2483 0.798 35693   2.7
  8.79  0.3473  1.2056 -0.0458  0.3057 -0.1333 -0.0086 -0.0086 -3.4710 -0.0296 -0.0296 -0.1574 -0.4585 0.797 35718   2.8
  9.29  0.4339  1.4729 -0.0107  0.3885 -0.0014 -0.0094 -0.0094 -3.3942 -0.0323 -0.0323 -0.0370 -0.0047 0.797 35718   2.9
  9.74  0.3977  1.3589 -0.0370  0.3503 -0.1019 -0.0087 -0.0087 -3.4173 -0.0299 -0.0299 -0.1274 -0.3507 0.796 35718   3.0
 10.21  0.4166  1.4240 -0.0370  0.3664 -0.0522 -0.0090 -0.0089 -3.4184 -0.0308 -0.0308 -0.1274 -0.1797 0.797 35742   3.1
 10.68  0.4230  1.4476 -0.0377  0.3701 -0.0770 -0.0089 -0.0089 -3.4222 -0.0306 -0.0306 -0.1297 -0.2647 0.796 35718   3.2
 11.16  0.4636  1.5590 -0.0331  0.4072 -0.0614 -0.0090 -0.0089 -3.3631 -0.0308 -0.0307 -0.1139 -0.2112 0.796 35742   3.3
 11.64  0.4997  1.6712 -0.0502  0.4398 -0.0869 -0.0093 -0.0092 -3.3445 -0.0319 -0.0317 -0.1727 -0.2988 0.795 35718   3.4
 12.11  0.4877  1.6437 -0.0563  0.4253 -0.1230 -0.0089 -0.0089 -3.3700 -0.0308 -0.0306 -0.1937 -0.4230 0.795 35718   3.5
 12.58  0.5402  1.7917 -0.0192  0.4736 -0.0107 -0.0092 -0.0092 -3.3168 -0.0318 -0.0316 -0.0661 -0.0367 0.795 35718   3.6
 13.06  0.5577  1.8456 -0.0701  0.4877 -0.1397 -0.0092 -0.0091 -3.3093 -0.0315 -0.0314 -0.2412 -0.4806 0.795 35718   3.7
 13.54  0.5736  1.9181 -0.0465  0.5001 -0.0709 -0.0095 -0.0095 -3.3297 -0.0328 -0.0327 -0.1600 -0.2440 0.796 35742   3.8
 14.00  0.6036  1.9784 -0.0386  0.5261 -0.0299 -0.0088 -0.0088 -3.2778 -0.0304 -0.0303 -0.1327 -0.1029 0.795 35693   3.9
 14.47  0.6414  2.0638 -0.0961  0.5596 -0.1724 -0.0098 -0.0097 -3.2177 -0.0336 -0.0334 -0.3307 -0.5932 0.796 35718   4.0
 14.82  0.6444  2.0565 -0.1203  0.5681 -0.2375 -0.0099 -0.0099 -3.1912 -0.0342 -0.0341 -0.4138 -0.8170 0.795 35718   4.1
 14.91  0.6730  2.1622 -0.1670  0.5871 -0.3905 -0.0101 -0.0101 -3.2129 -0.0347 -0.0346 -0.5773 -1.3435 0.794 35718   4.2
 14.99  0.6725  2.1977 -0.1770  0.5860 -0.4226 -0.0099 -0.0098 -3.2678 -0.0339 -0.0338 -0.6117 -1.4539 0.796 35718   4.3
```

FIGURE 40 - Typical results and data table layout of stability coefficient measurement tests, Able MK-VI-A 0.50 in balance, angle of attack sweep -5 deg to +15 deg, PD/2V = 0.294

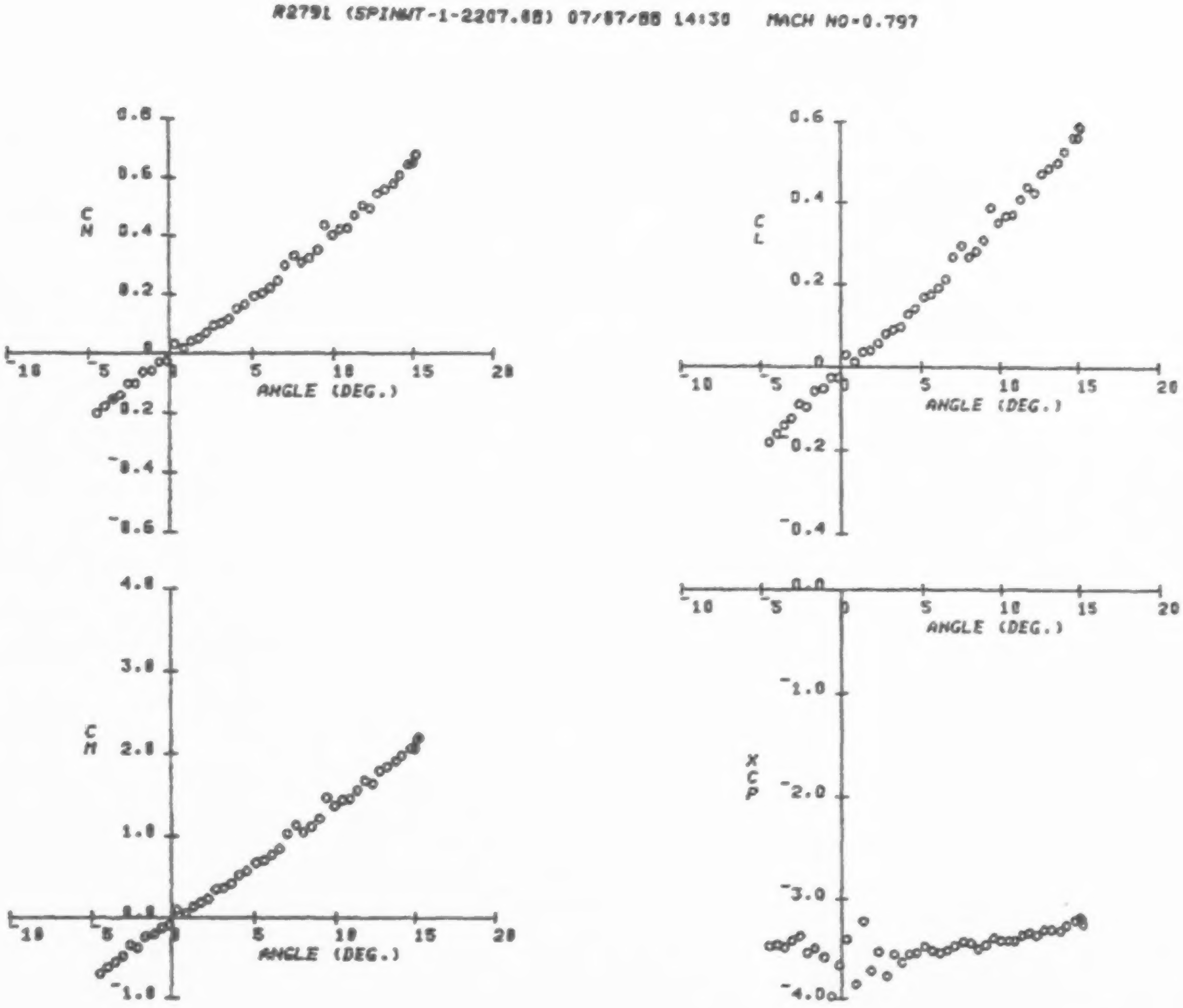

FIGURE 41 - Typical CN, CM, CL coefficients and center of pressure, graphical layout, Able MK-VI-A 0.50 in balance, angle of attack sweep -5 deg to +15 deg, Mach 0.80, spin rate 35,720 RPM, PD/2V = 0.294

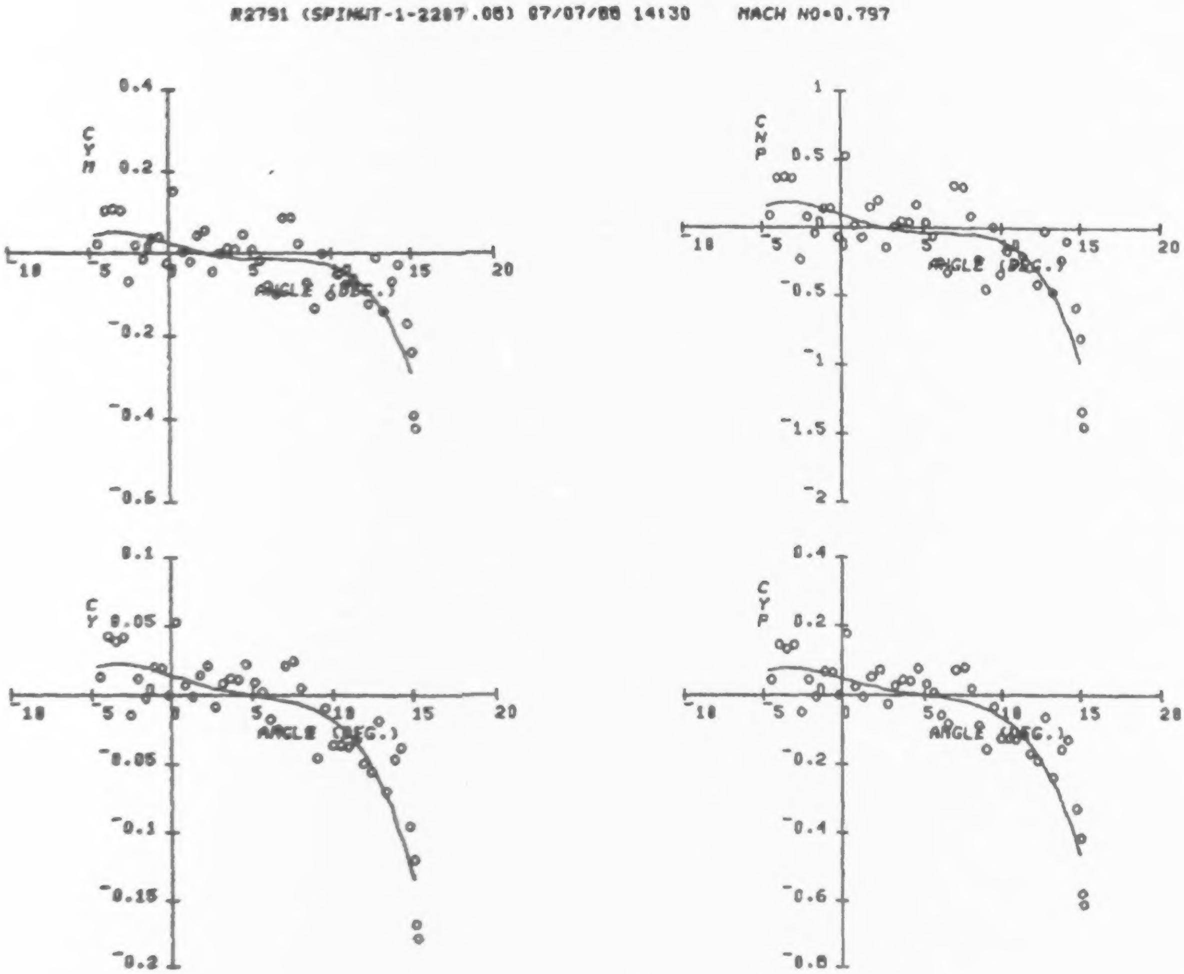

FIGURE 42 - Typical CY, CYM, CYP,CNP coefficients, graphical layout, Able MK-VI-A 0.50 in balance, angle of attack sweep -5 deg to + 15 deg, Mach 0.80, spin rate 35,720 RPM, PD/2V = 0.294

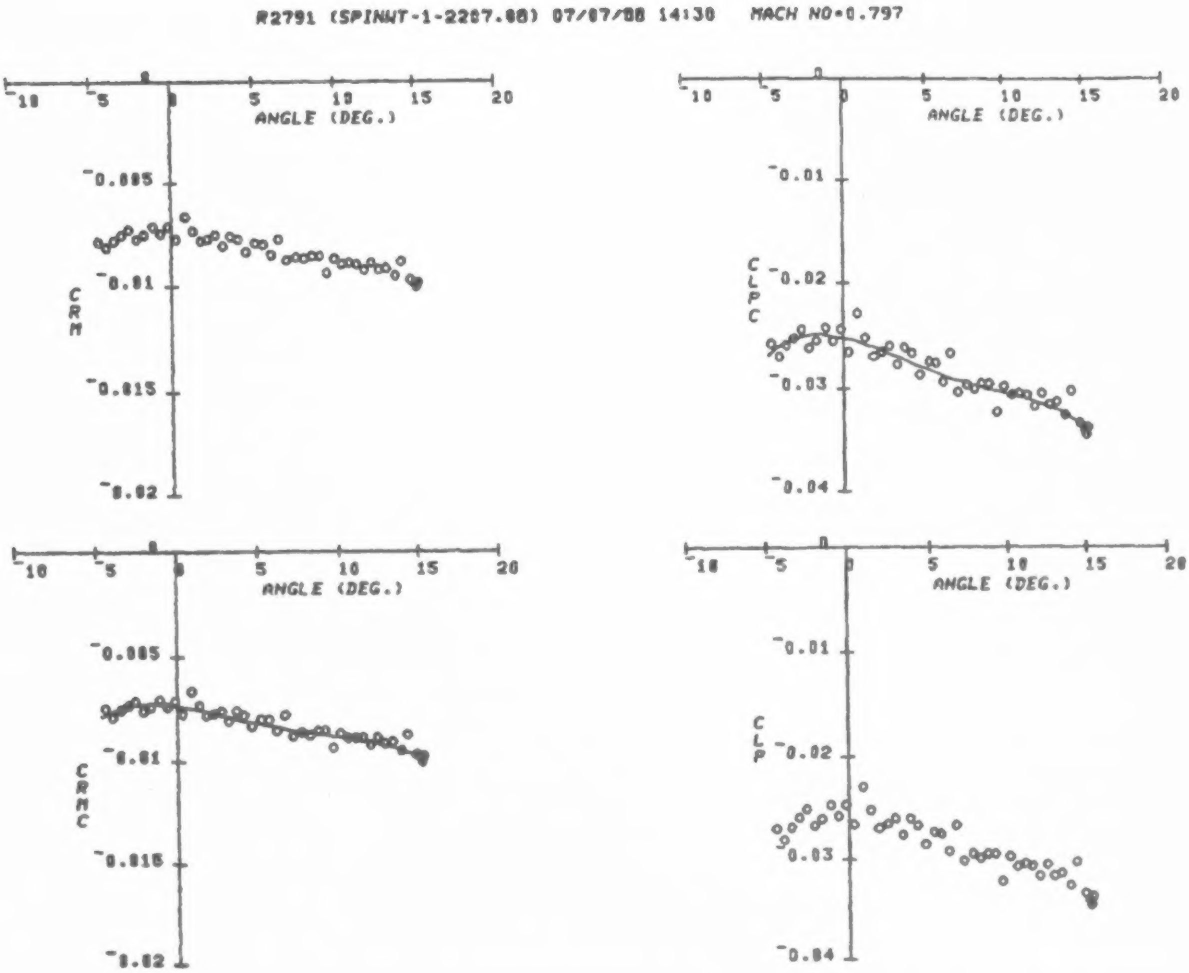

FIGURE 43 - Example of CRM, CRMC, CLP, CLPC coefficients, graphical layout, Able MK-VI-A 0.50 in balance, angle of attack sweep -5 deg to + 15 deg, Mach 0.80, spin rate 35,720 RPM, PD/2V = 0.294

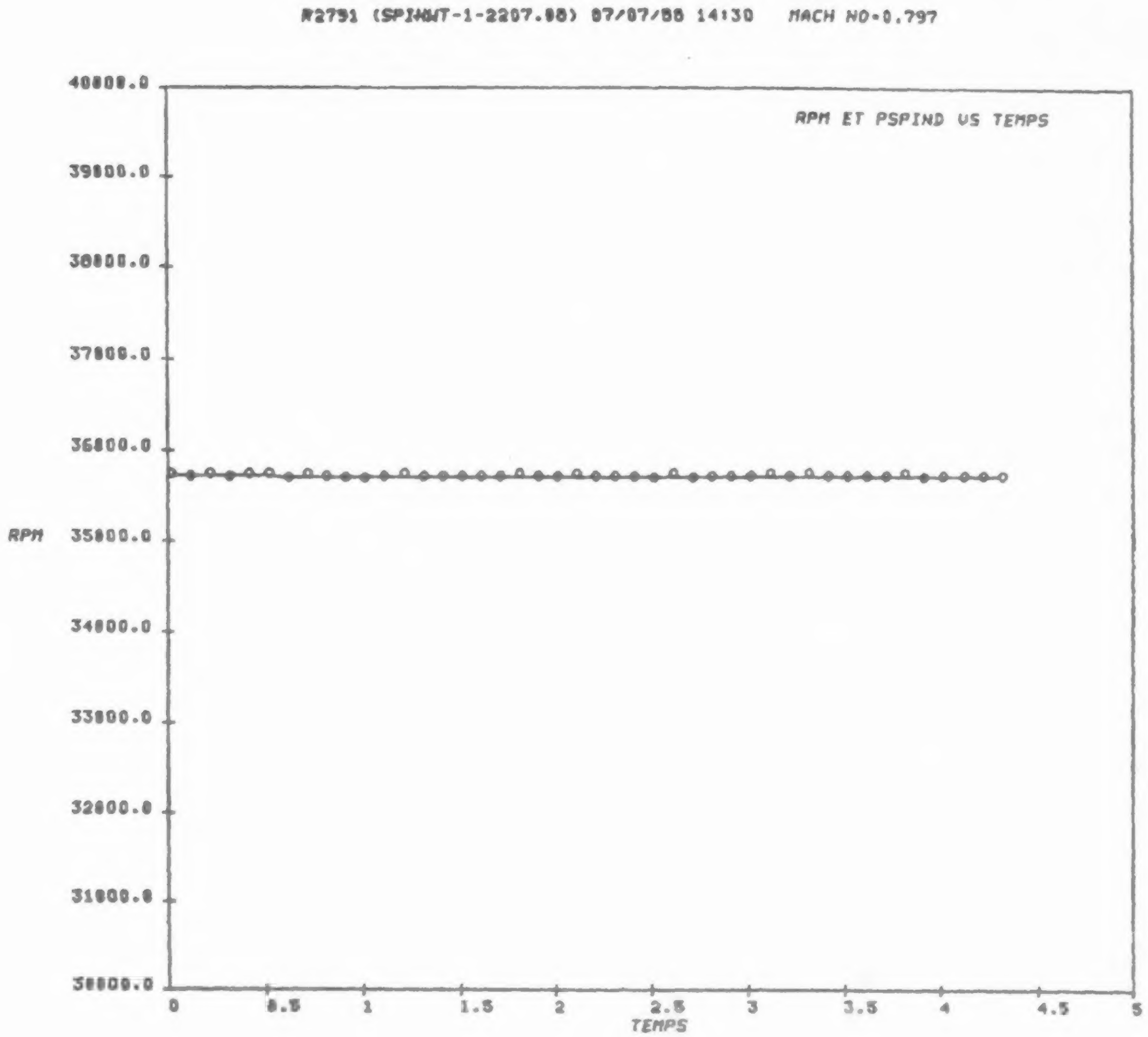

FIGURE 44 - Typical variation of spin rate versus time during a test run, angle of attack sweep -5 deg to + 15 deg, Mach 0.80, spin rate 35,720 RPM, PD/2V = 0.294

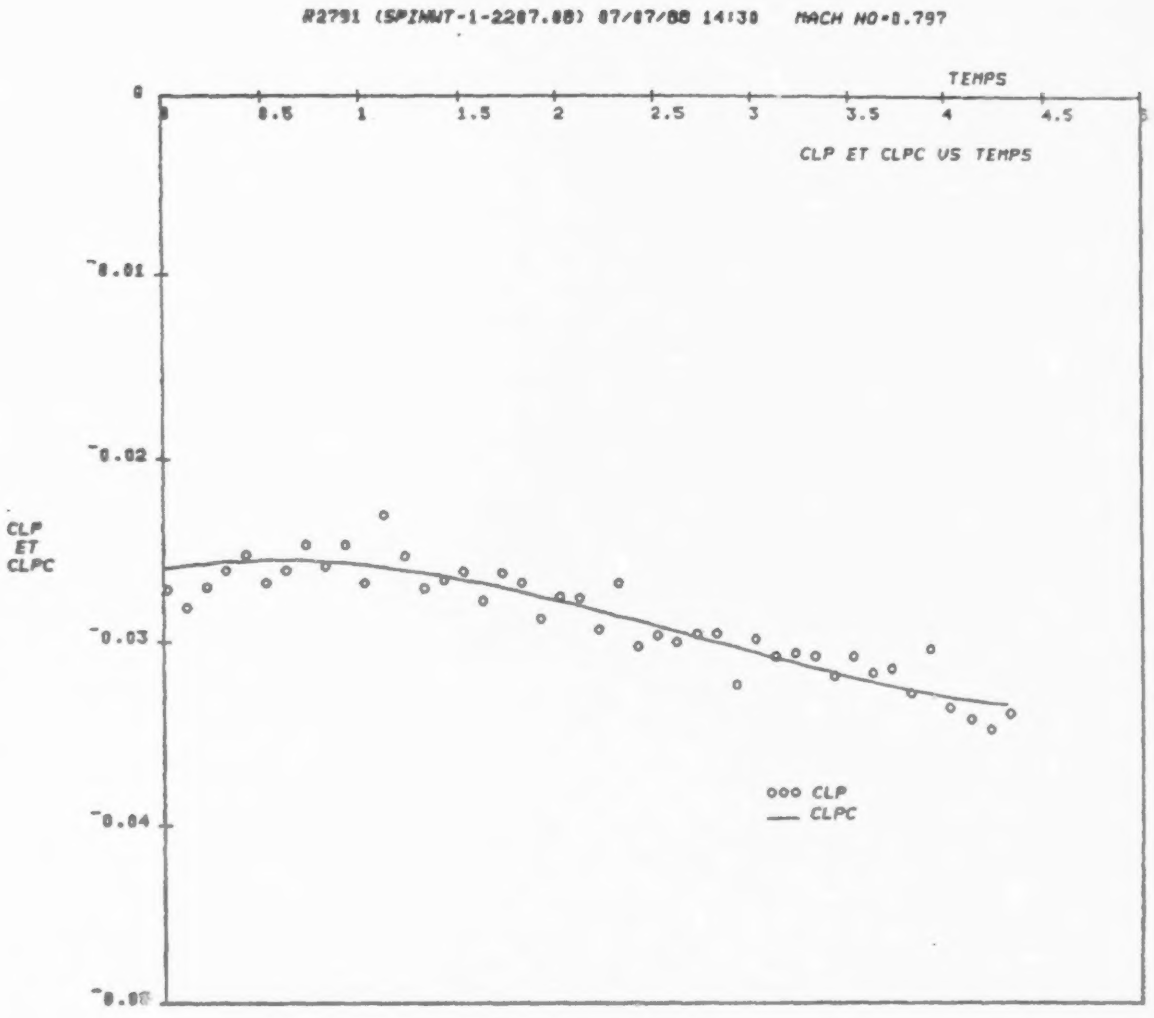

FIGURE 45 - Typical variation of CLP and CLPC versus time during a test run, angle of attack sweep -5 deg to + 15 deg, Mach 0.80, spin rate 35,720 RPM, PD/2V = 0.294

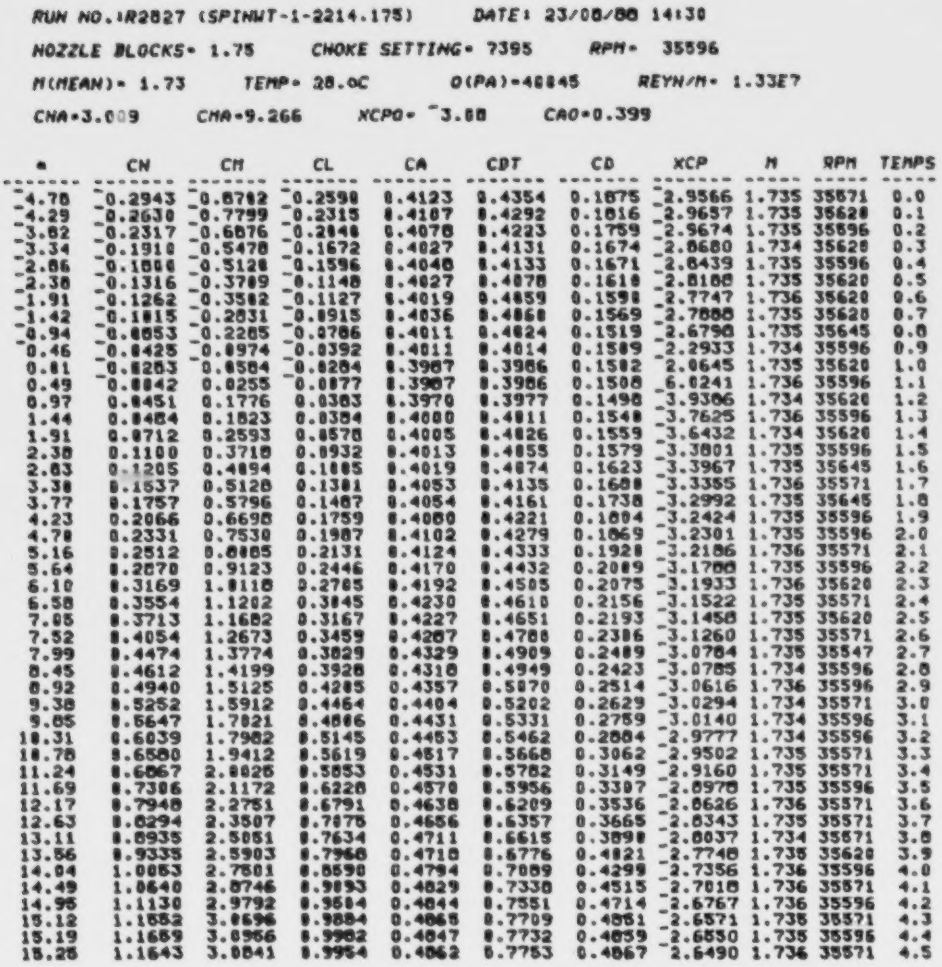

```
RUN NO.:R2827 (SPINWT-1-2214.175)      DATE: 23/08/88 14:30

NOZZLE BLOCKS= 1.75     CHOKE SETTING= 7395     RPM=  35596

M(MEAN)= 1.73     TEMP= 28.0C         Q(PA)=48845      REYN/M= 1.33E7

CNA=3.009     CMA=9.266     XCPO= -3.08     CAO=0.399

   α       CN       CM       CL       CA       CDT      CD       XCP      M     RPM   TEMPS
------- -------- -------- -------- -------- -------- -------- -------- ----- ----- -----
 -4.78  -0.2943  -0.8702  -0.2590   0.4123   0.4354   0.1875  -2.9566 1.735 35571   0.0
 -4.29  -0.2630  -0.7799  -0.2315   0.4107   0.4292   0.1816  -2.9657 1.735 35620   0.1
 -3.82  -0.2317  -0.6876  -0.2048   0.4078   0.4223   0.1759  -2.9674 1.735 35596   0.2
 -3.34  -0.1910  -0.5470  -0.1672   0.4027   0.4131   0.1674  -2.8680 1.734 35620   0.3
 -2.86  -0.1800  -0.5120  -0.1596   0.4040   0.4133   0.1671  -2.8439 1.735 35596   0.4
 -2.38  -0.1316  -0.3709  -0.1148   0.4027   0.4078   0.1618  -2.8188 1.735 35620   0.5
 -1.91  -0.1262  -0.3502  -0.1127   0.4019   0.4059   0.1598  -2.7747 1.736 35620   0.6
 -1.42  -0.1015  -0.2831  -0.0915   0.4036   0.4060   0.1569  -2.7888 1.735 35620   0.7
 -0.94  -0.0853  -0.2285  -0.0786   0.4011   0.4024   0.1519  -2.6790 1.735 35645   0.8
 -0.46  -0.0425  -0.0974  -0.0392   0.4011   0.4014   0.1509  -2.2933 1.734 35596   0.9
  0.01  -0.0283  -0.0584  -0.0204   0.3987   0.3986   0.1502   2.0645 1.735 35620   1.0
  0.49  -0.0042   0.0255  -0.0077   0.3987   0.3986   0.1508  -6.0241 1.736 35596   1.1
  0.97   0.0451   0.1776   0.0383   0.3970   0.3977   0.1498  -3.9386 1.734 35620   1.2
  1.44   0.0484   0.1823   0.0384   0.4000   0.4011   0.1540  -3.7625 1.736 35596   1.3
  1.91   0.0712   0.2593   0.0578   0.4005   0.4026   0.1559  -3.6432 1.734 35620   1.4
  2.38   0.1100   0.3718   0.0932   0.4013   0.4055   0.1579  -3.3801 1.735 35596   1.5
  2.83   0.1205   0.4094   0.1005   0.4019   0.4074   0.1623  -3.3967 1.735 35645   1.6
  3.30   0.1537   0.5128   0.1301   0.4053   0.4135   0.1680  -3.3355 1.736 35571   1.7
  3.77   0.1757   0.5796   0.1487   0.4054   0.4161   0.1738  -3.2992 1.735 35645   1.8
  4.23   0.2066   0.6698   0.1759   0.4080   0.4221   0.1804  -3.2424 1.735 35596   1.9
  4.70   0.2331   0.7530   0.1987   0.4102   0.4279   0.1869  -3.2301 1.735 35596   2.0
  5.16   0.2512   0.8085   0.2131   0.4124   0.4333   0.1928  -3.2186 1.736 35571   2.1
  5.64   0.2870   0.9123   0.2446   0.4170   0.4432   0.2089  -3.1788 1.735 35596   2.2
  6.10   0.3169   1.0118   0.2785   0.4192   0.4505   0.2075  -3.1933 1.736 35620   2.3
  6.58   0.3554   1.1202   0.3045   0.4230   0.4610   0.2156  -3.1522 1.735 35571   2.4
  7.05   0.3713   1.1682   0.3167   0.4227   0.4651   0.2193  -3.1458 1.735 35620   2.5
  7.52   0.4054   1.2673   0.3459   0.4287   0.4788   0.2306  -3.1260 1.735 35571   2.6
  7.99   0.4474   1.3774   0.3829   0.4329   0.4909   0.2409  -3.0784 1.735 35547   2.7
  8.45   0.4612   1.4199   0.3928   0.4318   0.4949   0.2423  -3.0785 1.734 35596   2.8
  8.92   0.4940   1.5125   0.4285   0.4357   0.5070   0.2514  -3.0616 1.736 35596   2.9
  9.38   0.5252   1.5912   0.4464   0.4404   0.5202   0.2629  -3.0294 1.734 35571   3.0
  9.85   0.5647   1.7021   0.4806   0.4431   0.5331   0.2759  -3.0140 1.734 35596   3.1
 10.31   0.6039   1.7982   0.5145   0.4463   0.5462   0.2884  -2.9777 1.734 35596   3.2
 10.78   0.6580   1.9412   0.5619   0.4517   0.5668   0.3062  -2.9502 1.735 35571   3.3
 11.24   0.6867   2.0026   0.5853   0.4531   0.5782   0.3149  -2.9160 1.735 35571   3.4
 11.69   0.7306   2.1172   0.6228   0.4570   0.5956   0.3307  -2.8978 1.735 35596   3.5
 12.17   0.7940   2.2751   0.6791   0.4638   0.6209   0.3536  -2.8626 1.736 35571   3.6
 12.63   0.8294   2.3507   0.7078   0.4656   0.6357   0.3665  -2.8343 1.735 35571   3.7
 13.11   0.8935   2.5051   0.7634   0.4711   0.6615   0.3898  -2.8037 1.734 35571   3.8
 13.56   0.9335   2.5903   0.7968   0.4710   0.6776   0.4021  -2.7748 1.735 35620   3.9
 14.04   1.0053   2.7501   0.8590   0.4794   0.7089   0.4299  -2.7356 1.736 35596   4.0
 14.49   1.0640   2.8746   0.9093   0.4829   0.7330   0.4515  -2.7018 1.736 35571   4.1
 14.96   1.1130   2.9792   0.9584   0.4844   0.7551   0.4714  -2.6767 1.736 35596   4.2
 15.12   1.1552   3.0696   0.9884   0.4865   0.7709   0.4851  -2.6571 1.735 35571   4.3
 15.19   1.1659   3.0966   0.9982   0.4847   0.7732   0.4859  -2.6550 1.735 35596   4.4
 15.28   1.1643   3.0841   0.9954   0.4862   0.7753   0.4867  -2.6490 1.736 35571   4.5
```

FIGURE 46 - Typical results and data table layout of stability coefficient measurement tests, Able MK-X-A 0.50 in balance, angle of attack sweep -5 deg to +15 deg, PD/2V = 0.160

. R2027 (SPINWT-1-2214.175) 23/08/88 14:30 MACH NO=1.735

α	CY	CYM	CRM	CRMC	CLP	CLPC	CYP	CNP	M	RPM	TEMPS
-4.78	0.0150	0.0283	-0.0041	-0.0046	-0.0256	-0.0290	0.0949	0.1789	1.735	35571	0.0
-4.29	0.0065	0.0046	-0.0037	-0.0042	-0.0236	-0.0265	0.0534	0.0298	1.735	35620	0.1
-3.82	0.0097	0.0169	-0.0040	-0.0044	-0.0253	-0.0276	0.0612	0.1066	1.735	35596	0.2
-3.34	0.0362	0.1142	-0.0038	-0.0041	-0.0242	-0.0260	0.2286	0.7203	1.734	35620	0.3
-2.86	0.0061	0.0113	-0.0030	-0.0032	-0.0190	-0.0203	0.0388	0.0710	1.735	35596	0.4
-2.38	-0.0080	-0.0220	-0.0026	-0.0027	-0.0161	-0.0171	-0.0507	-0.1437	1.735	35620	0.5
-1.91	0.0040	0.0243	-0.0026	-0.0027	-0.0163	-0.0170	0.0253	0.1532	1.736	35620	0.6
-1.42	0.0060	0.0291	-0.0024	-0.0025	-0.0152	-0.0155	0.0378	0.1833	1.735	35620	0.7
-0.94	0.0040	0.0243	-0.0022	-0.0023	-0.0141	-0.0142	0.0254	0.1531	1.735	35645	0.8
-0.46	-0.0050	-0.0005	-0.0023	-0.0023	-0.0146	-0.0144	-0.0367	-0.0834	1.734	35596	0.9
0.01	0.0051	0.0306	-0.0018	-0.0017	-0.0112	-0.0108	0.0323	0.1931	1.735	35620	1.0
0.49	0.0091	0.0420	-0.0021	-0.0020	-0.0133	-0.0128	0.0573	0.2697	1.736	35596	1.1
0.97	-0.0004	0.0202	-0.0024	-0.0023	-0.0154	-0.0147	-0.0025	0.1273	1.734	35620	1.2
1.44	0.0048	0.0284	-0.0019	-0.0018	-0.0123	-0.0115	0.0306	0.1789	1.736	35596	1.3
1.91	-0.0001	0.0151	-0.0023	-0.0022	-0.0140	-0.0139	-0.0006	0.0952	1.734	35620	1.4
2.38	0.0089	0.0482	-0.0023	-0.0022	-0.0146	-0.0137	0.0563	0.3844	1.735	35596	1.5
2.83	-0.0050	0.0093	-0.0027	-0.0026	-0.0170	-0.0161	-0.0317	0.0580	1.735	35645	1.6
3.30	-0.0020	0.0144	-0.0031	-0.0030	-0.0196	-0.0187	-0.0127	0.0908	1.736	35571	1.7
3.77	-0.0068	0.0040	-0.0035	-0.0034	-0.0223	-0.0213	-0.0431	0.0301	1.735	35645	1.8
4.23	0.0037	0.0305	-0.0035	-0.0034	-0.0221	-0.0211	0.0233	0.1926	1.735	35596	1.9
4.70	-0.0041	-0.0083	-0.0038	-0.0037	-0.0241	-0.0232	-0.0262	-0.0525	1.735	35596	2.0
5.16	-0.0027	0.0123	-0.0043	-0.0042	-0.0273	-0.0264	-0.0167	0.0777	1.736	35571	2.1
5.64	-0.0054	-0.0098	-0.0042	-0.0048	-0.0263	-0.0255	-0.0339	-0.0618	1.735	35596	2.2
6.10	-0.0101	-0.0186	-0.0051	-0.0049	-0.0319	-0.0312	-0.0635	-0.1177	1.736	35620	2.3
6.58	0.0003	0.0092	-0.0050	-0.0049	-0.0316	-0.0310	0.0019	0.0579	1.735	35571	2.4
7.05	0.0015	0.0260	-0.0050	-0.0049	-0.0317	-0.0311	0.0092	0.1641	1.735	35620	2.5
7.52	-0.0119	-0.0251	-0.0053	-0.0052	-0.0336	-0.0331	-0.0752	-0.1586	1.735	35571	2.6
7.99	-0.0135	-0.0293	-0.0047	-0.0047	-0.0298	-0.0294	-0.0854	-0.1051	1.735	35547	2.7
8.45	-0.0039	0.0171	-0.0053	-0.0052	-0.0332	-0.0338	-0.0249	0.1079	1.734	35596	2.8
8.92	-0.0016	0.0202	-0.0052	-0.0052	-0.0327	-0.0325	-0.0100	0.1278	1.736	35596	2.9
9.38	-0.0110	-0.0071	-0.0050	-0.0050	-0.0319	-0.0318	-0.0694	-0.0461	1.734	35571	3.0
9.85	-0.0241	-0.0321	-0.0054	-0.0054	-0.0343	-0.0342	-0.1524	-0.2026	1.734	35596	3.1
10.31	-0.0127	0.0055	-0.0059	-0.0059	-0.0372	-0.0372	-0.0888	0.0345	1.734	35596	3.2
10.78	-0.0219	-0.0159	-0.0057	-0.0057	-0.0361	-0.0361	-0.1383	-0.1085	1.735	35571	3.3
11.24	-0.0114	0.0117	-0.0057	-0.0057	-0.0361	-0.0362	-0.0723	0.0739	1.735	35571	3.4
11.69	-0.0134	0.0175	-0.0061	-0.0061	-0.0386	-0.0388	-0.0846	0.1184	1.735	35596	3.5
12.17	-0.0208	-0.0426	-0.0059	-0.0059	-0.0372	-0.0373	-0.1770	-0.2698	1.736	35571	3.6
12.63	-0.0232	-0.0159	-0.0058	-0.0058	-0.0368	-0.0369	-0.1463	-0.1002	1.735	35571	3.7
13.11	-0.0416	-0.0586	-0.0057	-0.0057	-0.0359	-0.0360	-0.2627	-0.3783	1.734	35571	3.8
13.56	-0.0310	-0.0195	-0.0061	-0.0061	-0.0385	-0.0386	-0.1956	-0.1231	1.735	35620	3.9
14.04	-0.0318	-0.0197	-0.0064	-0.0064	-0.0407	-0.0407	-0.2009	-0.1243	1.736	35596	4.0
14.49	-0.0158	0.0200	-0.0064	-0.0064	-0.0404	-0.0403	-0.0950	0.1264	1.736	35571	4.1
14.95	-0.0272	-0.0158	-0.0067	-0.0067	-0.0424	-0.0422	-0.1717	-0.0945	1.736	35596	4.2
15.12	-0.0200	-0.0136	-0.0061	-0.0061	-0.0387	-0.0383	-0.1262	-0.0850	1.735	35571	4.3
15.19	-0.0244	-0.0282	-0.0066	-0.0063	-0.0417	-0.0412	-0.1543	-0.1274	1.735	35596	4.4
15.28	-0.0239	-0.0194	-0.0066	-0.0065	-0.0417	-0.0410	-0.1508	-0.1224	1.736	35571	4.5

FIGURE 47 - Typical results and data table layout of stability coefficient measurement tests, Able MK-X-A 0.50 in balance, angle of attack sweep -5 deg to +15 deg, PD/2V = 0.160

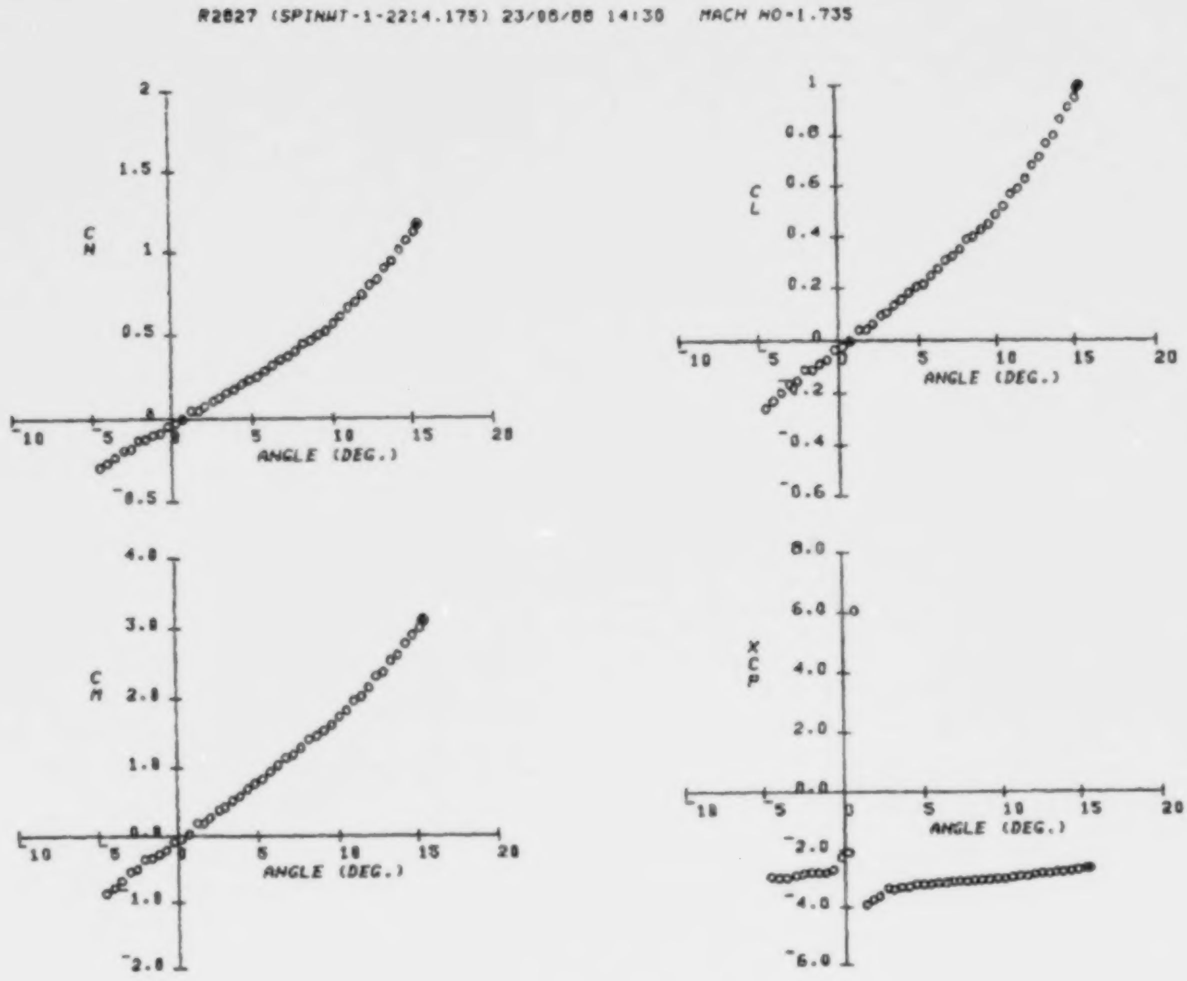

FIGURE 48 - Typical CN, CM, CL coefficients and center of pressure, graphical layout, Able MK-X-A 0.50 in balance, angle of attack sweep -5 deg to +15 deg, Mach 1.73, spin rate 35,600 RPM, PD/2V = 0.160

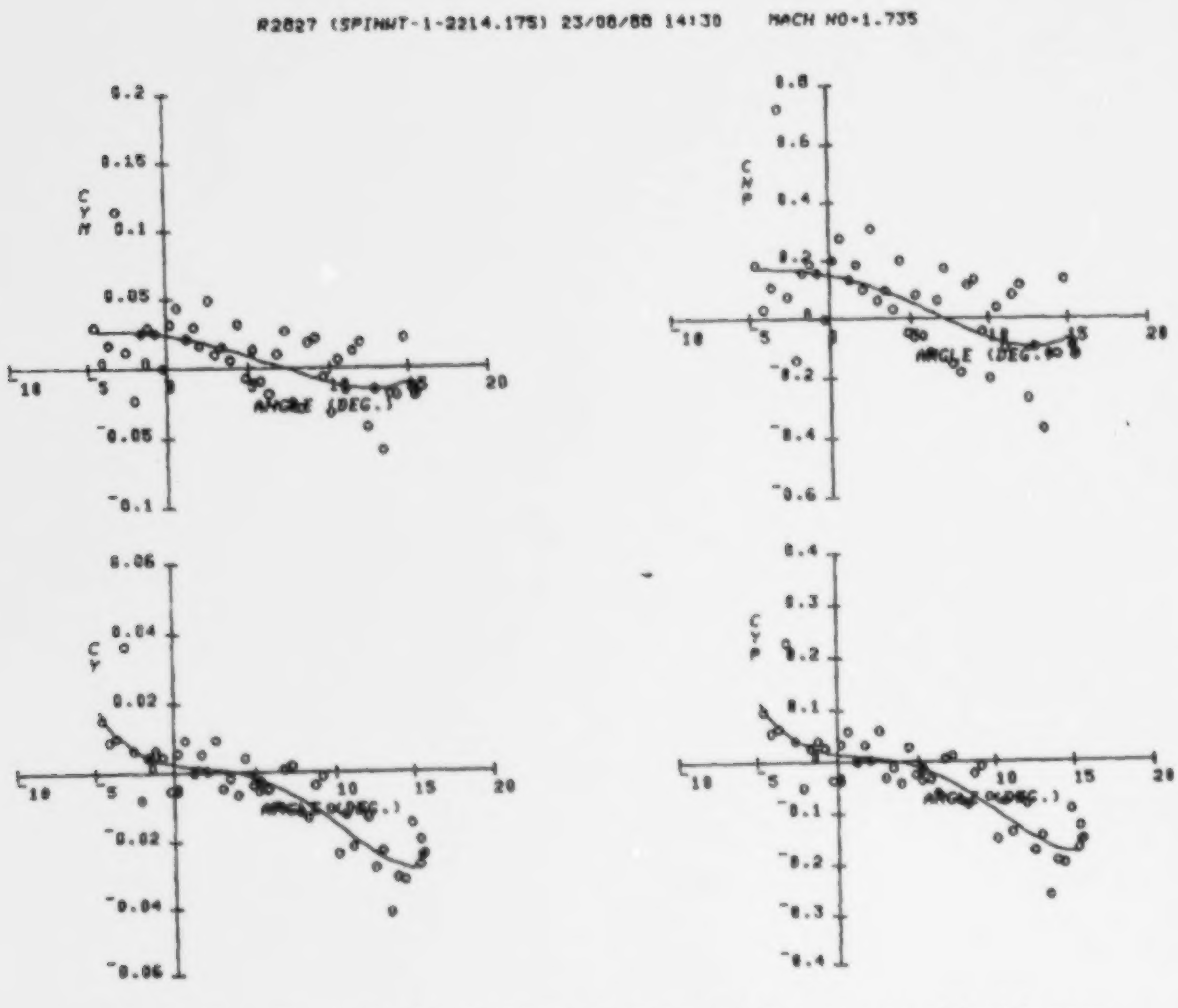

FIGURE 49 - Typical CY, CYM, CYP,CNP coefficients, graphical layout, Able MK-X-A 0.50 in balance, angle of attack sweep -5 deg to + 15 deg, Mach 1.73, spin rate 35,600 RPM, PD/2V = 0.160

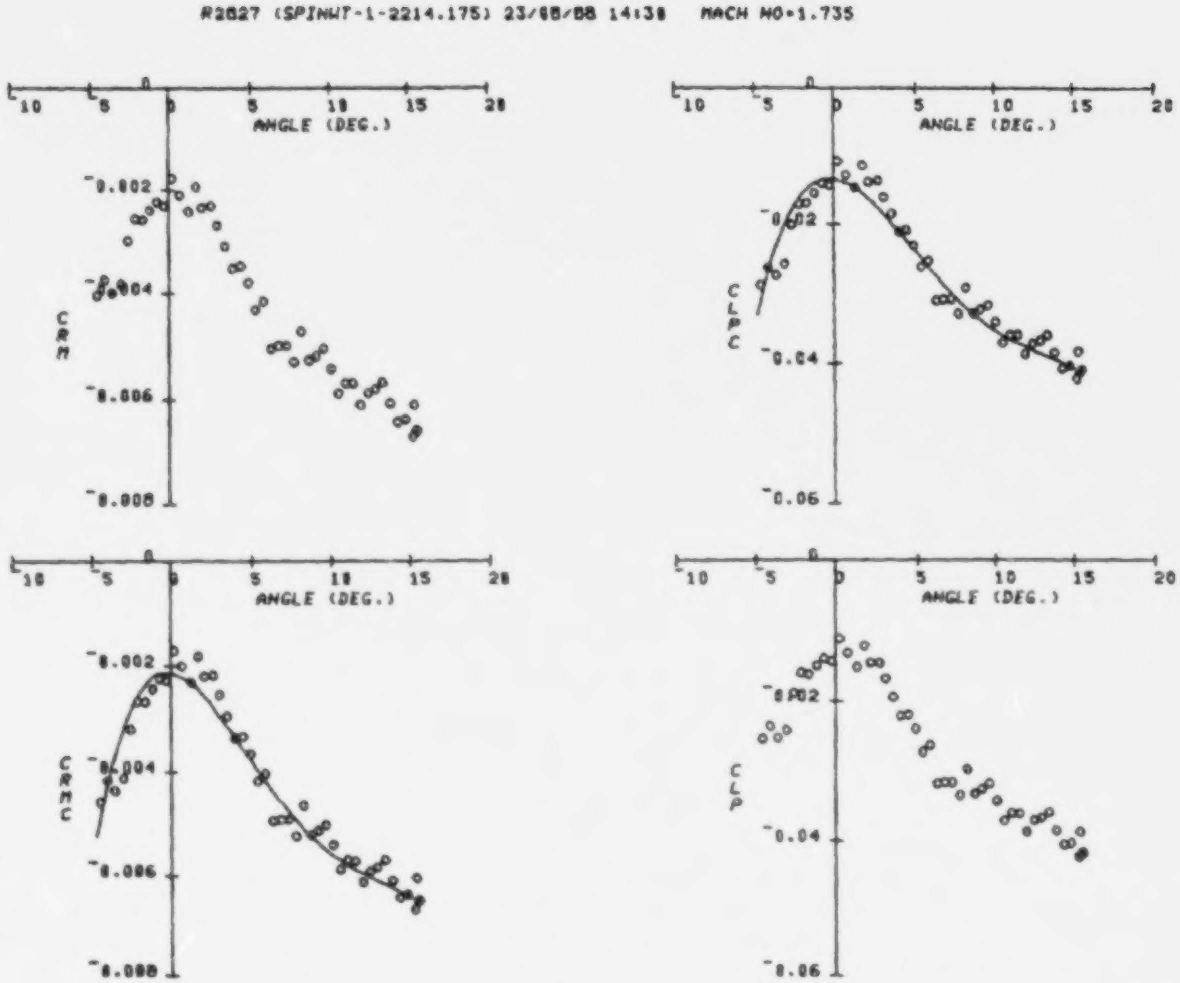

FIGURE 50 - Example of CRM, CRMC, CLP, CLPC coefficients, graphical layout, Able MK-VI-A 0.50 in balance, angle of attack sweep -5 deg to + 15 deg, Mach 1.73, spin rate 35,600 RPM, PD/2V = 0.160

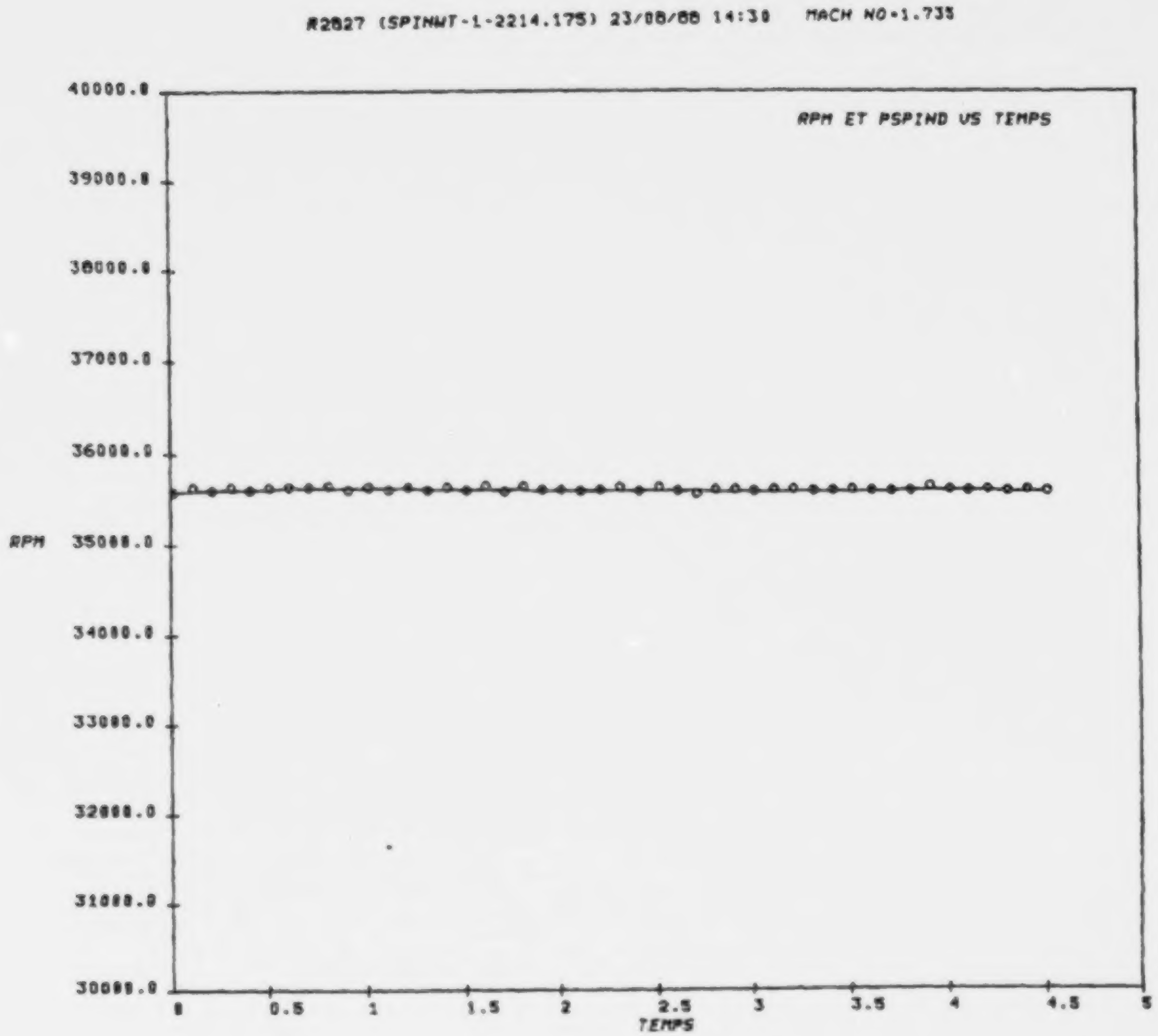

FIGURE 51 - Typical variation of spin rate versus time during a test run, angle of attack sweep -5 deg to + 15 deg, Mach 1.73, spin rate 35,600 RPM, PD/2V = 0.160

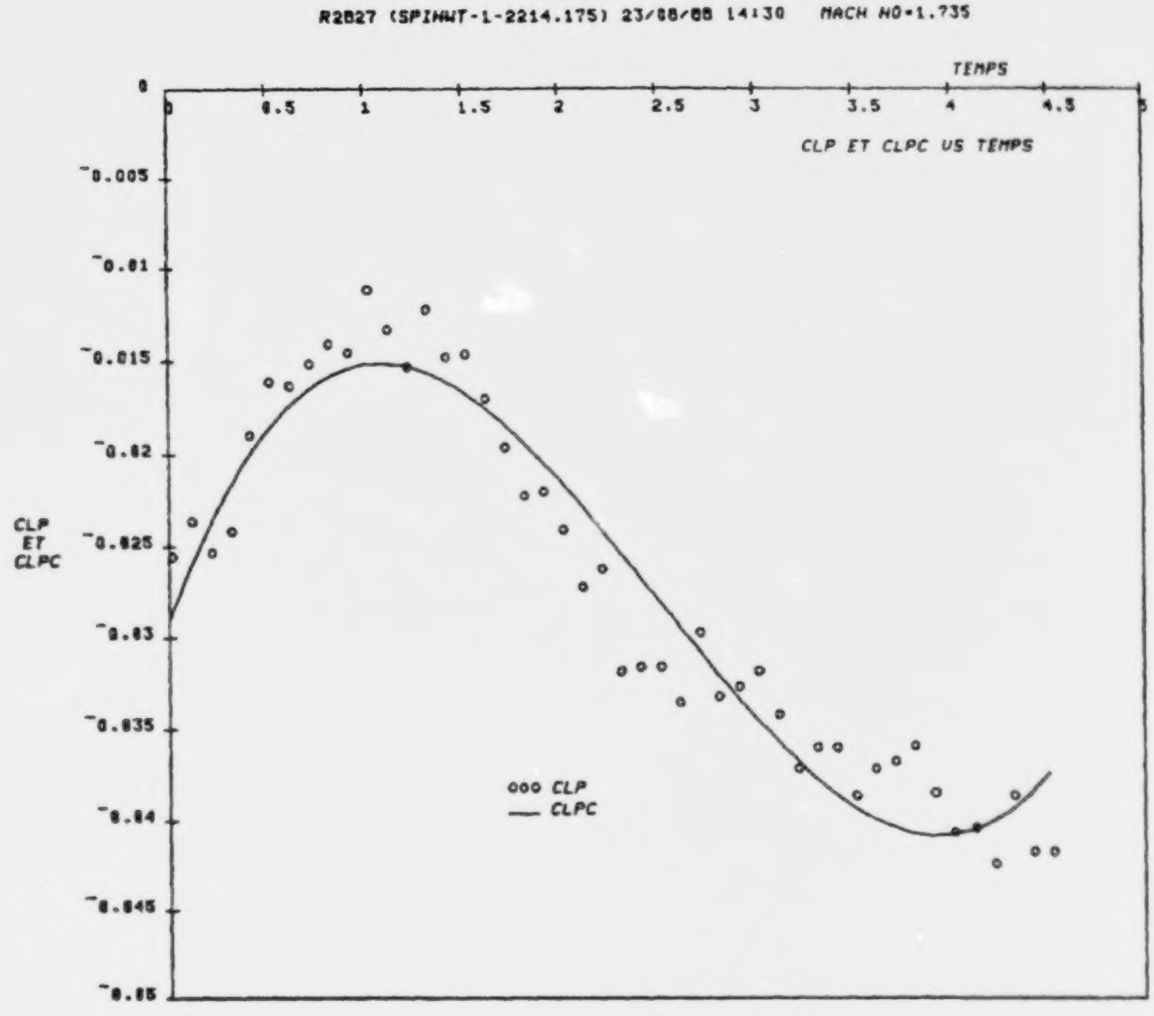

FIGURE 52 - Typical variation of CLP and CLPC versus time during a test run, angle of attack sweep -5 deg to + 15 deg, Mach 1.73, spin rate 35,600 RPM, PD/2V = 0.160

```
RUN NO.:R2990 (SPINWT-1-2090.110)     DATE: 08/12/88 14:50          ROTATION : LEFT

NOZZLE BLOCKS= 1.15     BOV SETTING= 70     RPM=  39947     PD/2V=  0.23901

M(MEAN)= 1.16      TEMP= 24.0C       Q(PA)=40103     REYN/M= 1.49E7

CNA=2.528       CMA=0.614       XCPO= ¯3.41      CAO=0.460

   α        CN       CM       CL        CA       CDT       CD       XCP      M     RPM   TEMPS
-------  -------  -------  -------  -------  -------  -------  -------  -----  -----  -----
¯2.63   ¯0.1342  ¯0.4255  ¯0.1128   0.4650   0.4707   0.1883  ¯3.1695  1.152  39966   0.0
¯2.47   ¯0.1032  ¯0.3195  ¯0.0832   0.4630   0.4670   0.1880  ¯3.0948  1.153  39941   0.1
¯2.32   ¯0.1023  ¯0.3245  ¯0.0834   0.4665   0.4702   0.1933  ¯3.1703  1.154  39941   0.2
¯2.10   ¯0.1010  ¯0.3083  ¯0.0842   0.4620   0.4656   0.1902  ¯3.0201  1.155  39966   0.3
¯2.04   ¯0.0996  ¯0.3091  ¯0.0831   0.4618   0.4650   0.1875  ¯3.1016  1.155  39941   0.4
¯1.91   ¯0.0771  ¯0.2412  ¯0.0618   0.4590   0.4613   0.1888  ¯3.1274  1.155  39966   0.5
¯1.77   ¯0.0658  ¯0.2104  ¯0.0515   0.4620   0.4639   0.1910  ¯3.1950  1.156  39941   0.6
¯1.64   ¯0.0922  ¯0.2854  ¯0.0790   0.4627   0.4651   0.1914  ¯3.0944  1.156  39941   0.7
¯1.49   ¯0.0711  ¯0.2187  ¯0.0589   0.4640   0.4657   0.1931  ¯3.0774  1.156  39941   0.8
¯1.34   ¯0.0378  ¯0.1146  ¯0.0269   0.4641   0.4648   0.1911  ¯3.0353  1.156  39941   0.9
¯1.21   ¯0.0512  ¯0.1545  ¯0.0414   0.4610   0.4620   0.1889  ¯3.0192  1.156  39941   1.0
¯1.07   ¯0.0466  ¯0.1310  ¯0.0380   0.4599   0.4607   0.1890  ¯2.8126  1.157  39941   1.1
¯0.95   ¯0.0505  ¯0.1542  ¯0.0428   0.4605   0.4613   0.1905  ¯3.0554  1.157  39941   1.2
¯0.81   ¯0.0304  ¯0.0805  ¯0.0238   0.4627   0.4630   0.1899  ¯2.6490  1.157  39941   1.3
¯0.67   ¯0.0327  ¯0.0827  ¯0.0273   0.4591   0.4595   0.1900  ¯2.5305  1.157  39966   1.4
¯0.53   ¯0.0121  ¯0.0243  ¯0.0079   0.4605   0.4606   0.1917  ¯2.0072  1.157  39966   1.5
¯0.39   ¯0.0110  ¯0.0205  ¯0.0079   0.4590   0.4590   0.1907  ¯1.8633  1.157  39966   1.6
¯0.26   ¯0.0238  ¯0.0661  ¯0.0217   0.4616   0.4617   0.1923  ¯2.7809  1.157  39966   1.7
¯0.10    0.0391   0.1635   0.0399   0.4588   0.4587   0.1891  ¯4.1770  1.157  39941   1.8
 0.01    0.0096   0.0660   0.0095   0.4595   0.4595   0.1905  ¯6.0744  1.157  39941   1.9
 0.14   ¯0.0056  ¯0.0029  ¯0.0067   0.4601   0.4600   0.1925  ¯0.5070  1.157  39893   2.0
 0.28    0.0011   0.0344  ¯0.0012   0.4610   0.4610   0.1924 ¯31.6078  1.157  39941   2.1
 0.44    0.0220   0.1128   0.0185   0.4595   0.4596   0.1918  ¯5.1340  1.157  39966   2.2
 0.56    0.0189   0.0824   0.0144   0.4613   0.4614   0.1921  ¯4.3502  1.157  39941   2.3
 0.71    0.0536   0.2015   0.0479   0.4605   0.4612   0.1924  ¯3.7875  1.157  39966   2.4
 0.84    0.0321   0.1354   0.0254   0.4620   0.4624   0.1933  ¯4.2127  1.156  39941   2.5
 0.98    0.0653   0.2342   0.0574   0.4617   0.4628   0.1911  ¯3.5879  1.156  39941   2.6
 1.11    0.0471   0.1873   0.0381   0.4611   0.4619   0.1899  ¯3.9809  1.157  39941   2.7
 1.24    0.0367   0.1457   0.0267   0.4638   0.4644   0.1925  ¯3.9680  1.157  39941   2.8
 1.38    0.0354   0.1617   0.0243   0.4594   0.4601   0.1914  ¯4.5718  1.157  39941   2.9
 1.53    0.0845   0.3112   0.0721   0.4636   0.4657   0.1908  ¯3.6802  1.156  39941   3.0
 1.65    0.0551   0.2190   0.0417   0.4646   0.4660   0.1944  ¯3.9759  1.156  39941   3.1
 1.78    0.0883   0.3113   0.0740   0.4615   0.4640   0.1930  ¯3.5249  1.156  39941   3.2
 1.85    0.0692   0.2554   0.0542   0.4610   0.4630   0.1925  ¯3.6911  1.156  39941   3.3
 1.95    0.1092   0.4018   0.0933   0.4653   0.4688   0.1961  ¯3.6807  1.156  39966   3.4
 2.02    0.0864   0.3342   0.0701   0.4619   0.4646   0.1957  ¯3.8672  1.156  39941   3.5
 2.09    0.0755   0.2851   0.0586   0.4630   0.4654   0.1958  ¯3.7741  1.156  39941   3.6
```

FIGURE 53 - Typical results and data table layout of stability coefficient measurement tests, Able MK-X-A 0.50 in balance, ,angle of attack sweep -2 deg to +2 deg, PD/2V = 0.239

```
R2990 (SPINWT-1-2090.110) 08/12/88 14:58  MACH NO=1.156

   *       CY       CYM      CRM      CRMC     CLP      CLPC     CYP      CNP      M     RPM   TEMPS
------- -------- -------- -------- -------- -------- -------- -------- -------- ----- ----- -----
 -2.63  -0.0139  -0.0249   0.0051   0.0053   0.0213   0.0221  -0.0582  -0.1043 1.152 39966   0.0
 -2.47  -0.0052  -0.0053   0.0054   0.0056   0.0227   0.0234  -0.0216  -0.0221 1.153 39941   0.1
 -2.32   0.0062   0.0363   0.0054   0.0055   0.0225   0.0230   0.0260   0.1519 1.154 39941   0.2
 -2.10   0.0073   0.0636   0.0053   0.0054   0.0224   0.0228   0.0306   0.2660 1.155 39966   0.3
 -2.04   0.0205   0.0071   0.0053   0.0054   0.0222   0.0224   0.0058   0.3643 1.155 39941   0.4
 -1.91   0.0143   0.0631   0.0051   0.0051   0.0211   0.0213   0.0598   0.2228 1.155 39966   0.5
 -1.77   0.0045   0.0176   0.0057   0.0057   0.0230   0.0239   0.0188   0.0735 1.156 39941   0.6
 -1.64   0.0072   0.0441   0.0054   0.0054   0.0227   0.0227   0.0302   0.1846 1.156 39941   0.7
 -1.49  -0.0010   0.0116   0.0057   0.0057   0.0237   0.0237  -0.0043   0.0487 1.156 39941   0.8
 -1.34   0.0272   0.1096   0.0048   0.0048   0.0201   0.0201   0.1137   0.4587 1.156 39941   0.9
 -1.21  -0.0153  -0.0374   0.0053   0.0052   0.0220   0.0219  -0.0640  -0.1563 1.156 39941   1.0
 -1.07  -0.0210  -0.0634   0.0057   0.0057   0.0240   0.0239  -0.0080  -0.2653 1.157 39941   1.1
 -0.95  -0.0080  -0.0032   0.0058   0.0058   0.0244   0.0244  -0.0334  -0.0134 1.157 39941   1.2
 -0.81  -0.0126  -0.0289   0.0060   0.0060   0.0250   0.0249  -0.0501  -0.1289 1.157 39941   1.3
 -0.67   0.0113   0.0640   0.0055   0.0054   0.0228   0.0228   0.0472   0.2678 1.157 39966   1.4
 -0.53  -0.0022   0.0138   0.0057   0.0057   0.0239   0.0239  -0.0093   0.0579 1.157 39966   1.5
 -0.39   0.0067   0.0154   0.0062   0.0062   0.0260   0.0260   0.0281   0.0644 1.157 39966   1.6
 -0.26   0.0045   0.0298   0.0061   0.0061   0.0253   0.0253   0.0189   0.1213 1.157 39966   1.7
 -0.10  -0.0150  -0.0245   0.0057   0.0058   0.0241   0.0241  -0.0628  -0.1025 1.157 39941   1.8
  0.01  -0.0070  -0.0128   0.0053   0.0053   0.0220   0.0220  -0.0293  -0.0503 1.157 39941   1.9
  0.14  -0.0089  -0.0147   0.0057   0.0057   0.0240   0.0240  -0.0373  -0.0613 1.157 39893   2.0
  0.28  -0.0133  -0.0353   0.0062   0.0062   0.0258   0.0259  -0.0558  -0.1477 1.157 39941   2.1
  0.44  -0.0018   0.0158   0.0058   0.0058   0.0242   0.0243  -0.0840   0.0626 1.157 39966   2.2
  0.56   0.0169   0.0680   0.0062   0.0062   0.0259   0.0260   0.0707   0.2845 1.157 39941   2.3
  0.71  -0.0155  -0.0444   0.0062   0.0062   0.0259   0.0261  -0.0648  -0.1858 1.157 39966   2.4
  0.84   0.0214   0.0935   0.0057   0.0057   0.0237   0.0239   0.0893   0.3912 1.156 39941   2.5
  0.98   0.0196   0.0681   0.0053   0.0053   0.0220   0.0222   0.0819   0.2850 1.156 39941   2.6
  1.11   0.0426   0.1398   0.0051   0.0052   0.0214   0.0216   0.1782   0.5858 1.157 39941   2.7
  1.24   0.0043   0.0194   0.0063   0.0063   0.0264   0.0265   0.0181   0.0818 1.157 39941   2.8
  1.38  -0.0015  -0.0189   0.0053   0.0053   0.0221   0.0222  -0.0063  -0.0458 1.157 39941   2.9
  1.53   0.0365   0.1358   0.0052   0.0052   0.0217   0.0217   0.1525   0.5648 1.156 39941   3.0
  1.65   0.0176   0.0695   0.0058   0.0058   0.0241   0.0241   0.0734   0.2909 1.156 39941   3.1
  1.78   0.0191   0.0647   0.0058   0.0058   0.0243   0.0241   0.0798   0.2709 1.156 39941   3.2
  1.85   0.0126   0.0325   0.0054   0.0053   0.0224   0.0222   0.0527   0.1358 1.156 39941   3.3
  1.95   0.0063   0.0106   0.0054   0.0053   0.0228   0.0224   0.0263   0.0443 1.156 39966   3.4
  2.02   0.0061   0.0187   0.0054   0.0053   0.0226   0.0221   0.0257   0.0782 1.156 39941   3.5
  2.09   0.0065   0.0105   0.0059   0.0057   0.0245   0.0238   0.0273   0.1694 1.156 39941   3.6
```

FIGURE 54 - Typical results and data table layout of stability coefficient measurement tests, Able MK-X-A 0.50 in balance, angle of attack sweep -2 deg to +2 deg, PD/2V = 0.239

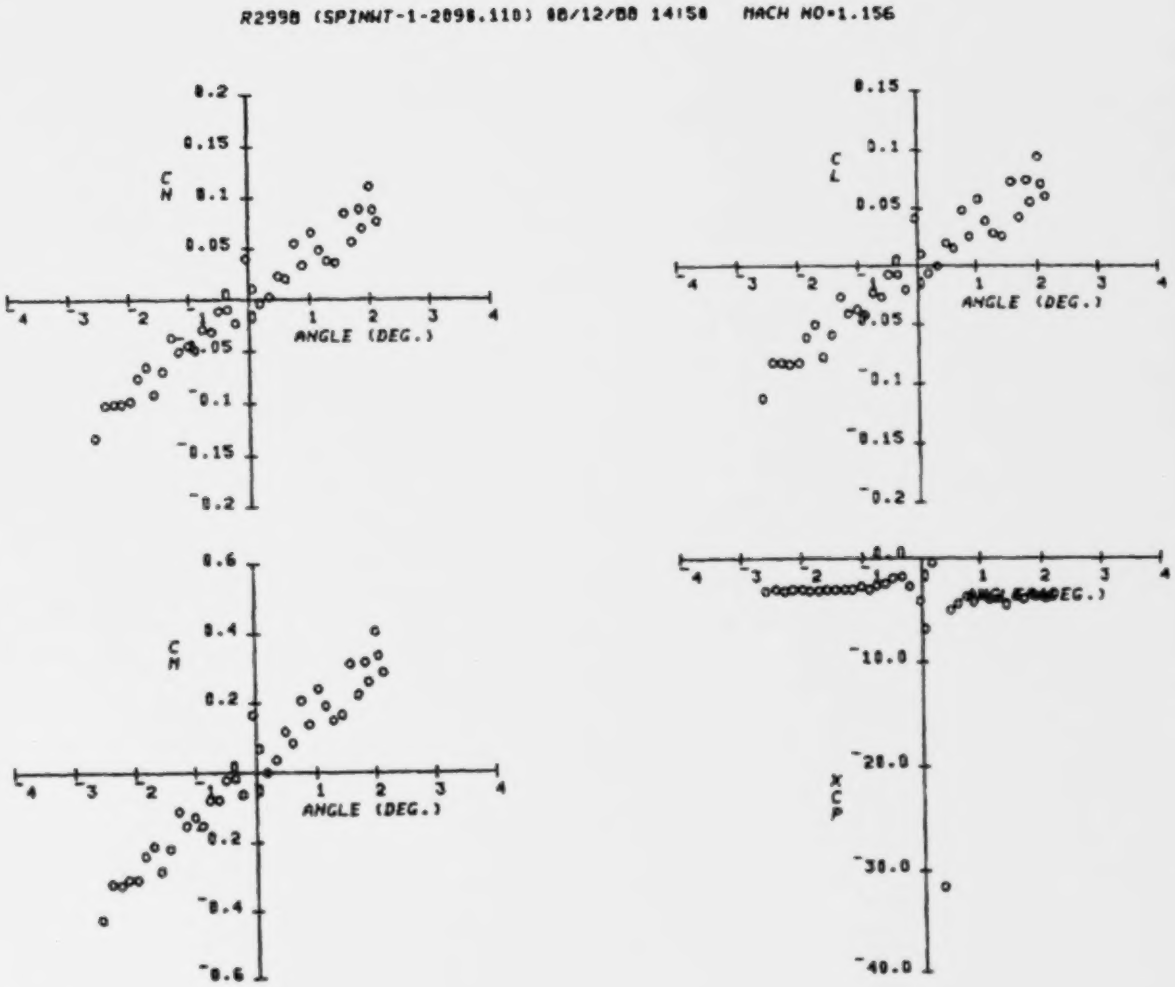

FIGURE 55 - Typical CN, CM, CL coefficients and center of pressure results, graphical layout, Able MK-X-A 0.50 in balance, angle of attack sweep -2 deg to +2 deg, Mach 1.16, spin rate 39,950 RPM, PD/2V = 0.239

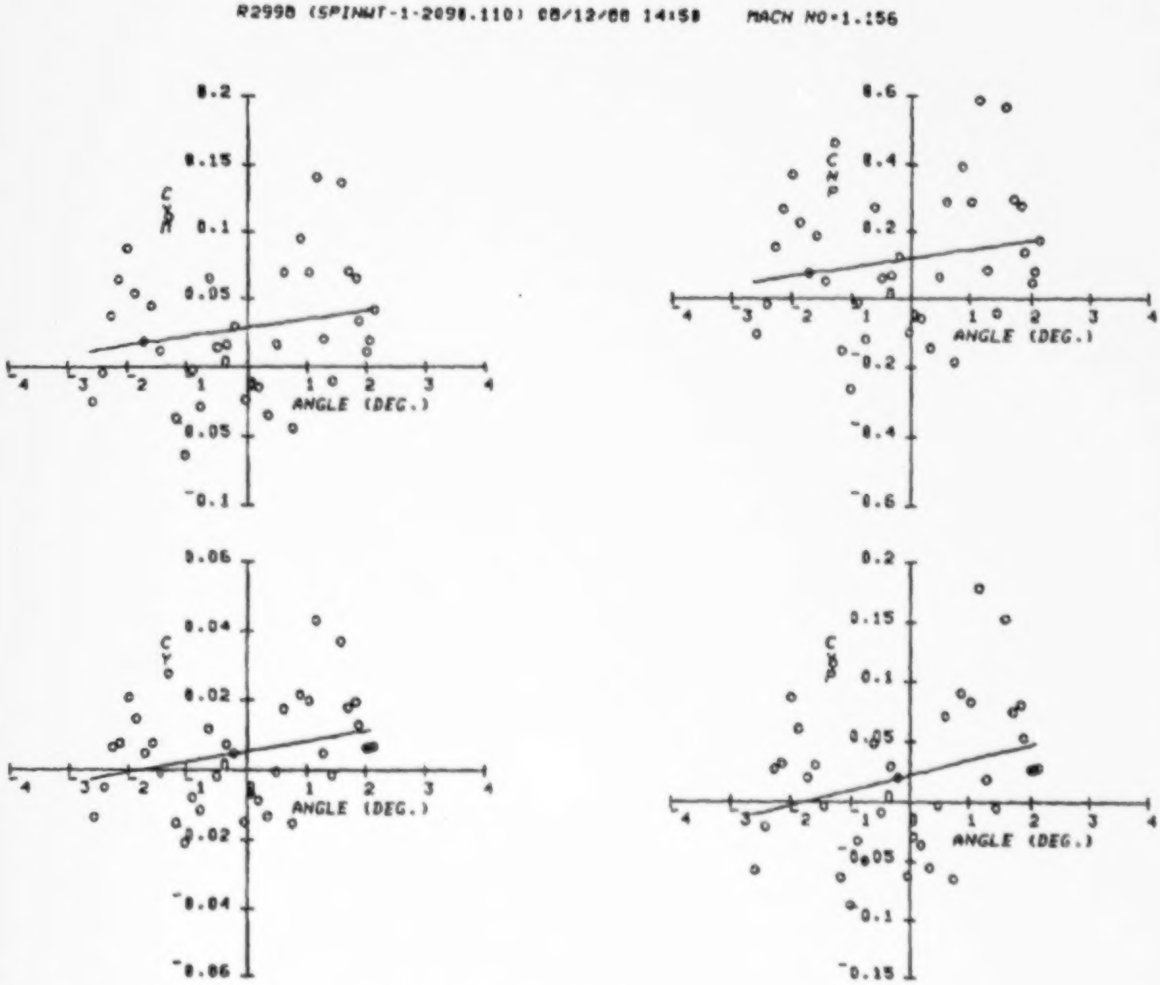

FIGURE 56 - Typical CY, CYM, CYP,CNP coefficients, graphical layout, Able MK-X-A 0.50 in balance, angle of attack sweep -2 deg to +2 deg, Mach 1.16, spin rate 39,950 RPM, PD/2V = 0.239

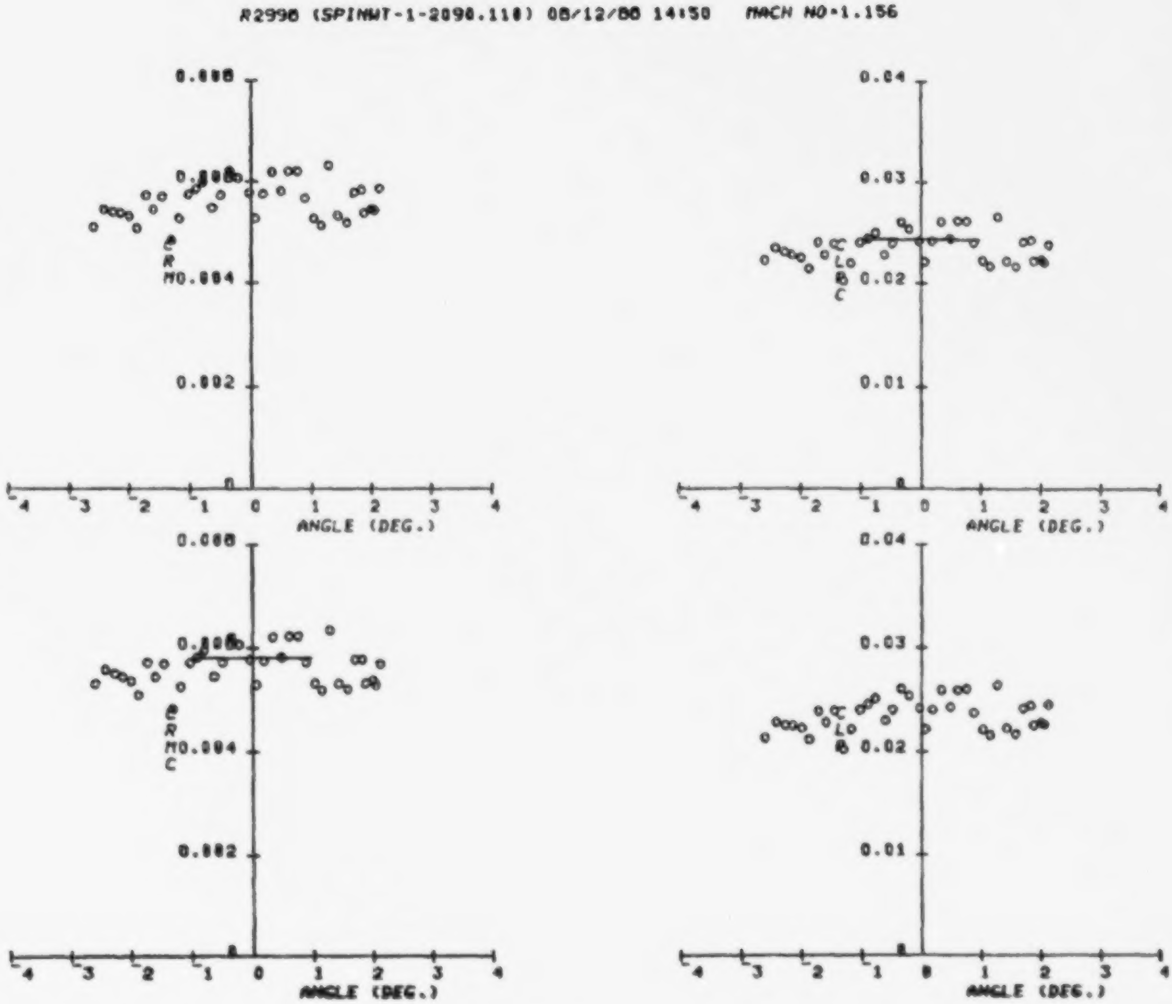

FIGURE 57 - Example of CRM, CRMC, CLP, CLPC coefficients, graphical layout, Able MK-VI-A 0.50 in balance, angle of attack sweep -2 deg to +2 deg, Mach 1.16, spin rate 39,950 RPM, PD/2V = 0.239

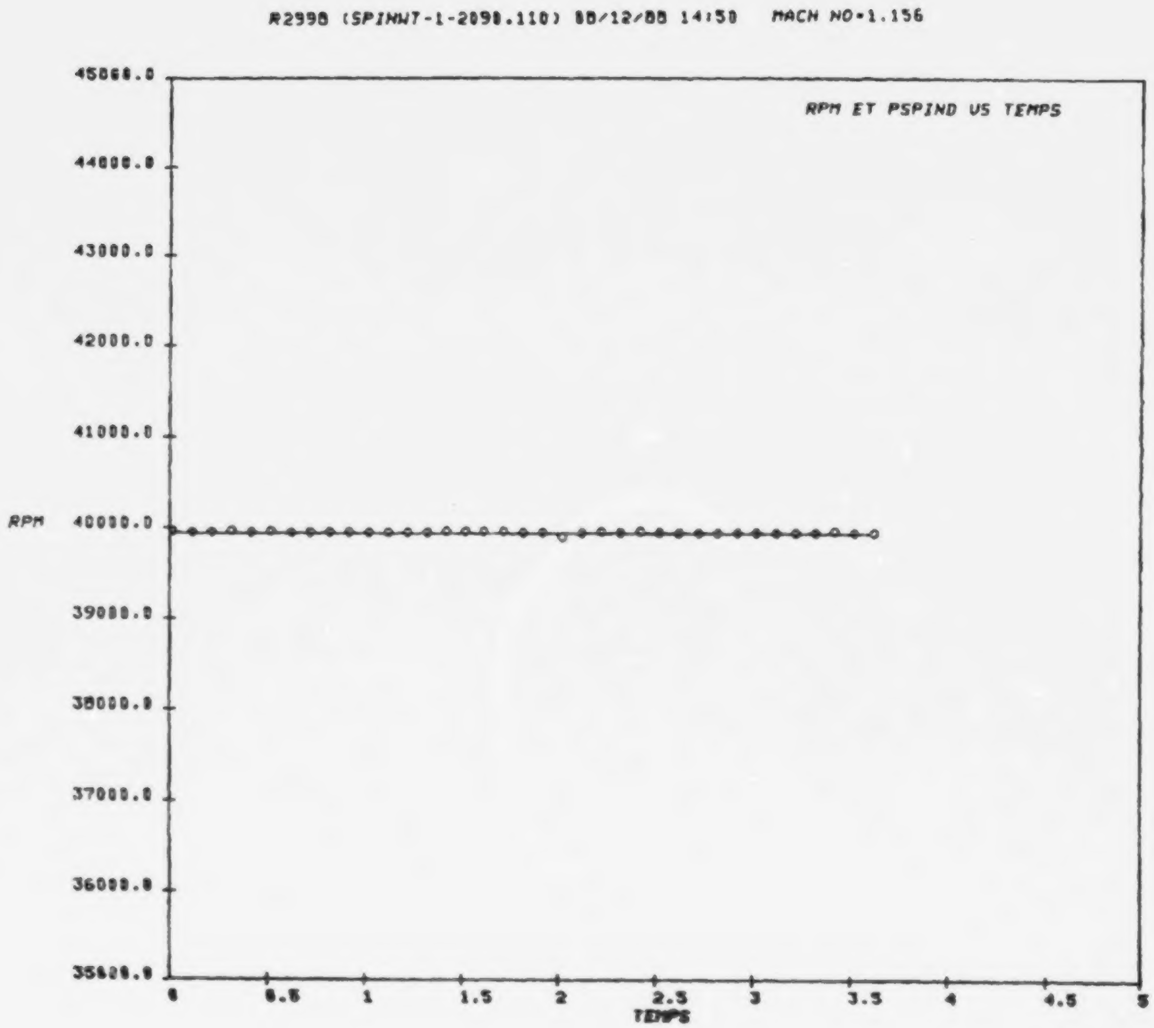

FIGURE 58 - Typical variation of spin rate versus time during a test run, angle of attack sweep -2 deg to +2 deg, Mach 1.16, spin rate 39,950 RPM, PD/2V = 0.239

R2998 (SPINWT-1-2090.118) 08/12/88 14:50 MACH NO=1.156

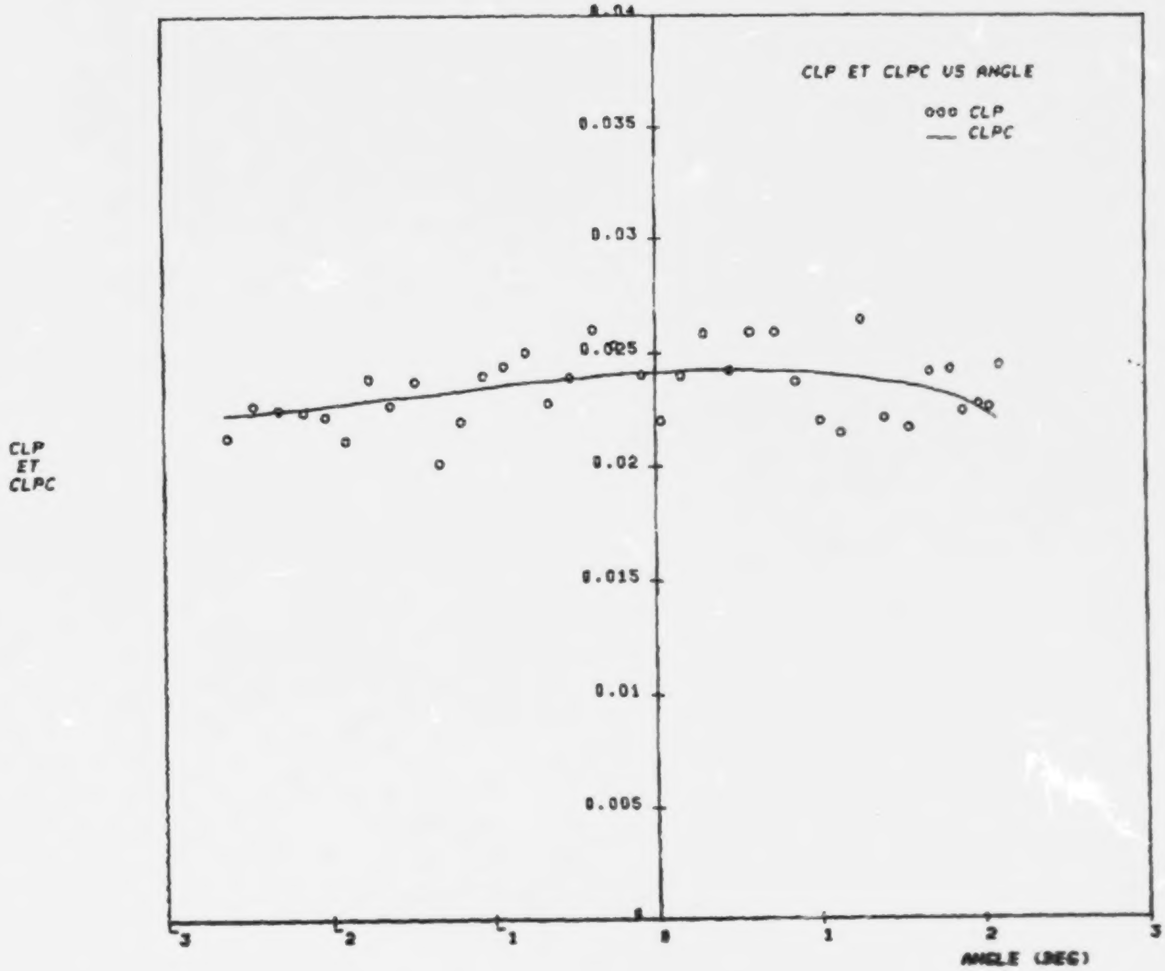

FIGURE 59 - Typical variation of CLP and CLPC versus angle of attack, angle of attack sweep -2 deg to +2 deg, Mach 1.16, spin rate 39,950 RPM, PD/2V = 0.239

9.2 Recorded Motor Data Results During Wind Tunnel and Calibration Tests

The spin rig motor controller provides output data results on the voltage, current, spin rate and temperature. Typical outputs are presented in Figures 60 and 61 that give the motor current and voltage versus time for various spin rate initial settings on the controller (no wind conditions). These results are complementary to Fig. 28 that gives the spin rate response versus time.

The results of Fig. 29 are typical of what is to be obtained from the experimental process to determine the model moment of inertia.

When a calibration of the motor current versus rolling moment (torque) and spin rate is performed with the Foucault braking system, the results of Fig. 30 are typical of what is to be obtained for each particular set of rolling moment and spin rate. A different curve shall be produced for each spin rate and rolling moment. Figure 62 presents results which are complementary to Fig. 30 and gives the voltage variation versus time recorded for the same calibration test conditions.

For each wind tunnel test runs of present series, the motor controller gave output data whose those of Fig. 63 are typical.

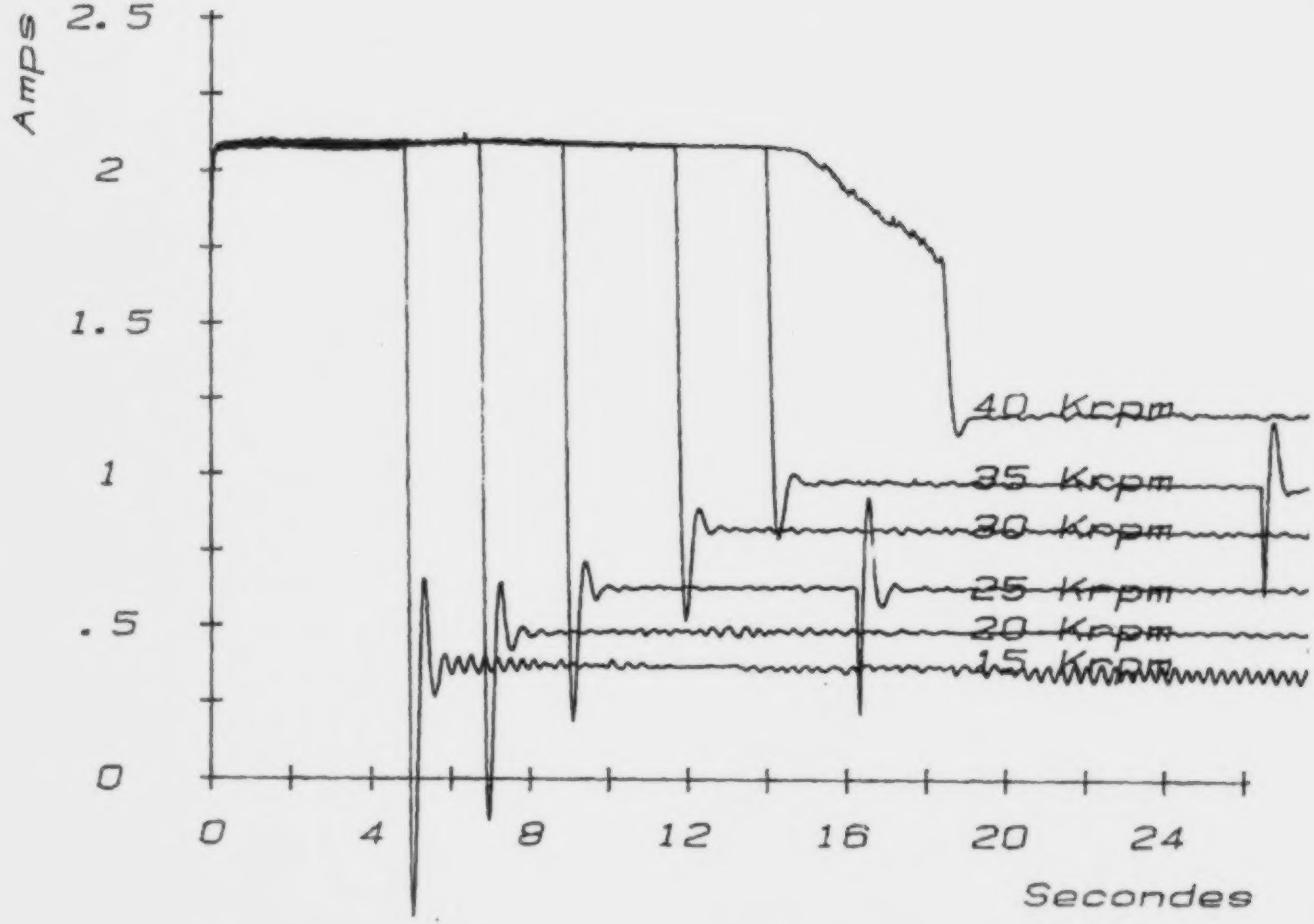

FIGURE 60 - Motor current variation versus time during spin rate acceleration, complementary to Fig. 28

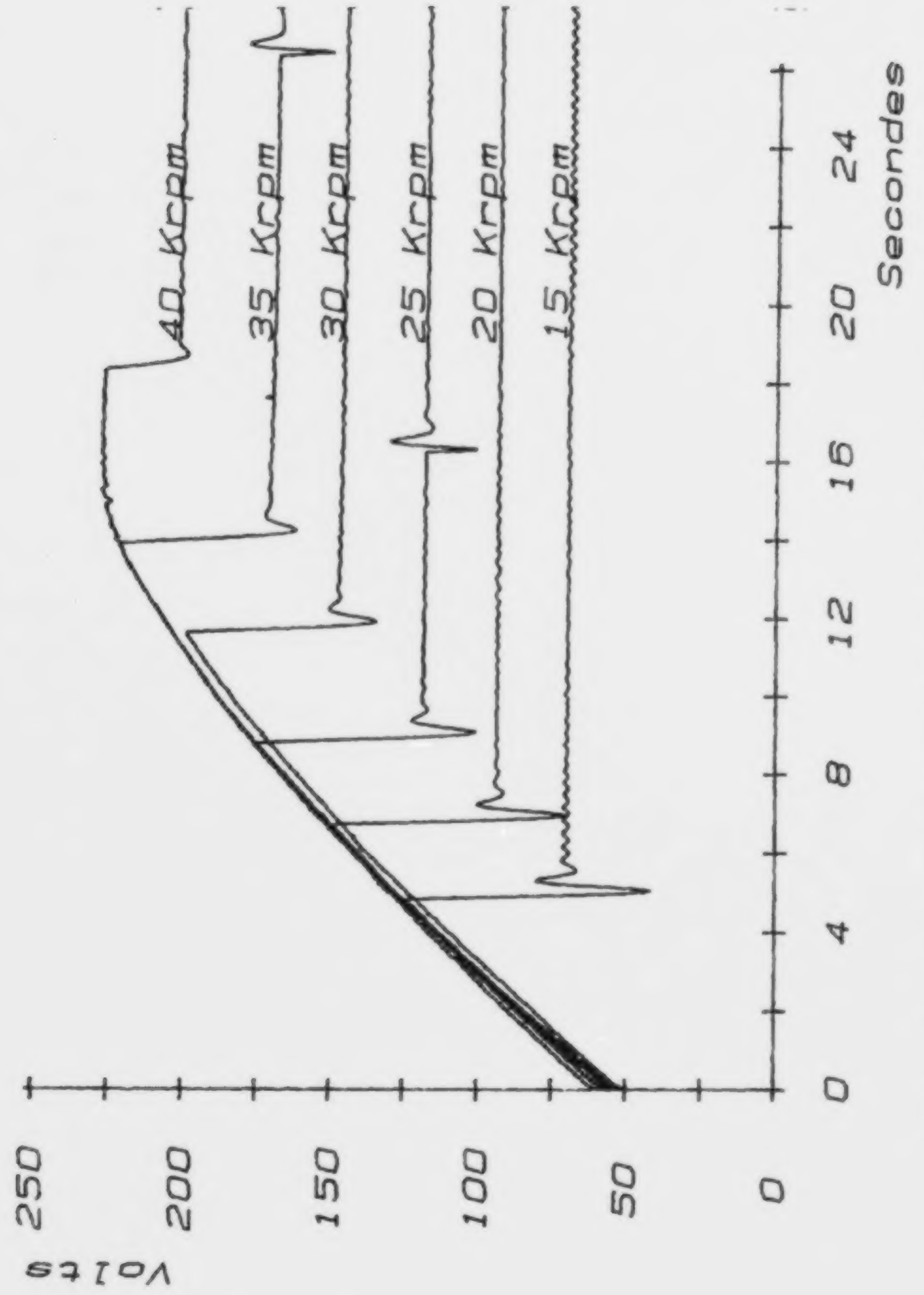

FIGURE 61 - Motor voltage variation versus time during spin rate acceleration, complementary to Fig. 28

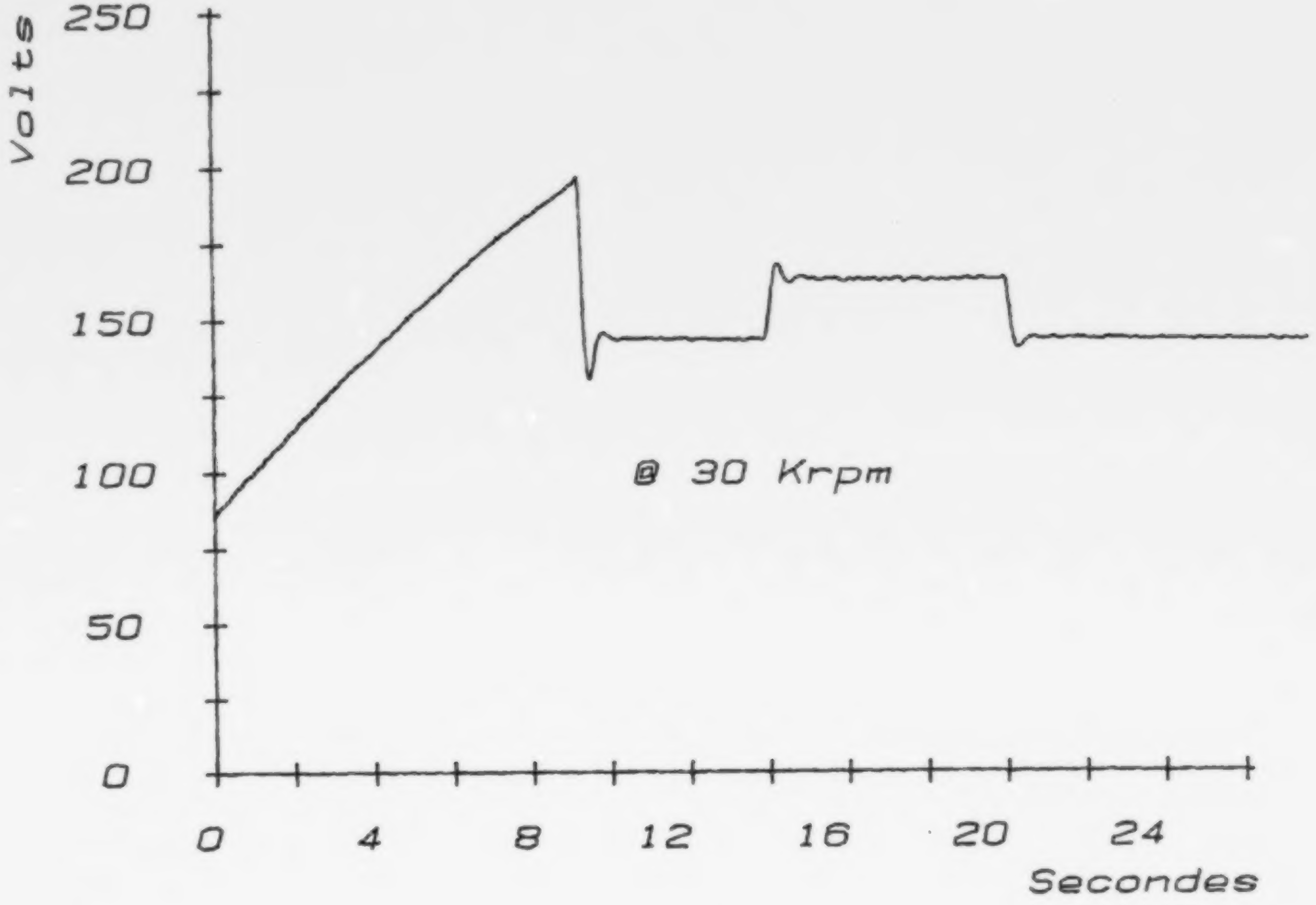

FIGURE 62 - Motor voltage variation versus time during calibration of current versus rolling moment with Foucault braking system, complementary to Fig. 30

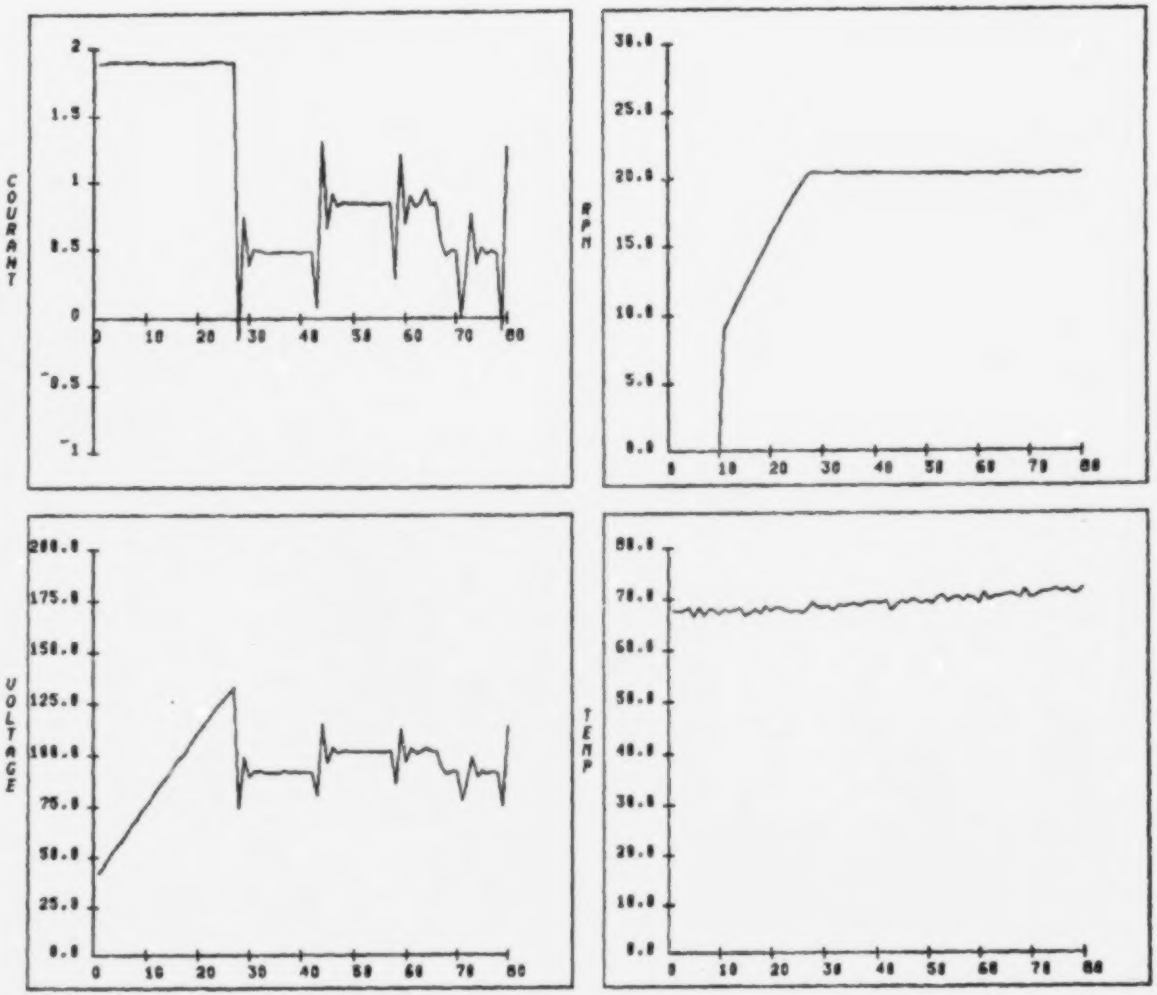

FIGURE 63 - Typical motor voltage, current, temp F deg and RPM variation versus time during a test run

10.0 AERODYNAMIC COEFFICIENTS MEASUREMENT ERRORS

This chapter attempts to determine the run-to-run repeatability or " precision " of measurements made in present tests series with the cone/cylinder with/without fins and flechette models. Wind tunnel results use to be under the form of aerodynamic coefficients and surface pressure ratios " P_{tap}/P_{∞} ", although only aerodynamic coefficient measurement were made in present test series, to the exception of the model base pressure. There are two sources of measurement errors that are assumed totally independent:

a - Residual Error which represents results dispersion that could not be explained by aleatory behavior of measurement instrumentation. Small variations of test conditions (from mechanical sources or atmospheric fluctuations) or the aerodynamic phenomena natural instability are the cause of the difference between overall measurement errors and systematic errors.

b - Systematic Error which represents results dispersion introduced all along the chain of instrumentation elements or modules. This aleatory error is usually repetitive and quantitatively known in advance. Systematic error is often named instrumentation noise.

The residual error and systematic error combine together to produce the measurement total error which is observed while compiling results. The standard deviation of measurement total error is related to the residual error and systematic error standard deviations as follows:

$$\text{Measurement total error} = \sqrt[2]{(\text{Residual error})^2+(\text{Systematic error})^2}$$

As far as experimental measurements are concerned, the concept of " precision " or " absolute accuracy " is related to the probable difference between result values that were measured during one test run and the average values that would have been obtained after repeating the same run for a large number of times. It is not possible to determine the " absolute accuracy " as true values are not known for free-flight conditions as well as for idealized wind tunnel test conditions. There are inaccurate flow parameters which are inherent to the wind tunnel test section, like Mach number and Reynolds number, that result in an environment that is different from atmospheric flight conditions. Also, the test section flow angularity combined with incorrect angles of attack (pitch and yaw) induced by misalignment between component fixations within the model/balance/sting/strut hub combination system, are other sources of measurement errors.

The statistical methodology to evaluate aerodynamic coefficient measurement errors is presented in Appendix D. Although some typical test runs were repeated several times in order to investigate results dispersion, most of the time, runs were performed twice only. Statistical analysis provided data on results interval limits, for levels of confidence of 95.0% and 80.0%, related to the case where a single test run was normally made. This data, which is presented in Tables VII and VIII, is expressed in percentage of experimental values.

Tables VII and VIII contain data on systematic error of the Able MK-X-A 0.50 in balance used for aerodynamic coefficient tests and that are expressed in percentage of the average measured value. This error is based on the known precision of the balance in terms of percentage of full range.

It can be observed in Table VII that the balance systematic error related to CNA, CMA and CA0 stay within an order of magnitude with respect to measurements interval limits for a level of confidence of 80.0%. It must be noted that since measurements were taken between -2 to +2 deg of angle of attack, the low level of forces and moments then involved did not help to obtain repeatable aerodynamic derivatives.

Nevertheless, the main objective of the test series was to investigate the possibility to effectively measure spin damping coefficients. The observed resolution of the balance, as rolling moment measurement were concerned, was approximately ±0.032% of its nominal capacity, which represents 1/6 of the balance accuracy (±0.2%) (see Appendix D). The balance accuracy systematic error varied from ±24% to ±350% of measured rolling moment values. The balance resolution systematic error varied from ±4% to ±50% of measured rolling moment values. The relation between test Mach number and balance accuracy and resolution systematic errors (for roll) were plotted in Figs. D2 and D4.

An apparent roll measurement shift of 0.0332% of the balance nominal capacity in absolute magnitude was observed for all tests made with the Able MK-X-A 0.50 in balance (Fig. D3). Although the apparent measurement shift can be compensated by making intentionally test runs in reverse (right and left) senses of rotation and averaging the rolling moment data results, it remained a residual balance offset unknown in magnitude but approximately equal to 0.05% of the balance nominal capacity (Fig. D3).

The minimum absolute value of measured rolling moment represented 0.0453% of balance nominal capacity and was made at Mach 2.95 while the maximum was 0.7270% for a Mach number of 0.93.

For those specific cases where runs were intentionally repeated in order to get data for statistics calculations, from Table VIII, it can be observed that the total error related to interval limits for level of confidence of 95.0% is well correlated to the balance systematic error. Such results suggest that run-to-run repeatability of aerodynamic phenomena and test conditions was probably very good and that result dispersion on spin damping measurement was imputable to the balance systematic error.

TABLE VII

AERODYNAMIC COEFFICIENT MEASUREMENT ERRORS

5-Calibre Army-Navy Spinner

Results are expressed in % of measured values

MACH NUMBER PD/2V	CNA	CMA	XCP0	CA0

TOTAL ERROR
Interval Limits for Level of Confidence of 95.0%

1.156±0.13% 0.185	±15.20%	±14.72%	±3.43%	±0.87%
1.272±0.11% 0.200	±10.34%	±10.53%	±5.76%	±2.56%
1.272±0.17% 0.220	±14.89%	±13.03%	±2.68%	±2.12%
2.953±0.12% 0.107	±4.71%	±3.05%	±12.41%	±8.30%

TOTAL ERROR
Interval Limits for Level of Confidence of 80.0%

1.156±0.13% 0.185	±7.82%	±7.58%	±1.77%	±0.45%
1.272±0.11% 0.200	±5.71%	±5.82%	±3.18%	±1.41%
1.272±0.17% 0.220	±7.66%	±6.71%	±1.38%	±1.09%
2.953±0.12% 0.107	±2.42%	±1.57%	±6.39%	±4.27%

SYSTEMATIC ERROR (in % of average value)

Mach 1.156 PD/2V 0.185	±9.72%	±2.40%	N/A	±1.82%
Mach 1.272 PD/2V 0.200	±9.31%	±2.32%	N/A	±1.85%
Mach 1.272 PD/2V 0.220	±9.37%	±2.30%	N/A	±1.87%
Mach 2.953 PD/2V 0.107	±16.65%	±5.44%	N/A	±9.08%

TABLE VIII

SPIN DAMPING COEFFICIENT MEASUREMENT ERRORS
5-Calibre Army-Navy Spinner

Results are expressed in % of measured values

MACH NUMBER PD/2V	CLPC

TOTAL ERROR
Interval limits for level of confidence of 95.0%

1.156±0.13% 0.185	±19.24%
1.272±0.11% 0.200	±5.69%
1.272±0.17% 0.220	±6.60%

TOTAL ERROR
Interval limits for level of confidence of 80.0%

1.156±0.13% 0.185	±8.43%
1.272±0.11% 0.200	±2.49%
1.272±0.17% 0.220	±2.89%

SYSTEMATIC ERROR (in % of average value)

Mach 1.156 PD/2V 0.185	±7.94%
Mach 1.272 PD/2V 0.200	±8.24%
Mach 1.272 PD/2V 0.220	±8.38%

11.0 DISCUSSIONS

The DREV 0.6-m x 0.6-m indraft wind tunnel performs very well in aerodynamic coefficient measurement through the use of wind tunnel balances but at low Reynolds numbers and low static pressures and densities in its test section.

There was no search for a specific aerodynamic phenomena related to this experiment but an interest to demonstrate the feasibility to perform measurements of spin-induced effects which are mainly the Magnus force/moment and spin damping characteristics. This is particularly true in the case of a smooth and sharp nose projectile such as the 5-Calibre Army-Navy Spinner model. Therefore, only Magnus force and spin damping data are discussed here. Also, several aspects on the behavior of the base pressure results and measured total drag coefficients are commented in the present discussions just as future prospects of testing spinning models, since present test series were to set basis for further work.

11.1 Measurement of Magnus Effects and Spin Damping

Figures 35 and 37 show that when tests are being performed with a sweep of angle of attack large enough (i.e -5 deg to +15 deg), it is possible to obtain results that follow predictable tendencies. The balance used for these tests had not the nominal capacities and the accuracy suitable for the level of side forces (i.e. Magnus effects) that were measured. Nevertheless, CY (Magnus force) versus angle of attack results presented in Fig. 35 show a very linear increase in spite of a relatively large scatter. If Magnus effects data similar to Fig. 35 could be obtained on a regular basis, average lines could be passed through the result scatter which would provide a level of confidence at least satisfactory for purposes of wind tunnel comparative studies.

It is worth to mention that Magnus effect results presented in Figs. 35 and 37 were in the correct and predicted sense. As mentioned in Refs. 10 and 39 to 60, the Magnus effects are viscous phenomena's almost entirely induced by the boundary layer. They are very difficult to reproduce in wind tunnel, and it is not rare that reverse Magnus effects are observed (i.e. Magnus forces or moments in reverse sense than they should be). Sometimes it can be due to the development of asymmetric vortices (Ref. 4) resulting into pressure distributions that produce forces making measurements to show spin-induced forces/moments in a reverse sense than expected.

Results of CY (Magnus force) versus angle of attack of Fig. 37 come from test runs performed at various spin rates (35,000, 31,000 and 26,000 RPM) but same Mach number. It shows that the slope of CY increase with angle of attack is less for lower spin rates. It suggests that measured Magnus forces were rather linearly dependent of spin rate (or PD/2V). By then, CYP coefficients (CY reduced with respect to PD/2V) to be obtained in DREV tunnel should to be rather consistent; i.e. CYP coefficients should be stable, at least for that configuration, and show similar values whatever a test is performed at medium or high spin rates. As wind tunnel testing is concerned, such behavior is highly desirable, but observations could be different for another model configuration.

Figures 64 and 65 show a comparison of free-flight data from Ref. 2 (BRL Report #876), Ref. 3 (AEDC-TR-70-12) and Ref. 4 (AGARDograph No.171) with data from present test series. From Fig. 64, it is observed that although few measurement data results of Magnus coefficient from DREV follow tendencies shown by free-flight tests, most of these results do not follow the same tendencies. It must be mentioned that CYP-ALPHA data from free-flight tests are based on smaller angle of attack variations (2-3 deg) than those from DREV wind tunnel test runs normally dedicated to such measurement (-5 to +15 deg). Also, in present wind tunnel test series, only few runs were done at ±15 deg in order to evaluate if Magnus effects could be observed. As most of tests runs were made from -2 to +2 deg with an unsuitable balance, it was not possible to identify with enough accuracy Magnus effects in these particular tests.

In spite of the low Reynolds numbers and low static pressures and densities in the DREV trisonic wind tunnel, reverse Magnus effects were not observed. The only detrimental condition was the unsuitability of the balance that was utilized.

In Fig. 36, spin damping coefficients from tests made in right and left senses of rotation were very similar from 0 to +8 deg of angle of attack. From +8 deg to +15 deg of angle of attack, left rotation test results display a sudden change of the slope versus

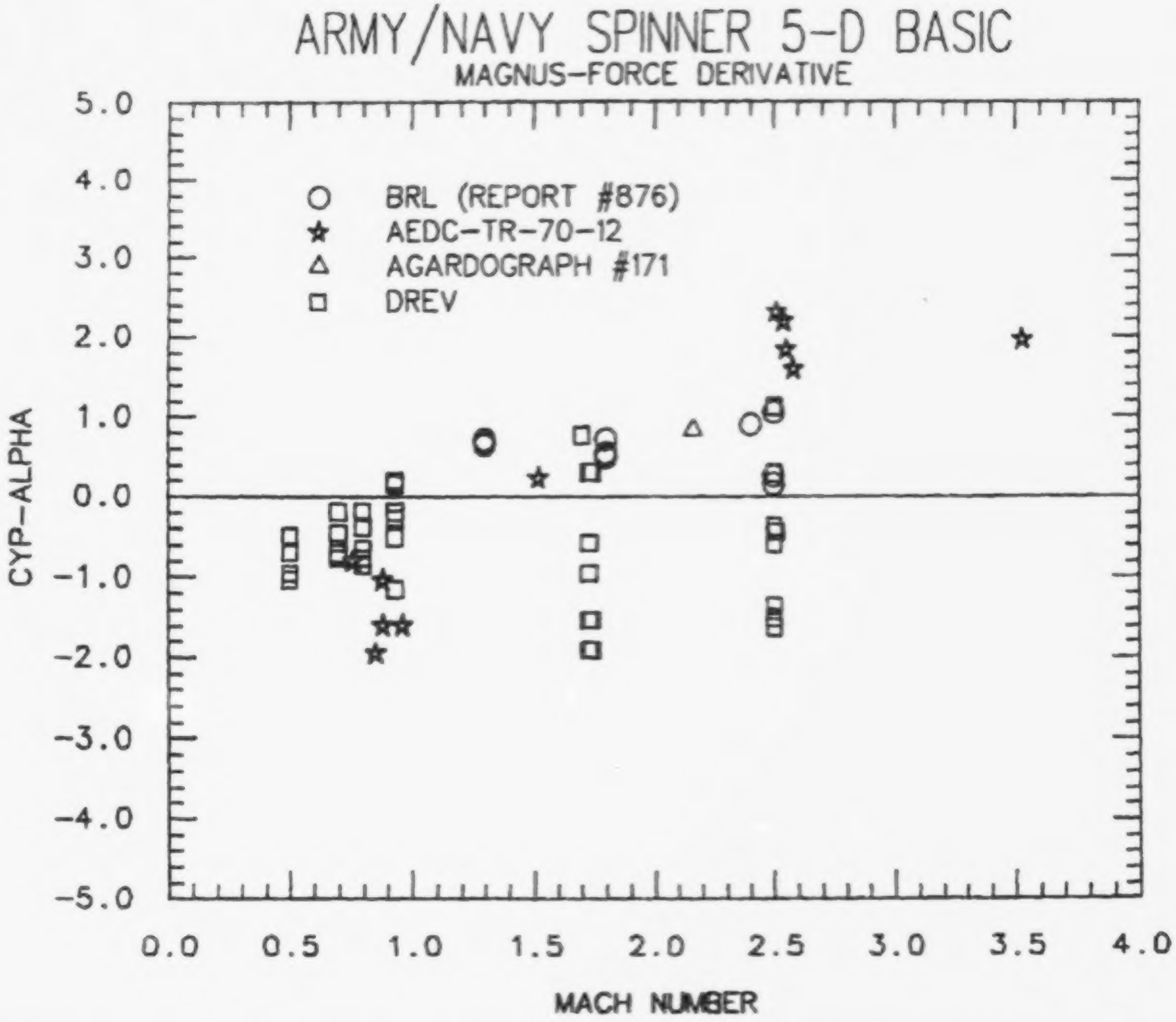

FIGURE 64 - Comparison with free-flight tests of CYP-ALPHA as measured in DREV trisonic wind tunnel

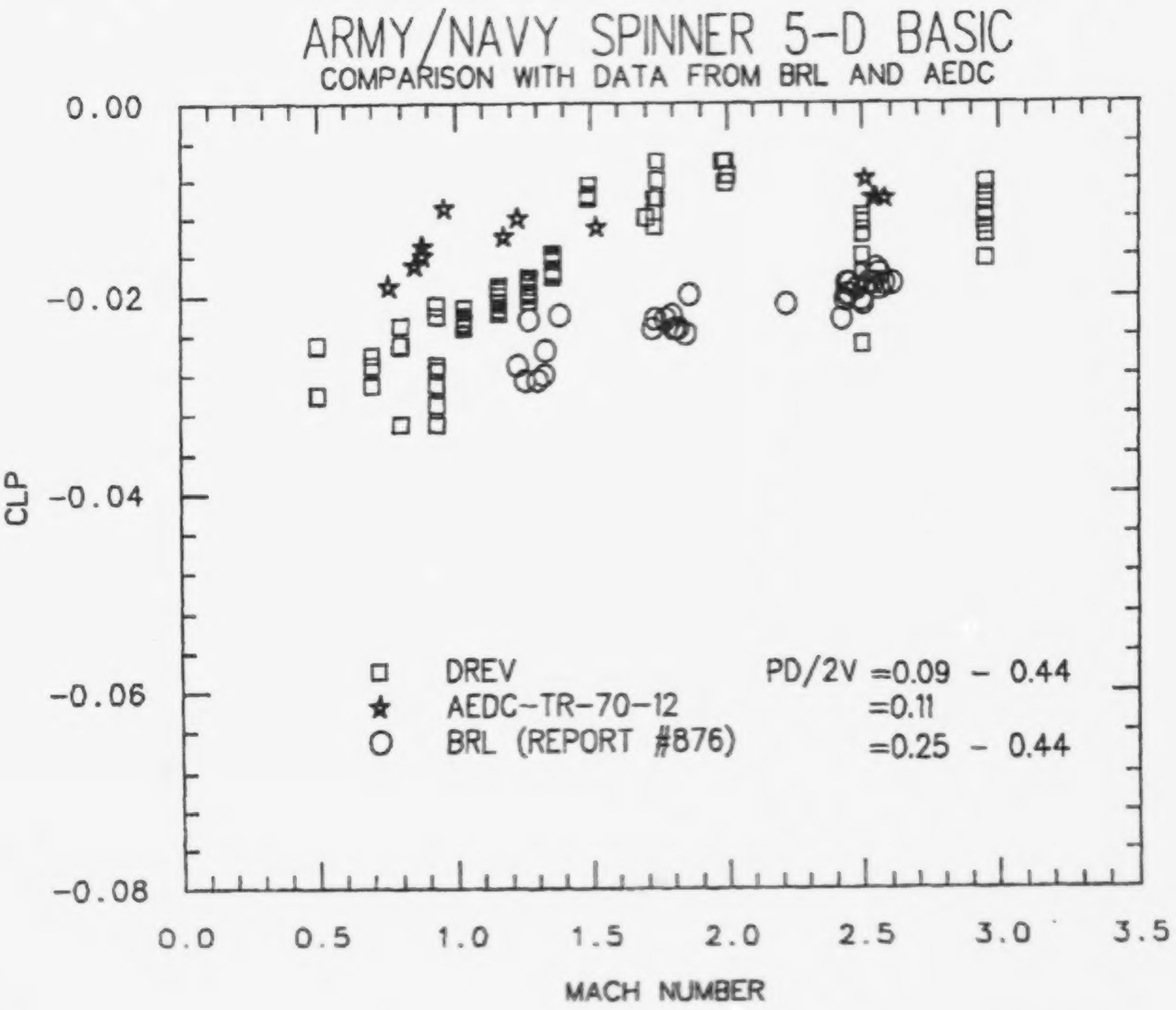

FIGURE 65 - Comparison with free-flight tests of spin damping coefficient as measured in DREV trisonic wind tunnel

angle of attack. As explained in Appendix D, the balance was utilized at a too low percentage of its nominal capacity and such inaccuracies were to be expected (and quantitatively predictable). In spite of such result scatter, by performing test runs in right and left senses of rotations and calculating the average (Chapter 6.0, Appendices A and D), it was possible to obtain data of a level of accuracy high enough for purposes like wind tunnel comparative studies. Much more accurate results should be obtained with the new balances and calibrator in development process.

Although from Fig. 65 it can be observed that CLP values obtained with the spin rig show large scatter, they are within the spread of free-flight data from Refs. 2 and 3. The lack of accuracy from the balance has produced this large result scatter.

It is to be noted that some authors non-dimensionalize spin damping using PD/V and care must be taken when comparisons are made. Since in the present memorandum all results use PD/2V, appropriate corrections to other experimental data from references have been made when necessary.

11.2 Influence of the Sting Interference on Model Base Pressure

As an attempt to consider the influence of sting support interference on model base flow and base pressure ratio (P_{base} / P_{inf}), a methodology was developed to calculate corrected values of CAO..

Figure 66 (Ref. 12) presents experimental data on the variation of axisymmetric supersonic base pressure ratio with respect to Mach number for slender bodies of revolution and also makes comparison with the 5-Calibre Army-Navy Spinner model base pressure data from present tests series.

From Fig. 66 (Ref. 12), it can be observed, for most practical purposes, that for a given Mach number (and $\gamma = 1.4$) the average pressure ratio on the base of a projectile can be considered constant. It is also well known that the base pressure depends on the relative thickness and character (i.e. laminar, transitional or turbulent) of the boundary layer approaching a blunt base. As an indication, Fig. 66 which shows some theoretical and experimental comparisons of base pressure ratio variation with Mach number, and

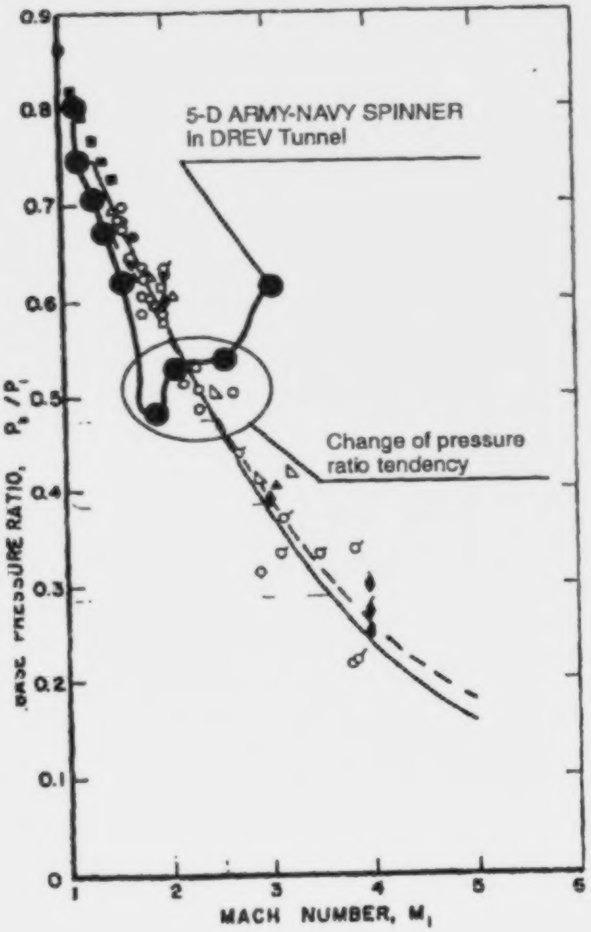

FIGURE 66 - Axisymmetric supersonic base pressure with respect to Mach number for slender bodies of revolution compared with 5-Calibre Army-Navy Spinner model base pressure behavior (from Ref. 12)

for different conditions of approaching boundary layer. It can be observed that base pressure is mainly influenced by the Mach number, and relatively small scatter of experimental data points representative of various conditions of approaching boundary layer suggests its relatively secondary effect.

The 5-Calibre Army-Navy Spinner model base pressure ratio data from present test series (Table IX) and plotted in Figs. 66 and 67 were derived from CAB data values with the following equations:

$$CAB_{\alpha=0} = CDT - CDF \quad \text{for } \alpha = 0 \text{ deg}$$

$$\frac{P_{base}}{P_{\infty}} \text{ DREV wind tunnel} = 1 - \frac{\gamma \cdot M^2}{2} \cdot CAB_{\alpha=0}$$

Values of averaged CAO from Table BIV were then recalculated (Table IX) by replacing measurement base pressure ratios by values given in Fig. 66 (Ref. 12). The following equation was used:

$$CA0_{corrected} = CAO - CAB_{\alpha=0} + \left[\left(Pinf - Pbase \right) / Pinf \cdot \frac{2}{\gamma \cdot M^2} \right]$$

where values of (Pinf - Pbase)/Pinf are presented in graphical form in Fig. 67. Values of $CA0_{corrected}$ were plotted in Fig. 68.

TABLE IX

5-D Army - Navy Spinner

MACH	$\frac{P_{base}}{P_{\infty}}$ CORR	CAO	$\frac{P_{base}}{P_{\infty}}$ DREV	$CAB_{\alpha=0}$	$CA0_{corrected}$
1.03	0.850	0.397	0.825	0.236	0.364
1.16	0.825	0.468	0.749	0.267	0.387
1.27	0.780	0.442	0.710	0.257	0.380
1.36	0.765	0.415	0.681	0.247	0.350
1.48	0.680	0.406	0.627	0.243	0.372
1.73	0.630	0.406	0.480	0.248	0.334
1.99	0.572	0.328	0.530	0.169	0.313
2.50	0.450	0.252	0.537	0.106	0.272
2.95	0.373	0.205	0.614	0.0633	0.245

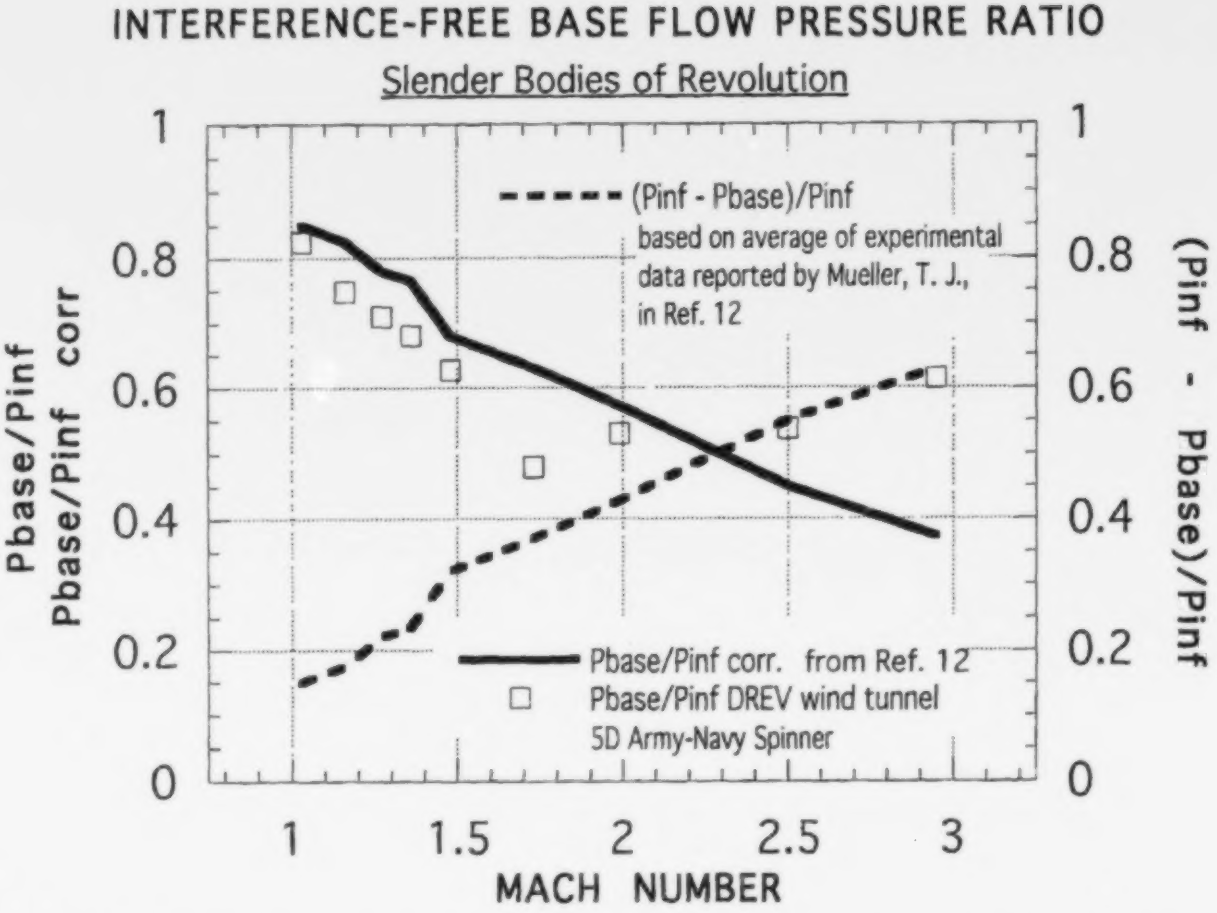

FIGURE 67 - Base pressure ratio data used to calculate corrected CAO coefficients

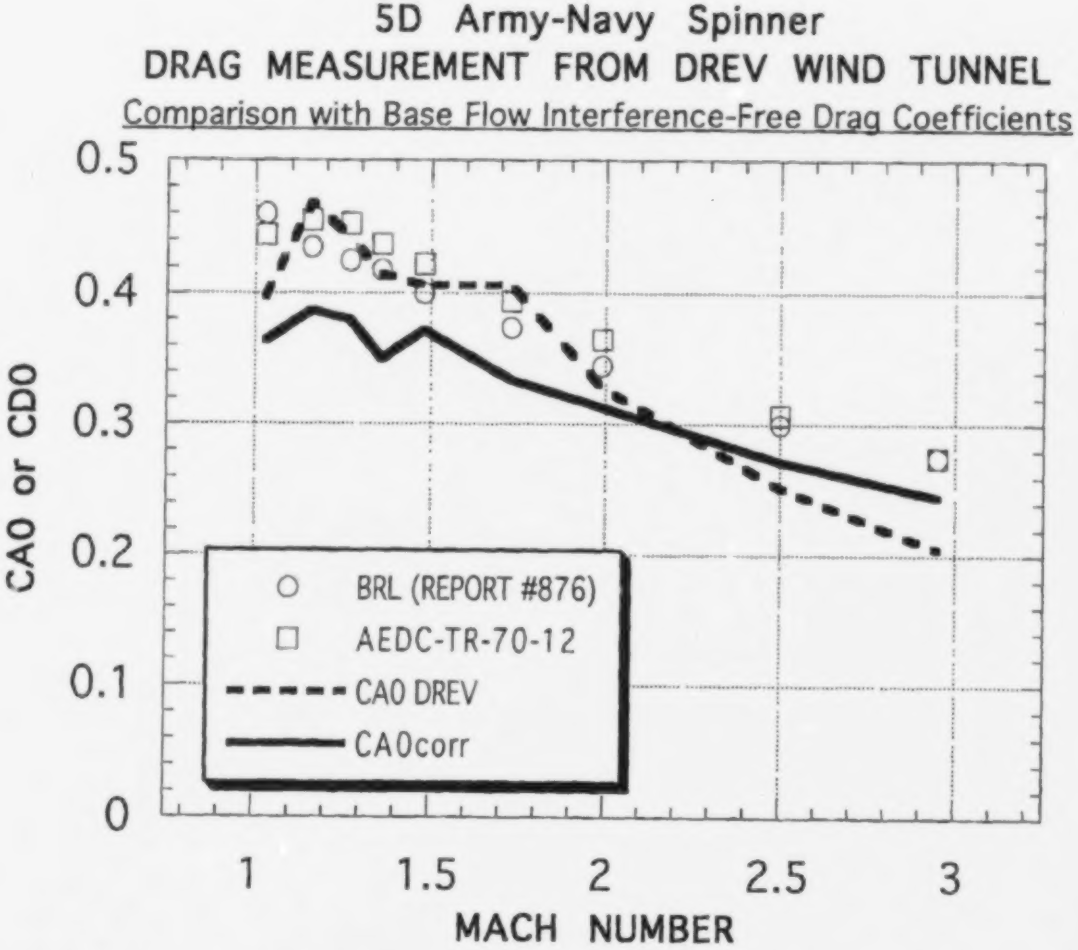

FIGURE 68 - Corrected CAO coefficients for base pressure variations induced by sting support interference and comparison with free-flight tests

It can be seen from Fig. 66 that base pressure ratio measured with the 5-D Army-Navy Spinner model would be close to experimental data for slender bodies of revolution between Mach 1.0 to 1.5, and follow a similar tendency up to Mach 1.75. Results at Mach 2.0 would also be similar. Results suggest that variation of the base pressure ratio versus Mach number showed a tendency in reverse sense for the 5-D Army-Navy Spinner model in presence of the sting support. Also, the base pressure ratio swerve (Fig. 6) observed between Mach 1.75 and Mach 3.0 would be an indication for the base pressure to behave more normally up to Mach 1.75 and that a reverse tendency would happen only at higher Mach number. To confirm such assumption more tests should be made between Mach 1.0 and 4.0.

From Fig. 68, it can be observed that recalculated values of CAO have smoothed the step at Mach 1.75 displayed by measured CA0 (CA0 DREV). Below Mach 2.2, corrected CA0 values have decreased while they have increased between Mach 2.2 to 3.0. A tendency for the drag to increase while approaching Mach 1.0 is considered as typical.

It is recognized that experimental conditions providing a similitude in the velocity profile and in the relative thickness of the boundary layer approaching the model blunt base (i.e. laminar, transitional or turbulent) should result into a base pressure distribution rather similar to that of a projectile in free-flight (as per Ref. 12 mainly and associated Refs. 13 to 36). At the present state of knowledge, theories suggest that primordial dependence of the base pressure ratio would be on the relative location of the recompression zone downstream of the model base and value of recompression (or reattachment) pressure (see Refs. 12, 19, 20, 21, 22, 29, 32, 33, 34). It is generally recognized that:

a- A turbulent boundary layer results into a higher base pressure than a laminar one,

b- A higher Mach number results into a lower base pressure.

It appears with evidence that presence of the sting support just inside the reattachment (recompression) zone affect for a great deal the value of that recompression and also create a new location (virtual) for that recompression.

Such variations of the base pressure ratio attributed to the presence of the sting support were already observed in the DREV trisonic wind tunnel. Tests had been made with the DREV-ISL reference models which reproduced the "Southampton University Calibration Model, 2D Configuration" and featured mainly a nose-cone/cylinder with/without trapezoidal fins. The base pressure measurement results obtained with these models were reproduced in Fig. 69 (Ref. 37) where the curve related to the DREV-ISL Cone/Cylinder model without fins present a remarkable similarity with that of Fig. 66. As base drag and base pressure measurement are concerned for the DREV wind tunnel, Ref. 38 present the description and results of test run series that were made and dedicated to find the " real " values of base drag and base pressure for several projectile base configurations.

11.3 Rationale of Testing Spinning Models and Future Prospects

Such a discussion is a rather current practice with wind tunnel facilities in the presentation of their experiment description reports. It comes from the imperative necessity to constantly update their own balance-sheet of practical interests why their facilities are being used and also to yield new experimental potentials, diversification and evolution of measurement capabilities which are as much secondary effects of their sustained activities.

Primordial tests in DREV 0.6 m x 0.6 m wind tunnel were usually made under the form of experimental comparative studies in order to identify optimized flight body configurations under development (more discussions on that aspect are made below).

For those tests, experimentalist did not had a control on the Reynolds numbers obtained in test section although they were able to determine their values. By then, the results had to be accepted as they were with the consequences related to the unmatched Reynolds numbers. That is why, most of the time, preliminary investigations had to be made with so-called reference

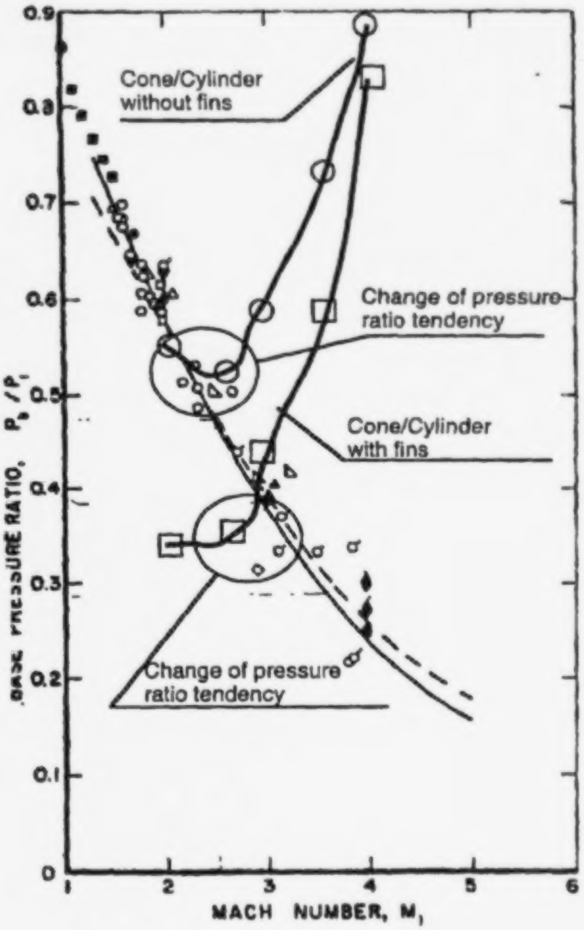

FIGURE 69 - Axisymmetric supersonic base pressure with respect to Mach number for slender bodies of revolution compared with cone/cylinder models base pressure behavior (from Ref. 37)

or calibration models in order to determine if discrepancies in Reynolds numbers could have invalidated a part of the experiment, if not all.

While reporting such wind tunnel test series, it was (and should always be) mandatory, to ascertain reliability of data, to present the results from the preliminary tests with calibration models and compare them with those from other wind tunnel facilities (and from which abundant data are usually available). At DREV, it has been frequent to use an AGARD-B or an Army/Navy Spinner 5D model as reference models.

As a secondary application, the DREV indraft wind tunnel facility has been used several times to produce preliminary aerodynamic data dedicated as input figures for flight simulation programs. These trajectory simulations were usually utilized in a first time to generate interim bombing tables or artillery firing tables, and this before trajectory data obtained from air bomb releases or gun firings were used to finalize firing/bombing tables.

In the last few years, very powerful computational fluid dynamic (CFD) programs have been available on the market. Their use is rapidly increasing for research and development work oriented towards improvement for performance of various flight vehicle aerodynamic configurations. It results that CFD (and analytical) works and experimental aerodynamics will be intricate together more than ever in further aerodynamic scientific research work as two complementary activities. It is unlikely that new aerodynamic configuration developments will rely on experimental aerodynamics in the same manner as it was the case in the past.

For some particular test cases where small bullets have to be experimented in the DREV trisonic facility while using rather large spinning models, it shall be possible to reproduce simultaneously the Mach number, the Reynolds number and the streamline helix angle over the model surface (PD/2V). For most of the time, with other types of projects, it will be only possible to match the Mach number and PD/2V values with those of the real flight body. The Reynolds number in the wind tunnel being usually several times less than for free-flight conditions. The effect of such discrepancies shall be minimized if the laminar and/or turbulent flow regime conditions proper to real free-flight cases can be reproduced for the wind tunnel tests (although at "much" different Reynolds numbers).

The results then obtained should constitute a valuable help to validate CFD studies and new codes if numerical simulations are being made to take into account the specific conditions encountered in the DREV wind tunnel facility. Although the real free-flight conditions are different, if computations can be compatible with wind tunnel measurements, it is believed that chances are good for those simulations of interest (proper to real flight) to be reliable. The subsequent extrapolated data from CFD calculations (simulating free-flight aerodynamics) are used to verify and study the flight dynamics of the project flight vehicle.

Because there is no deterministic solution (i.e. analytical or numerical) to optimize forever an aerodynamic configuration, it will always be possible to imagine improvements never seen before. Then more and more sophisticated configurations that will imply unforeseen phenomena's surpassing those deterministic calculation capabilities shall make necessary a direct experimental observation (it is believed for some while).

Because the flow characteristics encountered in the DREV wind tunnel rarely reproduced conditions of free-flight, wind tunnel tests shall often give overall aerodynamic coefficients that differ from those obtained from aeroballistic range facilities or C~~DF~~FD calculations. Although it could be argued that such aerodynamics data are only valuable to constitute a data bank, they are very useful for comparison purposes in order to identify/differentiate the particular characteristics of some particular configurations when large series are being studied; (i.e. although aerodynamics coefficients obtained from the wind tunnel could present some non-linear apparent shifts, a best lifting configuration in the wind tunnel, for example, will remain a best lifting body in free-flight).

The DREV wind tunnel facility offers a testing environment that makes possible to perform a diversity of flow measurements. In the past, this data used to be of a very useful help to understand the aerodynamics related to a specific configuration because measuring apparatus can be localized in a particular area on the model surface or in the surrounding flow. Then, almost any particularities of the aerodynamics of any configuration can be studied in isolation.

As future prospects of testing spinning model in the DREV trisonic facility are concerned, primordial interests could be listed as follows:

a - The new DREV balances (high precision) specially designed to be used in conjunction with the spin rig apparatus shall be available in a near future. When ready, a wind tunnel test series should be initiated in order to verify the accuracy of Magnus effects and spin damping measurements that can be achieved in the DREV trisonic facility.

b - The new 6-DOF calibrator that will provide simultaneous balance loading, increase accuracy and resolution will be available in a short while. It could be used to perform multi-load calibration of one of the Able MK-X-A 0.50 in or (preferably) Able MK-VI-A 0.50 in balance (but in repaired or undamaged conditions). A noticeable increase of accuracy would then result, rendering Magnus effects and spin damping measurements probably within the standards of today's.

c - The aerodynamics effects induced by the spinning motion of a flight body are entirely dependent on the behavior of the boundary layer, which is affected by the spinning motion. In consequence of that, the experimental study of the boundary layer over the surface of spinning models would be a next logical step. As the DREV trisonic facility is concerned, it could be achieved as follows:

Reference 61 presents a typical wind tunnel investigation of the boundary of a spinning wind tunnel model whose configuration approached the Army/Navy Spinner 5D model. Measurements were made within the boundary layer by using dedicated pitot probes configured for the purpose (flat beak shape) to approach the surface as close as possible. Figures 70 and 71 are reproduced from Ref. 61 and show the model and probe apparatus in the test section of the Naval Ordnance Laboratory's Supersonic Tunnel No.2. Tests were conducted at Mach numbers of 3.02 and 4.10 and spin rates around 23,000 rpm (PD/2V=0.2).

At DREV, in order to make it possible to explore the flow over the surface of a projectile model, the necessary instrumentation has been developed and built for that purpose (was tested with static wind tunnel models). A boundary layer and flow exploration system was built in order to measure the velocity profile and static pressure. The static and total pressure probe tips can be adjusted at various distances from the projectile, and also at various angles. Flat beak configured probe tips are being used to explore the near-to-surface boundary layer, while cylindrical probe tips are substituted to explore the flow at distances over 0.5 in from the model surface.

With time, electronic pressure measurement devices have been developed, making possible some very elaborated surface static pressure and boundary layer wind tunnel surveys. A crucial problem remain the adapted configuration to be given to the static/total pressure probes, the dimensioning of pressure taps and the design/development of non-intrusive transverse mechanical probe support. A great deal of research was made in the past on the subject and Refs. 62 to 69, although not recent, present an overview of these apparatus which are still in use but ~~use~~ need to be connected to more sophisticated electronics.

An ONERA 5-holes-type non-intrusive probe designed for the measurement of orthogonal flow velocity components was designed and fabricated at DREV (but has not yet been experimented). It is described in Figs. 72 to 75. This probe would be very useful to explore the aerodynamic effects in the surrounding flow of a spinning wind tunnel model.

The whole system features a telescopic arrangement allowing the 0.120 in diameter non-intrusive probe to extent up to 6.5 in from its streamline main support (Fig. 72) which is 0.50 in in diameter. The length adjustment is made by using the 5-40 UNC x 1/8 LG set screw (Fig. 73) to maintain the telescopic probe at a desired location. The probe miniature fore end cone (Fig. 74), which is 0.120 in in diameter, bears five 0.016 in total pressure taps whose

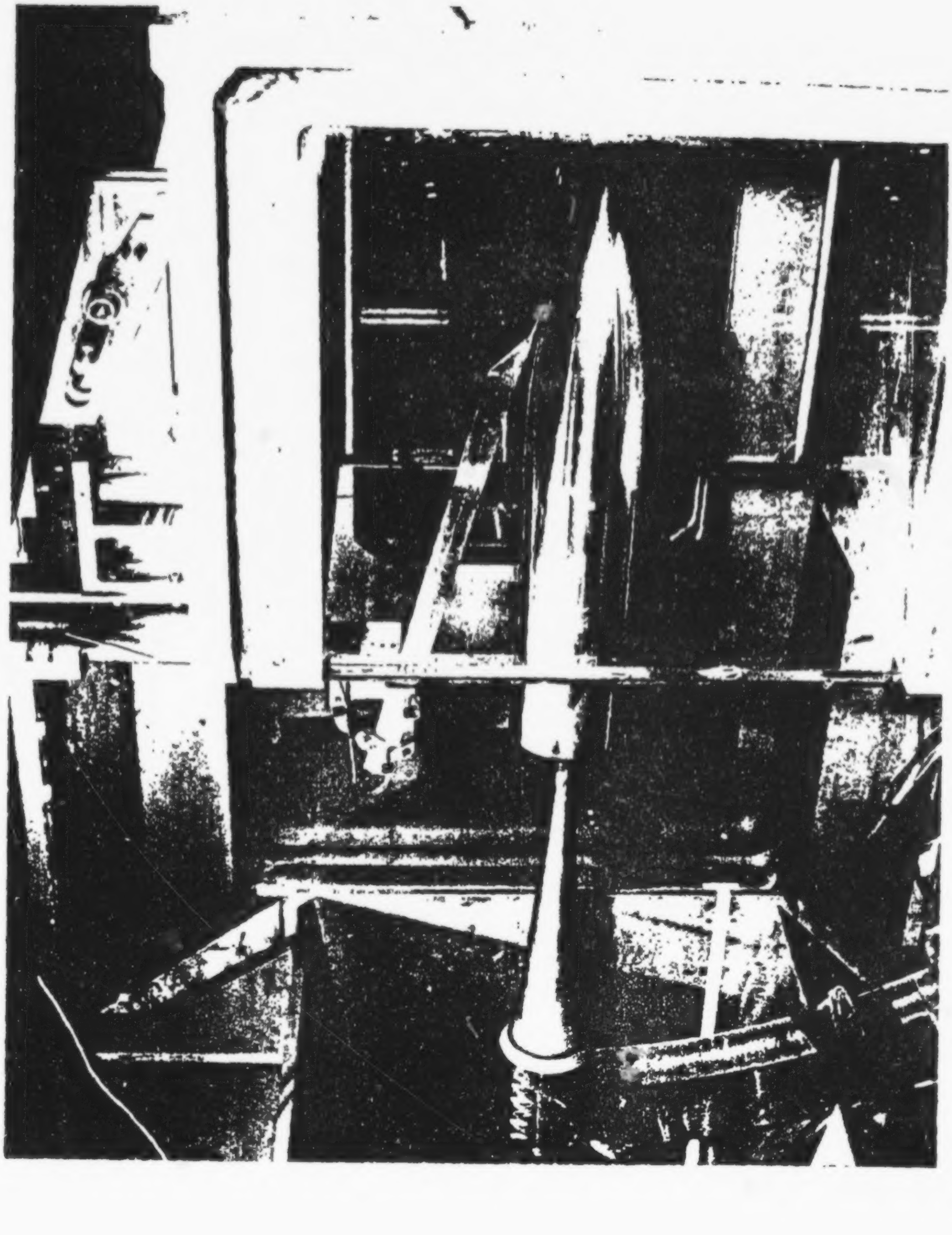

FIGURE 70 - Ogive-Cylinder 5-D model and traversing mechanism in Naval Ordnance Laboratory's Supersonic Tunnel No. 2

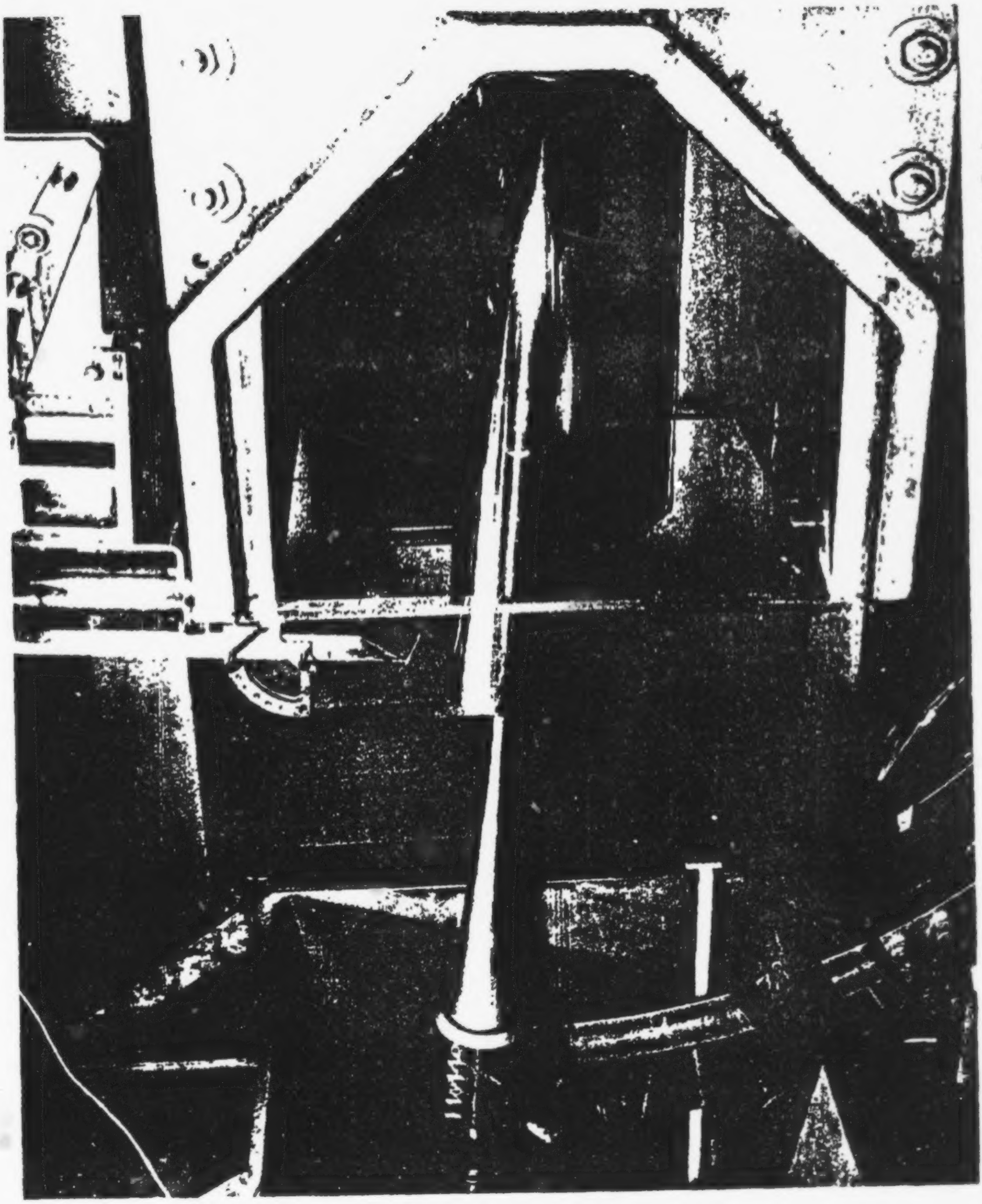

FIGURE 71 - Ogive-Cylinder 5-D model and traversing mechanism in Naval Ordnance Laboratory's Supersonic Tunnel No. 2

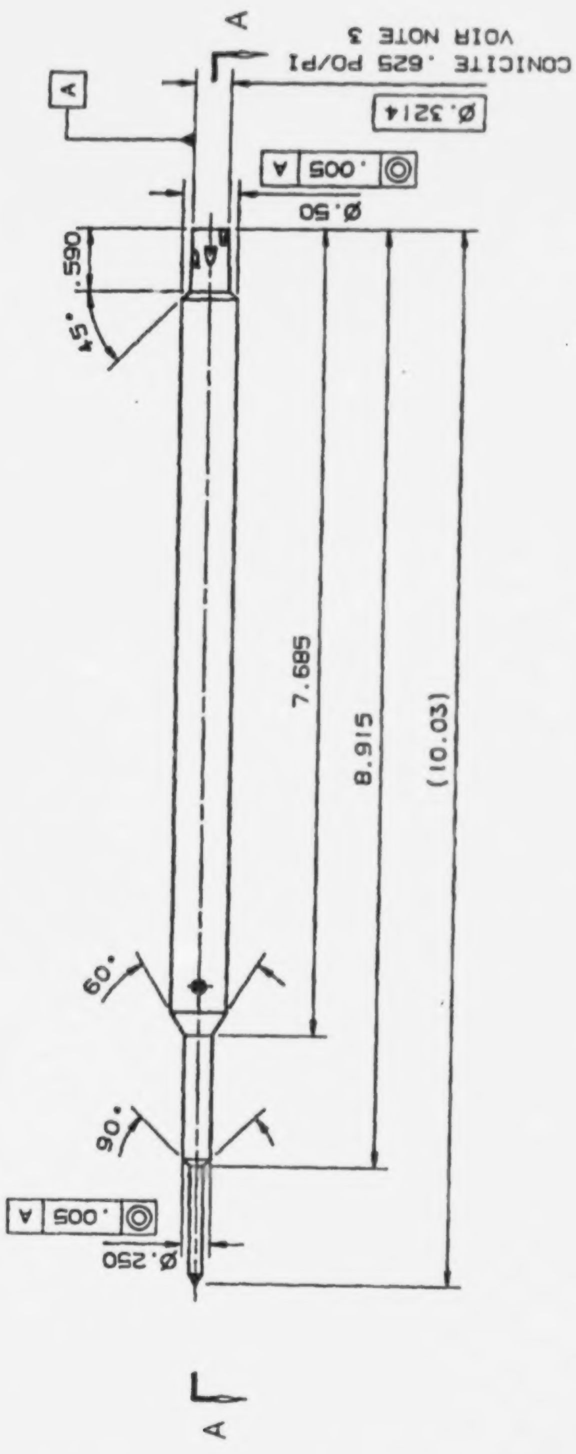
A
CONICITE .625 PO/PI
VOIR NOTE 3
Ø.3214
.005 A
Ø.50
.590
45°
7.685
8.915
(10.03)
60°
90°
.005 A
Ø.250
A

FIGURE 72 - ONERA type non intrusive probe, orthogonal flow velocity component measurements, dim. in in

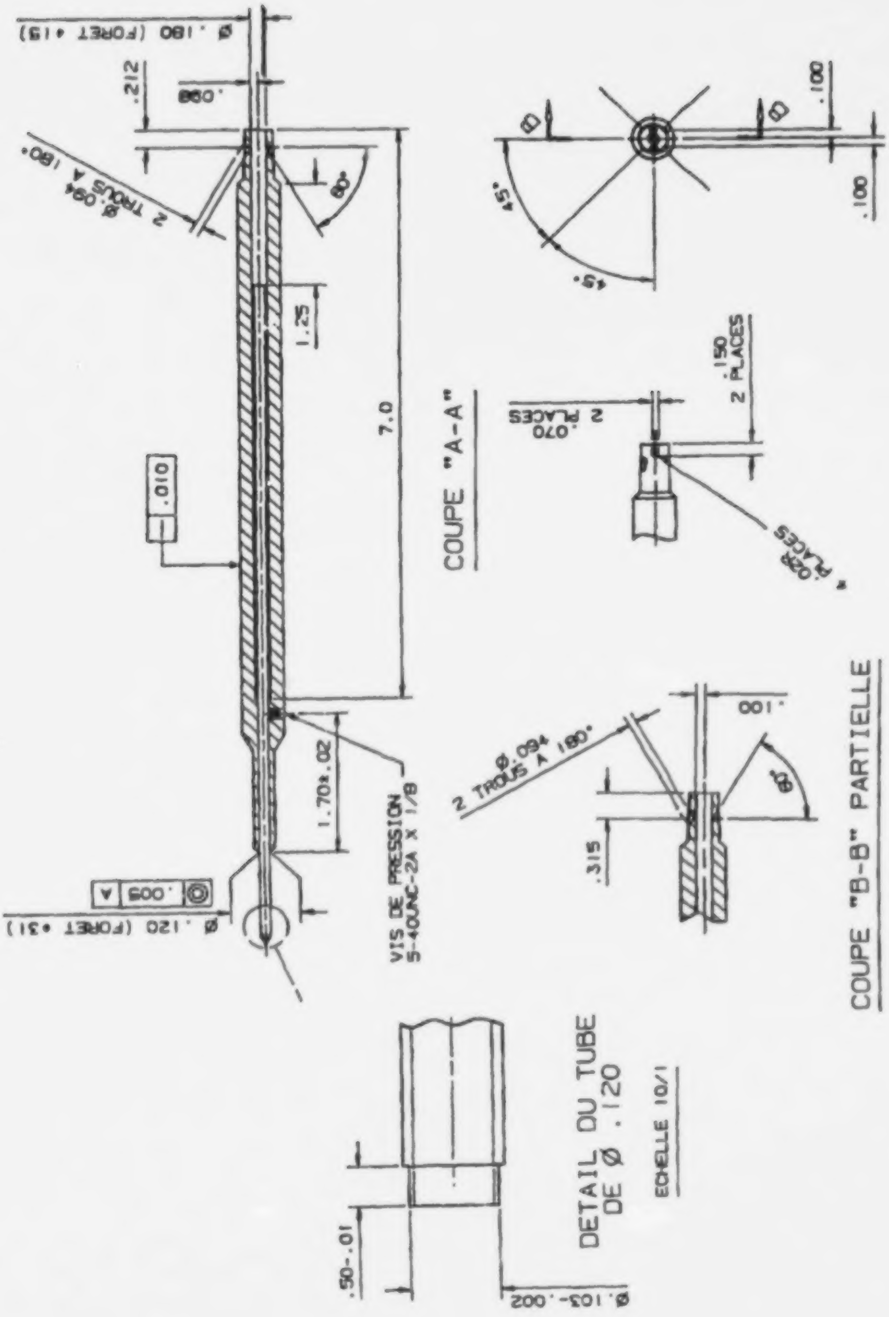
Ø .180 (FORET #15)
.212
.088
Ø.094
2 TROUS A 180°
60°
1.25
7.0
.010
COUPE "A-A"
45°
45°
.100
.100
.070
2 PLACES
.150
2 PLACES
.028
PLACES
COUPE "B-B" PARTIELLE
.100
Ø.094
2 TROUS A 180°
60°
.315
1.70±.02
VIS DE PRESSION
5-40UNC-2A X 1/8
Ø .120 (FORET #31)
.005 A
DETAIL DU TUBE
DE Ø .120
ECHELLE 10/1
.50-.01
Ø.103-.002

FIGURE 73 - ONERA type non intrusive probe, orthogonal flow velocity components measurement, dim. in in

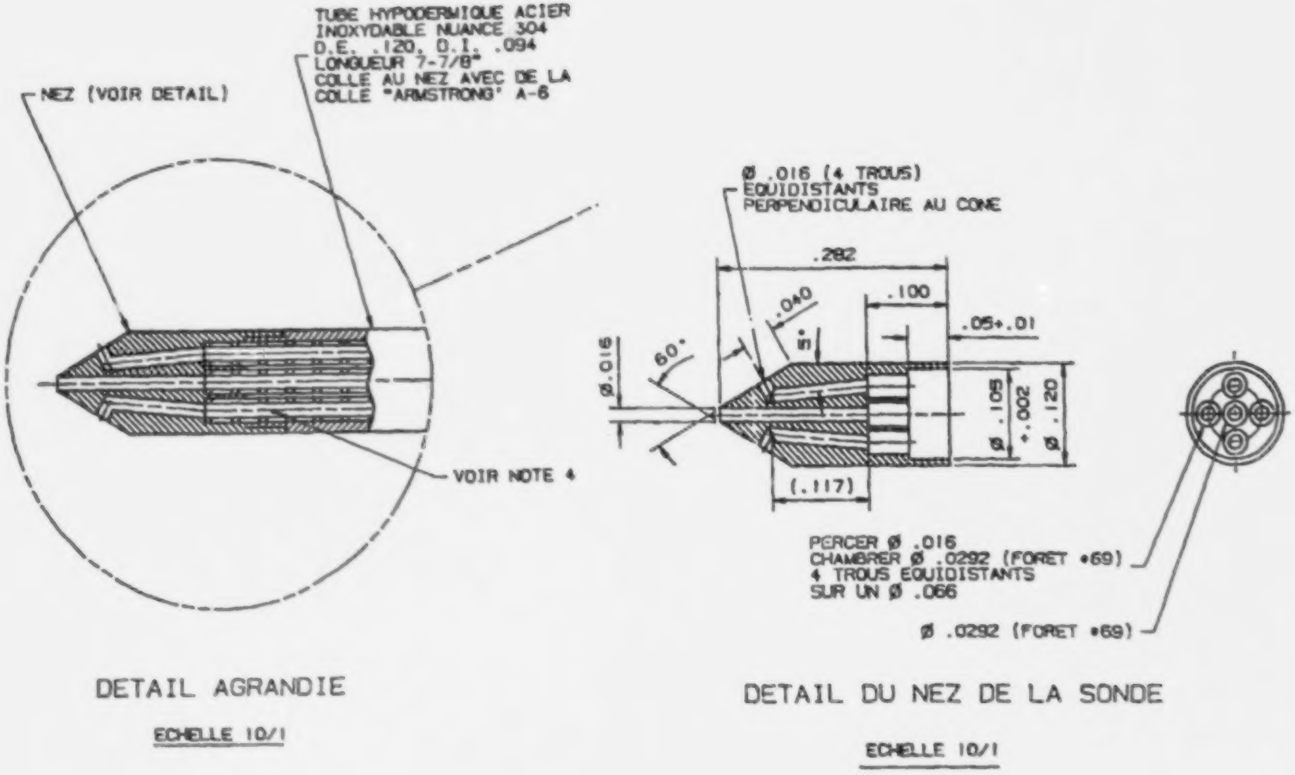
NEZ (VOIR DETAIL)
TUBE HYPODERMIQUE ACIER
INOXYDABLE NUANCE 304
D.E. .120, D.I. .094
LONGUEUR 7-7/8"
COLLE AU NEZ AVEC DE LA
COLLE "ARMSTRONG" A-6
VOIR NOTE 4
Ø .016 (4 TROUS)
EQUIDISTANTS
PERPENDICULAIRE AU CONE
.282
.040
.100
.05+.01
5°
Ø.016
60°
Ø .105
+.002
Ø .120
(.117)
PERCER Ø .016
CHAMBRER Ø .0292 (FORET #69)
4 TROUS EQUIDISTANTS
SUR UN Ø .066
Ø .0292 (FORET #69)

DETAIL AGRANDIE

ECHELLE 10/1

DETAIL DU NEZ DE LA SONDE

ECHELLE 10/1

FIGURE 74 - ONERA type non intrusive probe, 5 pressure taps conical nose tip, dim. in in

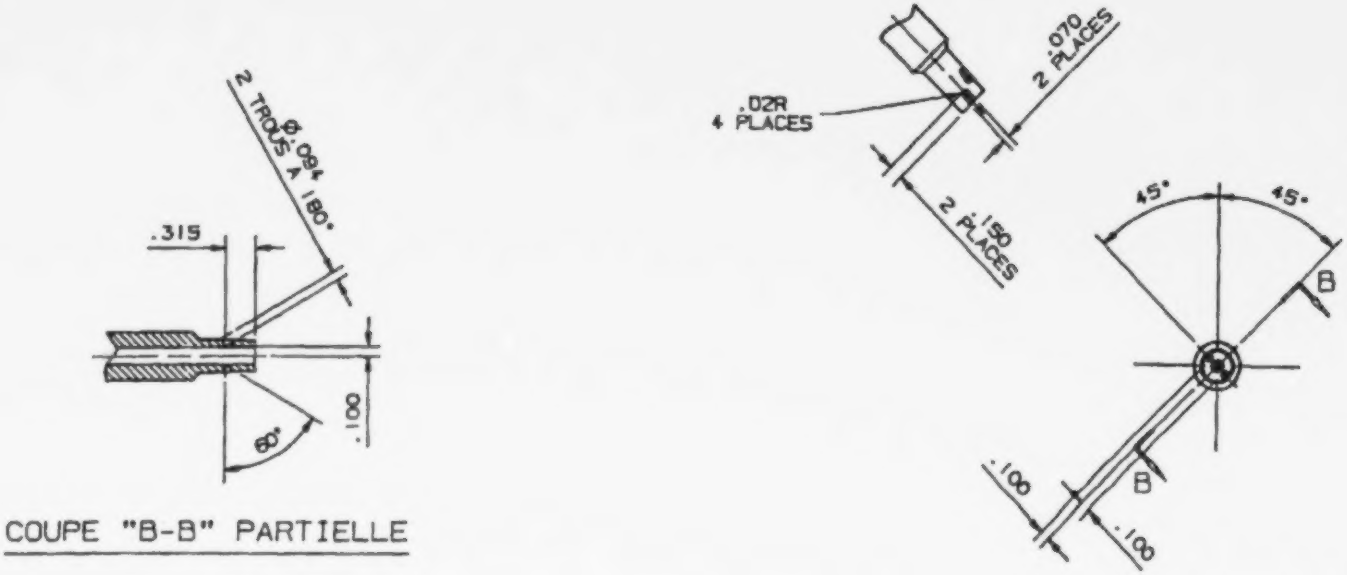
.315
Ø.094
2 TROUS A 180°
.100
60°
COUPE "B-B" PARTIELLE
.02R
4 PLACES
.070
2 PLACES
.150
2 PLACES
45°
45°
B
B
.100
.100

FIGURE 75 - ONERA type non intrusive probe, conical fixation, dim. in in

individual tubings exit through the aft end main support conical fixation. This fixation is similar to the one on the 0.50 in ABLE balances and adequate adaptor/s must be used in order to hold the ONERA probe at a desirable location somewhere around a spinning projectile model. Figure 76 presents generic diagrams (from Ref. 70) that show the functioning (see also Refs. 71 and 72).

The final resultant of Magnus effects is an alteration to the pressure distribution over the surface of a spinning body. The possibility to measure the static pressure at some point on the surface of a spinning wind tunnel model would provide useful data to the comprehension of Magnus effects.

In order to make it possible to explore the static surface pressure on a spinning model, the necessary instrumentation has been developed and built at DREV for that purpose (has not yet been tested). The apparatus was originally designed to study the influence of approaching boundary layer on the base pressure distribution. In order to not disturb the base flow by any kind of downstream sting-support, the test model had to be held from its fore end by the upstream sting/pivot/after-body combination system (designed and built at DREV for testing in the 0.6m x 0.6m Indraft Wind Tunnel). Because of such a mechanical arrangement, only part-model consisting of base/after-body could be tested.

In order to make possible (base/after-body) flow surveys as a function of boundary layer characteristics, the upstream sting was fitted with aspiration holes connected to a proper aspiration system in order to alter the boundary layer velocity profile around the base/after-body test model.

The principle of work is based on sliding seal technique. It consists of series of pressure holes, localized on a same radial plane and fitted with seals that slide on the inside surface of the model spinning outer shell. The outer shell itself bears pressure taps localized on four radial planes and at a same distance with respect to the model base, in order to let them match the pressure holes four times per revolution. During a test run, while the model is spinning, the static pressure inside each pressure holes come to a state of equilibrium after a short time. Measurements can then be made. By

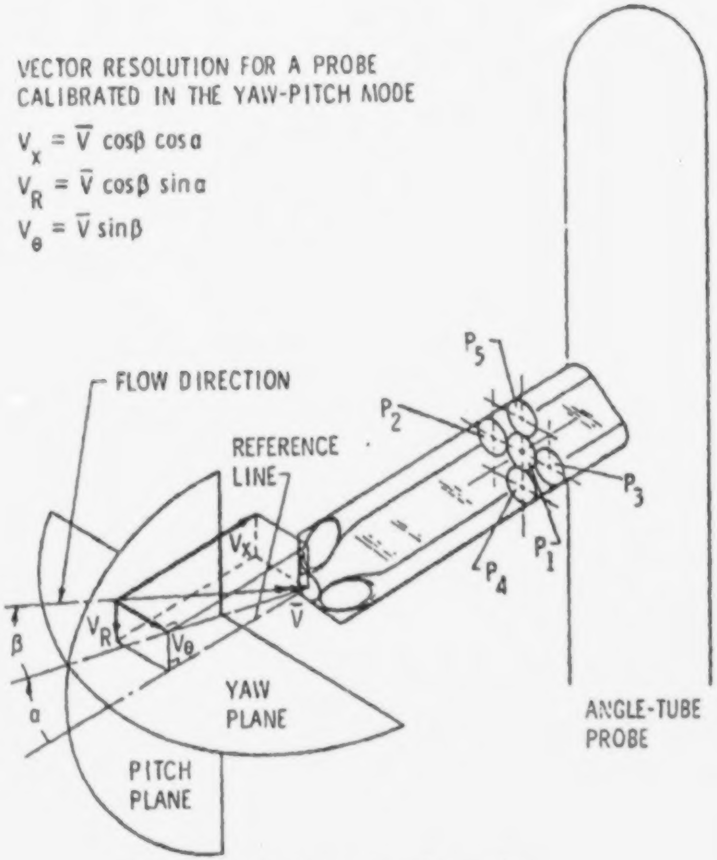
VECTOR RESOLUTION FOR A PROBE CALIBRATED IN THE YAW-PITCH MODE
$V_x = \bar{V} \cos\beta \cos\alpha$
$V_R = \bar{V} \cos\beta \sin\alpha$
$V_\theta = \bar{V} \sin\beta$
FLOW DIRECTION
REFERENCE LINE
P_2
P_5
P_3
P_1
P_4
V_{X1}
V_R
V_θ
$\bar{V}$
β
α
YAW PLANE
PITCH PLANE
ANGLE-TUBE PROBE

Geometry of the angle-tube probes.

$$C_{P_{yaw}} = (P_2 - P_3)/(P_1 - \overline{P}) \quad (1)$$

$$C_{P_{pitch}} = (P_4 - P_5)/(P_1 - \overline{P}) \quad (2)$$

$$C_{P_{total}} = (P_1 - P_{total})/(P_1 - \overline{P}) \quad (3)$$

$$C_{P_{static}} = (\overline{P} - P_{static})/(P_1 - \overline{P}) \quad (4)$$

$$\overline{P} = (P_2 + P_3 + P_4 + P_5)/4 \quad (5)$$

FIGURE 76 - Diagrams showing the working of Five-hole Probe (ONERA type), extracted from Ref. 70

indexing the center core that bear pressure holes in a single radial plane, it is possible to make surface pressure measurements for several radial planes. Figure 77 shows the general arrangement of the two models (a short and a long one) that were built at DREV.

A similar system was designed by the U.S. Army Ballistics Research Laboratory under the supervision of Dr. Charles H. Murphy, for the U.S. Army Chemical Research, Development and Engineering Center, Aberdeen Proving Ground, Maryland (that has built the model). Their system support the model from the base by a standard sting arrangement, then making possible the testing of complete projectile configuration, (although some base flow interferences are to be induced by the sting support). A complete description is given in Ref. 73, and Refs. 74 to 77 provide more information on the measurement of surface static pressure on spinning wind tunnel models.

Figures 78 and 79 show the model whose configuration was a secant ogive, cylinder, boattail configuration with a 8 in diameter and 5.5 caliber length. It was tested in the NASA-Ames 14 Foot Transonic Wind Tunnel at Mach 0.94 and 4,900 rpm.

The interests of surface pressure measurements to the comprehension of Magnus effects can be emphasises by these two comments extracted from introduction of Ref. 73:

> *" Although the Magnus force is only a 10th to a 100th of the normal force, it can have a large detrimental influence on range and accuracy. "*
>
> *" The tests were conducted to extend the data base for this projectile configuration and represent the first time that the aerodynamic surface pressures have been experimentally determined on any spinning projectile ".*

The DREV surface pressure measurement spinning model has not been tested yet, but new adapted design that would feature the standard sting supported electrical spin rig and sliding seal technique in order to test complete configuration (in a similar fashion to BRL arrangement) could be considered in the future. Since there are some questions about the efficiency of the sliding seal system, the conclusion No.1 of the U.S. Army Chemical Research,

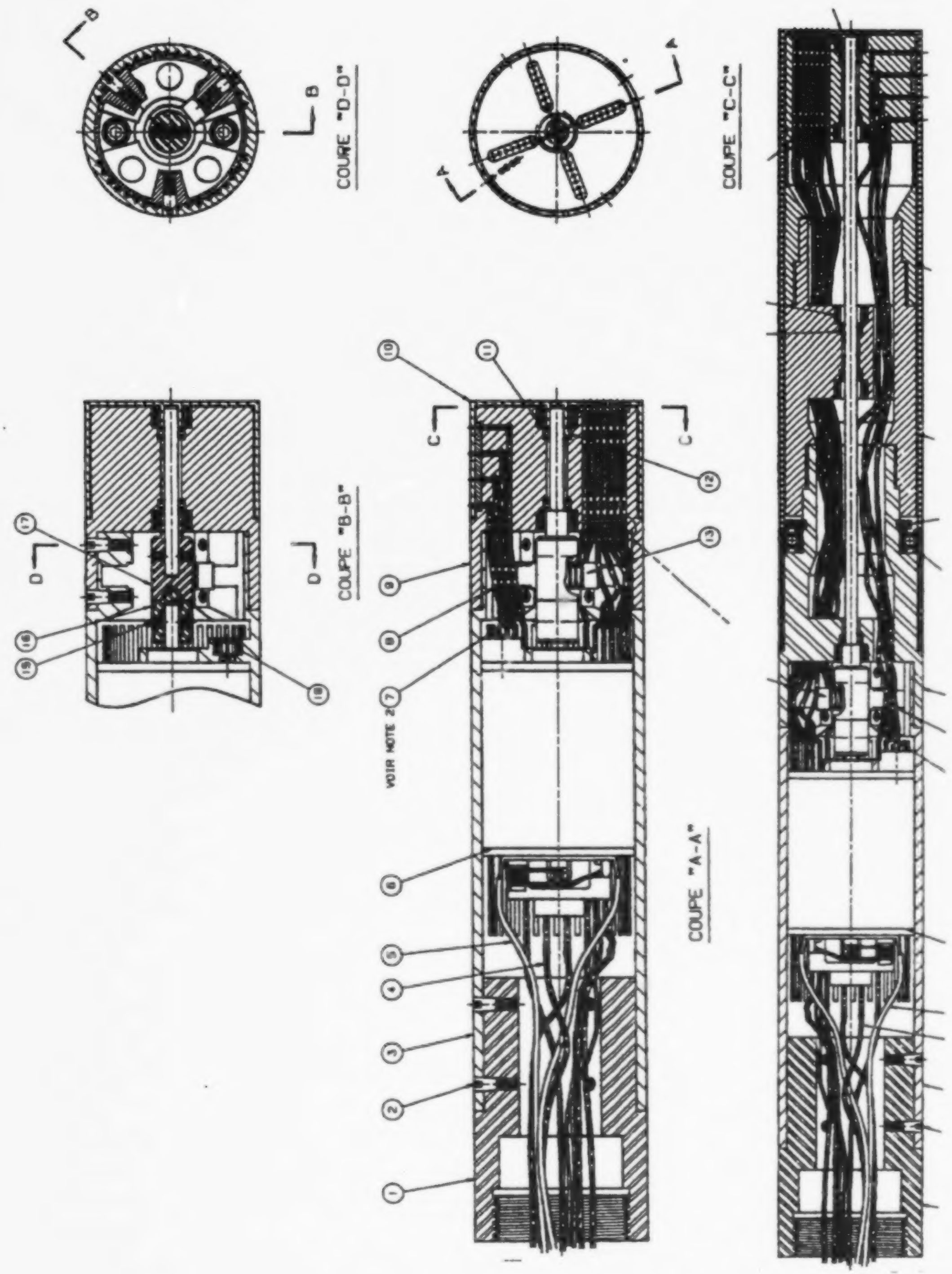
COUPE "D-D"
B
B
COUPE "C-C"
A
A
COUPE "B-B"
D
D
COUPE "A-A"
C
C
VOIR NOTE 2
1
2
3
4
5
6
7
8
9
10
11
12
13
15
16
17
18

FIGURE 77 - General arrangement of DREV surface pressure distribution spinning models based on sliding seal technique and standard pressure module as measuring device

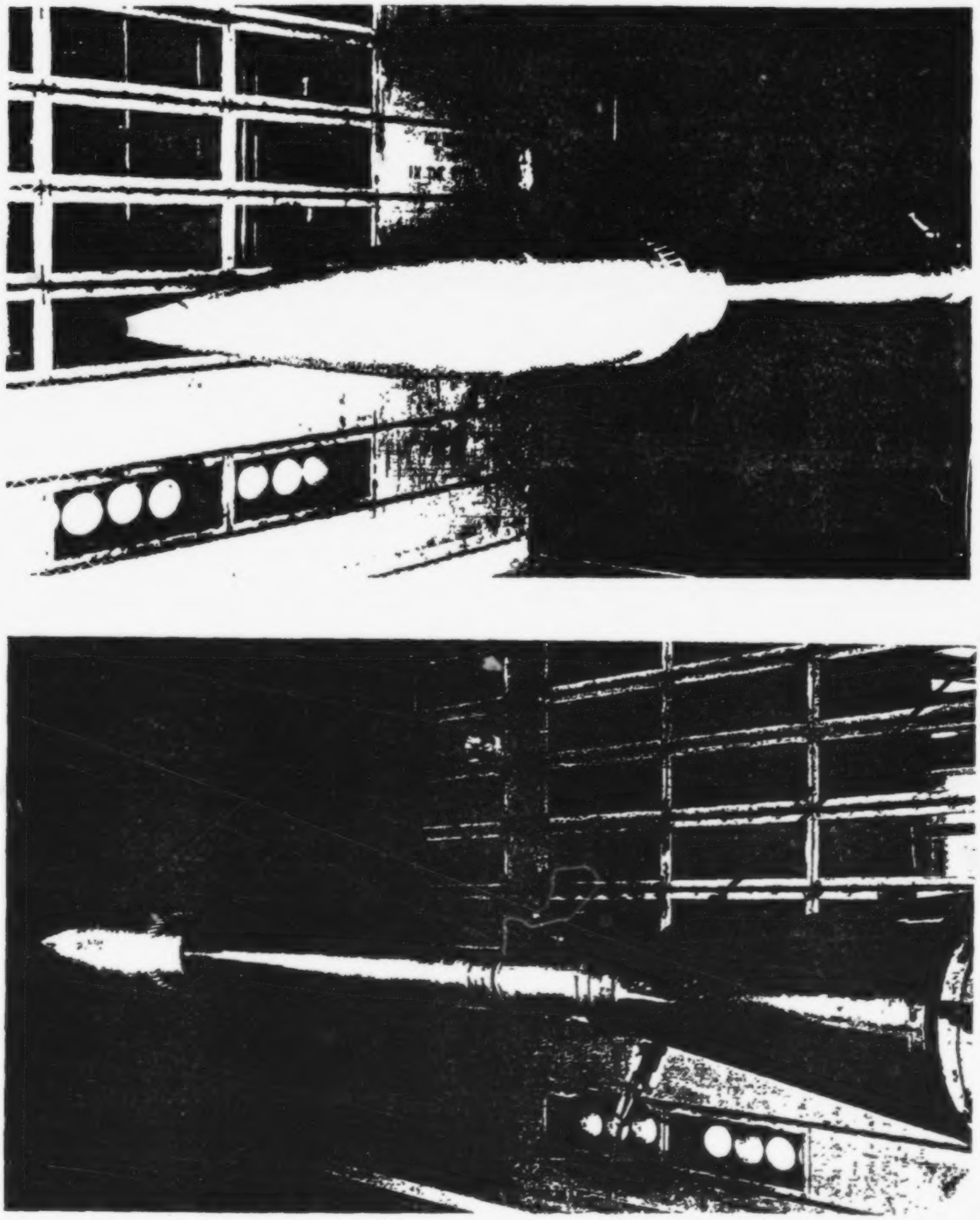

FIGURE 78 - BRL model in NASA-Ames 14 Foot Transonic Wind Tunnel

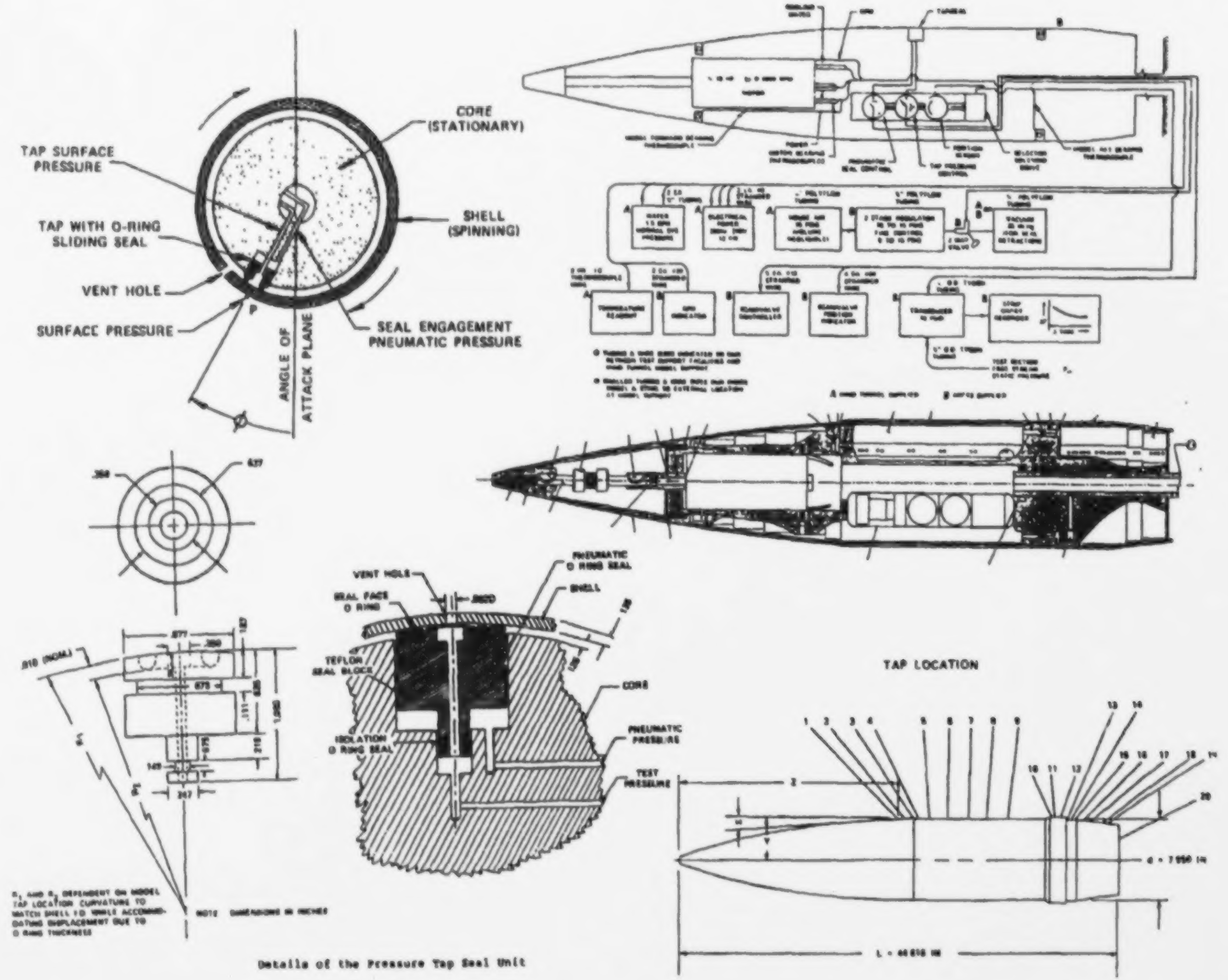
CORE (STATIONARY)
SHELL (SPINNING)
TAP SURFACE PRESSURE
TAP WITH O-RING SLIDING SEAL
VENT HOLE
SURFACE PRESSURE
SEAL ENGAGEMENT PNEUMATIC PRESSURE
ANGLE OF ATTACK PLANE
P
A
B
.359
.637
.877
.250
.675
1.060
.218
.145
.247
.010 (NOM)
VENT HOLE
.0620
SEAL FACE O RING
PNEUMATIC O RING SEAL
SHELL
TEFLON SEAL BLOCK
ISOLATION O RING SEAL
CORE
PNEUMATIC PRESSURE
TEST PRESSURE
NOTE DIMENSIONS IN INCHES
TAP LOCATION
1
2
3
4
5
6
7
8
9
10
11
12
13
14
15
16
17
18
19
20
L = 46.616 IN

Details of the Pressure Tap Seal Unit

FIGURE 79 - BRL model surface pressure measurement arrangement

Development and Engineering Center wind tunnel series (Ref. 73) is reproduced here:

> *" The sliding seal technique is capable of accurately measuring the Magnus-induced surface pressures on a spinning projectile wind tunnel model at transonic Mach numbers. "*

There are several other technologies that can be employed to measured the surface pressure of a spinning model like the laser velocimeter, telemetry systems, etc... The system based on sliding seal technique is of a particular interest for DREV, because it employs standard electronic multi-port pressure sensor modules whose technology is already implemented at the 0.6 m x 0.6 m trisonic facility.

12.0 CONCLUSIONS

This study demonstrated the feasibility of using a D.C. electric motor for purposes of driving a low costs spinning rig for projectile configuration testing in the DREV 0.6m x 0.6m trisonic wind tunnel facility. When only modest resources are available, it appears to be a suitable replacement to these early types of spinning model tests (Hotchkiss-Brandt model) in NAE 5 ft x 5 ft (1.5 m x 1.5 m) trisonic wind tunnel. Although tests performed in the NAE facility reproduced free-flight conditions and that Reynolds numbers per unit length in the DREV facility test section are much lower than for atmospheric flight conditions, aerodynamic coefficient measurement results can be used as input data for trajectory simulation programmes.

New technologies in small permanent magnet-type D.C. motors provide a power-to-volume ratio high enough to house the motor inside the spinning shell of a wind tunnel model of less than 1.6 in diameter. This departure from current practice of using air turbine was made principally because of size constraints and control factors, i.e. ease, simplicity and accuracy of controling a small electric motor compare to an air turbine. It is concluded that measurements of better accuracy would be obtained by using stiff and high accuracy balances. Tests demonstrated the rig suitability.

Values of spin damping and Magnus forces and moments, for a smooth ogive-cylinder projectile, usually represent only 10th to 100th of the normal force and pitching moment. The balances used for testing were damaged and of rated loads (i.e. nominal capacities) unsuitable for the level of forces and moments that were measured. Although with that kind of instrumentation measured values of CLP and CYP-ALPHA were apparently near zero, DREV results stay within scatter of data from other sources.

In present test series, the precision of results was limited by balance accuracy. An improvement on the balance signal quality is expected from new DREV balance design to reduce noise level. These balances, whose characteristics are appropriate for testing of spinning models in DREV trisonic facility, shall be available in a near future. Their main characteristics are an increased resistance to overloads and vibrations while having more accuracy and resolution (Refs. 7 to 9). Also, a new balance calibrator was designed and constructed. Its innovative properties are 6-DOF multi-loading and increase accuracy and resolution. This instrumentation has not yet been tested.

Even with the low density in its test section and the low Reynolds numbers related with the testing of small models in the DREV trisonic facility, it was possible to measure spin damping and clearly recognize Magnus effects and quantify them. But the accuracy can be considered as low with respect to standards of today's. When new DREV balances will be available, more testing shall be made to evaluate the accuracy of Magnus measurements that can be achieved.

The use of this apparatus in conjunction with the new DREV balances and multi-loading calibrator shall be very useful to make experimental comparative study of range-limited small-calibre training ammunition concepts. Model of larger sizes could be used and the forward or aft fins (that provide spin deceleration) would results into much greater spin damping (rolling moment) and Magnus effects, rendering measurement easier. In these tests, reliable measurement of spin damping coefficients, Magnus Forces and moments and spin effects on drag are important.

The specific testing of small/portable arm bullet configurations in the DREV trisonic facility offer the opportunity to reproduce simultaneously the Reynolds number, the Mach number and PD/2V (i.e. helix angle of streamlines around the model) that are characteristic of free-flight conditions. This is achievable because the wind tunnel model being of a much larger size than the real projectile, it compensate for the low characteristic Reynolds/m. Since small arm bullet configurations that are tested in aeroballistic range facilities are often larger than full size, resulting Reynolds numbers are larger than for normal bullet free-flight conditions. These conditions make the DREV trisonic facility a laboratory of predilection to experiment small arm bullet aerodynamics.

The possibility to perform pitot probe measurements within the boundary layer on rapidly spinning ogive-cylinder ~~or~~ projectile configurations is considered as an important help to the comprehension of Magnus effects and to the others spin induced effects. Since the necessary probes and related instrumentation to explore the boundary layer already exist at DREV, dedicated wind tunnel test series should be planned. The probes are of the following types:

a- conical inlet insensible to flow direction,

b- flat beak to approach the spinning model surface,

c- ONERA 5-holes non-intrusive type to measure the orthogonal flow velocity components.

It makes that exploration of the boundary layer on spinning configurations is a type of measurement specific to wind tunnel testing (i.e. could not be obtained with an aeroballistic range).

Spinning base/after-body models dedicated to measurement of surface pressure have already been developed at DREV but not tested yet. They use the sliding seal technique. A similar system, designed by BRL, was used successfully to measure surface pressure on spinning models. These BRL models represented complete projectile configurations.

It would be possible to merge the DREV concepts of electrical spin rig and sliding seal technique which is used on the base/after-body models. Then, an electrical spin rig dedicated to measurement of surface pressure on complete configuration spinning models could be designed and built. Since this technique uses pressure tap holes through the wall of the rotating outer shell, it avoids much problems and limitations encountered with other techniques like Laser velocimetry, impact probe and telemetry. The DREV (and BRL) sliding seal technique allows surface pressures to be measured on spinning models at any attitude and flow regime. In addition, the body can include indentations or protuberances.

The measurement of the Magnus induced surface pressure on spinning configurations is another type of measurement specific to wind tunnel testing (i.e. could not be obtained with an aeroballistic range facility unless complex apparatus of telemetry, projectile roll angle detection etc... be embarked inside the free-flight shell).

Once free-flight test results or data from aeroballistics range tests are available, there is rather little purposes to make direct comparisons with wind tunnel aerodynamic coefficient test results, since test conditions are often much different because of the Reynolds numbers that cannot be reproduced. Also, wind tunnel wall interferences, longitudinal pressure gradients along test section, non-uniform transverse low velocity distribution, base flow interference caused by the sting-support etc... can only be partly corrected in the data reduction process.

Because of the numerous types of dedicated measurement tests that can be made in isolation in the DREV trisonic wind tunnel, test results from spinning models (as well as from static model tests) have the primordial purposes to help in the comprehension of aerodynamics of configurations of interest. Aerodynamic coefficient tests (or force tests performed with 6-DOF balances) can be of a great usefulness at the beginning of a project or in those circumstances where it is not possible to make free-flight tests.

13.0 ACKNOWLEDGEMENTS

The author wishes to thank Messrs. R. Bilodeau, R. Fiset and P. Bélanger for their valuable contribution to the development of this project and their continuous assistance was very appreciated particularly for the development of a controller compatible with the data acquisition system. Also, the primordial contribution of Dr. Nguyen Dinh from Laval University (Department of Mechanical Engineering) was highly usefull and appreciated. As a contractor, he finalized the spin rig mechanical configuration and gave it its present general arrangement. He also imagined and conceived the calibration rig/vacuum chamber system. The spin rig, its spinning model outer shell and the calibration rig were machined and constructed in the Department of Mechanical Engineering machine shop at the Laval University. They also designed and built the initial version of the controller. Their work was outstanding.

14.0 REFERENCES

1. Dinh, N. Nguyen, " Conception et construction d'un modèle de projectile tournant ", Département de génie mécanique, Université Laval, Rapport du contrat M. A. S.No. 11 SD, 97701-5-27752, juin 1986, UNCLASSIFIED

2. Murphy, C.H. and Schmidt, L.E., " The Effect on the Aerodynamic Characteristics of Bodies of Revolution in Supersonic Flight ", Ballistic Research Laboratories, Report No. 876, Project No. TB3-0240 of the Research and Development Division, Ordnance Corps, August 1953, UNCLASSIFIED

3. Winchenbach, G.L., Watt, R.M. and Skinner, A.G., " Free-Flight Range Tests of Basic and Boattail Configurations of 3- and 5-Caliber ARMY-NAVY SPINNER PROJECTILES ", Von Kármán Gas Dynamics Facility, Arnold Engineering Development Center, Air Force Systems Command, Arnold Air Force Station, Tennessee, AEDC-TR-70-12, March 1970, UNCLASSIFIED

4. Jacobson, I.D., " Magnus Characteristics of Arbitrary Rotating Bodies ", AGARDograph No. 171, AGARD-AG-171, UNCLASSIFIED

5. Laviolette, M., and Dixon, R. C., " Static Aerodynamic Characteristics, including Magnus Force and Moment Coefficients, of the Spin-Stabilized 120-mm Hotchkiss-Brant Mortar Shell ", DREV R-625/70, October 1970, UNCLASSIFIED

6. Girard, B., " Electrical Spin Rig for Projectile Wind Tunnel Testing " , DREV M-2860/87, September 1987, UNCLASSIFIED, LIMITED DISTRIBUTION

7. Girard, B., Drouin, G., Faucher, G., Paradis, M.-A. and Normand, M., " A Study of a Monopiece Six-Component Sting-Supported Wind Tunnel Balance ", DREV M-2984/89, October 1989, UNCLASSIFIED, LIMITED DISTRIBUTION

8. Paradis, M.-A. and Faucher, G., " Etude théorique et expérimentale d'un nouveau concept de balance pour la soufflerie à aspiration du CRDV ", Sorenco Ltée, Volumes 1 and 2, Volume 2 Annexe A, contract no: MAS W7701-8-0877/01-XSK, March 1991, UNCLASSIFIED, LIMITED DISTRIBUTION

9. Grondin, R., " Etude de faisabilité du montage des ponts de jauges et des circuits de compensation ", Société de Microélectronique Industrielle de Sherbrooke Inc., Volume 2 Annexe A, subcontract no: SOREN1-E1008-01, contract no: MAS W7701-8-0877/01-XSK, Marsh 1991, UNCLASSIFIED, LIMITED DISTRIBUTION

10. Seginer, A. and Ringel, M., " Magnus Effects at High Angles of Attack and Critical Reynolds Numbers ", Technion - Israel Institute of Technology, Haïfa, Israel, J. Spacecraft, Vol. 23, No. 3, pp. 237-244, May-June 1986, UNCLASSIFIED

11. Dupuis, A.D. and Giraud, M., " Sur les Méthodes Pratiques d'Évaluation du Coéfficient de Trainée de Frottement d'un Projectile en Vol Libre ", France, Institut Saint-Louis de Recherches, 1989, UNCLASSIFIED

12. Mueller, Thomas J., " Determination of the Turbulent Base Pressure in Supersonic Axisymmetric Flow ", University of Notre Dame, Notre Dame, Indiana USA, AIAA Paper No. 67-446, AIAA 3rd Propulsion Joint Specialist Conference, Washington, D.C./July 17-21, 1967, UNCLASSIFIED

13. Zumwalt, G. W., " Analytical and experimental Study of the Axially-Symmetric Supersonic Base Pressure Problem", Ph. D. Thesis, University of Illinois, Dissertation, Department of Mechanical Engineering, MIC 59-4589, University Microfilms, Inc., Ann Harbor, 1959, UNCLASSIFIED

14. Beheim, M. A., " Flow in the Base Region of Axisymmetric and Two-Dimensional Configurations ", Lewis Research Center, NASA TR R-77, 1961, UNCLASSIFIED

15. McDonald, H., " An Analysis of the Turbulent Base Pressure Problem in Supersonic Axi-Symmetric Flow ", Report Ae.200, British Aircraft Corp., Preston Division, Lancashire, Englang, April 1964, UNCLASSIFIED

16. Vereshchagina, L. I., " On Base Pressure for Solids of Revolution in a Supersonic Gas Flow ", Herald of Leningrad University, Issue 3, No. 13, pp 208-214 (See STARR N66-17406 08-23), UNCLASSIFIED

17. Badrinarayanan, M. A., " An Experimental Investigation of Base Flows at Supersonic Speeds ", Journal of the Royal Aeronautical Society, Vol. 65, pp. 475-482, July 1961, UNCLASSIFIED

18. Love, E. S., " Base Pressure at Supersonic Speeds on Two-Dimensional Airfoils and on Bodies of Revolution with and without Fins Having Turbulent Boundary Layers, NACA TN-3819, January 1957, UNCLASSIFIED

19. Chapman, D. R., " An Analysis of Base Pressure at Supersonic Velocities and Comparison with Experiment ", NACA Report 1051, 1951, (Supersedes NACA TN-2137, 1950), UNCLASSIFIED

20. Potter, J. L., Whitfield, J. D., Strike, W. T., " Transition Measurements and the Correlation of Transition Sensitive Data ", AEDC-TR-59-4, February 1959, UNCLASSIFIED

21. Graham, D. K., Binion, T. W. Jr., " Base Drag Measurements on an Ogive Cylinder Model with Base Nozzle Flow ", AEDC-TDR-64-8, May 1964, UNCLASSIFIED

22. Karpov, B. G., " The Effect of Various Boattail Shapes on Base Pressure and Other Aerodynamic Characteristics of a 7-Caliber Long Body of Revolution at M=1.70 ", Ballistic Research Laboratories Report No. 1295, August 1965, UNCLASSIFIED

23. Nash, J. F., " An Analysis of Two-Dimensional Turbulent Base Flow Including the Effect of the Approaching Boundary Layer ", NPL Aero. Report 1036, A. R. C. 24000, July 1962, UNCLASSIFIED

24. McDonald, H., " Turbulent Shear Layer Reattachment with Special Emphasis on the Base Pressure Problem ", British Aircraft Corp., Preston Division, Lancashire, England, August 1963, UNCLASSIFIED

25. Roshko, A., Thomke G. J., " Flow Separation and Reattachament Behind a Downstream-Facing Step ", Douglas Report SM-43056-1, January 1964, UNCLASSIFIED

26. Roshko, A., Thomke G. J., " Observations of turbulent Reattachment Behind an Axisymmetric Downstream-Facing Step in Supersonuc Flow ", Douglas MSSD Report SM-43068, April 1965, UNCLASSIFIED

27. McDonald, H., " The Turbulent Supersonic Base Pressure Problem; a Comparison between a Theory and some External Evidence ", British Aircraft Corp., Report Ae 194, Preston Division, Lancashire, England, April 1965, UNCLASSIFIED

28. Nash, J. F., " Comments on " Review of Recent Development in Turbulent Supersonic Base Flow ", AIAA Journal, pp. 574-575, March 1966, UNCLASSIFIED

29. Tanner, M., " Boundary- Layer Thickness and Base Pressure ", Institut für Theoretische Strömungsmechanik, DFVLR Göttingen, Federal Replublic of Germany, AIAA Thecnical Notes 1985, UNCLASSIFIED

30. Tanner, M., " Steady base Flows ", Progress of Aerospace Sciences, Vol. 21, No. 2, pp. 81-157, 1984, UNCLASSIFIED

31. Goecke, S., " Flifht-Measured Pressure Characteristics of Aft-Facing Steps in High Reynolds Number Flow at Mach Numbers of 2.20, 2.50 and 2.80 and Comparison with Other Data", NASA TM-72855, 1978, UNCLASSIFIED

32. Korst, H. H., " A Theory for Base Pressures in Transonic and Supersonic Flow ", Journal of Applied Mechanics, Vol. 23 pp. 593-600, 1956, UNCLASSIFIED

33. Nash, J. F., " An Analysis of Two-Dimensional Turbulent Base Flow, Including the Effect of the Approaching Boundary Layer", British Aeronautical Research council, R and M 3434, 1966, UNCLASSIFIED

34. Roberts, J. B., " On the Prediction of Base Pressure in Two-Dimensional Supersonic Turbulent Flow ", British Aeronautical Research Council, R and M 3434, 1966, UNCLASSIFIED

35. Tanner, M., " Theoretical Prediction of Base Pressure for Steady Base Flow ", Progress of Aerospace Sciences, Vol. 14, pp. 177-225, 1973, UNCLASSIFIED

36. Hong Yong, Shik, " A Study of Axially-Symmetric Supersonic Base Flow With Turbulent Initial Boundary Layer ", PHD Thesis 1968, University of Washington USA, UMI Dissertation Information Service, Ann Harbor Michigan, 1991, UNCLASSIFIED

37. Girard, B., " Wind Tunnel Tests on DREV - ISL Reference Models at Supersonic Speeds (Series ISLFPWT- 1) ", DREV - TM - 9704, August 1997, UNCLASSIFIED

38. Girard, B., " Direct Base Drag Measurement Wind Tunnel Tests of Projectile Base Configurations (Series BDWT-1) ", DREV - TM- 1999-028, February 1999, UNCLASSIFIED

39. Green, J.E., " A Summary of Experimental Magnus Characteristics of a 7- and 5-Caliber Body of Revolution at Subsonic Through Supersonic Speeds ", Naval Ordnance Lab., White Oak, Silver Spring, MD, NAVORD Rept. 6110, August 1958, UNCLASSIFIED

40. Platou, A.S., " Magnus Characteristics of Finned and Nonfinned Projectiles ", AIAA Journal, Vol. 3 January 1965, pp. 83-90, UNCLASSIFIED

41. Murphy, C.H., " Effect of Roll on Dynamic Instability of Symmetric Missiles ", Journal of the Aeronautical Sciences, Vol. 21, September 1954, pp. 643-644, UNCLASSIFIED

42. Nicolaides, J.D., " Two Nonlinear Problems in the Flight Dynamics of Modern Ballistics Missiles ", Institute of Aerospace Sciences, Notre Dame University, Notre Dame, IN, IAS Rep 59-17, January 1959, UNCLASSIFIED

43. Green, J.E., " Static Stability and Magnus Characteristics of the 5-Caliber and 7-Caliber Army-Navy Spinner Rocket at Low Subsonic Speeds ", Naval Ordnance Lab., White Oak, Silver Spring, MD, NAVORD Rept. 3884, December 1954, UNCLASSIFIED

44. Martin, J.C., " On Magnus Effects Caused by the Boundary Layer Displacement Thickness on Bodies of Revolution at Small Angles of Attack ", Ballistics Research Lab., Aberdeen Proving Ground, MD, BRL Rept. 870, June 1955; also Journal of the Aeronautical Sciences, Vol. 24, March 1957, pp 421-429, UNCLASSIFIED

45. Fletcher, C.A.J., " Investigation of the Magnus Characteristics of a Spinning Inclined Ogive-Cylinder Body at M=0.2 ", Weapons Research Establishment, Salisbury, South Australia, TN HSA 159, October 1969, UNCLASSIFIED

46. Kegelman, J.T., Nelson, R.C., and Mueller, T.J., " Boundary Layer and Side Force Characteristics of a Spinning Axisymmetric Body ", AIAA Paper 80-1584, August 1980, UNCLASSIFIED

47. Krahn, E., " Negative Magnus Force ", Journal of the Aeronautical Sciences, Vol. 23, April 1956, pp 377-378, UNCLASSIFIED

48. Swanson, W.M., " Magnus Effect: A Summary of Investigations to Date ", Journal of Basic Engineering, Vol. 83, Sept. 1961, pp. 461-470, UNCLASSIFIED

49. Fletcher, C.A.J., " Negative Magnus Forces in the Critical Reynolds Number Regime ", Journal of Aircraft, Vol. 9, December 1972, pp. 826-834, UNCLASSIFIED

50. Tani, I., " Low-Speed Flows Involving Bubble Separation ", Progress in Aeronautical Science, Vol. 5, 1965, pp. 70-103, UNCLASSIFIED

51. Birtwell, E.P., Coffin, J.B., Covert, E.E., and Haldeman, C.W., " Reverse Magnus Force on a Magnetically Suspended Ogive Cylinder at Subsonic Speeds ", AIAA Journal, Vol. 16, Feb. 1978, pp 111-116, UNCLASSIFIED

52. Ingram, C.W., Lusardi, R.J., and Nicolaides, J.D., " Effects of Rifling and N-Vanes on the Magnus Characteristics of Bodies of Revolution ", AIAA Paper 72-970, September 1972, UNCLASSIFIED

53. Zehentner, R.J., Nelson, R.C., and Mueller, T.J., " A Visual Study of the influence of Nose Bluntness on the Boundary Layer Characteristics of a Spinning Axisymmetric Body ", AIAA Paper 81-1901, August 1981, UNCLASSIFIED

54. Rosenwasser, I., and Seginer, A., " The Measurement of Magnus Forces on Spinning Models ", Proceedings of the 23rd Israel Annual Conference on Aviation and Astronautics, Tel-Aviv and Haïfa, Israel, Feb. 1981, pp. 81-88, UNCLASSIFIED

55. Seginer, A., and Ringel, M., " Magnus Effects at High Angles of Attack and Critical Reynolds Numbers ", AIAA Paper 83-2145, August 1983, UNCLASSIFIED

56. Iversen, J.D., " Correletion of Magnus Force Data for Slender Spinning Cylinders ", AIAA Paper 72-966, September 1972, UNCLASSIFIED

57. Uselton, J.C., and Carman, J.B., " A Study of the Magnus Effects on a Sounding Rocket at Supersonic Speeds ", Journal of Spacecraft and Rockets, Vol. 8, January 1971, pp. 28-34, UNCLASSIFIED

58. Stureck, W.B., " Boundary Layer Studies on a Spinning Cone ", AIAA Paper 72-967, September 1972, UNCLASSIFIED

59. Vaughn, H.R. and Reis, G.E., " A Magnus Theory ", AIAA Paper 73-124, January 1973, UNCLASSIFIED

60. Kahn, D., Oskay, V., and Whiteside, J., " Verification of Ground Test Data by Instrumented Flight Test of an Artillery Shell ", AIAA Paper 72-979, September 1972, UNCLASSIFIED

61. George, O. L. Jr., Ragsdale, W.C., " Pitot Probe Measurements Within the Laminar Boundary layer on a Rapidly Spinning Ogive-Cylinder in Supersonic Flow ", Sandia Laboratories, SLA-73-0940, November 1973, UNCLASSIFIED

62. Thorman, H. C., " Boundary Layer Measurements on an Axisymmetric Body with Spin and Yaw ", Ph. D. Thesis, Calfifornia Institute of Technology, Pasadena, California, 1958, UNCLASSIFIED

63. Potter, J. L., Kinslow, M. and Boylan, D. E., " An Influence of the Orifice on Measured Pressures in Rarefied Flow ", AEDC-TDR-64-175, AEDC, Arnold Air Force Station, Tennessee, September 1964, UNCLASSIFIED

64. Arney, G. D. and Bailey, A. B., " Effect of Temperature on Pressure Measurements ", AIAA Journal, Vol. 1 No. 12, pp. 2863-2864, December 1963, UNCLASSIFIED

65. Vaughn, H. R. and George, O. L., " Surface Flow Angles on an Ogive Cylinder at Angle of Attack in Supersonic Flow ", SC-RR-71 0781, Sandia Laboratories, Albuquerque, New Mexico, December 1971, UNCLASSIFIED

66. Ludwig, G. R., " Effects of Probes Size on Measurement in a Laminar Boundary Layer in Supersonic Flow ", Technical Note No. 9, University of Toronto, Institute of Aerophysics, Canada, November 1956, UNCLASSIFIED

67. Ragsdale, W.C., Brown, M. A. and Ball, R. G., " An Experimental Investigation of the Laminar Boundary Layer on a Spinning Ogive Cylinder in Supersonic Flow ", NOLTR-72-265, Naval Ordnance Laboratory, Silver Spring, Maryland, November 1972, UNCLASSIFIED

68. Ragsdale, W. C. " Boundary-Layer Survey Test for Sandia Corporation ", Wind Tunnel Report No. 65, Naval Ordance Laboratory, Silver Spring, Maryland, October 1972, UNCLASSIFIED

69. Vaughn, H. R. and Reis, G. E., " A Magnus Theory for Bodies of Revolution ", SC-RR-72 0537, Sandia Laboratories, Albuqierque, New Mexico, January 1973, UNCLASSIFIED

70. Treaster, A. L., Yocum, A. M., " The Calibration and Application of Five-hole Probes ", Applied Research Laboratory, Presented at the Aerospace Industries/Tests Measurements Divisions Symposium, 1978, Albuquerque, ISA Transactions, Vol. 18, No.3, 34 pages, 0019-0578/79/03/0023/12, ISA 1979, UNCLASSIFIED

71. Pien, P.C., " Five-hole Sperical Pitot Tube ", David Taylor Model Basin Report 1229, May 1958, UNCLASSIFIED

72. Krause, L. N. and Dudzinski, T. J., " Flow-Direction Measurement with Fixed Position Probes in Subsonic Flows over a Range of Reynolds Number ", NASA TMX-52576, May 1969, UNCLASSIFIED

73. Miller, M. C. and Molnar, J. W., " Wind Tunnel Measurement of the Magnus Induced Surface Pressures on a Spinning Artillery Projectile Model in the Transonic Speed Regime ", Chemical Research, Development & Engineering Center, CRDEC-TR-86081, September 1986, UNCLASSIFIED

74. Miller, M. C., " Surface Pressure Measurements on a Spinning Wind Tunnel Model ", Am. Instit. Aeronaut. Astronaut. J. 14, 1669, December 1976, UNCLASSIFIED

75. Miller, M. C., " A technique to Measure the Pressure Distribution Acting on the Surface of a Spinning Body in a Wind Tunnel ", Edgewood Arsenal, ED-TR-76070, September 1976, UNCLASSIFIED

76. Miller, M. C., " Wind Tunnel Measurements of the Surface Pressure Distribution on a Spinning Magnus Rotor ", Am. Instit. Aeronaut. Astronaut. Journal of Aircraft 16 (no. 12), 815, December 1979, UNCLASSIFIED

77. Miller, M. C. " Experimental Measurement of the Aerodynamics Surface Pressures on Spinning Bodies ", Proceedings of the International Congress of Instrumentation in Aerospace Simulation Facilities, pp. 117-130, September 1983, UNCLASSIFIED

APPENDIX A

Summary of Runs

SUMMARY OF RUNS

TRIAL SPINWT-1

STABILITY COEFFICIENTS - FORCE AND MOMENT MEASUREMENTS

Configuration data reduction input parameters

Diameters of reference

- d = Body diameter (or calibre) = 1.596 in = 40.54 mm

- d^1 = Base diameter = 1.596 in = 40.54 mm

Able MK-X-A 0.50 in balance and Able MK-VI-A 0.50 in balance Resolving Center with respect to Moment Resolving Center located at model base

- c = Distance of BRC aft of MRC = -1.28 in = -32.51 mm

Note: as " c " is defined as: " Distance of BRC aft of MRC " , the moment resolving center being located at the model base which is aft of the balance resolving center, the value of " c " is negative.

TABLE AI

AERODYNAMIC COEFFICIENTS								
TEST RUN NUMBER ----------- TUNNEL LOG RUN NUMBER ----------- TYPE OF BALANCE USED	SPIN RATE in RPM --------- SWEPT ANGLE of ATTACK in deg	MEASUREMENT RESULTS of SPIN DAMPING COEFFICIENT $\alpha = 0.0$ deg average value need to be calculated with data from test made in reverse sense of rotation to compensate for roll measurement shift	TEST MACH NUMBER	CNA	CMA	XCPO	CAO	SENSE of ROTATION R or L
2205.05 R2794 0.50 MK-VI-A	35809 -5 to +15	-0.0300	0.50	2.486	8.591	-3.46	N/A	R
2206.07-1 R2793 0.50 MK-VI-A	35796 -5 to +15	-0.0265	0.70	2.153	7.536	-3.50	N/A	R
2207.08 R2791 0.50 MK-VI-A	35722 -5 to +15	-0.0250	0.80	2.102	7.483	-3.56	N/A	R
2178.09 R2795 0.50 MK-VI-A	30494 -5 to +15	-0.0230	0.93	2.500	8.634	-3.45	N/A	R
2209.09-1 R2790 0.50 MK-VI-A	35721 -5 to +15	-0.0205	0.93	2.309	8.173	-3.54	N/A	R

2190.05 R2812 0.50 MK-X-A	0.0 -5 to +15	N/A	0.50	2.024	6.515	-3.22	0.172	N/A
2160.05 R2821 0.50 MK-X-A	20746 -5 to +15	-0.0300	0.50	2.368	7.741	-3.27	0.174	R
2130.05 R2805 0.50 MK-X-A	25529 -5 to +15	-0.0250	0.50	2.315	7.549	-3.26	0.184	R
2175.05 R2802 0.50 MK-X-A	30771 -5 to +15	-0.0300	0.50	2.586	8.312	-3.21	0.170	R
2191.07 R2811 0.50 MK-X-A	0.0 -5 to +15	N/A	0.70	2.136	6.996	-3.28	0.171	N/A
2161.07 R2820 0.50 MK-X-A	20816 -5 to +15	-0.0270	0.70	2.212	7.268	-3.29	0.176	R
2131.07-1 R2807 0.50 MK-X-A	25892 -5 to +15	-0.0260	0.70	2.475	7.933	-3.21	0.168	R
2131.07 R2804 0.50 MK-X-A	25812 -5 to +15	-0.0290	0.70	2.691	9.120	-3.39	0.172	R
2176.07 R2803 0.50 MK-X-A	30749 -5 to +15	-0.0270	0.70	2.120	7.063	-3.33	0.168	R
2192.08 R2810 0.50 MK-X-A	0.0 -5 to +15	N/A	0.80	2.502	8.322	-3.33	0.164	N/A
2162.08 R2817 0.50 MK-X-A	21394 -5 to +15	-0.0325	0.80	2.435	8.071	-3.31	0.177	R
2162.08-2 R2819 0.50 MK-X-A	20671 -5 to +15	-0.0250	0.80	2.395	7.970	-3.33	0.178	R

2132.08 R2806 0.50 MK-X-A	25842 -5 to +15	-0.0230	0.80	2.165	7.407	-3.42	0.172	R
2177.08-3 R2800 0.50 MK-X-A	30688 -5 to +15	-0.0030	0.80	2.060	7.031	-3.41	0.161	R
2177.08-4 R2801 0.50 MK-X-A	30720 -5 to +15	-0.0260	0.80	2.612	8.960	-3.43	0.162	R
2210.110-2 R2975 0.50 MK-X-A	36236 -2 to +2	-0.0260	0.81	2.329	7.797	-3.35	0.249	R
2193.09 R2808 0.50 MK-X-A	0.0 -5 to +15	N/A	0.93	2.768	9.314	-3.36	0.222	N/A
2163.09 R2816 0.50 MK-X-A	21085 -5 to +15	-0.0330	0.93	2.184	7.389	-3.38	0.229	R
2133.09 R2814 0.50 MK-X-A	25895 -5 to +15	-0.0320	0.93	2.402	8.131	-3.39	0.227	R
2133.09-1 R2815 0.50 MK-X-A	25784 -5 to +15	-0.0280	0.93	2.494	8.391	-3.36	0.235	R
2178.09-1 R2813 0.50 MK-X-A	30779 -5 to +15	-0.0300	0.93	2.480	8.132	-3.28	0.237	R
2209.09-2 R2809 0.50 MK-X-A	35714 -5 to +15	-0.0275	0.93	2.418	8.324	-3.44	0.241	R
2194.100 R2980 0.50 MK-X-A	0.0 -2 to +2	N/A	1.03	2.427	8.568	-3.53	0.390	N/A
2194.100-1 R2981 0.50 MK-X-A	0.0 -2 to +2	N/A	1.03	2.425	8.336	-3.44	0.405	N/A

2134.100 R2978 0.50 MK-X-A	26066 -2 to +2	-0.0180	1.02	2.496	8.634	-3.46	0.403	R
2134.100-1 R2979 0.50 MK-X-A	26073 -2 to +2	-0.0210	1.03	2.581	8.903	-3.45	0.404	R
2119.100 R2982 0.50 MK-X-A	26048 -2 to +2	-0.0252	1.03	2.548	8.838	-3.47	0.403	L
2119.100-1 R2983 0.50 MK-X-A	26062 -2 to +2	-0.0240	1.03	2.546	8.726	-3.43	0.405	L
2149.100 R2984 0.50 MK-X-A	31093 -2 to +2	-0.0250	1.03	2.616	9.056	-3.46	0.395	L
2149.100-1 R2985 0.50 MK-X-A	31097 -2 to +2	-0.0243	1.03	2.465	8.462	-3.43	0.389	L
2179.100 R2986 0.50 MK-X-A	31060 -2 to +2	-0.0220	1.03	2.490	8.668	-3.48	0.397	R
2179.100-1 R2987 0.50 MK-X-A	31057 -2 to +2	-0.0206	1.03	2.593	9.006	-3.47	0.396	R
2209.100 R2988 0.50 MK-X-A	35995 -2 to +2	-0.0185	1.03	2.622	8.976	-3.42	0.394	R
2209.100-1 R2989 0.50 MK-X-A	35987 -2 to +2	-0.0205	1.03	2.640	8.911	-3.38	0.398	R
2104.100 R2990 0.50 MK-X-A	36035 -2 to +2	-0.0250	1.03	2.550	8.742	-3.43	0.396	L
2104.100-1 R2991 0.50 MK-X-A	36033 -2 to +2	-0.0262	1.03	2.492	8.580	-3.44	0.377	L

2089.100 R2992 0.50 MK-X-A	39305 -2 to +2	-0.0245	1.03	2.441	8.471	-3.47	0.398	L
2089.100-1 R2993 0.50 MK-X-A	39968 -2 to +2	-0.0235	1.03	2.504	8.645	-3.45	0.400	L
2224.100 R2994 0.50 MK-X-A	39927 -2 to +2	-0.0210	1.02	2.441	8.557	-3.50	0.396	R
2224.100-1 R2995 0.50 MK-X-A	39929 -2 to +2	-0.0207	1.02	2.703	9.358	-3.46	0.401	R
2195.110 R2967 0.50 MK-X-A	0.0 -2 to +2	N/A	1.16	2.391	8.362	-3.50	0.464	N/A
2195.110-1 R2968 0.50 MK-X-A	0.0 -2 to +2	N/A	1.16	2.431	8.487	-3.49	0.465	N/A
2120.110 R2958 0.50 MK-X-A	25927 -2 to +2	-0.0220	1.16	2.365	8.196	-3.47	0.473	L
2120.110-1 R2959 0.50 MK-X-A	25998 -2 to +2	-0.0218	1.16	2.393	8.402	-3.51	0.476	L
2135.110 R2969 0.50 MK-X-A	26082 -2 to +2	-0.0195	1.16	2.546	8.881	-3.49	0.471	R
2135.110-1 R2970 0.50 MK-X-A	26099 -2 to +2	-0.0217	1.16	2.400	8.364	-3.48	0.470	R
2150.110 R2960 0.50 MK-X-A	31007 -2 to +2	-0.0200	1.16	2.384	8.363	-3.51	0.472	L
2150.110-1 R2961 0.50 MK-X-A	31063 -2 to +2	-0.0225	1.16	2.636	9.173	-3.48	0.471	L

2150.110-2 R2962 0.50 MK-X-A	31090 -2 to +2	-0.0235	1.16	2.642	9.181	-3.47	0.469	L
2150.110-3 R2963 0.50 MK-X-A	31116 -2 to +2	-0.0260	1.16	2.693	9.135	-3.39	0.471	L
2180.110 R2971 0.50 MK-X-A	31120 -2 to +2	-0.0190	1.16	2.518	8.625	-3.42	0.470	R
2180.110-1 R2972 0.50 MK-X-A	31079 -2 to +2	-0.0205	1.16	2.492	8.548	-3.43	0.459	R
2105.110 R2964 0.50 MK-X-A	35786 -2 to +2	-0.0250	1.16	2.423	8.371	-3.45	0.474	L
2105.110-1 R2965 0.50 MK-X-A	35955 -2 to +2	-0.0240	1.16	2.639	9.123	-3.46	0.470	L
2210.110 R2973 0.50 MK-X-A	35785 -2 to +2	-0.0190	1.16	2.511	8.742	-3.48	0.469	R
2210.110 R2973 0.50 MK-X-A	35785 -2 to +2	-0.0190	1.16	2.511	8.742	-3.48	0.469	R
2210.110-1 R2974 0.50 MK-X-A	35875 -2 to +2	-0.0191	1.16	2.510	8.600	-3.43	0.469	R
2210.110-3 R2976 0.50 MK-X-A	36260 -2 to +2	-0.0200	1.16	2.529	8.657	-3.42	0.465	R
2225.100 R2996 0.50 MK-X-A	39919 -2 to +2	-0.0190	1.16	2.519	8.708	-3.46	0.460	R
2225.100-1 R2997 0.50 MK-X-A	39895 -2 to +2	-0.0175	1.16	2.636	8.952	-3.40	0.459	R

2090.110 R2998 0.50 MK-X-A	39947 -2 to +2	-0.0245	1.16	2.528	8.614	-3.41	0.460	L
2090.110-1 R2999 0.50 MK-X-A	39930 -2 to +2	-0.0225	1.16	2.375	8.194	-3.45	0.463	L
2121.125 R2943 0.50 MK-X-A	26041 -2 to +2	-0.0230	1.22	2.683	9.092	-3.39	0.451	L
2196.125 R2940 0.50 MK-X-A	0.0 -2 to +2	N/A	1.27	2.541	8.857	-3.49	0.428	N/A
2196.125-1 R2941 0.50 MK-X-A	0.0 -2 to +2	N/A	1.27	2.568	8.907	-3.47	0.439	N/A
2136.125 R2931 0.50 MK-X-A	26072 -2 to +2	-0.0175	1.27	2.296	7.880	-3.43	0.439	R
2136.125-1 R2932 0.50 MK-X-A	26074 -2 to +2	-0.0190	1.27	2.449	8.279	-3.38	0.440	R
2121.125-1 R2944 0.50 MK-X-A	26050 -2 to +2	-0.0230	1.27	2.364	8.184	-3.46	0.441	L
2121.125-2 R2945 0.50 MK-X-A	26053 -2 to +2	-0.0225	1.27	2.412	8.242	-3.42	0.441	L
2181.125 R2933 0.50 MK-X-A	31096 -2 to +2	-0.0185	1.27	2.860	9.781	-3.42	0.441	R
2181.125-1 R2934 0.50 MK-X-A	31102 -2 to +2	-0.0195	1.27	2.613	8.855	-3.39	0.441	R
2151.125-2 R2948 0.50 MK-X-A	31224 -2 to +2	-0.0195	1.27	2.449	8.602	-3.51	0.448	L

2151.125-3 R2949 0.50 MK-X-A	31224 -2 to +2	-0.0185	1.27	2.391	8.224	-3.45	0.450	L
2211.125 R2935 0.50 MK-X-A	36008 -2 to +2	-0.0175	1.27	2.494	8.482	-3.40	0.441	R
2211.125-1 R2936 0.50 MK-X-A	36031 -2 to +2	-0.0180	1.27	2.544	8.744	-3.44	0.440	R
2211.125-2 R2937 0.50 MK-X-A	36022 -2 to +2	-0.0190	1.27	2.673	9.119	-3.41	0.440	R
2106.125-2 R2952 0.50 MK-X-A	35942 -2 to +2	-0.0205	1.27	2.472	8.741	-3.54	0.449	L
2106.125-3 R2953 0.50 MK-X-A	36017 -2 to +2	-0.0200	1.27	2.470	8.629	-3.49	0.445	L
2106.125-4 R2954 0.50 MK-X-A	36018 -2 to +2	-0.0185	1.27	2.631	9.328	-3.55	0.446	L
2106.125-4 R2954 0.50 MK-X-A	36018 -2 to +2	-0.0185	1.27	2.631	9.328	-3.55	0.446	L
2091.125-2 R2957 0.50 MK-X-A	38119 -2 to +2	-0.0200	1.27	2.513	8.824	-3.51	0.445	L
2091.125-1 R2956 0.50 MK-X-A	39334 -2 to +2	-0.0200	1.27	2.422	8.535	-3.52	0.443	L
2091.125 R2955 0.50 MK-X-A	39476 -2 to +2	-0.0190	1.27	2.587	8.958	-3.46	0.442	L
2226.125 R2938 0.50 MK-X-A	40005 -2 to +2	-0.0180	1.27	2.709	9.413	-3.47	0.438	R

2197.135-1 R2929 0.50 MK-X-A	0.0 -2 to +2	N/A	1.33	2.611	9.123	-3.49	0.420	N/A
2197.135 R2928 0.50 MK-X-A	0.0 -2 to +2	N/A	1.36	2.619	8.986	-3.43	0.409	N/A
2137.135-3 R2912 0.50 MK-X-A	26293 -2 to +2	-0.0130	1.32	2.598	9.005	-3.47	0.424	R
2137.134-4 R2913 0.50 MK-X-A	26318 -2 to +2	-0.0130	1.36	2.534	8.713	-3.44	0.415	R
2122.135 R2918 0.50 MK-X-A	26269 -2 to +2	-0.0200	1.36	2.648	8.975	-3.39	0.417	L
2122.135-1 R2919 0.50 MK-X-A	26270 -2 to +2	-0.0195	1.36	2.747	9.366	-3.41	0.417	L
2182.135 R2914 0.50 MK-X-A	31293 -2 to +2	-0.0150	1.36	2.650	9.138	-3.45	0.412	R
2182.135-1 R2915 0.50 MK-X-A	31226 -2 to +2	-0.0130	1.36	2.740	9.267	-3.38	0.417	R
2152.135 R2920 0.50 MK-X-A	31185 -2 to +2	-0.0190	1.36	2.831	9.537	-3.37	0.416	L
2152.135-1 R2921 0.50 MK-X-A	31140 -2 to +2	-0.0190	1.36	2.697	9.153	-3.39	0.412	L
2152.135-2 R2930 0.50 MK-X-A	31058 -2 to +2	-0.0172	1.35	2.761	9.554	-3.46	0.419	R
2112.135 R2916 0.50 MK-X-A	36169 -2 to +2	-0.0135	1.36	2.718	9.353	-3.44	0.416	R

2112.135-1 R2917 0.50 MK-X-A	36169 -2 to +2	-0.0160	1.36	2.586	8.691	-3.36	0.412	R
2107.135 R2922 0.50 MK-X-A	35957 -2 to +2	-0.0200	1.36	2.708	9.240	-3.41	0.413	L
2107.135-1 R2923 0.50 MK-X-A	35949 -2 to +2	-0.0200	1.32	2.539	8.630	-3.40	0.416	L
2092.135 R2924 0.50 MK-X-A	40646 -2 to +2	-0.0200	1.36	2.593	8.960	-3.45	0.405	L
2092.135-1 R2925 0.50 MK-X-A	39750 -2 to +2	-0.0192	1.36	2.824	9.612	-3.40	0.410	L
2227.135 R2926 0.50 MK-X-A	39762 -2 to +2	-0.0170	1.36	2.541	8.642	-3.40	0.413	R
2227.135-1 R2927 0.50 MK-X-A	39749 -2 to +2	-0.0172	1.36	2.634	8.996	-3.42	0.416	R
2198.150 R2880 0.50 MK-X-A	0.0 -2 to +2	N/A	1.45	2.909	9.595	-3.30	0.415	N/A
2198.150-1 R2881 0.50 MK-X-A	0.0 -2 to +2	N/A	1.46	2.638	8.887	-3.37	0.410	N/A
2123.150 R2874 0.50 MK-X-A	26075 -2 to +2	-0.0120	1.49	2.901	9.583	-3.30	0.404	L
2138.150 R2876 0.50 MK-X-A	26095 -2 to +2	-0.0050	1.49	2.658	8.748	-3.29	0.402	R
2183.150 R2877 0.50 MK-X-A	31095 -2 to +2	-0.0075	1.49	2.853	9.314	-3.26	0.406	R

2153.150 R2873 0.50 MK-X-A	31080 -2 to +2	-0.0125	1.49	2.973	9.615	-3.23	0.403	L
2108.150 R2872 0.50 MK-X-A	36041 -2 to +2	-0.0130	1.49	2.678	8.807	-3.29	0.410	L
2213.150 R2878 0.50 MK-X-A	35947 -2 to +2	-0.0075	1.49	2.801	9.100	-3.25	0.404	R
2093.150 R2875 0.50 MK-X-A	40695 -2 to +2	-0.0120	1.49	2.879	9.316	-3.24	0.406	L
2228.150 R2879 0.50 MK-X-A	40675 -2 to +2	-0.0080	1.49	2.964	9.712	-3.28	0.404	R
2199.175 R2828 0.50 MK-X-A	0.0 -5 to +15	N/A	1.75	2.964	9.123	-3.08	0.380	N/A
2199.175-1 R2829 0.50 MK-X-A	0.0 -15 to +15	N/A	1.73	2.977	9.337	-3.14	0.410	N/A
2199.175-2 R2833 0.50 MK-X-A	0.0 +15 to -15	N/A	1.74	2.875	8.912	-3.10	0.399	N/A
2169.175 R2822 0.50 MK-X-A	20771 -5 to +15	-0.0120	1.70	3.022	9.299	-3.08	0.425	R
2139.175 R2823 0.50 MK-X-A	25867 -5 to +15	-0.0120	1.73	2.974	9.163	-3.08	0.400	R
2139.175-1 R2835 0.50 MK-X-A	25782 +15 to -15	-0.0100	1.73	3.091	9.693	-3.14	0.403	L
2184.175-1 R2825 0.50 MK-X-A	30709 -5 to +15	-0.0100	1.74	3.053	9.251	-3.03	0.405	R

2184.175-2 R2836 0.50 MK-X-A	30763 +15 to -15	-0.0110	1.73	3.334	10.597	-3.18	0.410	L
2019.175 R2826 0.50 MK-X-A	30727 -1 to +1	-0.0050	1.74	2.944	9.195	-3.12	0.399	R
2214.175 R2827 0.50 MK-X-A	35596 -5 to +15	-0.0140	1.73	3.009	9.266	-3.08	0.399	R
2214.175-1 R2830 0.50 MK-X-A	35667 -15 to +15	-0.0100	1.73	3.046	9.470	-3.11	0.415	L
2214.175-2 R2831 0.50 MK-X-A	35315 -15 to +15	-0.00800	1.73	3.031	9.574	-3.16	0.422	R
2214.175-3 R2832 0.50 MK-X-A	35860 +5 to -15	-0.0100	1.74	2.991	9.189	-3.07	0.402	R
2214.175-4 R2834 0.50 MK-X-A	35599 +15 to -15	-0.0100	1.74	3.157	9.588	-3.04	0.415	L
2200.200-1 R2871 0.50 MK-X-A	0.0 -2 to +2	N/A	2.00	3.149	9.480	-3.01	0.320	N/A
2125.200 R2863 0.50 MK-X-A	26077 -2 to +2	-0.0055	1.98	3.023	9.166	-3.03	0.338	L
2140.200 R2864 0.50 MK-X-A	26098 -2 to +2	-0.0070	1.98	3.226	9.833	-3.05	0.329	R
2140.200 R2864 0.50 MK-X-A	26098 -2 to +2	-0.0070	1.98	3.226	9.833	-3.05	0.329	R
2155.200 R2861 0.50 MK-X-A	30832 -2 to +2	-0.0040	1.99	3.201	9.700	-3.03	0.319	L

2185.200 R2865 0.50 MK-X-A	31135 -2 to +2	-0.0060	1.99	3.044	9.323	-3.06	0.338	R
2110.200 R2860 0.50 MK-X-A	35904 -2 to +2	-0.0130	1.98	3.057	9.314	-3.05	0.313	L
2215.200 R2866 0.50 MK-X-A	36103 -2 to +2	-0.0040	2.00	3.151	9.753	-3.10	0.334	R
2230.200 R2867 0.50 MK-X-A	40953 -2 to +2	-0.0070	2.00	3.146	9.512	-3.02	0.335	R
2095.200 R2869 0.50 MK-X-A	40950 -2 to +2	-0.0075	2.00	3.491	10.333	-2.96	0.322	L
2201.250 R2858 0.50 MK-X-A	0.0 -5 to +15	-0.0075	2.50	3.690	9.923	-2.96	0.256	N/A
2171.250 R2842 0.50 MK-X-A	20671 -5 to +15	-0.0075	2.50	3.355	9.599	-2.86	0.243	R
2134.250 R2848 0.50 MK-X-A	20602 -2 to +2	-0.0200	2.50	3.330	9.470	-2.84	0.242	R
2135.250 R2854 0.50 MK-X-A	20677 -2 to +2	-0.0285	2.50	3.370	9.675	-2.87	0.226	L
2141.250 R2841 0.50 MK-X-A	25754 -5 to +15	N/A	2.50	3.244	9.337	-2.88	0.247	R
2126.250 R2843 0.50 MK-X-A	25782 -5 to +15	-0.0080	2.50	3.304	9.452	-2.86	0.251	L
2132.250 R2847 0.50 MK-X-A	25606 -2 to +2	-0.0188	2.50	3.345	9.529	-2.85	0.251	R

2033.250 R2853 0.50 MK-X-A	25819 -2 to +2	-0.0100	2.50	3.235	9.401	-2.91	0.252	L
2186.250 R2840 0.50 MK-X-A	30467 -5 to +15	-0.0050	2.50	3.379	9.581	-2.84	0.240	R
2030.250 R2846 0.50 MK-X-A	30766 -2 to +2	-0.0150	2.50	3.303	9.402	-2.85	0.259	R
2030.250 R2846 0.50 MK-X-A	30766 -2 to +2	-0.0150	2.50	3.303	9.402	-2.85	0.259	R
2031.250 R2852 0.50 MK-X-A	30854 -2 to +2	-0.0205	2.50	3.262	9.380	-2.88	0.241	L
2156.250 R2855 0.50 MK-X-A	30823 -5 to +15	-0.0063	2.50	3.227	9.342	-2.89	0.264	L
2156.250-1 R2856 0.50 MK-X-A	30763 -5 to +15	-0.0100	2.51	3.336	9.622	-2.88	0.269	L
2216.250 R2839 0.50 MK-X-A	35780 -5 to +15	-0.0050	2.50	3.347	9.634	-2.88	0.258	R
2029.250 R2844 0.50 MK-X-A	35566 -2 to +2	-0.0175	2.50	3.368	9.692	-2.88	0.256	L
2028.250 R2845 0.50 MK-X-A	35639 -2 to +2	-0.0100	2.50	3.209	9.392	-2.93	0.271	R
2111.250-2 R2857 0.50 MK-X-A	35689 -5 to +15	-0.0190	2.50	3.270	9.494	-2.90	0.251	L
2036.250 R2849 0.50 MK-X-A	40434 -2 to +2	-0.0180	2.50	3.344	9.509	-2.84	0.262	L

2018.250 R2850 0.50 MK-X-A	40456 -2 to +2	-0.0050	2.50	3.254	9.417	-2.89	0.251	R
2018.250-1 R2851 0.50 MK-X-A	39651 -2 to +2	-0.0075	2.50	3.326	9.558	-2.87	0.247	R
2202.300 R2901 0.50 MK-X-A	0.0 -2 to +2	N/A	2.95	3.324	9.251	-2.78	0.173	N/A
2202.300-1 R2902 0.50 MK-X-A	0.0 -2 to +2	N/A	2.95	3.280	9.199	-2.80	0.208	N/A
2142.300 R2882 0.50 MK-X-A	26101 -2 to +2	-0.0130	2.95	3.326	9.334	-2.81	0.200	R
2142.300-1 R2888 0.50 MK-X-A	26105 -2 to +2	-0.0130	2.95	3.318	9.355	-2.82	0.203	R
2127.300 R2892 0.50 MK-X-A	26125 -2 to +2	-0.0138	2.95	3.325	9.362	-2.82	0.207	L
2127.300-1 R2893 0.50 MK-X-A	26158 -2 to +2	-0.0220	2.95	3.216	9.109	-2.83	0.208	L
2187.300-4 R2908 0.50 MK-X-A	31063 -2 to +2	-0.0100	2.95	3.379	9.476	-2.80	0.213	R
2187.300-3 R2904 0.50 MK-X-A	31017 -2 to +2	N/A	2.95	3.322	9.297	-2.80	0.211	R
2187.300 R2883 0.50 MK-X-A	31065 -2 to +2	-0.0050	2.95	3.221	9.101	-2.83	0.206	R
2187.300-1 R2885 0.50 MK-X-A	31062 -2 to +2	-0.0077	2.95	3.310	9.372	-2.83	0.202	R

2187.300-2 R2886 0.50 MK-X-A	31079 -2 to +2	-0.0040	2.95	3.317	9.298	-2.80	0.203	R
2157.300 R2894 0.50 MK-X-A	31008 -2 to +2	-0.0108	2.95	3.260	9.259	-2.84	0.214	L
2157.300-1 R2895 0.50 MK-X-A	31016 -2 to +2	-0.0116	2.95	3.328	9.341	-2.81	0.211	L
2217.300 R2884 0.50 MK-X-A	35948 -2 to +2	-0.0080	2.95	3.273	9.243	-2.82	0.205	R
2112.300-1 R2897 0.50 MK-X-A	35826 -2 to +2	-0.0080	2.95	3.385	9.425	-2.78	0.194	L
2117.300-1 R2891 0.50 MK-X-A	35962 -2 to +2	-0.0100	2.95	3.313	9.328	-2.82	0.208	R
2112.300 R2896 0.50 MK-X-A	35815 -2 to +2	-0.0172	2.95	3.379	9.440	-2.79	0.205	L
2117.300-1 R2887 0.50 MK-X-A	35938 -2 to +2	N/A	2.95	3.317	9.332	-2.81	0.208	R
2232.300 R2889 0.50 MK-X-A	40682 -2 to +2	-0.0100	2.95	3.318	9.355	-2.82	0.203	R
2232.300-1 R2890 0.50 MK-X-A	40723 -2 to +2	-0.0080	2.95	3.232	9.250	-2.86	0.193	R
2097.300 R2898 0.50 MK-X-A	40500 -2 to +2	N/A	2.95	3.365	9.457	-2.81	0.204	L
2097.300-2 R2900 0.50 MK-X-A	40504 -2 to +2	-0.0128	2.95	3.355	9.405	-2.80	0.207	L

2097.300-5 R2907 0.50 MK-X-A	40622 -2 to +2	-0.0140	2.95	3.472	9.471	-2.73	0.215	L

APPENDIX B

Summary of Results

REDUCTION OF SPIN DAMPING COEFFICIENT

The Able MK-VI-A 0.50 in balance was intended to be used for present test series. It was a very precise but old and some rolling element strain gages had their bounding defective at the beginning of the test series. The Able MK-X-A 0.50 in balance was then used in replacement. This balance had its rolling element already damaged before the beginning of the tests. The consequence was a shift of the bridge offset (natural offset) that was just a little to high to be compensated by the balance excitation apparatus. Nevertheless, it was still possible to perform a calibration by using a different procedure than usual. Also, a testing methodology was set up in order to make possible to perform some spin damping measurements with enough precision to explore the feasibility of such experiment in the DREV trisonic facility.

While performing the rolling moment calibration, the difference with current DREV methodology consisted in that only single slope coefficients were derived for positive and negative rolling moment and an additive constant calculated to compensate for the bridge zero offset. Also, the non-linearities occurring when a balance is to be utilized within less than 1.0 % of its nominal capacity had to be investigated in order to choose an appropriate data reduction methodology.

It was then decided that the graphical plot of data results obtained from a testing methodology based on an image system would make evident roll measurement shifts induced by the balance. Since that present test series were to be made with a spinning model, it was decided, for test conditions at supersonic regime, to perform each test twice: one was be made with the model spinning in the right rotation sense while the second test was made in the opposite sense of rotation (left). All other test conditions were maintained constant.

Since two types of balances were utilized and that the Able MK-VI-A 0.50 in balance was damaged at the beginning of test run series, some data results were published and plotted directly without further treatment. Also, at the beginning of the test series, runs with spin in reverse senses of rotation were not performed. The data results related to the cases of single test run measurements are summarized in Table BI and mainly concern test runs made at Mach 0.50 to 0.93 (and some at Mach 1.73 that were left untouched because of their relative precision, i.e. right and left rotation tests gave similar results).

Table BII presents results, as the spin damping coefficients are concerned, for tests that were mainly made at Mach 1.03 to 3.00 and where runs in reverse senses of rotation were performed. The measured rolling moments felt by the balance for the right and left rotation tests were converted into % of the balance nominal capacity (see Table BIII) and plotted in Fig. B1. Also, the observed differences between roll measurements from right and left rotation tests were plotted.

It can be observed from Fig. B1, that most of the measurements were made in a region outside the ±0.2% balance accuracy (expressed in % of balance nominal capacity). Also, while the curve of absolute difference stays consistently positive it converges towards zero within the ±0.2% region. This behavior suggests the presence of non-linearities output signals when measurements made were less in absolute values than the balance accuracy (±0.2% of nominal capacity).

It was concluded, in a first time, that:

a- This process provided one roll measurement in the linear part of the positive roll element calibration curve, and one in the linear part of the negative roll element calibration curve.

b- The consistent positive difference between roll measurements from right and left rotation tests was an indication of a measurement shift that could be compensated by averaging results (average of spin damping coefficients obtained from right and left rotation tests). It must be mentioned that there was no way to compensate any symmetrical balance offset, unless an appropriate very precise calibration could be made. More details are given on that aspect in Appendix D.

The physical meaning of averaging right and left rotation test results is explained graphically in the Fig. B2 that presents a typical example. It can be observed that although the rolling moment measurements provided data with a measurement shift, the absolute difference between rolling moment measurements of right and left rotation represented twice the rolling moment measurement of a single run with a spinning model. Also, the right and left rotation test respective tables show that test conditions were kept identical in both cases.

The CLPC coefficients from right and left rotation tests were reduced in a first time by giving a positive value for the spin rate in order to help differentiating them and to verify the balance functionning. This has produced CLPC data results of positive values for the left rotation tests and negative values for the right rotation tests.

The measurement shift on spin damping coefficients can be calculated as follows (see Fig. B2):

$$\text{Measurement Shift on CLPC} = \underset{\text{positive value}}{\text{CLPC}_{\text{left rotation}}} - \left|\Delta\text{CLPC}/2\right|$$

where:

$$\Delta\text{CLPC} = \underset{\text{positive value}}{\text{CLPC}_{\text{left rotation}}} - \underset{\text{negative value}}{\text{CLPC}_{\text{right rotation}}}$$

$$\text{CLPC}_{\text{average}} = - \left|\Delta\text{CLPC}/2\right| = \underset{\text{measurement shift}}{\text{CLPC}_{\text{corrected for}}}$$

The spin damping coefficients published in Tables BI and BII show negative values as it should normally results when the data reduction is made by using positive spin rate values for the right sense of rotation and negative spin rate values for the left sense of rotation.

The calculation of the spin damping coefficient implies the used of a spin rate. In order to give to the apparent spin damping measurement shift a physical correlation with the balance, the apparent roll measurement shifts for right and left rotation tests were calculated and plotted in Fig. B3. These results, also presented in Table BIII, are expressed in % of the balance nominal capacity. In Fig. B3, the measured rolling moments from right and left rotation tests were plotted vs the average rolling moment calculated from the values of $CLPC_{average}$. The diagonal line represents the averaged rolling moments calculated from right and left rotation tests data results.

Figure B3 indicates that an average roll measurement shift having a magnitude of +0.0332% of the balance nominal capacity was observed. The standard deviation was ±0.032%. The linearity of the results is to be remarked. Also, it can be observed (Fig. B3) that although measurements made within the balance accuracy (±0.2%) present a measurement fluctuations of ±0.032%, the relative linearity of results is convincing that average values of spin damping coefficients can be used for comparison purposes.

The values of spin damping coefficients presented in Table BI and averaged values from right and left rotation tests presented in Table BII are plotted together in Fig. B4.

Table BIV gives the averages of longitudinal stability coefficients vs Mach numbers that were calculated by using all data from the whole test series. These results are plotted in Figs. B5 to B8.

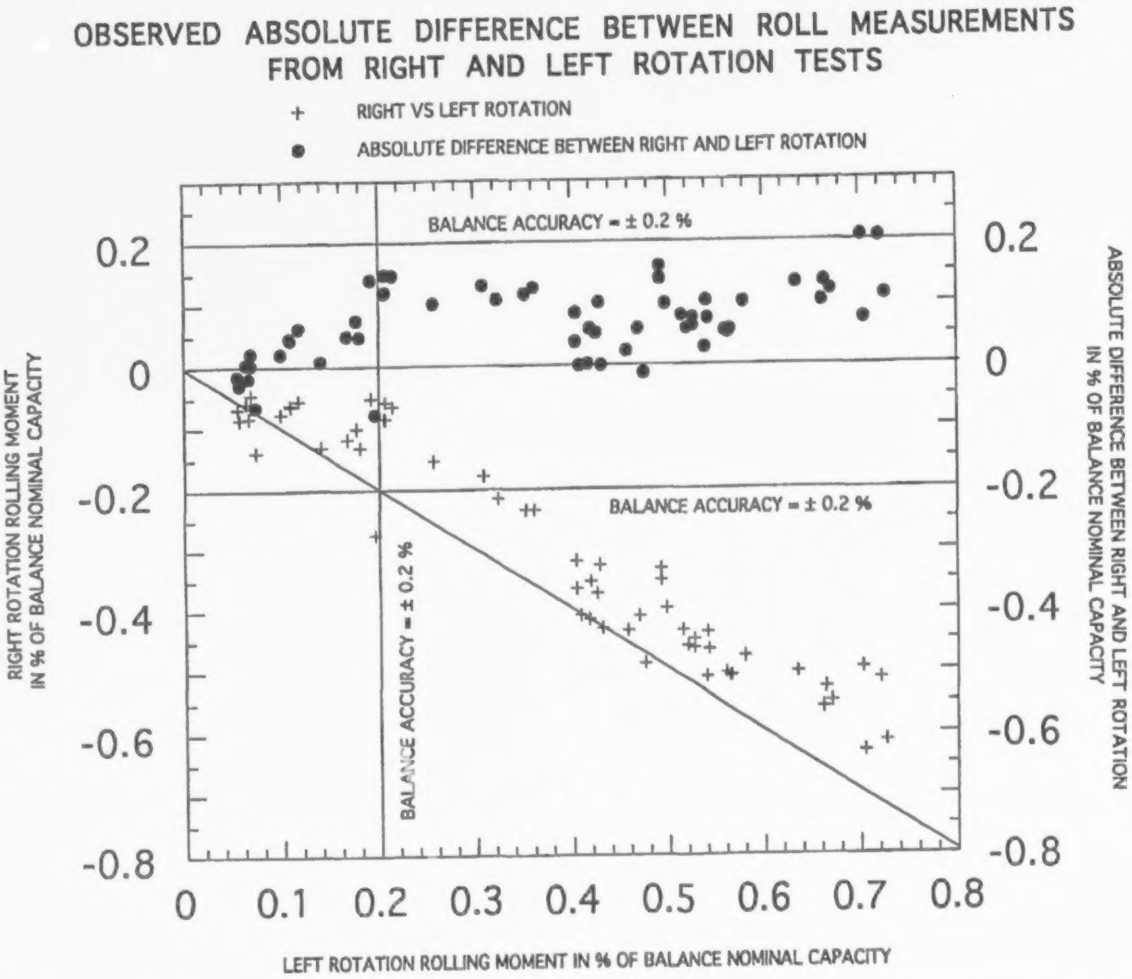

FIGURE B1 - Observed differences between measured rolling moment measurements from right and left rotation tests, expressed in % of balance nominal capacity

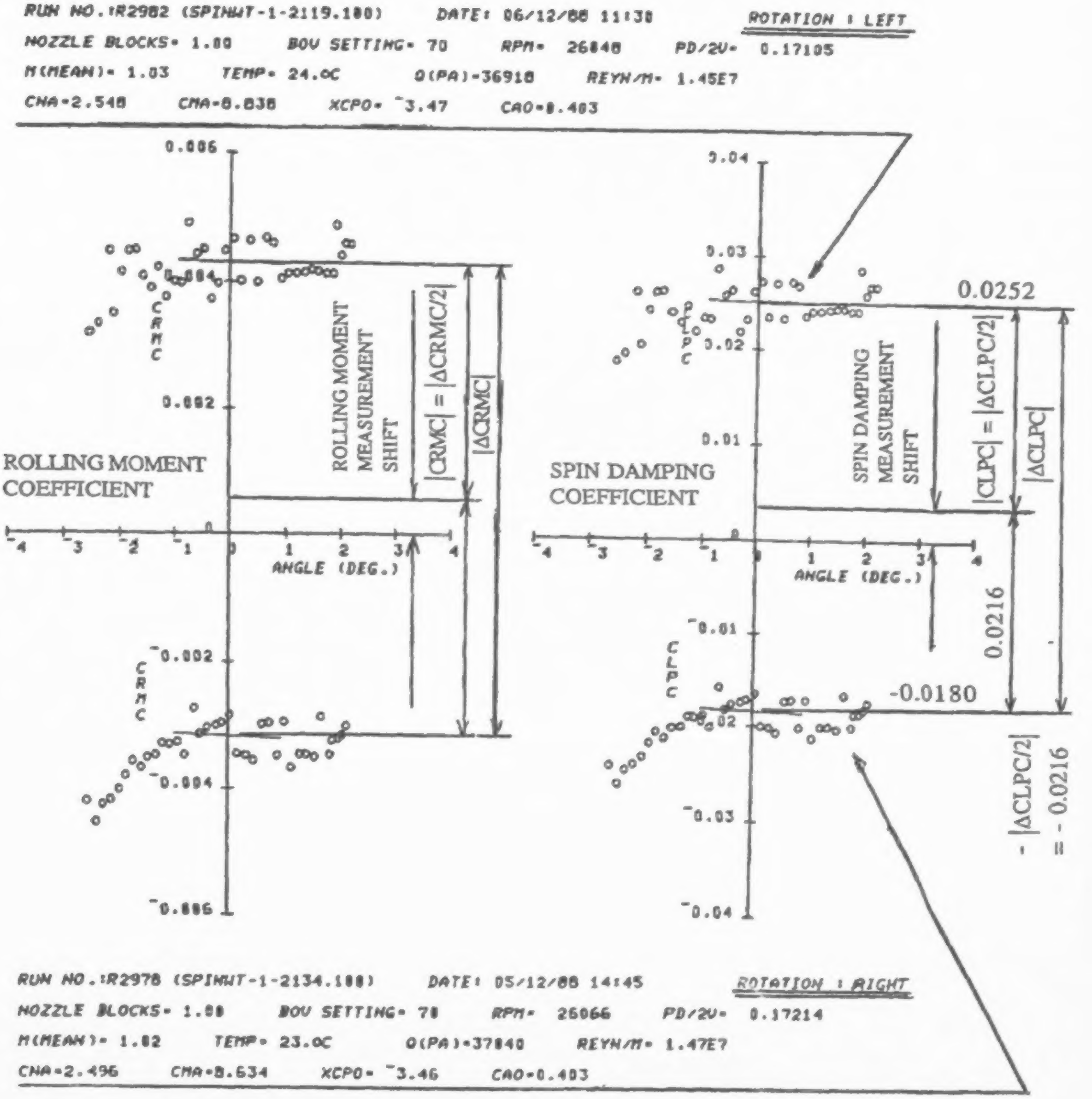

RUN NO.:R2982 (SPINWT-1-2119.100) DATE: 06/12/88 11:38 ROTATION : LEFT
NOZZLE BLOCKS= 1.00 BOV SETTING= 70 RPM= 26840 PD/2V= 0.17105
M(MEAN)= 1.03 TEMP= 24.0C Q(PA)=36910 REYN/M= 1.45E7
CNA=2.540 CMA=8.838 XCPO= ¯3.47 CAO=0.403

RUN NO.:R2978 (SPINWT-1-2134.100) DATE: 05/12/88 14:45 ROTATION : RIGHT
NOZZLE BLOCKS= 1.00 BOV SETTING= 70 RPM= 26066 PD/2V= 0.17214
M(MEAN)= 1.02 TEMP= 23.0C Q(PA)=37040 REYN/M= 1.47E7
CNA=2.496 CMA=8.634 XCPO= ¯3.46 CAO=0.403

0.006
0.004
0.002
0
¯0.002
¯0.004
¯0.006
CRMC
ROLLING MOMENT COEFFICIENT
ROLLING MOMENT MEASUREMENT SHIFT
|CRMC| = |ΔCRMC/2|
|ΔCRMC|
¯4 ¯3 ¯2 ¯1 0 1 2 3 4
ANGLE (DEG.)
0.04
0.03
0.02
0.01
¯0.01
¯0.02
¯0.03
¯0.04
CLPC
SPIN DAMPING COEFFICIENT
SPIN DAMPING MEASUREMENT SHIFT
|CLPC| = |ΔCLPC/2|
|ΔCLPC|
0.0252
0.0216
-0.0180
- |ΔCLPC/2|
= - 0.0216

FIGURE B2 - Averaging of spin damping coefficient values from right and left rotation tests to compensate for an apparent measurement shift

OBSERVED SHIFT BETWEEN ROLL MEASUREMENTS
FROM RIGHT AND LEFT ROTATION SPIN TESTS

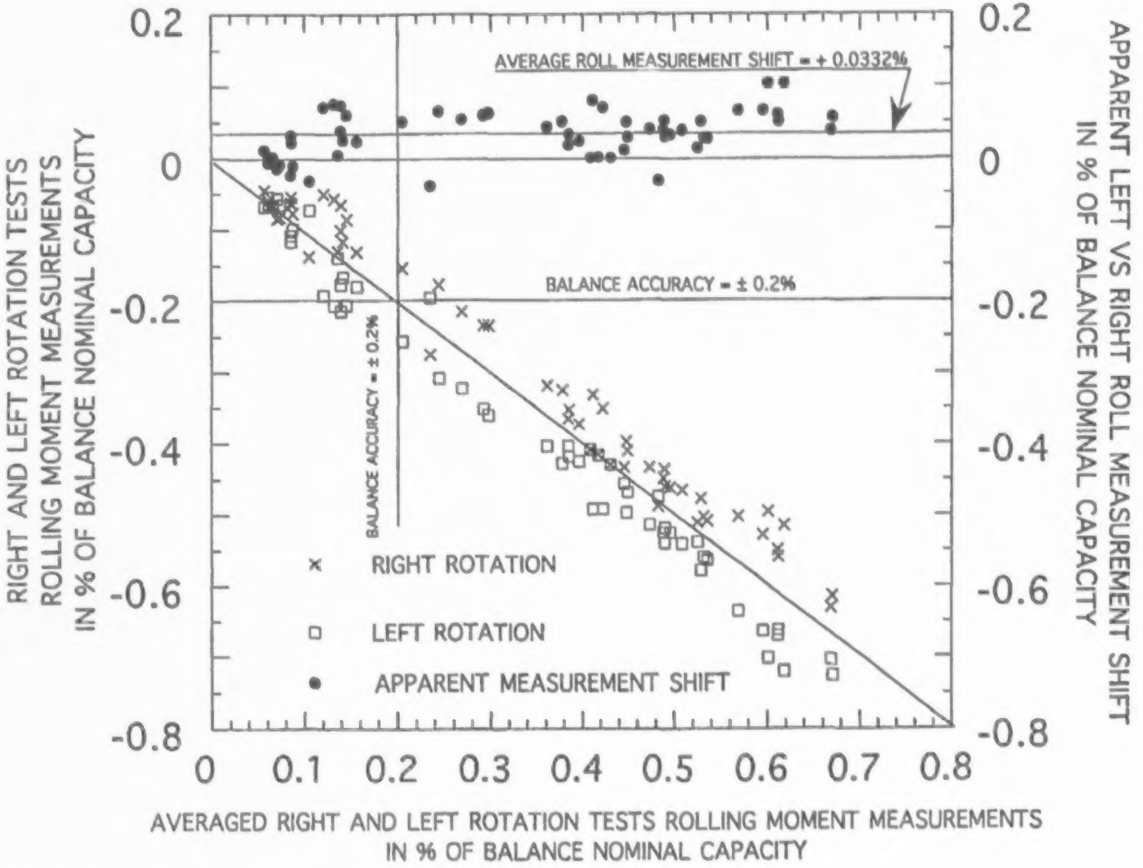

FIGURE B3 - Observed relative magnitude of roll measurement shift vs rolling moment measurements from right and left rotation tests

TABLE BI

Spin Damping Coefficients Plotted Directly Without Averaging with Data from Reverse Sense of Rotation Tests to Compensate for Roll Measurement Shift

Run numbers of **right rotation tests**	Run numbers of **left rotation tests**	MACH NUMBER	CLPC $\alpha = 0$ deg Test Spin Damping Coefficient **corrected for inertial effects** due to spin rate variations during test run **but not for roll measurement shift**	Pd/2V	Test RPM
R2821 QA= QA•d =	 18.81 N 0.7626 N•m	0.50	-0.0300 ℓ_{roll} = -.3398% bal.cap	0.251	20746
R2805 QA= QA•d =	 18.81 N 0.7626 N•m	0.50	-0.0250 ℓ_{roll} = -.3599% bal.cap	0.319	25529
R2802 QA= QA•d =	 18.81 N 0.7626 N•m	0.50	-0.0300 ℓ_{roll} = -.5212% bal.cap	0.385	30771
R2794 QA= QA•d =	 18.81 N 0.7626 N•m	0.50	-0.0300 ℓ_{roll} = -.5956% bal.cap	0.440	35809
R2820 QA= QA•d =	 31.13 N 1.2621 N•m	0.70	-0.0270 ℓ_{roll} = -.3831% bal.cap	0.190	20816
R2807 QA= QA•d =	 31.13 N 1.2621 N•m	0.70	-0.0260 ℓ_{roll} = -.4582% bal.cap	0.236	25892

R2804 QA= QA•d =	 31.13 N 1.2621 N•m	0.70	-0.0290 ℓ_{roll} = -.5111% bal.cap	0.236	25812
R2803 QA= QA•d =	 31.13 N 1.2621 N•m	0.70	-0.0270 ℓ_{roll} = -.5706% bal.cap	0.283	30749
R2793 QA= QA•d =	 31.13 N 1.2621 N•m	0.70	-0.0265 ℓ_{roll} = -.4354% bal.cap	0.330	35796
R2817 QA= QA•d =	 36.77 N 1.4908 N•m	0.80	-0.0325 ℓ_{roll} = -.4988% bal.cap	0.174	21394
R2819 QA= QA•d =	 36.77 N 1.4908 N•m	0.80	-0.0250 ℓ_{roll} = -.3837% bal.cap	0.174	20671
R2806 QA= QA•d =	 36.77 N 1.4908 N•m	0.80	-0.0230 ℓ_{roll} = -.4281% bal.cap	0.211	25842
R2801 QA= QA•d =	 36.77 N 1.4908 N•m	0.80	-0.0260 ℓ_{roll} = -.5711% bal.cap	0.249	30720
R2975 QA= QA•d =	 36.77 N 1.4908 N•m	0.81	-0.0260 ℓ_{roll} = -.6743% bal.cap	0.294	36236
R2791 QA= QA•d =	 36.77 N 1.4908 N•m	0.80	-0.0250 ℓ_{roll} = -.6484% bal.cap	0.294	35721
R2816 QA= QA•d =	 43.39 N 1.7589 N•m	0.93	-0.0330 ℓ_{roll} = -.5152% bal.cap	0.150	21085
R2814 QA= QA•d =	 43.39 N 1.7589 N•m	0.93	-0.0320 ℓ_{roll} = -.6161% bal.cap	0.185	25895
R2815 QA= QA•d =	 43.39 N 1.7589 N•m	0.93	-0.0280 ℓ_{roll} = -.5391% bal.cap	0.185	25895
R2795 QA= QA•d =	 43.39 N 1.7589 N•m	0.93	-0.0230 ℓ_{roll} = -.5219% bal.cap	0.218	30497

R2813 QA= QA•d =	 43.39 N 1.7589 N•m	0.93	-0.0300 ℓ_{roll} = -.6807% bal.cap	0.218	30779
R2790 QA= QA•d =	 43.39 N 1.7589 N•m	0.93	-0.0205 ℓ_{roll} = -.5419% bal.cap	0.254	35721
R2809 QA= QA•d =	 43.39 N 1.7589 N•m	0.93	-0.0275 ℓ_{roll} = -.7270% bal.cap	0.254	35714
R2974 QA= QA•d =	 51.54 N 2.0893 N•m	1.16	-0.0191 ℓ_{roll} = -.5053% bal.cap	0.214	35875
R2822 QA= QA•d =	 51.10 N 2.0717 N•m	1.70	-0.0120 ℓ_{roll} = -.1339% bal.cap	0.091	20771
 QA= QA•d =	R2835 51.10 N 2.0717 N•m	1.73	-0.0100 ℓ_{roll} = -.1397% bal.cap	0.114	25782
R2825 QA= QA•d =	 51.10 N 2.0717 N•m	1.74	-0.0100 ℓ_{roll} = -.1679% bal.cap	0.137	30709
 QA= QA•d =	R2836 51.10 N 2.0717 N•m	1.73	-0.0110 ℓ_{roll} = -.1847% bal.cap	0.137	30763
R2832 QA= QA•d =	 51.10 N 2.0717 N•m	1.74	-0.0100 ℓ_{roll} = -.1961% bal.cap	0.160	35860
 QA= QA•d =	R2834 51.10 N 2.0717 N•m	1.74	-0.0100 ℓ_{roll} = -.1961% bal.cap	0.160	35599

TABLE BII

Reduction of Spin Damping Coefficients to Compensate for Roll Measurement Shift

(Calculations Are Made by Using Data from Two Test Runs Performed in Same Test Conditions but with Model Spinning in Right and Left Senses of Rotation)

Run numbers of **right rotation tests** used to calculate spin damping coefficients corrected for roll measurement shift	Run numbers of **left rotation tests** used to calculate spin damping coefficients corrected for roll measurement shift	MACH NUMBER	CLPC $\alpha = 0$ deg Test Spin Damping Coefficient **corrected for inertial effects** due to spin rate variations during test run **but not for roll measurement shift**	Pd/2V	Test RPM
R2978		1.02	-0.0180	0.172	26066
	R2982	1.03	-0.0252	0.171	26048
AVERAGED FOR ROLL	SPIN DAMPING MEAS. SHIFT	**MACH 1.03**	**$C\ell_p$ -0.0216**	**Pd/2V 0.172**	ℓ_{roll} average = -.4222% bal.cap
R2979		1.03	-0.0210	0.172	26073
	R2983	1.03	-0.0240	0.171	26062
AVERAGED FOR ROLL	SPIN DAMPING MEAS. SHIFT	**MACH 1.03**	**$C\ell_p$ -0.0230**	**Pd/2V 0.172**	ℓ_{roll} average= -.4496% bal.cap
R2986		1.03	-0.0220	0.204	31060
	R2985	1.03	-0.0243	0.205	31097
AVERAGED FOR ROLL	SPIN DAMPING MEAS. SHIFT	**MACH 1.03**	**$C\ell_p$ -0.0231**	**Pd/2V 0.204**	ℓ_{roll} average= -.5355% bal.cap
R2987		1.03	-0.0206	0.204	31057
	R2984	1.03	-0.0250	0.204	31093
AVERAGED FOR ROLL	SPIN DAMPING MEAS. SHIFT	**MACH 1.03**	**$C\ell_p$ -0.0228**	**Pd/2V 0.204**	ℓ_{roll} average= -.5286% bal.cap

R2989		1.03	-0.0205	0.236	35987
	R2990	1.03	-0.0250	0.237	36035
AVERAGED FOR ROLL	SPIN DAMPING MEAS. SHIFT	**MACH** **1.03**	Cℓp **-0.0228**	**Pd/2V** **0.236**	ℓ_{roll} average= -.6115% bal.cap
R2988		1.03	-0.0185	0.236	35995
	R2991	1.03	-0.0262	0.236	36033
AVERAGED FOR ROLL	SPIN DAMPING MEAS. SHIFT	**MACH** **1.03**	Cℓp **-0.0224**	**Pd/2V** **0.236**	ℓ_{roll} average= -.6007% bal.cap
R2994		1.02	-0.0210	0.264	39927
	R2993	1.03	-0.0235	0.265	39968
AVERAGED FOR ROLL	SPIN DAMPING MEAS. SHIFT	**MACH** **1.03**	Cℓp **-0.0223**	**Pd/2V** **0.264**	ℓ_{roll} average= -.6690% bal.cap
R2995		1.02	-0.0207	0.264	39929
	R2992	1.03	-0.0245	0.258	39305
AVERAGED FOR ROLL	SPIN DAMPING MEAS. SHIFT	**MACH** **1.03**	Cℓp **-0.0226**	**Pd/2V** **0.261**	ℓ_{roll} average= -.6703% bal.cap
R2970		1.16	-0.0217	0.156	26099
	R2959	1.16	-0.0218	0.155	25998
AVERAGED FOR ROLL	SPIN DAMPING MEAS. SHIFT	**MACH** **1.16**	Cℓp **-0.0218**	**Pd/2V** **0.155**	ℓ_{roll} average= -.4177% bal.cap
R2969		1.16	-0.0195	0.156	26082
	R2958	1.16	-0.0220	0.155	25927
AVERAGED FOR ROLL	SPIN DAMPING MEAS. SHIFT	**MACH** **1.16**	Cℓp **-0.0207**	**Pd/2V** **0.155**	ℓ_{roll} average= -.3966% bal.cap
R2971		1.16	-0.0190	0.186	31120
	R2960	1.16	-0.0200	0.185	31007
AVERAGED FOR ROLL	SPIN DAMPING MEAS. SHIFT	**MACH** **1.16**	Cℓp **-0.0195**	**Pd/2V** **0.185**	ℓ_{roll} average= -.4460% bal.cap
R2971		1.16	-0.0190	0.186	31120
	R2962	1.16	-0.0235	0.186	31090
AVERAGED FOR ROLL	SPIN DAMPING MEAS. SHIFT	**MACH** **1.16**	Cℓp **-0.0213**	**Pd/2V** **0.186**	ℓ_{roll} average= -.4898% bal.cap
R2971		1.16	-0.0190	0.186	31120
	R2961	1.16	-0.0225	0.185	31063
AVERAGED FOR ROLL	SPIN DAMPING MEAS. SHIFT	**MACH** **1.16**	Cℓp **-0.0207**	**Pd/2V** **0.185**	ℓ_{roll} average= -.4734% bal.cap

R2973		1.16	-0.0190	0.214	35785
	R2965	1.16	-0.0240	0.215	35955
AVERAGED FOR ROLL	SPIN DAMPING MEAS. SHIFT	MACH 1.16	$C\ell_p$ -0.0215	Pd/2V 0.214	ℓ_{roll} average= -.5688% bal.cap
R2976		1.16	-0.0200	0.216	36260
	R2964	1.16	-0.0250	0.213	35786
AVERAGED FOR ROLL	SPIN DAMPING MEAS. SHIFT	MACH 1.16	$C\ell_p$ -0.0225	Pd/2V 0.214	ℓ_{roll} average= -.5953% bal.cap
R2996		1.16	-0.0190	0.239	39919
	R2999	1.16	-0.0225	0.238	39930
AVERAGED FOR ROLL	SPIN DAMPING MEAS. SHIFT	MACH 1.16	$C\ell_p$ -0.0208	Pd/2V 0.238	ℓ_{roll} average= -.6120% bal.cap
R2997		1.16	-0.0175	0.238	39895
	R2998	1.16	-0.0245	0.239	39947
AVERAGED FOR ROLL	SPIN DAMPING MEAS. SHIFT	MACH 1.16	$C\ell_p$ -0.0210	Pd/2V 0.238	ℓ_{roll} average= -.6179% bal.cap
R2931		1.27	-0.0175	0.146	26072
	R2944	1.27	-0.0230	0.145	26050
AVERAGED FOR ROLL	SPIN DAMPING MEAS. SHIFT	MACH 1.27	$C\ell_p$ -0.0203	Pd/2V 0.145	ℓ_{roll} average= -.3781% bal.cap
R2932		1.27	-0.0190	0.146	26074
	R2945	1.27	-0.0225	0.144	26053
AVERAGED FOR ROLL	SPIN DAMPING MEAS. SHIFT	MACH 1.27	$C\ell_p$ -0.0207	Pd/2V 0.145	ℓ_{roll} average= -.3855% bal.cap
R2933		1.27	-0.0185	0.171	31096
	R2949	1.27	-0.0185	0.174	31224
AVERAGED FOR ROLL	SPIN DAMPING MEAS. SHIFT	MACH 1.27	$C\ell_p$ -0.0185	Pd/2V 0.172	ℓ_{roll} average= -.4087% bal.cap
R2934		1.27	-0.0195	0.172	31102
	R2948	1.27	-0.0195	0.172	31224
AVERAGED FOR ROLL	SPIN DAMPING MEAS. SHIFT	MACH 1.27	$C\ell_p$ -0.0195	Pd/2V 0.172	ℓ_{roll} average= -.4308% bal.cap
R2935		1.27	-0.0175	0.200	36008
	R2952	1.27	-0.0205	0.200	35942
AVERAGED FOR ROLL	SPIN DAMPING MEAS. SHIFT	MACH 1.27	$C\ell_p$ -0.0190	Pd/2V 0.200	ℓ_{roll} average= -.4881% bal.cap

R2936		1.27	-0.0180	0.200	36031
	R2952	1.27	-0.0205	0.200	35942
AVERAGED FOR ROLL	SPIN DAMPING MEAS. SHIFT	**MACH 1.27**	**$C\ell_p$ -0.0193**	**Pd/2V 0.200**	ℓ_{roll} average= -.4958% bal.cap
R2937		1.27	-0.0190	0.200	36022
	R2954	1.27	-0.0185	0.200	36018
AVERAGED FOR ROLL	SPIN DAMPING MEAS. SHIFT	**MACH 1.27**	**$C\ell_p$ -0.0188**	**Pd/2V 0.200**	ℓ_{roll} average= -.4829% bal.cap
R2938		1.27	-0.0180	0.223	40005
	R2957	1.27	-0.0200	0.213	38119
AVERAGED FOR ROLL	SPIN DAMPING MEAS. SHIFT	**MACH 1.27**	**$C\ell_p$ -0.0190**	**Pd/2V 0.218**	ℓ_{roll} average= -.5320% bal.cap
R2938		1.27	-0.0180	0.223	40005
	R2956	1.27	-0.0200	0.217	39334
AVERAGED FOR ROLL	SPIN DAMPING MEAS. SHIFT	**MACH 1.27**	**$C\ell_p$ -0.0190**	**Pd/2V 0.220**	ℓ_{roll} average= -.5369% bal.cap
R2938		1.27	-0.0180	0.223	40005
	R2955	1.27	-0.0190	0.219	39476
AVERAGED FOR ROLL	SPIN DAMPING MEAS. SHIFT	**MACH 1.27**	**$C\ell_p$ -0.0185**	**Pd/2V 0.221**	ℓ_{roll} average= -.5252% bal.cap
R2912		1.32	-0.0130	0.142	26293
	R2918	1.36	-0.0200	0.139	26269
AVERAGED FOR ROLL	SPIN DAMPING MEAS. SHIFT	**MACH 1.34**	**$C\ell_p$ -0.0165**	**Pd/2V 0.140**	ℓ_{roll} average= -.2978% bal.cap
R2913		1.36	-0.0130	0.140	26318
	R2919	1.36	-0.0195	0.139	26270
AVERAGED FOR ROLL	SPIN DAMPING MEAS. SHIFT	**MACH 1.36**	**$C\ell_p$ -0.0162**	**Pd/2V 0.140**	ℓ_{roll} average= -.2924% bal.cap
R2914		1.36	-0.0150	0.165	31293
	R2920	1.36	-0.0190	0.165	31185
AVERAGED FOR ROLL	SPIN DAMPING MEAS. SHIFT	**MACH 1.36**	**$C\ell_p$ -0.0170**	**Pd/2V 0.165**	ℓ_{roll} average= -.3616% bal.cap
R2930		1.35	-0.0172	0.165	31058
	R2921	1.36	-0.0190	0.165	31140
AVERAGED FOR ROLL	SPIN DAMPING MEAS. SHIFT	**MACH 1.36**	**$C\ell_p$ -0.0181**	**Pd/2V 0.165**	ℓ_{roll} average= -.3850% bal.cap

R2916		1.36	-0.0135	0.192	36169
	R2922	1.36	-0.0200	0.190	35957
AVERAGED FOR ROLL	SPIN DAMPING MEAS. SHIFT	**MACH** **1.36**	**$C_{\ell p}$** **-0.0167**	**Pd/2V** **0.191**	ℓ_{roll} average= -.4112% bal.cap
R2917		1.36	-0.0160	0.191	36169
	R2923	1.32	-0.0200	0.195	35949
AVERAGED FOR ROLL	SPIN DAMPING MEAS. SHIFT	**MACH** **1.34**	**$C_{\ell p}$** **-0.0180**	**Pd/2V** **0.193**	ℓ_{roll} average= -.4479% bal.cap
R2926		1.36	-0.0170	0.210	39762
	R2925	1.36	-0.0192	0.210	39750
AVERAGED FOR ROLL	SPIN DAMPING MEAS. SHIFT	**MACH** **1.36**	**$C_{\ell p}$** **-0.0181**	**Pd/2V** **0.210**	ℓ_{roll} average= -.4900% bal.cap
R2927		1.36	-0.0172	0.210	39749
	R2924	1.36	-0.0200	0.215	40646
AVERAGED FOR ROLL	SPIN DAMPING MEAS. SHIFT	**MACH** **1.36**	**$C_{\ell p}$** **-0.0186**	**Pd/2V** **0.212**	ℓ_{roll} average= -.5083% bal.cap
R2876		1.49	-0.0050	0.129	26095
	R2874	1.49	-0.0120	0.130	26075
AVERAGED FOR ROLL	SPIN DAMPING MEAS. SHIFT	**MACH** **1.49**	**$C_{\ell p}$** **-0.0085**	**Pd/2V** **0.129**	ℓ_{roll} average= -.1461% bal.cap
R2877		1.49	-0.0075	0.153	31095
	R2873	1.49	-0.0125	0.155	31080
AVERAGED FOR ROLL	SPIN DAMPING MEAS. SHIFT	**MACH** **1.49**	**$C_{\ell p}$** **-0.0100**	**Pd/2V** **0.154**	ℓ_{roll} average= -.2052% bal.cap
R2878		1.49	-0.0075	0.177	35947
	R2872	1.49	-0.0130	0.179	36041
AVERAGED FOR ROLL	SPIN DAMPING MEAS. SHIFT	**MACH** **1.49**	**$C_{\ell p}$** **-0.0103**	**Pd/2V** **0.178**	ℓ_{roll} average= -.2443% bal.cap
R2879		1.49	-0.0080	0.202	40675
	R2875	1.49	-0.0120	0.201	40695
AVERAGED FOR ROLL	SPIN DAMPING MEAS. SHIFT	**MACH** **1.49**	**$C_{\ell p}$** **-0.0100**	**Pd/2V** **0.202**	ℓ_{roll} average= -.2692% bal.cap
R2827		1.73	-0.0140	0.160	35596
	R2830	1.73	-0.0100	0.160	35667
AVERAGED FOR ROLL	SPIN DAMPING MEAS. SHIFT	**MACH** **1.73**	**$C_{\ell p}$** **-0.0120**	**Pd/2V** **0.160**	ℓ_{roll} average= -.2354% bal.cap

R2864		1.98	-0.0070	0.108	26098
	R2863	1.98	-0.0055	0.108	26077
AVERAGED FOR ROLL	SPIN DAMPING MEAS. SHIFT	**MACH** **1.98**	$C_{\ell p}$ **-0.0062**	**Pd/2V** **0.108**	ℓ_{roll} average= -.0740% bal.cap
R2865		1.99	-0.0060	0.129	31135
	R2861	1.99	-0.0040	0.128	30832
AVERAGED FOR ROLL	SPIN DAMPING MEAS. SHIFT	**MACH** **1.99**	$C_{\ell p}$ **-0.0050**	**Pd/2V** **0.128**	ℓ_{roll} average= -.0708% bal.cap
R2866		2.00	-0.0040	0.149	36103
	R2860	1.98	-0.0130	0.150	35904
AVERAGED FOR ROLL	SPIN DAMPING MEAS. SHIFT	**MACH** **1.99**	$C_{\ell p}$ **-0.0085**	**Pd/2V** **0.149**	ℓ_{roll} average= -.1400% bal.cap
R2867		2.00	-0.0070	0.169	40953
	R2869	2.00	-0.0075	0.169	40950
AVERAGED FOR ROLL	SPIN DAMPING MEAS. SHIFT	**MACH** **2.00**	$C_{\ell p}$ **-0.0073**	**Pd/2V** **0.169**	ℓ_{roll} average= -.1364% bal.cap
R2848		2.50	-0.0200	0.076	20602
	R2854	2.50	-0.0285	0.076	20677
AVERAGED FOR ROLL	SPIN DAMPING MEAS. SHIFT	**MACH** **2.50**	$C_{\ell p}$ **-0.0243**	**Pd/2V** **0.076**	ℓ_{roll} average= -.1424% bal.cap
R2847		2.50	-0.0188	0.095	25606
	R2853	2.50	-0.0100	0.095	25819
AVERAGED FOR ROLL	SPIN DAMPING MEAS. SHIFT	**MACH** **2.50**	$C_{\ell p}$ **-0.0144**	**Pd/2V** **0.095**	ℓ_{roll} average= -.1055% bal.cap
R2846		2.50	-0.0150	0.114	30766
	R2852	2.50	-0.0205	0.114	30854
AVERAGED FOR ROLL	SPIN DAMPING MEAS. SHIFT	**MACH** **2.50**	$C_{\ell p}$ **-0.0178**	**Pd/2V** **0.114**	ℓ_{roll} average= -.1565% bal.cap
R2839		2.50	-0.0050	0.132	35780
	R2857	2.51	-0.0190	0.131	35689
AVERAGED FOR ROLL	SPIN DAMPING MEAS. SHIFT	**MACH** **2.50**	$C_{\ell p}$ **-0.0120**	**Pd/2V** **0.131**	ℓ_{roll} average= -.1213% bal.cap
R2845		2.50	-0.0100	0.130	35639
	R2844	2.50	-0.0175	0.131	35566
AVERAGED FOR ROLL	SPIN DAMPING MEAS. SHIFT	**MACH** **2.50**	$C_{\ell p}$ **-0.0138**	**Pd/2V** **0.131**	ℓ_{roll} average= -.1394% bal.cap

R2850		2.50	-0.0050	0.149	40456
	R2849	2.50	-0.0180	0.149	40434
AVERAGED FOR ROLL	SPIN DAMPING MEAS. SHIFT	**MACH** **2.50**	$C\ell_p$ **-0.0115**	**Pd/2V** **0.149**	ℓ_{roll} average= -.1322% bal.cap
R2851		2.50	-0.0075	0.146	39651
	R2849	2.50	-0.0180	0.149	40434
AVERAGED FOR ROLL	SPIN DAMPING MEAS. SHIFT	**MACH** **2.50**	$C\ell_p$ **-0.0128**	**Pd/2V** **0.148**	ℓ_{roll} average= -.1461% bal.cap
R2882		2.95	-0.0130	0.090	26101
	R2892	2.95	-0.0138	0.090	26125
AVERAGED FOR ROLL	SPIN DAMPING MEAS. SHIFT	**MACH** **2.95**	$C\ell_p$ **-0.0134**	**Pd/2V** **0.090**	ℓ_{roll} average= -.0663% bal.cap
R2888		2.95	-0.0130	0.090	26105
	R2893	2.95	-0.0220	0.090	26158
AVERAGED FOR ROLL	SPIN DAMPING MEAS. SHIFT	**MACH** **2.95**	$C\ell_p$ **-0.0175**	**Pd/2V** **0.090**	ℓ_{roll} average= -.0865% bal.cap
R2908		2.95	-0.0100	0.107	31063
	R2894	2.95	-0.0108	0.107	31008
AVERAGED FOR ROLL	SPIN DAMPING MEAS. SHIFT	**MACH** **2.95**	$C\ell_p$ **-0.0104**	**Pd/2V** **0.107**	ℓ_{roll} average= -.0611% bal.cap
R2885		2.95	-0.0077	0.107	31062
	R2895	2.95	-0.0116	0.107	31016
AVERAGED FOR ROLL	SPIN DAMPING MEAS. SHIFT	**MACH** **2.95**	$C\ell_p$ **-0.0097**	**Pd/2V** **0.107**	ℓ_{roll} average= -.0570% bal.cap
R2884		2.95	-0.0080	0.124	35948
	R2896	2.95	-0.0172	0.124	35815
AVERAGED FOR ROLL	SPIN DAMPING MEAS. SHIFT	**MACH** **2.95**	$C\ell_p$ **-0.0126**	**Pd/2V** **0.124**	ℓ_{roll} average= -.0858% bal.cap
R2891		2.95	-0.0100	0.124	35962
	R2897	2.95	-0.0080	0.124	35826
AVERAGED FOR ROLL	SPIN DAMPING MEAS. SHIFT	**MACH** **2.95**	$C\ell_p$ **-0.0090**	**Pd/2V** **0.124**	ℓ_{roll} corrected= -.0613% bal.cap
R2890		2.95	-0.0080	0.141	40723
	R2907	2.95	-0.0140	0.140	40622
AVERAGED FOR ROLL	SPIN DAMPING MEAS. SHIFT	**MACH** **2.95**	$C\ell_p$ **-0.0110**	**Pd/2V** **0.141**	ℓ_{roll} average= -.0852% bal.cap

R2889		2.95	-0.0100	0.141	40682
	R2900	2.95	-0.0128	0.140	40504
CORRECTED FOR ROLL	SPIN DAMPING MEAS. OFFSET	**MACH** **2.95**	**$C\ell_p$** **-0.0114**	**Pd/2V** **0.141**	ℓ_{roll} average= -.0883% bal.cap

TABLE BIII

Calculation of Observed Roll Measurement Shift

(Calculations Are Made by Using Data from Two Test Runs Performed in Same Test Conditions but with Model Spinning in Right and Left Senses of Rotation)

Run numbers of **right rotation tests** used to calculate spin damping coefficients corrected for roll measurement shift	Run numbers of **left rotation tests** used to calculate spin damping coefficients corrected for roll measurement shift	MACH NUMBER	CLPC $\alpha = 0$ deg Test Spin Damping Coefficient **corrected for inertial effects** due to spin rate variations during test run **but not for roll measurement shift**	Pd/2V	Test RPM
R2978		1.02	-0.0180	0.172	26066
	R2982	1.03	-0.0252	0.171	26048
QA = 47.37 N QA•d = 1.9205 N•m Right ℓ_{roll} % = **- 0.3518 %** Left ℓ_{roll} % = **+ 0.4926 %**		**MACH 1.03**	$C\ell_p$ shift = **0.0036** CRMC shift = **0.000619**	**Pd/2V 0.172**	ℓ_{roll} shift = +0.001189N•m = 0.070% balan. nominal capaci.
R2979		1.03	-0.0210	0.172	26073
	R2983	1.03	-0.0240	0.171	26062
QA = 47.37 N QA•d = 1.9205 N•m Right ℓ_{roll} % = **- 0.4105 %** Left ℓ_{roll} % = **+ 0.4691 %**		**MACH 1.03**	$C\ell_p$ shift = **0.0015** CRMC shift = **0.000258**	**Pd/2V 0.172**	ℓ_{roll} shift = +0.000495N•m = 0.029% balan. nominal capaci.
R2986		1.03	-0.0220	0.204	31060
	R2985	1.03	-0.0243	0.205	31097
QA = 47.37 N QA•d = 1.9205 N•m Right ℓ_{roll} % = **- 0.5100 %** Left ℓ_{roll} % = **+ 0.5633 %**		**MACH 1.03**	$C\ell_p$ shift = **0.0012** CRMC shift = **0.000235**	**Pd/2V 0.204**	ℓ_{roll} shift = +0.000451N•m = 0.027% balan. nominal capaci.

R2987		1.03	-0.0206	0.204	31057
	R2984	1.03	-0.0250	0.204	31093
QA = 47.37 N QA•d = 1.9205 N•m Right ℓ_{roll} % = - 0.4776 % Left ℓ_{roll} % = + 0.5796 %		MACH 1.03	$C\ell_p$ shift = 0.0022 CRMC shift = 0.000449	Pd/2V 0.204	ℓ_{roll} shift = +0.000862N•m ≡ 0.051% balan. nominal capaci.
R2989		1.03	-0.0205	0.236	35987
	R2990	1.03	-0.0250	0.237	36035
QA = 47.37 N QA•d = 1.9205 N•m Right ℓ_{roll} % = - 0.5498 % Left ℓ_{roll} % = + 0.6705 %		MACH 1.03	$C\ell_p$ shift = 0.0023 CRMC shift = 0.000531	Pd/2V 0.236	ℓ_{roll} shift = +0.001020N•m ≡ 0.060% balan. nominal capaci.
R2988		1.03	-0.0185	0.236	35995
	R2991	1.03	-0.0262	0.236	36033
QA = 47.37 N QA•d = 1.9205 N•m Right ℓ_{roll} % = - 0.4961 % Left ℓ_{roll} % = + 0.7027 %		MACH 1.03	$C\ell_p$ shift = 0.0039 CRMC shift = 0.000909	Pd/2V 0.236	ℓ_{roll} shift = +0.001745N•m ≡ 0.103% balan. nominal capaci.
R2994		1.02	-0.0210	0.264	39927
	R2993	1.03	-0.0235	0.265	39968
QA = 47.37 N QA•d = 1.9205 N•m Right ℓ_{roll} % = - 0.6300 % Left ℓ_{roll} % = + 0.7050 %		MACH 1.03	$C\ell_p$ shift = 0.0013 CRMC shift = 0.000330	Pd/2V 0.264	ℓ_{roll} shift = +0.000634N•m ≡ 0.038% balan. nominal capaci.
R2995		1.02	-0.0207	0.264	39929
	R2992	1.03	-0.0245	0.258	39305
QA = 47.37 N QA•d = 1.9205 N•m Right ℓ_{roll} % = - 0.6140 % Left ℓ_{roll} % = + 0.7267 %		MACH 1.03	$C\ell_p$ shift = 0.0019 CRMC shift = 0.000496	Pd/2V 0.261	ℓ_{roll} shift = +0.000952N•m ≡ 0.056% balan. nominal capaci.
R2970		1.16	-0.0217	0.156	26099
	R2959	1.16	-0.0218	0.155	25998
QA = 51.54 N QA•d = 2.0893 N•m Right ℓ_{roll} % = - 0.4158 % Left ℓ_{roll} % = + 0.4177 %		MACH 1.16	$C\ell_p$ shift = 0.00005 CRMC shift = 0.000008	Pd/2V 0.155	ℓ_{roll} shift = +0.000016N•m ≡ .0010% balan. nominal capaci.

R2969		1.16	-0.0195	0.156	26082
	R2958	1.16	-0.0220	0.155	25927
QA = 51.54 N QA•d = 2.0893 N•m Right ℓ_{roll} % = - 0.3737 % Left ℓ_{roll} % = + 0.4257 %		**MACH** **1.16**	$C\ell_p$ shift = **0.0013** CRMC shift = **0.000194**	**Pd/2V** **0.155**	ℓ_{roll} shift = +0.000405N•m ≡ 0.024% balan. nominal capaci.
R2971		1.16	-0.0190	0.186	31120
	R2960	1.16	-0.0200	0.185	31007
QA = 51.54 N QA•d = 2.0893 N•m Right ℓ_{roll} % = - 0.4345 % Left ℓ_{roll} % = + 0.4574 %		**MACH** **1.16**	$C\ell_p$ shift = **0.0005** CRMC shift = **0.000093**	**Pd/2V** **0.185**	ℓ_{roll} shift = +0.000193N•m ≡ 0.011% balan. nominal capaci.
R2971		1.16	-0.0190	0.186	31120
	R2962	1.16	-0.0235	0.186	31090
QA = 51.54 N QA•d = 2.0893 N•m Right ℓ_{roll} % = - 0.4369 % Left ℓ_{roll} % = + 0.5404 %		**MACH** **1.16**	$C\ell_p$ shift = **0.0023** CRMC shift = **0.000419**	**Pd/2V** **0.186**	ℓ_{roll} shift = +0.000874N•m ≡ 0.052% balan. nominal capaci.
R2971		1.16	-0.0190	0.186	31120
	R2961	1.16	-0.0225	0.185	31063
QA = 51.54 N QA•d = 2.0893 N•m Right ℓ_{roll} % = - 0.4345 % Left ℓ_{roll} % = + 0.5146 %		**MACH** **1.16**	$C\ell_p$ shift = **0.0018** CRMC shift = **0.000324**	**Pd/2V** **0.185**	ℓ_{roll} shift = +0.000676N•m ≡ 0.040% balan. nominal capaci.
R2973		1.16	-0.0190	0.214	35785
	R2965	1.16	-0.0240	0.215	35955
QA = 51.54 N QA•d = 2.0893 N•m Right ℓ_{roll} % = - 0.5027 % Left ℓ_{roll} % = + 0.6349 %		**MACH** **1.16**	$C\ell_p$ shift = **0.0025** CRMC shift = **0.000535**	**Pd/2V** **0.214**	ℓ_{roll} shift = +0.001118N•m ≡ 0.066% balan. nominal capaci.
R2976		1.16	-0.0200	0.216	36260
	R2964	1.16	-0.0250	0.213	35786
QA = 51.54 N QA•d = 2.0893 N•m Right ℓ_{roll} % = - 0.5291 % Left ℓ_{roll} % = + 0.6641 %		**MACH** **1.16**	$C\ell_p$ shift = **0.0025** CRMC shift = **0.000535**	**Pd/2V** **0.214**	ℓ_{roll} shift = +0.001118N•m ≡ 0.066% balan. nominal capaci.

R2996		1.16	-0.0190	0.239	39919
	R2999	1.16	-0.0225	0.238	39930
QA = 51.54 N QA•d = 2.0893 N•m Right ℓ_{roll} % = - 0.5590 % Left ℓ_{roll} % = + 0.6620 %		**MACH** **1.16**	$C\ell_p$ shift = **0.0018** CRMC shift = **0.000417**	**Pd/2V** **0.238**	ℓ_{roll} shift = +0.000870N•m = 0.051% balan. nominal capaci.
R2997		1.16	-0.0175	0.238	39895
	R2998	1.16	-0.0245	0.239	39947
QA = 51.54 N QA•d = 2.0893 N•m Right ℓ_{roll} % = - 0.5149 % Left ℓ_{roll} % = + 0.7209 %		**MACH** **1.16**	$C\ell_p$ shift = **0.0035** CRMC shift = **0.000833**	**Pd/2V** **0.238**	ℓ_{roll} shift = +0.001740N•m = 0.103% balan. nominal capaci.
R2931		1.27	-0.0175	0.146	26072
	R2944	1.27	-0.0230	0.145	26050
QA = 53.55 N QA•d = 2.1708 N•m Right ℓ_{roll} % = - 0.3259 % Left ℓ_{roll} % = + 0.4284 %		**MACH** **1.27**	$C\ell_p$ shift = **0.0028** CRMC shift = **0.000399**	**Pd/2V** **0.145**	ℓ_{roll} shift = +0.000866N•m = 0.051% balan. nominal capaci.
R2932		1.27	-0.0190	0.146	26074
	R2945	1.27	-0.0225	0.144	26053
QA = 53.55 N QA•d = 2.1708 N•m Right ℓ_{roll} % = - 0.3539 % Left ℓ_{roll} % = + 0.4191 %		**MACH** **1.27**	$C\ell_p$ shift = **0.0018** CRMC shift = **0.000254**	**Pd/2V** **0.145**	ℓ_{roll} shift = +0.000551N•m = 0.033% balan. nominal capaci.
R2933		1.27	-0.0185	0.171	31096
	R2949	1.27	-0.0185	0.174	31224
QA = 53.55 N QA•d = 2.1708 N•m Right ℓ_{roll} % = - 0.4087 % Left ℓ_{roll} % = + 0.4087 %		**MACH** **1.27**	$C\ell_p$ shift = **0.0000** CRMC offset = **0.000000**	**Pd/2V** **0.172**	ℓ_{roll} shift = +0.000000N•m = 0.000% balan. nominal capaci.
R2934		1.27	-0.0195	0.172	31102
	R2948	1.27	-0.0195	0.172	31224
QA = 53.55 N QA•d = 2.1708 N•m Right ℓ_{roll} % = - 0.4308 % Left ℓ_{roll} % = + 0.4308 %		**MACH** **1.27**	$C\ell_p$ shift = **0.0000** CRMC shift = **0.000000**	**Pd/2V** **0.172**	ℓ_{roll} shift = +0.000000N•m = 0.000% balan. nominal capaci.

R2935		1.27	-0.0175	0.200	36008
	R2952	1.27	-0.0205	0.200	35942
QA = 53.55 N QA•d = 2.1708 N•m Right ℓ_{roll} % = - 0.4496 % Left ℓ_{roll} % = + 0.5266 %		**MACH** **1.27**	Cℓ_p shift = 0.0015 CRMC shift = 0.000300	**Pd/2V** **0.200**	ℓ_{roll} shift = +0.000651N•m ≡ 0.039% balan. nominal capaci.
R2936		1.27	-0.0180	0.200	36031
	R2952	1.27	-0.0205	0.200	35942
QA = 53.55 N QA•d = 2.1708 N•m Right ℓ_{roll} % = - 0.4624 % Left ℓ_{roll} % = + 0.5266 %		**MACH** **1.27**	Cℓ_p shift = 0.0013 CRMC shift = 0.000250	**Pd/2V** **0.200**	ℓ_{roll} shift = +0.000543N•m ≡ 0.032% balan. nominal capaci.
R2937		1.27	-0.0190	0.200	36022
	R2954	1.27	-0.0185	0.200	36018
QA = 53.55 N QA•d = 2.1708 N•m Right ℓ_{roll} % = - 0.4881 % Left ℓ_{roll} % = + 0.4753 %		**MACH** **1.27**	Cℓ_p shift = -0.0013 CRMC shift = -0.000250	**Pd/2V** **0.200**	ℓ_{roll} shift = -0.000543N•m ≡ 0.032% balan. nominal capaci.
R2938		1.27	-0.0180	0.223	40005
	R2957	1.27	-0.0200	0.213	38119
QA = 53.55 N QA•d = 2.1708 N•m Right ℓ_{roll} % = - 0.5040 % Left ℓ_{roll} % = + 0.5600 %		**MACH** **1.27**	Cℓ_p shift = 0.0010 CRMC shift = 0.000218	**Pd/2V** **0.218**	ℓ_{roll} shift = +0.000473N•m ≡ 0.028% balan. nominal capaci.
R2938		1.27	-0.0180	0.223	40005
	R2956	1.27	-0.0200	0.217	39334
QA = 53.55 N QA•d = 2.1708 N•m Right ℓ_{roll} % = - 0.5087 % Left ℓ_{roll} % = + 0.5652 %		**MACH** **1.27**	Cℓ_p shift = 0.0010 CRMC shift = 0.000220	**Pd/2V** **0.220**	ℓ_{roll} shift = +0.000478N•m ≡ 0.028% balan. nominal capaci.
R2938		1.27	-0.0180	0.223	40005
	R2955	1.27	-0.0190	0.219	39476
QA = 53.55 N QA•d = 2.1708 N•m Right ℓ_{roll} % = - 0.5110 % Left ℓ_{roll} % = + 0.5394 %		**MACH** **1.27**	Cℓ_p shift = 0.0005 CRMC shift = 0.000111	**Pd/2V** **0.221**	ℓ_{roll} shift = +0.000240N•m ≡ 0.014% balan. nominal capaci.

R2912		1.32	-0.0130	0.142	26293
	R2918	1.36	-0.0200	0.139	26269
QA = 53.74 N QA•d = 2.1787 N•m Right ℓ_{roll} % = - 0.2346 % Left ℓ_{roll} % = + 0.3610 %		**MACH** **1.34**	$C\ell_p$ shift = **0.0035** CRMC shift = **0.000490**	**Pd/2V** **0.140**	ℓ_{roll} shift = +0.001068N•m ≡ 0.063% balan. nominal capaci.
R2913		1.36	-0.0130	0.140	26318
	R2919	1.36	-0.0195	0.139	26270
QA = 53.74 N QA•d = 2.1787 N•m Right ℓ_{roll} % = - 0.2346 % Left ℓ_{roll} % = + 0.3519 %		**MACH** **1.36**	$C\ell_p$ shift = **0.0033** CRMC shift = **0.000455**	**Pd/2V** **0.140**	ℓ_{roll} shift = +0.000991N•m ≡ 0.059% balan. nominal capaci.
R2914		1.36	-0.0150	0.165	31293
	R2920	1.36	-0.0190	0.165	31185
QA = 53.74 N QA•d = 2.1787 N•m Right ℓ_{roll} % = - 0.3191 % Left ℓ_{roll} % = + 0.4042 %		**MACH** **1.36**	$C\ell_p$ shift = **0.0020** CRMC shift = **0.000330**	**Pd/2V** **0.165**	ℓ_{roll} shift = +0.000719N•m ≡ 0.043% balan. nominal capaci.
R2930		1.35	-0.0172	0.165	31058
	R2921	1.36	-0.0190	0.165	31140
QA = 53.74 N QA•d = 2.1787 N•m Right ℓ_{roll} % = - 0.3659 % Left ℓ_{roll} % = + 0.4042 %		**MACH** **1.36**	$C\ell_p$ shift = **0.0009** CRMC shift = **0.000149**	**Pd/2V** **0.165**	ℓ_{roll} shift = +0.000324N•m ≡ 0.019% balan. nominal capaci.
R2916		1.36	-0.0135	0.192	36169
	R2922	1.36	-0.0200	0.190	35957
QA = 53.74 N QA•d = 2.1787 N•m Right ℓ_{roll} % = - 0.3324 % Left ℓ_{roll} % = + 0.4925 %		**MACH** **1.36**	$C\ell_p$ shift = **0.0033** CRMC shift = **0.000621**	**Pd/2V** **0.191**	ℓ_{roll} shift = +0.001352N•m ≡ 0.080% balan. nominal capaci.
R2917		1.36	-0.0160	0.191	36169
	R2923	1.32	-0.0200	0.195	35949
QA = 53.74 N QA•d = 2.1787 N•m Right ℓ_{roll} % = - 0.3981 % Left ℓ_{roll} % = + 0.4976 %		**MACH** **1.34**	$C\ell_p$ shift = **0.0020** CRMC shift = **0.000386**	**Pd/2V** **0.193**	ℓ_{roll} shift = +0.000841N•m ≡ 0.050% balan. nominal capaci.

R2926		1.36	-0.0170	0.210	39762
	R2925	1.36	-0.0192	0.210	39750
QA = 53.74 N QA•d = 2.1787 N•m Right ℓ_{roll} % = - 0.4602 % Left ℓ_{roll} % = + 0.5198 %		**MACH** **1.36**	$C\ell_p$ shift = **0.0011** CRMC shift = **0.000231**	**Pd/2V** **0.210**	ℓ_{roll} shift = +0.000503N•m ≡ 0.030% balan. nominal capaci.
R2927		1.36	-0.0172	0.210	39749
	R2924	1.36	-0.0200	0.215	40646
QA = 53.74 N QA•d = 2.1787 N•m Right ℓ_{roll} % = - 0.4656 % Left ℓ_{roll} % = + 0.5415 %		**MACH** **1.36**	$C\ell_p$ shift = **0.0014** CRMC shift = **0.000294**	**Pd/2V** **0.210**	ℓ_{roll} shift = +0.000641N•m ≡ 0.038% balan. nominal capaci.
R2876		1.49	-0.0050	0.129	26095
	R2874	1.49	-0.0120	0.130	26075
QA = 55.54 N QA•d = 2.2518 N•m Right ℓ_{roll} % = - 0.0859 % Left ℓ_{roll} % = + 0.2063 %		**MACH** **1.49**	$C\ell_p$ shift = **0.0035** CRMC shift = **0.000452**	**Pd/2V** **0.129**	ℓ_{roll} shift = +0.001017N•m ≡ 0.060% balan. nominal capaci.
R2877		1.49	-0.0075	0.153	31095
	R2873	1.49	-0.0125	0.155	31080
QA = 55.54 N QA•d = 2.2518 N•m Right ℓ_{roll} % = - 0.1539 % Left ℓ_{roll} % = + 0.2565 %		**MACH** **1.49**	$C\ell_p$ shift = **0.0025** CRMC shift = **0.000385**	**Pd/2V** **0.154**	ℓ_{roll} shift = +0.000867N•m ≡ 0.051% balan. nominal capaci.
R2878		1.49	-0.0075	0.177	35947
	R2872	1.49	-0.0130	0.179	36041
QA = 55.54 N QA•d = 2.2518 N•m Right ℓ_{roll} % = - 0.1779 % Left ℓ_{roll} % = + 0.3083 %		**MACH** **1.49**	$C\ell_p$ shift = **0.0028** CRMC shift = **0.000490**	**Pd/2V** **0.178**	ℓ_{roll} shift = +0.001102N•m ≡ 0.065% balan. nominal capaci.
R2879		1.49	-0.0080	0.202	40675
	R2875	1.49	-0.0120	0.201	40695
QA = 55.54 N QA•d = 2.2518 N•m Right ℓ_{roll} % = - 0.2153 % Left ℓ_{roll} % = + 0.3230 %		**MACH** **1.49**	$C\ell_p$ shift = **0.0020** CRMC shift = **0.000404**	**Pd/2V** **0.202**	ℓ_{roll} shift= +0.000910N•m ≡ 0.054% balan. nominal capaci.

R2827		1.73	-0.0140	0.160	35596
	R2830	1.73	-0.0100	0.160	35667
QA = 51.10 N QA•d = 2.0717 N•m Right ℓ_{roll} % = - 0.2746 % Left ℓ_{roll} % = + 0.1961 %		**MACH** **1.73**	$C\ell_p$ shift = **-0.0020** CRMC shift = **-0.000320**	**Pd/2V** **0.160**	ℓ_{roll} shift = -0.000663N•m ≡ 0.039% balan. nominal capaci.
R2864		1.98	-0.0070	0.108	26098
	R2863	1.98	-0.0055	0.108	26077
QA = 46.09 N QA•d = 1.8686 N•m Right ℓ_{roll} % = - 0.0836 % Left ℓ_{roll} % = + 0.0657 %		**MACH** **1.98**	$C\ell_p$ shift = **-0.0008** CRMC shift = **-0.000081**	**Pd/2V** **0.108**	ℓ_{roll} shift = -0.000151N•m ≡ 0.009% balan. nominal capaci.
R2865		1.99	-0.0060	0.129	31135
	R2861	1.99	-0.0040	0.128	30832
QA = 46.09 N QA•d = 1.8686 N•m Right ℓ_{roll} % = - 0.0849 % Left ℓ_{roll} % = + 0.0566 %		**MACH** **1.99**	$C\ell_p$ shift = **-0.0010** CRMC shift = **-0.000128**	**Pd/2V** **0.128**	ℓ_{roll} shift = -0.000239N•m ≡ 0.014% balan. nominal capaci.
R2866		2.00	-0.0040	0.149	36103
	R2860	1.98	-0.0130	0.150	35904
QA = 46.09 N QA•d = 1.8686 N•m Right ℓ_{roll} % = - 0.0659 % Left ℓ_{roll} % = + 0.2142 %		**MACH** **1.99**	$C\ell_p$ shift = **0.0045** CRMC shift = **0.000671**	**Pd/2V** **0.149**	ℓ_{roll} shift = +0.001253N•m ≡ 0.074% balan. nominal capaci.
R2867		2.00	-0.0070	0.169	40953
	R2869	2.00	-0.0075	0.169	40950
QA = 46.09 N QA•d = 1.8686 N•m Right ℓ_{roll} % = - 0.1308 % Left ℓ_{roll} % = + 0.1401 %		**MACH** **2.00**	$C\ell_p$ shift = **0.0003** CRMC shift = **0.0000423**	**Pd/2V** **0.169**	ℓ_{roll} shift = +0.000079N•m ≡ .0047% balan. nominal capaci.
R2848		2.50	-0.0200	0.076	20602
	R2854	2.50	-0.0285	0.076	20677
QA = 32.16 N QA•d = 1.3036 N•m Right ℓ_{roll} % = - 0.1172 % Left ℓ_{roll} % = + 0.1671 %		**MACH** **2.50**	$C\ell_p$ shift = **0.0043** CRMC shift = **0.000323**	**Pd/2V** **0.076**	ℓ_{roll} shift = +0.000421N•m ≡ 0.025% balan. nominal capaci.

R2847		2.50	-0.0188	0.095	25606
	R2853	2.50	-0.0100	0.095	25819
QA = 32.16 N QA•d = 1.3036 N•m Right ℓ_{roll} % = - 0.1378 % Left ℓ_{roll} % = + 0.0733 %		**MACH** **2.50**	$C\ell_p$ shift = **-0.0044** CRMC shift = **-0.000418**	**Pd/2V** **0.095**	ℓ_{roll} shift = -0.000545N•m ≡ 0.032% balan. nominal capaci.
R2846		2.50	-0.0150	0.114	30766
	R2852	2.50	-0.0205	0.114	30854
QA = 32.16 N QA•d = 1.3036 N•m Right ℓ_{roll} % = - 0.1319 % Left ℓ_{roll} % = + 0.1803 %		**MACH** **2.50**	$C\ell_p$ shift = **0.0028** CRMC shift = **0.000314**	**Pd/2V** **0.114**	ℓ_{roll} shift = +0.000409N•m ≡ 0.024% balan. nominal capaci.
R2839		2.50	-0.0050	0.132	35780
	R2857	2.51	-0.0190	0.131	35689
QA = 32.16 N QA•d = 1.3036 N•m Right ℓ_{roll} % = - 0.0505 % Left ℓ_{roll} % = + 0.1920 %		**MACH** **2.50**	$C\ell_p$ shift = **0.0070** CRMC shift = **0.000917**	**Pd/2V** **0.131**	ℓ_{roll} shift = +0.001195N•m ≡ 0.071% balan. nominal capaci.
R2845		2.50	-0.0100	0.130	35639
	R2844	2.50	-0.0175	0.131	35566
QA = 32.16 N QA•d = 1.3036 N•m Right ℓ_{roll} % = - 0.1010 % Left ℓ_{roll} % = + 0.1768 %		**MACH** **2.50**	$C\ell_p$ shift = **0.0038** CRMC shift = **0.000491**	**Pd/2V** **0.131**	ℓ_{roll} shift = +0.000640N•m ≡ 0.038% balan. nominal capaci.
R2850		2.50	-0.0050	0.149	40456
	R2849	2.50	-0.0180	0.149	40434
QA = 32.16 N QA•d = 1.3036 N•m Right ℓ_{roll} % = - 0.0575 % Left ℓ_{roll} % = + 0.2069 %		**MACH** **2.50**	$C\ell_p$ shift = **0.0065** CRMC shift = **0.000969**	**Pd/2V** **0.149**	ℓ_{roll} shift = +0.001263N•m ≡ 0.075% balan. nominal capaci.
R2851		2.50	-0.0075	0.146	39651
	R2849	2.50	-0.0180	0.149	40434
QA = 32.16 N QA•d = 1.3036 N•m Right ℓ_{roll} % = - 0.0856 % Left ℓ_{roll} % = + 0.2055 %		**MACH** **2.50**	$C\ell_p$ shift = **0.0053** CRMC shift = **0.000777**	**Pd/2V** **0.148**	ℓ_{roll} shift = +0.001013N•m ≡ 0.060% balan. nominal capaci.

R2882		2.95	-0.0130	0.090	26101
	R2892	2.95	-0.0138	0.090	26125
QA = 22.90 N QA•d = 0.9284 N•m Right ℓ_{roll} % = - 0.0643 % Left ℓ_{roll} % = + 0.0682 %		**MACH** **2.95**	$C\ell_p$ shift = **0.00040** CRMC shift = **0.000036**	**Pd/2V** **0.090**	ℓ_{roll} shift = +0.000033N•m ≡ 0.002% balan. nominal capaci.
R2888		2.95	-0.0130	0.090	26105
	R2893	2.95	-0.0220	0.090	26158
QA = 22.90 N QA•d = 0.9284 N•m Right ℓ_{roll} % = - 0.0643 % Left ℓ_{roll} % = + 0.1088 %		**MACH** **2.95**	$C\ell_p$ shift = **0.0045** CRMC shift = **0.000405**	**Pd/2V** **0.090**	ℓ_{roll} shift = +0.000376N•m ≡ 0.022% balan. nominal capaci.
R2908		2.95	-0.0100	0.107	31063
	R2894	2.95	-0.0108	0.107	31008
QA = 22.90 N QA•d = 0.9284 N•m Right ℓ_{roll} % = - 0.0588 % Left ℓ_{roll} % = + 0.0635 %		**MACH** **2.95**	$C\ell_p$ shift = **0.00040** CRMC shift = **0.0000428**	**Pd/2V** **0.107**	ℓ_{roll} shift = +0.000040N•m ≡ .0024% balan. nominal capaci.
R2885		2.95	-0.0077	0.107	31062
	R28 95	2.95	-0.0116	0.107	31016
QA = 22.90 N QA•d = 0.9284 N•m Right ℓ_{roll} % = - 0.0453 % Left ℓ_{roll} % = + 0.0682 %		**MACH** **2.95**	$C\ell_p$ shift = **0.00195** CRMC shift = **0.0002087**	**Pd/2V** **0.107**	ℓ_{roll} shift = +0.000194N•m ≡ .0115% balan. nominal capaci.
R2884		2.95	-0.0080	0.124	35948
	R2896	2.95	-0.0172	0.124	35815
QA = 22.90 N QA•d = 0.9284 N•m Right ℓ_{roll} % = - 0.0545 % Left ℓ_{roll} % = + 0.1172 %		**MACH** **2.95**	$C\ell_p$ shift = **0.00460** CRMC shift = **0.0005704**	**Pd/2V** **0.124**	ℓ_{roll} shift = +0.000530N•m ≡ .0313% balan. nominal capaci.
R2891		2.95	-0.0100	0.124	35962
	R2897	2.95	-0.0080	0.124	35826
QA = 22.90 N QA•d = 0.9284 N•m Right ℓ_{roll} % = - 0.0681 % Left ℓ_{roll} % = + 0.0545 %		**MACH** **2.95**	$C\ell_p$ shift = **-0.00100** CRMC shift = **-0.000124**	**Pd/2V** **0.124**	ℓ_{roll} shift = -0.000115N•m ≡ .0068% balan. nominal capaci.

R2890		2.95	-0.0080	0.141	40723
	R2907	2.95	-0.0140	0.140	40622
QA = 22.90 N QA•d = 0.9284 N•m Right ℓ_{roll} % = - **0.0620** % Left ℓ_{roll} % = + **0.1084** %		**MACH** **2.95**	**$C\ell_p$** shift = **-0.00300** CRMC shift = **-0.000423**	**Pd/2V** **0.141**	ℓ_{roll} shift = -0.000393N•m = .0232% balan. nominal capaci.
R2889		2.95	-0.0100	0.141	40682
	R2900	2.95	-0.0128	0.140	40504
QA = 22.90 N QA•d = 0.9284 N•m Right ℓ_{roll} % = - **0.0775** % Left ℓ_{roll} % = + **0.0991** %		**MACH** **2.95**	**$C\ell_p$** shift = **-0.00140** CRMC shift = **-0.000197**	**Pd/2V** **0.141**	ℓ_{roll} shift = -0.000183N•m = .0108% balan. nominal capaci.

TABLE BIV

Average of Longitudinal Stability Coefficients Versus Mach Number Based on the Whole Test Series

MACH NUMBER	CNA $\alpha = 0$ deg	CMA $\alpha = 0$ deg	XCP0 in model calibre with respect to base	CA0
0.50	2.356	7.742	-3.28	0.175
0.70	2.298	7.653	-3.33	0.171
0.80	2.325	7.880	-3.39	0.169
0.93	2.444	8.311	-3.40	0.232
1.03	2.532	8.747	-3.45	0.397
1.16	2.503	8.651	-3.46	0.468
1.27	2.531	8.747	-3.46	0.442
1.36	2.662	9.102	-3.42	0.415
1.48	2.825	9.268	-3.28	0.406
1.73	3.033	9.404	-3.10	0.406
1.99	3.165	9.602	-3.03	0.328
2.50	3.306	9.499	-2.87	0.252
2.95	3.314	9.138	-2.81	0.205

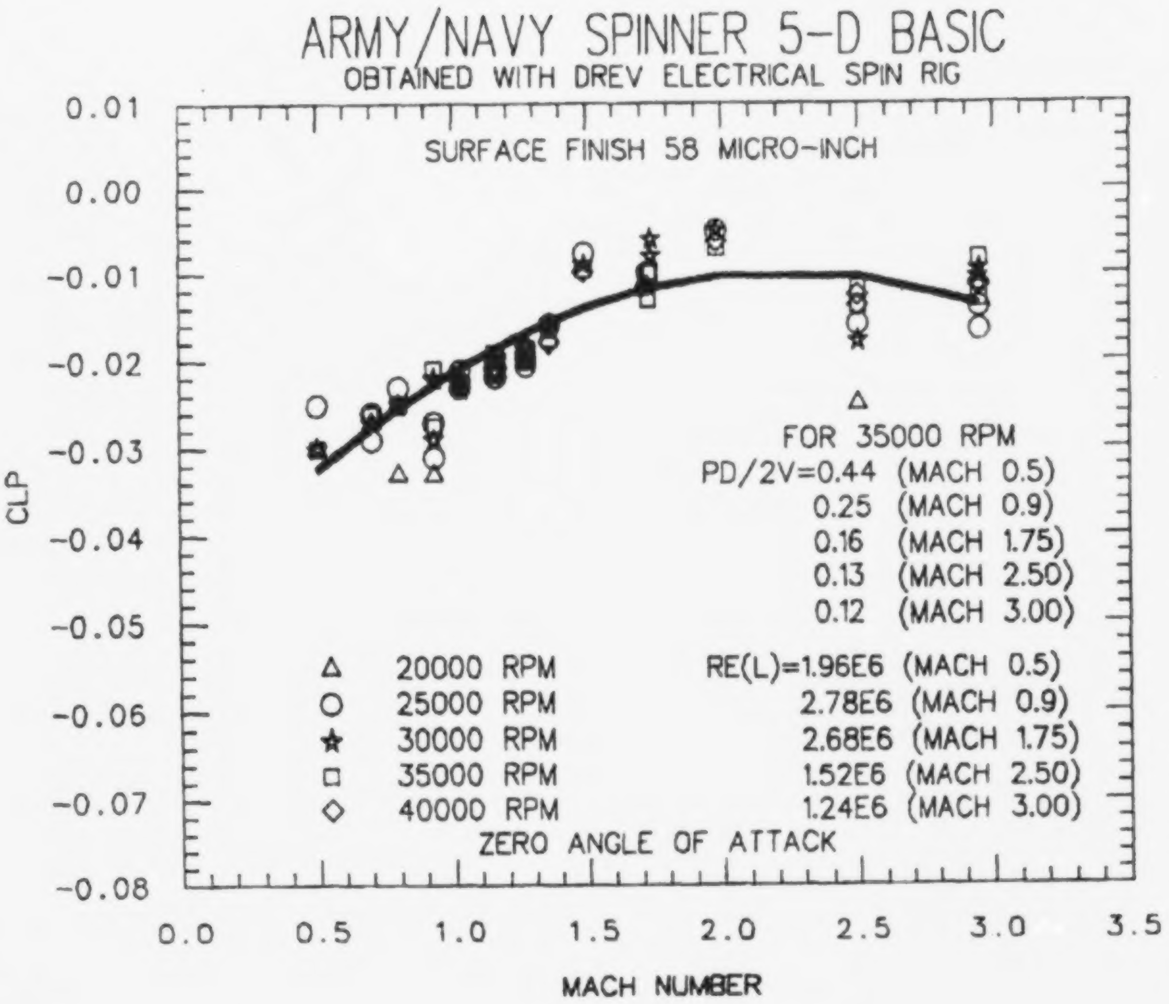

FIGURE B4 - Variation of spin damping coefficient with Mach number and spin rate

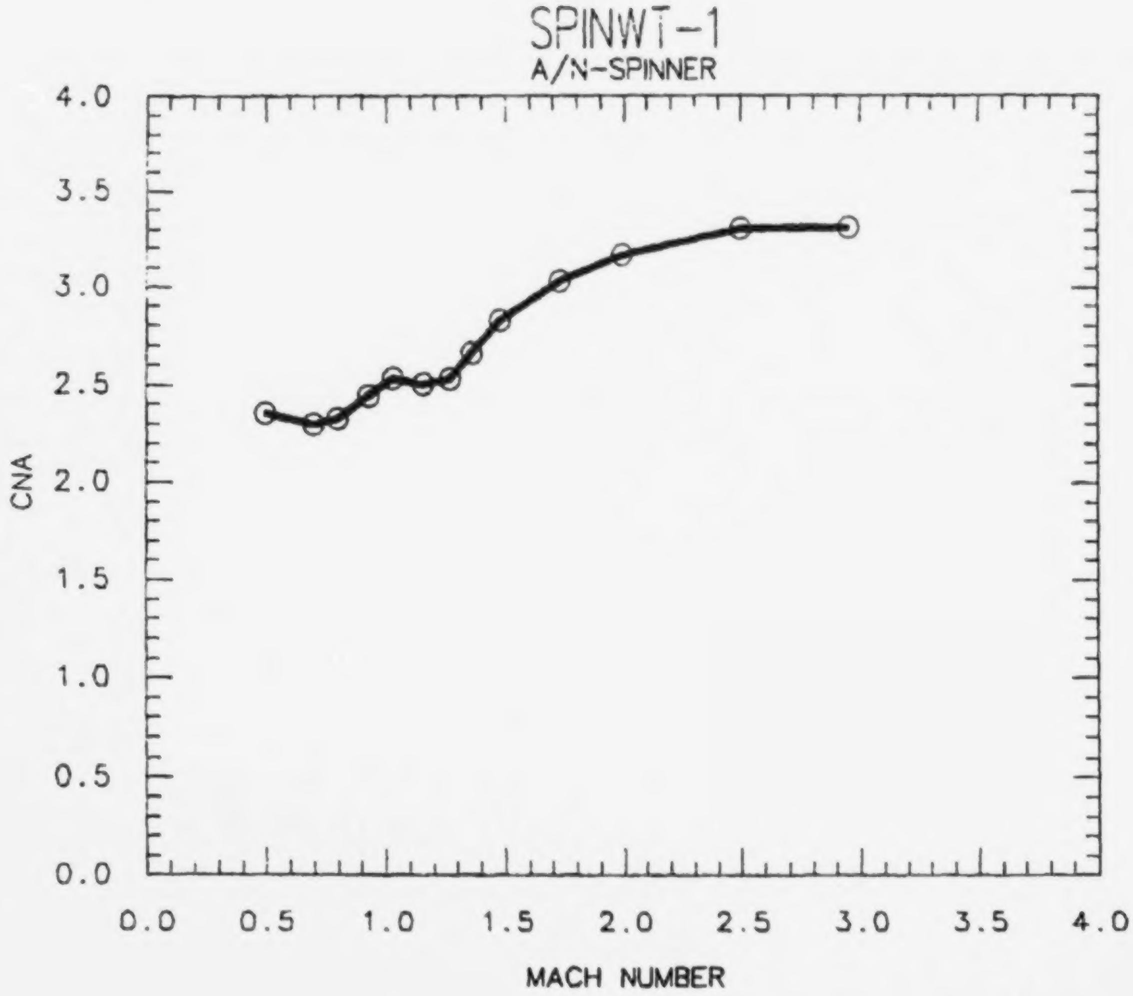

FIGURE B5 - 5-D Army-Navy Spinner, average of CNA versus Mach number obtained in DREV Trisonic facility with a spinning model

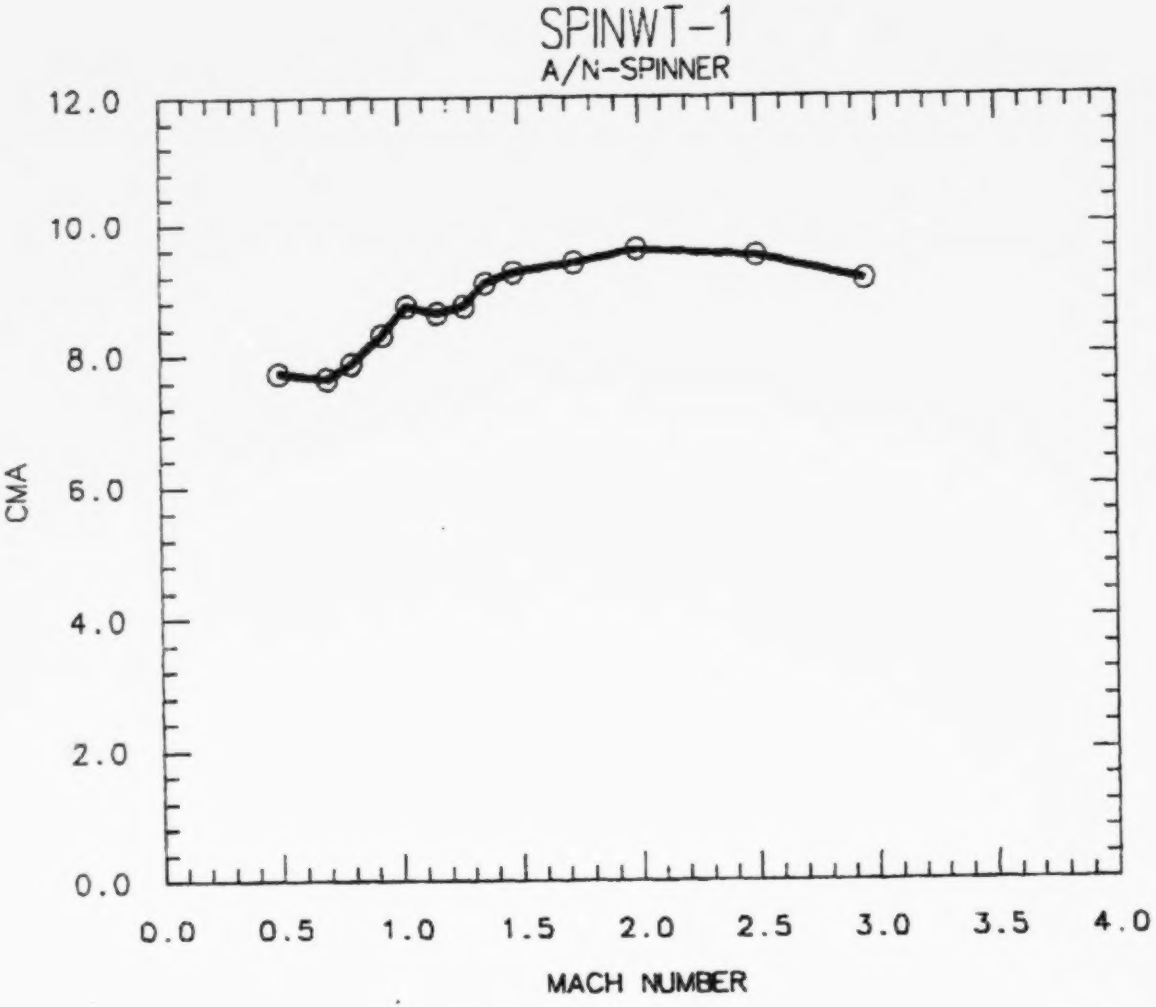

FIGURE B6 - 5-D Army-Navy Spinner, average of CMA versus Mach number obtained in DREV Trisonic facility with a spinning model

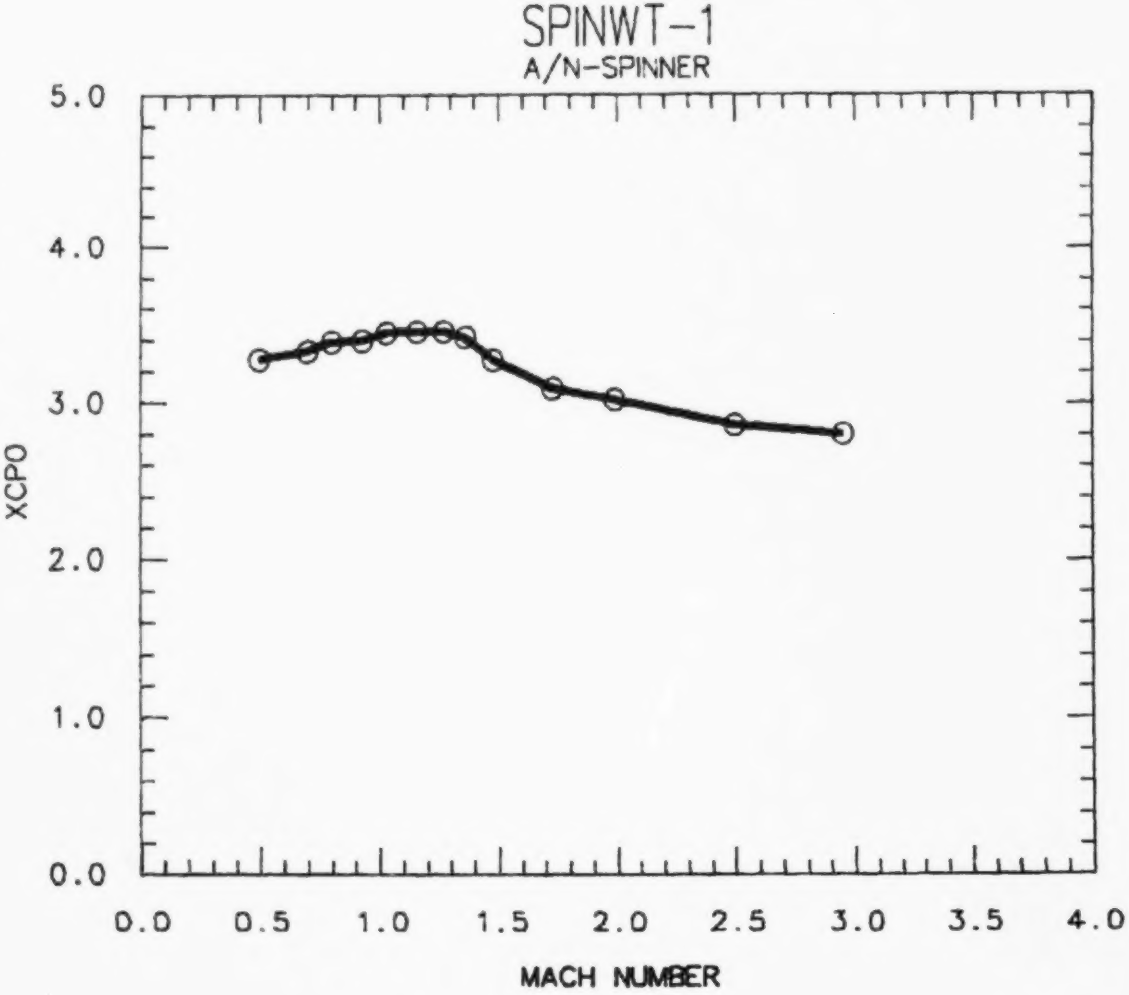

FIGURE B7 - 5-D Army-Navy Spinner, average of XCP0 versus Mach number obtained in DREV Trisonic facility with a spinning model, with respect to base

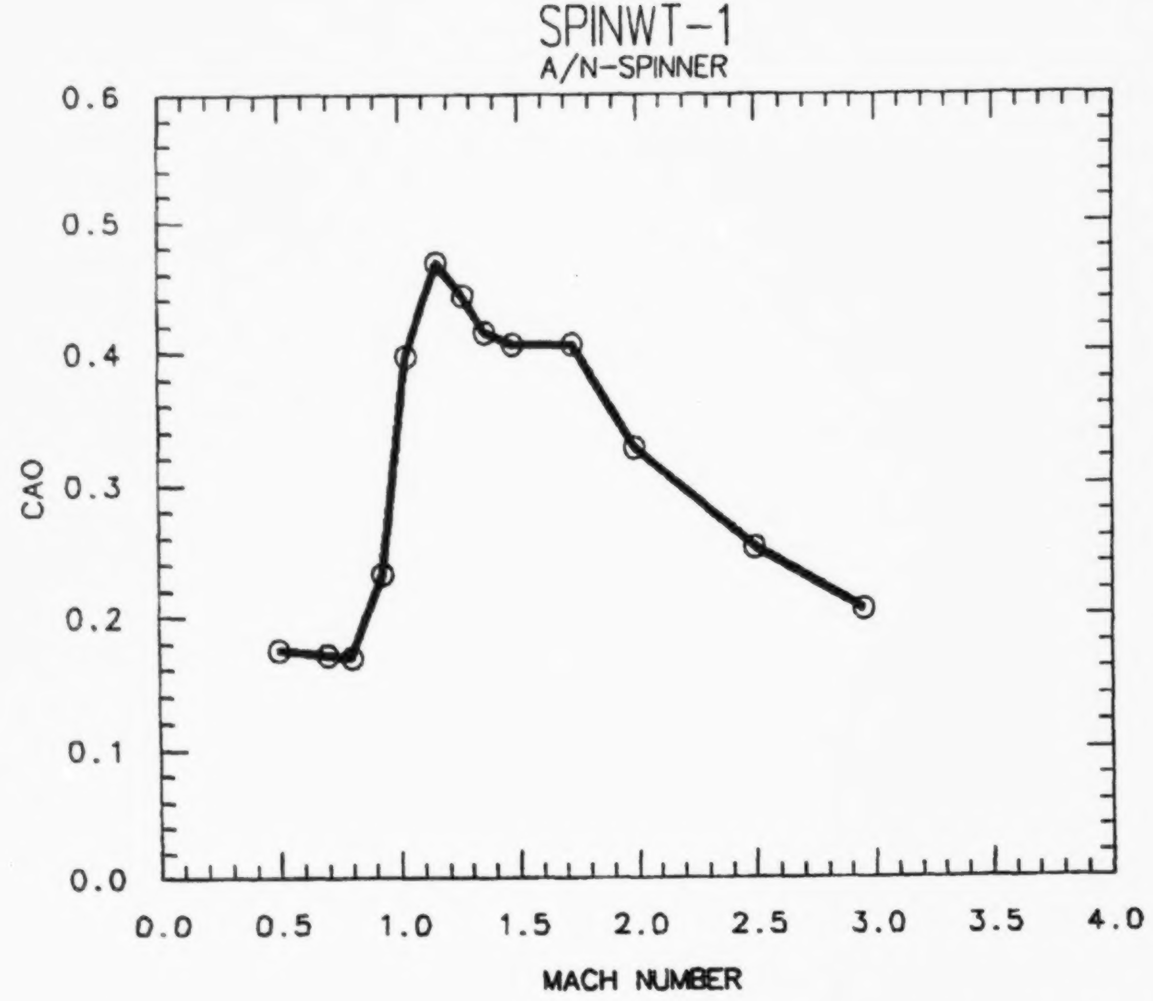

FIGURE B8 - 5-D Army-Navy Spinner, average of CA0 versus Mach number obtained in DREV Trisonic facility with a spinning model

APPENDIX C

Balance Overloads

BALANCE OVERLOADS

Because of the spinning model complex mechanics leading to potential vibration coupling with the balance elastic response, a standard calculation process to determine balance maximum loads expected from present test series was not made prior to tunnel testing. Instead, overload experiments were performed. Normally, it should be made with an appropriate overload balance to be selected from several that are in use at DREV.

Since the electrical spin rig has been designed to accommodate very short model projectile configurations, its balance housing can only receive a 0.50 in balance configured exactly as per ABLE MK balances geometry. The DREV 0.50 in overload balances have their floating outer shell retained at the fore end by a socket head cap screw whose the head protruded too far to permit installation inside the spin rig.

a - Static Overload Tests with Rigid Dummy Spin Rig Supports

In a first time, static overload tests were performed by using a rigid dummy spin rig support in place of the spin rig/ balance combination in order to use the same model spinning outer shell(s) but without spin motion (Fig. C1). Since there was no motor to be housed inside the dummy support, the balance housing could be made longer to accommodate the overload balance extended length.

Also, this rigid support had to be used in conjunction with a special U-shape double key (that engaged on the support dummy motor shaft), in order to be able to remove it with pliers (Fig. C2). Individual keys must not be used. Otherwise, with dummy support, if normal keys are used, the model will be completely locked closed without a possibility to recuperate the balance, the model outer shell and the sting. If such a case happened, the method used was to drill and tap each key (US 0-80 NF) and remove them independently with long 0-80 screws and press system (or pliers if easily sliding).

b - Dynamic Tests with 0.50 in ABLE Balances

In a second time, dynamic overload tests were performed

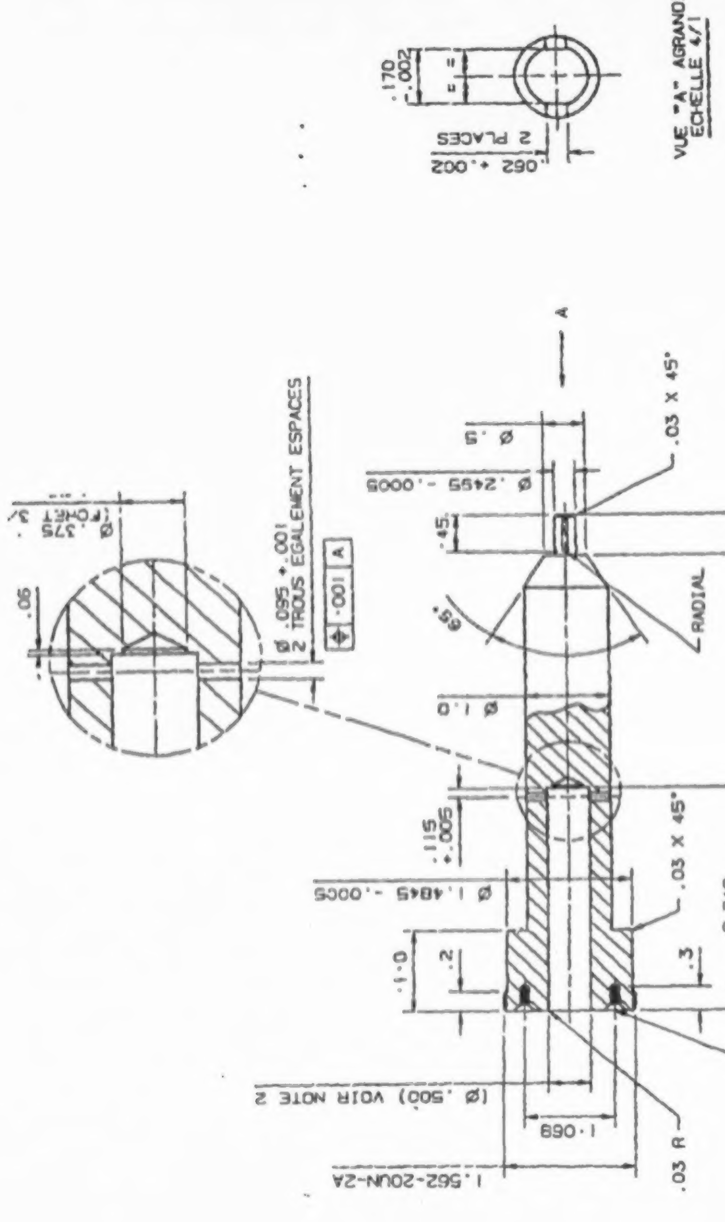
.170
-.002
.062 +.002
2 PLACES
VUE "A" AGRANDI
ECHELLE 4/1
A
.03 X 45°
Ø .5
Ø .2495 -.0005
.45
.5
Ø .375
(FORET 3/...)
.06
Ø .095 +.001
2 TROUS EGALEMENT ESPACES
.001 A
65°
RADIAL
Ø 1.0
5.675
(6.175)
.115
+.005
.03 X 45°
Ø 1.4845 -.0005
2.740
1.0
.2
.3
(Ø .500) VOIR NOTE 2
1.068
1.562-20UN-2A
.03 R
#4-40UNC-2B
FRAISER 82° X Ø .25
2 TROUS

FIGURE C1 - Static test rigid dummy spin rig support, dim. in in

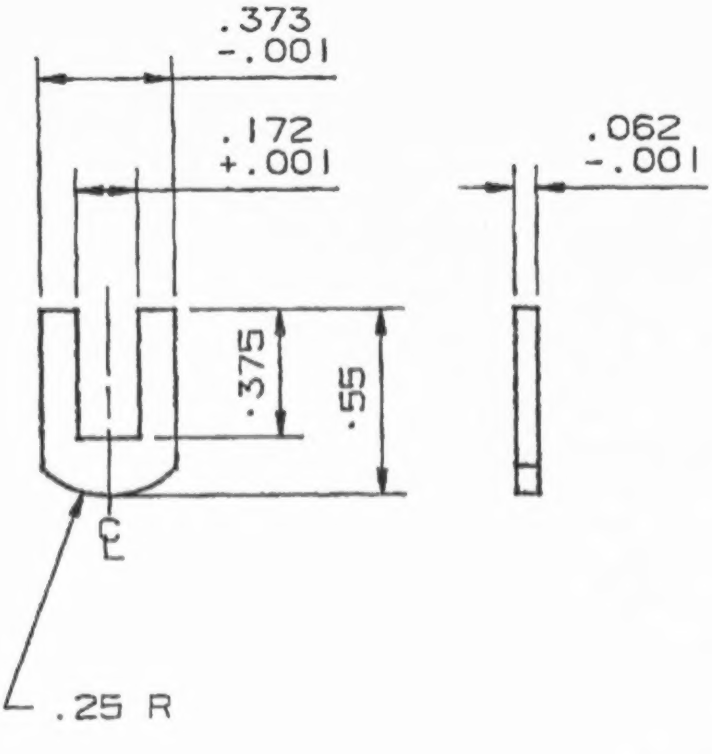
.373
-.001
.172
+.001
.062
-.001
.375
.55
.25 R
℄

FIGURE C2 - Static test U - shape double key (to be used in conjunction with dummy spin rig support), dim. in in

by using a standard 0.5 in ABLE balance. For each particular test Mach number, series of test runs were made by increasing the spin rate gradually and observing maximum loads then generated.

c - Conclusions from Overloads Tests

Since values of spin damping, Magnus forces and moments, for a smooth ogive-cylinder projectile, usually represent only 10th to 100th of the normal force and pitching moment, it was not surprising that only very small differences (almost not noticeable) were observed between the static and dynamic (spinning) test starting/stopping loads and maximum loads (encountered during a run with the model at angle of attack) .

It was observed that an improperly balanced model outer shell is to be considered as a major cause of severe high frequency vibrations that could damage a balance even if maximum rated loads have not been overpassed.

Overload test results showed that most critical conditions were to be encountered when the starting and stopping shock waves passed through the test section, and particularly for the balance longitudinal components, i.e. normal force and pitching moment. It was suspected that test section straight side walls induced a lateral propagation component of starting and stopping shock waves which sensibly differed from the vertical propagation component, being under influence of tunnel floor and ceiling made of configured nozzle blocks.

Although overload test recorded results were not retrievable at present time, Figs. C3 and C4 present typical overload test data from another test run series. The overload conditions represented by Figs. C3 and C4 could be considered as very severe. Conditions encountered in present test series were much less important in amplitude.

The time duration where flow conditions in the test section are effectively constant, can varies depending on the test Mach number, the model cross-section area and the amount of obstruction to the flow produced by model particular configuration. (Not to mention several other factors like the pressure at which the

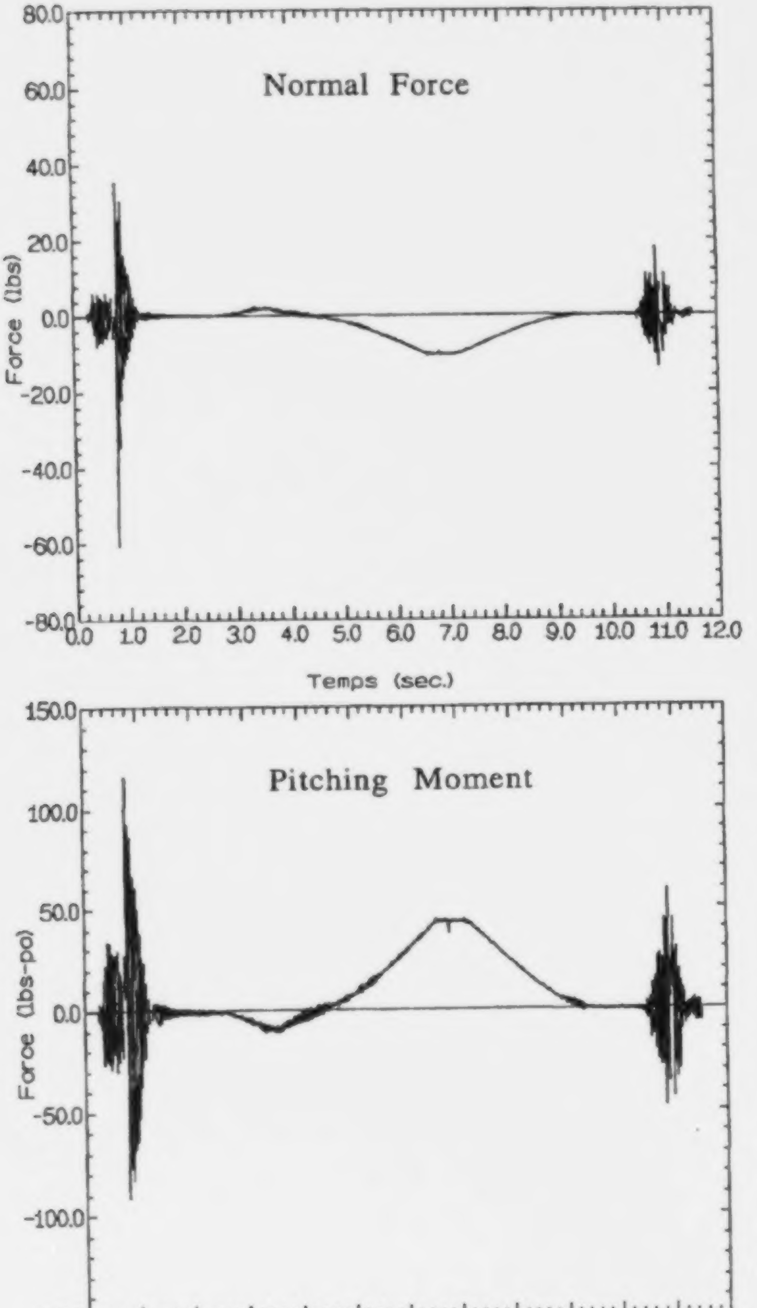

FIGURE C3 - Normal force (top) and pitching moment (bottom) loads caused by starting and stopping shock waves.

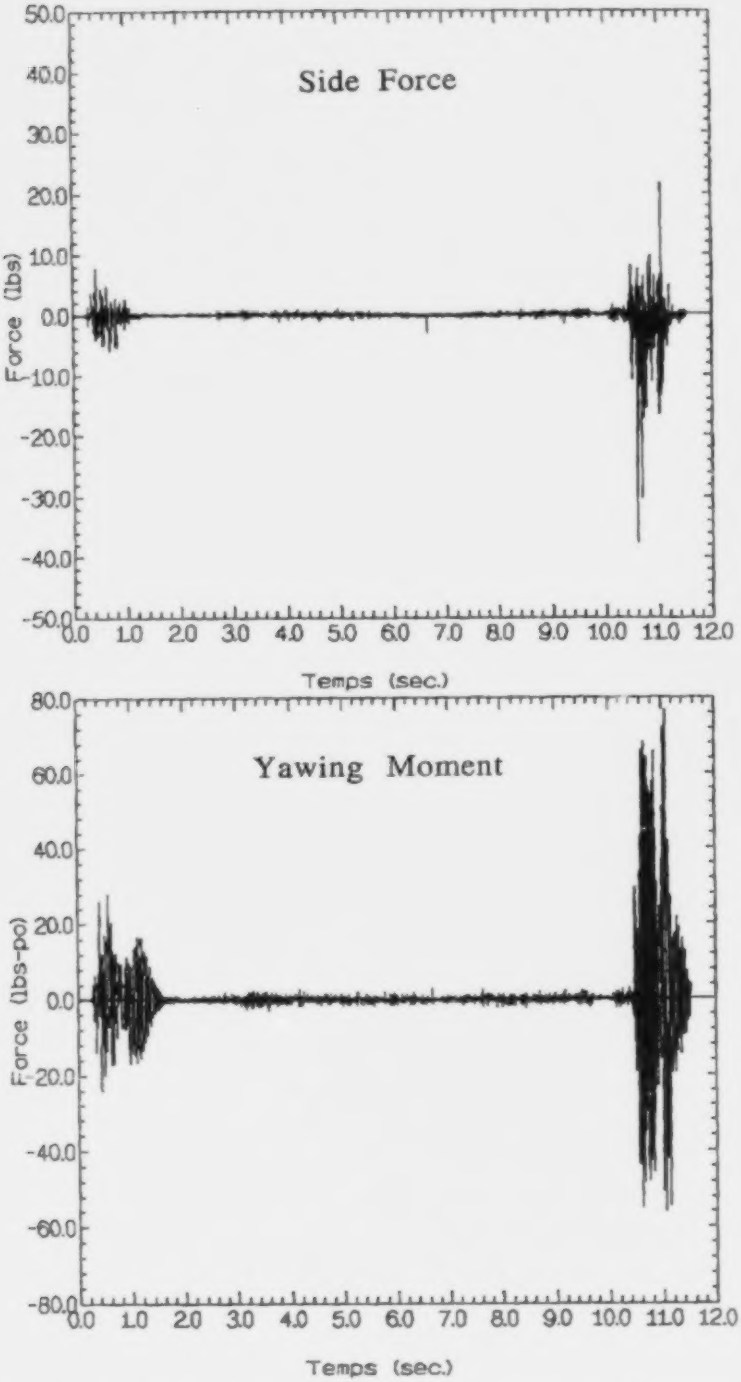

FIGURE C4 - Side force (top) and yawing moment (bottom) loads caused by starting and stopping shock waves.

vacuum tank was previously pumped etc... Since the main valve shall not close until the sting-strut mechanism has been returned to zero angle of attack, depending on the loads applied on it during a test run (also internal friction due to adjustment of its roller bearings or a lack of grease etc...), the main valve can close after the flow conditions have ceased to be constant in the test section, i.e. the pressure in the vacuum tank has become too high.

It results that very strong transient shock waves travel from the vacuum tank towards the test section and the nozzle blocks. They can damage the model and make the balance unserviceable. A source of preoccupation during overload tests as well as during normal test runs is to make sure that high loads observed at the end of a run is really coming from the closure of the main valve and not from run duration having overpassed the steady-state conditions time.

By plotting the static pressure in the test section versus time (Fig. C5) it is possible to differentiate between the both types of stopping loads. Shock waves happening after that test section static pressure has returned to atmospheric pressure are caused by the closing of the main valve. If shock waves happen before, the steady-state flow conditions time has been overpassed. Then, the swept of angle of attack should be reduced and/or the drive motor voltage augmented (which can be made from the control console) and possibly a maintenance be made to the sting-strut mechanism (in order to reduce its internal friction which shall reduce the load on the motor and augment its speed). As an indication, typical maximum usable times versus Mach numbers for a test run are given in Table CI.

TABLE CI
Typical Test Run Duration Times vs Mach Numbers

Mach Number	Effective Run Duration (s)	Mach Number	Effective Run Duration (s)
0.50	6.5	1.38	9.1
0.70	7.0	1.50	9.2
0.80	8.3	1.75	9.3
0.90	9.3	2.00	9.3
1.00	8.4	2.50	9.6
1.15	8.5	3.00	9.2
1.28	8.9		

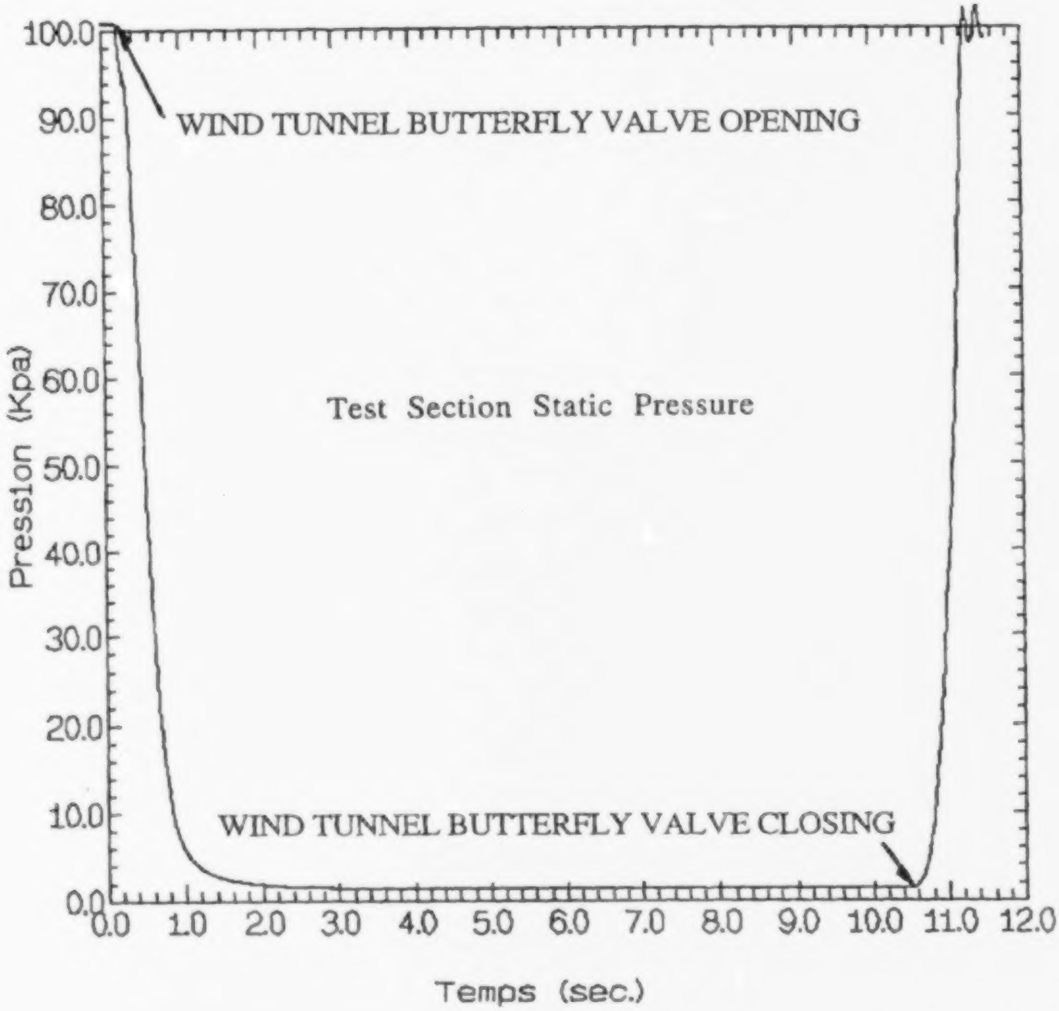

FIGURE C5 - Plot of test section static pressure versus time used to identify the closing time of the main valve

APPENDIX D

Measurement Errors

STATISTICAL METHODOLOGY TO EVALUATE AERODYNAMIC COEFFICIENT MEASUREMENT ERRORS

In present test series, the primordial aim was to explore the possibility to measure spin damping coefficients by using and adapting the technology of rotating models in the DREV trisonic facility. To that purpose, rolling moments as well as spin rate had to be measured. Since the accuracy of the model spin rate detection and of the recording instrumentation was better than 0.06% of the measured values, only the measurements errors generated by the balance are considered in the present experimental error analysis.

During aerodynamic coefficient test runs, the projectile model was pitched through a range of angles of attack, and a single set of measurements was recorded for each discrete value of angle of attack. It was assumed, for statistical calculations, that normally only one test run was to be made for each set of experimental conditions. Then, several wind tunnel test runs of typical interest were intentionally repeated in order to provide additional data to determine the 95.0% confidence interval limits to be used for the prediction of future single observation (single run) tests. The interval limits are defined as the upper and lower values of results that correspond to a specified level of confidence. The higher is the level of confidence (i.e. 97.5%, 99.0%, 99.9% etc...), and the larger shall be the interval length, which is defined as the difference between the interval limits.

The statistical calculations were based on a methodology that needed the data from at least three different test runs. At the end of the "Demonstration of Measurement Errors Calculation Methodology" which is presented below, a table of multiple factors, which are all less than unity, make possible the conversion of the statistical results of Tables D-I to D-V for the cases where more than a single test run was made for same test conditions.

The statistical results related to the aerodynamic coefficient tests are presented in Table D-I to D-V. At the bottom of these tables, calculations were made to approximate the balance systematic error by using data on balance accuracy (Ref. 7).

Longitudinal Aerodynamic Coefficient Measurement Errors

Since CNA and CMA coefficients are derivatives, it was necessary to find a mean to correlate them with the balance force and moment systematic errors. Most of the tests were performed at angle of attack swepts from -2.0 to +2.0 deg. and the derivative coefficients calculations based on theses small ranges of angles of attacks. As a consequence, the systematic errors induced by the balance on CNA and CMA derivatives were arbitrarily based on the forces and moments that were felt by the balance at an angle of attack of 2.0 deg.

From Tables D-I to D-IV, it can be observed that CNA's, CMA's and CA0's ratios of interval lengths over average values and for a confidence level of 95.0% show a tendency to stay within a same order of magnitude than balance systematic error (but still being about of 3 to 4 times larger). Since the results of the longitudinal position of the aerodynamic center " XCP0 " come from a combination of CNA and CMA, the related statistical results are more complicated to justified. Nevertheless, it can be observed (Tables D-I to D-IV) that dispersion of XCP0 results is similar to that of CNA and CMA.

Rolling Moment and Spin Damping Coefficients Measurement Errors

As CLPC is concerned, a major problem was the very low magnitude of the rolling moments that had to be measured for the part of the test series to be performed at supersonic Mach numbers above 1.5. These rolling moment measurements were necessary to derive the spin damping coefficients at high Mach numbers, which was one of the primordial aims of present test series. For tests at supersonic regimes, a multiple runs procedure was adopted and spin tests were performed in both senses of rotation (right and left). Their average was calculated to provide a final result. The related test conditions are presented in Table BII.

The idea to proceed that way came from the observation of a systematic positive roll measurement shift, making the left rotation tests (positive rolling moment) to be always larger than right rotation tests (negative rolling moments). In order to make possible a graphical comparison of the measured rolling moments, the left rotation test rolling moments were made negative and plotted versus the rolling moment from right rotation tests in Fig. D1.

Figure D1 shows the dispersion of the rolling moment measurements then obtained for right and left rotation spin tests. The diagonal line represents the average but also the condition of right and left rotation measurements of same absolute values. It can be observed that experimental results for right and left rotation tests set apart each side of the diagonal line, emphasizing the idea of a measurement shift. The linear behavior of the balance for each sense of rotation taken individually is remarkable.

It can be observed from Fig. D1, that rolling moment measurements were made at a level of magnitude less than 0.7% of the balance nominal capacity. Also, it can be seen that several measurements were less, in absolute magnitude, than 0.2% of the balance nominal capacity. The balance accuracy being also ±0.2% of its nominal capacity, the accuracy systematic error which then resulted was rather high.

By referring at the left scale of Fig. D1, it appears that the rolling moment measurement dispersion of right rotation tests and left rotation tests considered separately, was much less than the ±0.2% of the balance nominal capacity.

This is because the balance absolute accuracy remains at ±0.2% independently of the magnitude of the rolling moments that are being measured. The resolution of the balance being the smallest measurable increment or variation of forces and moments (and even if their absolute values can only be determined with less accuracy), the resolution of the balance represents a smaller figure than its accuracy. While plotted, the observed dispersion of the results shall appear less than the accuracy (while expressed in % of balance nominal capacity).

This can be observed from results of Table D-V where the ratios of interval lengths over average values, for a confidence level of 95.0%, are 2 to 6 times less in magnitude than balance systematic error. As statistical results of Table D-V are concerned, it must be noted that since only 3 data results were available for the calculations, the degree of approximation is high.

In order to determine an observed value for the balance resolution from the present test series, the run-to-run standard deviation was calculated independently for the right and left rotation spin tests. It shows that the resolution of the balance was approximately ±0.032% of its nominal capacity, which represents 1/6 of the balance accuracy. The variations of the balance accuracy systematic error and of the balance resolution systematic error were calculated with respect to the magnitude of the rolling moment measurements and plotted in Figs. D1 and D2.

Figure D3 presents, in a generic form, the working principle of the methodology of making intentionally test runs in reverse (right and left) senses of rotation and averaging the rolling moment data results. It shows that although the apparent measurement shift can be compensated by proceeding that way, a residual balance offset will always be there and remain unknown in magnitude. In fact, the apparent measurement shift is equaled to the half of the difference of balance offsets (between positive and negative rolling moments).

From the data contained in the Able MK-X-A 0.50 in balance instructions manual, it can be deduced that balance offsets should be of a similar magnitude than the observed hysteresis. As the rolling element is concerned, it is approximately equal to 0.05% of the balance nominal capacity. The calculated average of the roll measurement shift in present test series was 0.0332% of the balance nominal capacity.

Such a behavior is typical of instrumentations whose designs utilize strain gages as sensing elements. It must be noted that one of the primordial behaviors of strain gages is to response with an offset in their output signals. (And usually, the offset is negative, i.e. the output signal is less than it should be). In fact, when an extreme accuracy is required from an instrumentation apparatus, strain gages are not being used. Instead, other form of displacement sensors are utilized in these circumstances. Normally, strain gages are included in the design of aerodynamic balances and provide ample accuracy and resolution for the purpose of wind tunnel testing.

The experimentalisms are not usually preoccupied by these balance offsets that represent less than 1/2000 of the balance nominal capacities. If conditions are such that the balance offsets become a problem, it only means that another balance with some lower nominal capacities should be selected for the tests. It is worth to mention that balance offsets are not necessarily constant or repetitive, although they shall always remain inferior to some known and observable percentages of the balance nominal capacities.

It can be concluded that:

a- Since the behavior of non-linearities of the balance for very low rolling moments are not known usually (unless some calibration apparatus would permit to measure it), the advantage of the procedure is to make sure that the error related to the apparent measurement shift is compensated.

b- Depending on the shape of balance non-linearities and on relative values of the measurement shift and balance offset, it could happen that results from a particular sense of rotation (right or left) would have been closer to the real value than the average. In Fig. D3, for example, the results from left rotation tests would be a best choice (and possibly was). But due to the lack of reliable measured data on the balance offsets, it would be, generally speaking, hazardous to privilege data results obtained from one sense of rotation to the detriment of results obtained in reverse sense of rotation.

c- In the absence of measured calibration data to support a data reduction procedure, the best alternative was to make sure that the apparent measurement shift was removed from results, the balance offsets being considered as unavoidable imprecisions typical of that type of instrumentation.

For the tests conditions presented in Table BI where runs were made only a single sense of rotation (right or left), the related balance accuracy and resolution systematic errors were plotted in Fig. D4.

In Figs. D2 and D4, horizontal bars show the spread of rolling moment magnitude related to each test Mach number. Each bar indicate the minimum and the maximum rolling moment (in % of balance nominal capacity) that was measured. The corresponding sections of the curves representing the balance accuracy and resolution systematic error are to be used to qualify the results for each test Mach number. Since a same range of model spin rate was not experimented for each test Mach number, these bars display irregular lengths, i.e. these bars were plotted only as a mean to characterize the results and not to draw any conclusions of aerodynamic nature.

Spread of Rolling Moment Measurements vs Mach Number

TEST MACH NUMBER	MINIMUM MEASURED ROLLING MOMENT IN % BAL CAP.	MAXIMUM MEASURED ROLLING MOMENT IN % BAL CAP.
0.50	0.3398	0.5212
0.70	0.3831	0.5706
0.80	0.3837	0.6743
0.93	0.5152	0.7270
1.03	0.3318	0.6705
1.16	0.3737	0.7204
1.27	0.3259	0.5652
1.36	0.2346	0.5415
1.49	0.0859	0.3230
1.73	0.1339	0.2746
2.00	0.0657	0.2142
2.50	0.0733	0.2069
2.95	0.0453	0.1084

ESTIMATED BALANCE SYSTEMATIC ERROR
VS ROLLING MOMENT MEASUREMENT VALUES

Assuming a Balance Accuracy of ±0.2 % Nom. Cap. and Observed Balance Resolution of ±0.032% Nom. Cap.
Calculated from Run-to-Run Standard Deviation of Individual Right and Left Rotation Tests Series

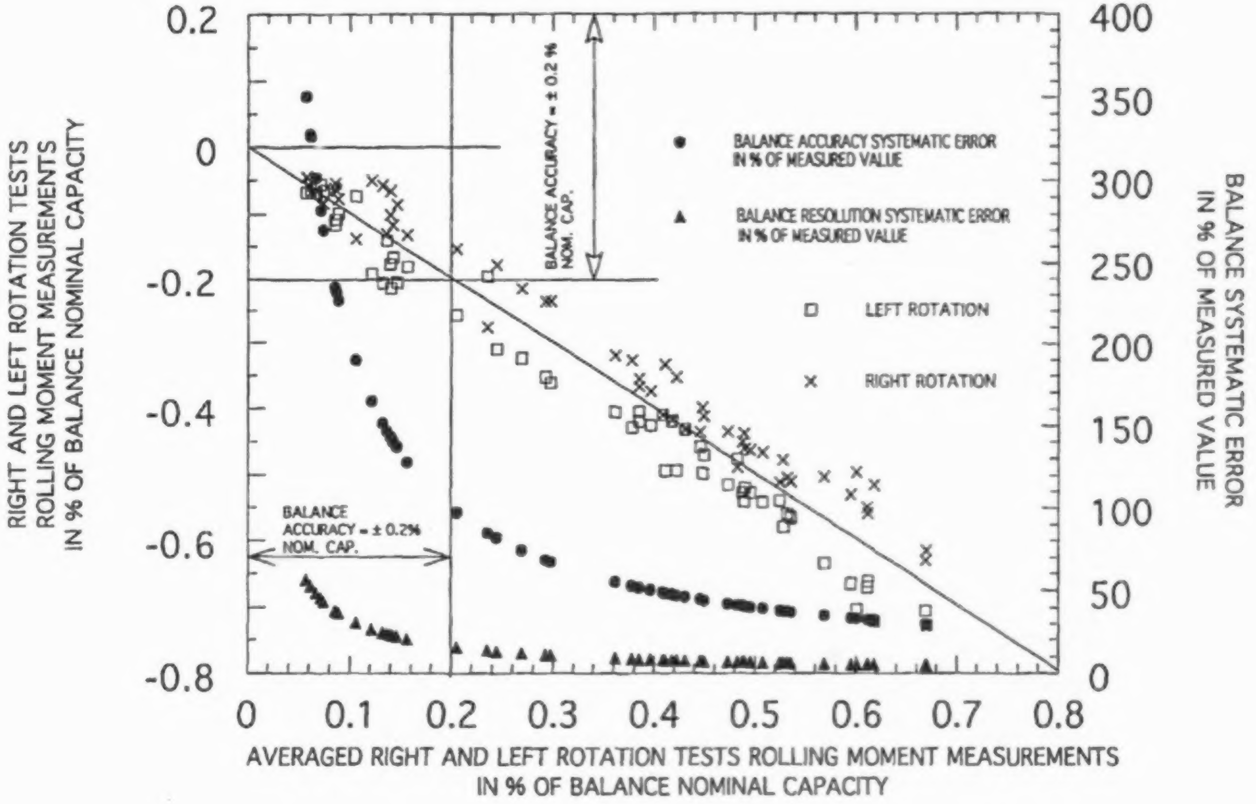

FIGURE D1 - Right and left rotation tests rolling moment measurements, to be remarked the linearity of the results and constant behavior of the balance under the form of a consistent measurement shift

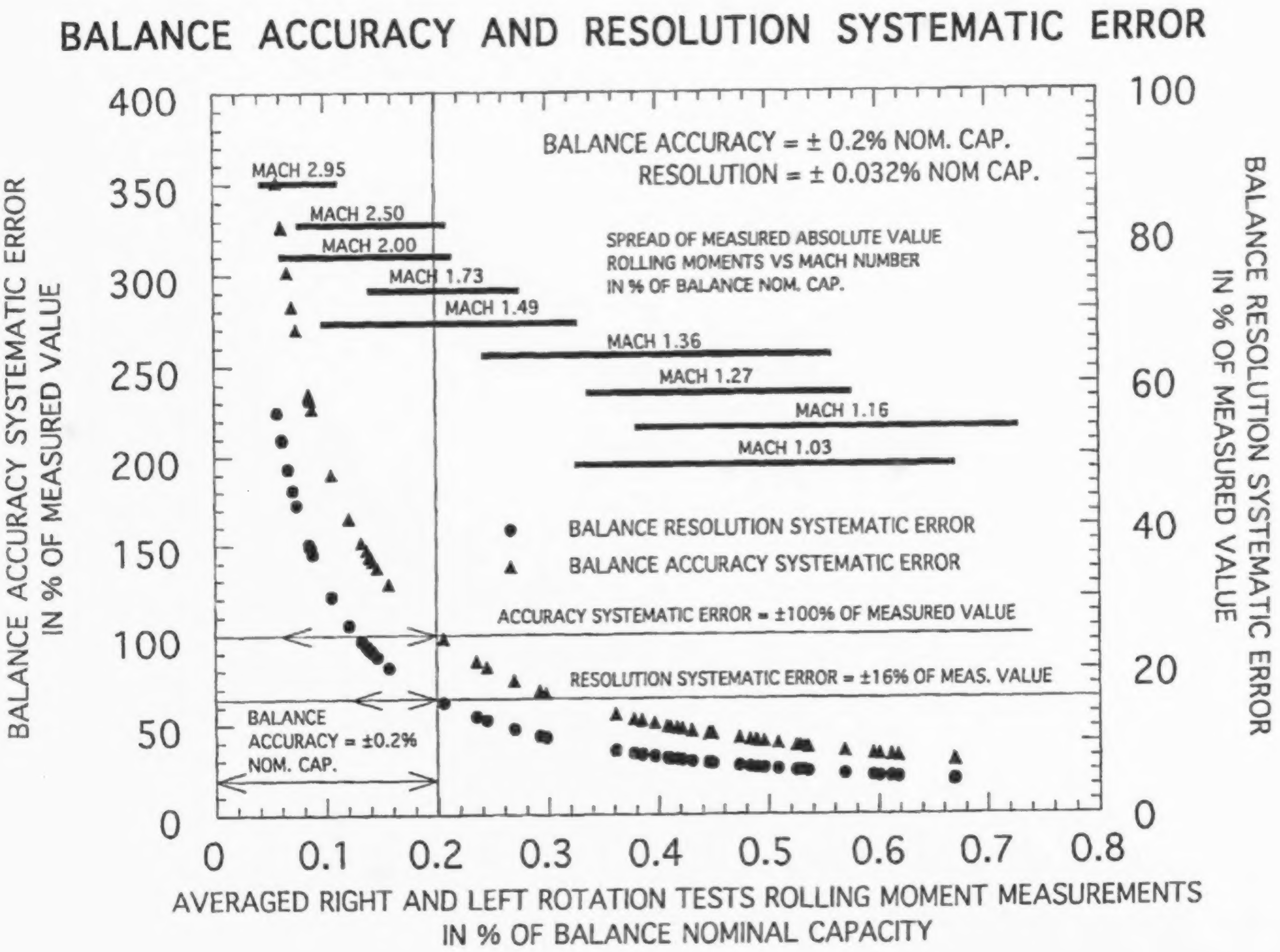

FIGURE D2 - Characterization of rolling moment measurements calculated from the average of spin tests made in reverse senses of rotation

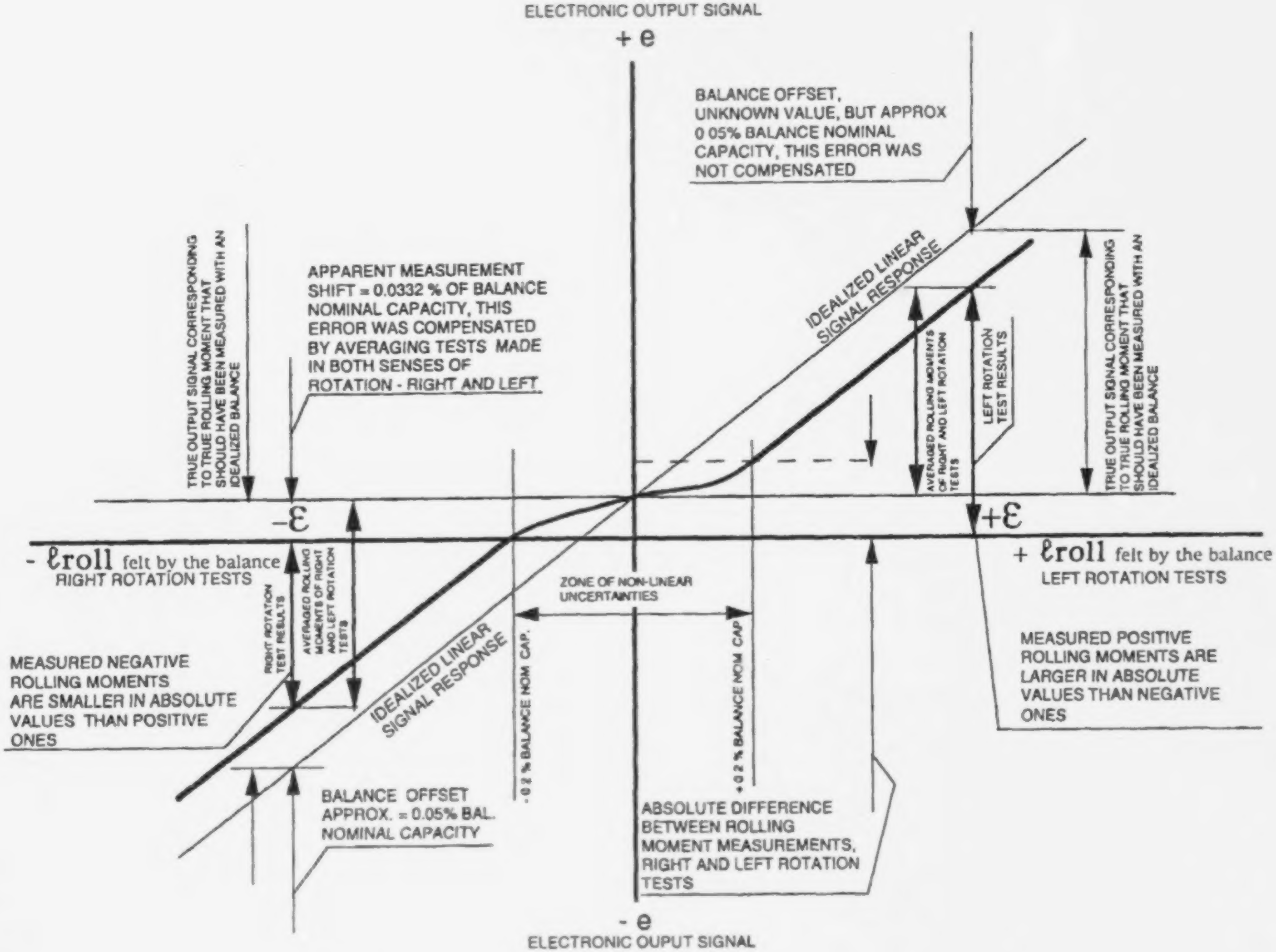
ELECTRONIC OUTPUT SIGNAL
+ e
BALANCE OFFSET, UNKNOWN VALUE, BUT APPROX 0 05% BALANCE NOMINAL CAPACITY, THIS ERROR WAS NOT COMPENSATED
TRUE OUTPUT SIGNAL CORRESPONDING TO TRUE ROLLING MOMENT THAT SHOULD HAVE BEEN MEASURED WITH AN IDEALIZED BALANCE
APPARENT MEASUREMENT SHIFT = 0.0332 % OF BALANCE NOMINAL CAPACITY, THIS ERROR WAS COMPENSATED BY AVERAGING TESTS MADE IN BOTH SENSES OF ROTATION - RIGHT AND LEFT
IDEALIZED LINEAR SIGNAL RESPONSE
AVERAGED ROLLING MOMENTS OF RIGHT AND LEFT ROTATION TESTS
LEFT ROTATION TEST RESULTS
TRUE OUTPUT SIGNAL CORRESPONDING TO TRUE ROLLING MOMENT THAT SHOULD HAVE BEEN MEASURED WITH AN IDEALIZED BALANCE
-ε
+ε
- ℓroll felt by the balance
RIGHT ROTATION TESTS
+ ℓroll felt by the balance
LEFT ROTATION TESTS
ZONE OF NON-LINEAR UNCERTAINTIES
RIGHT ROTATION TEST RESULTS
AVERAGED ROLLING MOMENTS OF RIGHT AND LEFT ROTATION TESTS
MEASURED NEGATIVE ROLLING MOMENTS ARE SMALLER IN ABSOLUTE VALUES THAN POSITIVE ONES
IDEALIZED LINEAR SIGNAL RESPONSE
- 0 2 % BALANCE NOM CAP.
+ 0 2 % BALANCE NOM CAP
MEASURED POSITIVE ROLLING MOMENTS ARE LARGER IN ABSOLUTE VALUES THAN NEGATIVE ONES
BALANCE OFFSET APPROX. = 0.05% BAL. NOMINAL CAPACITY
ABSOLUTE DIFFERENCE BETWEEN ROLLING MOMENT MEASUREMENTS, RIGHT AND LEFT ROTATION TESTS
- e
ELECTRONIC OUPUT SIGNAL

FIGURE D3 - Generic diagram showing the interrelation between the balances errors and the working of the methodology of spin tests in reverse senses of rotation

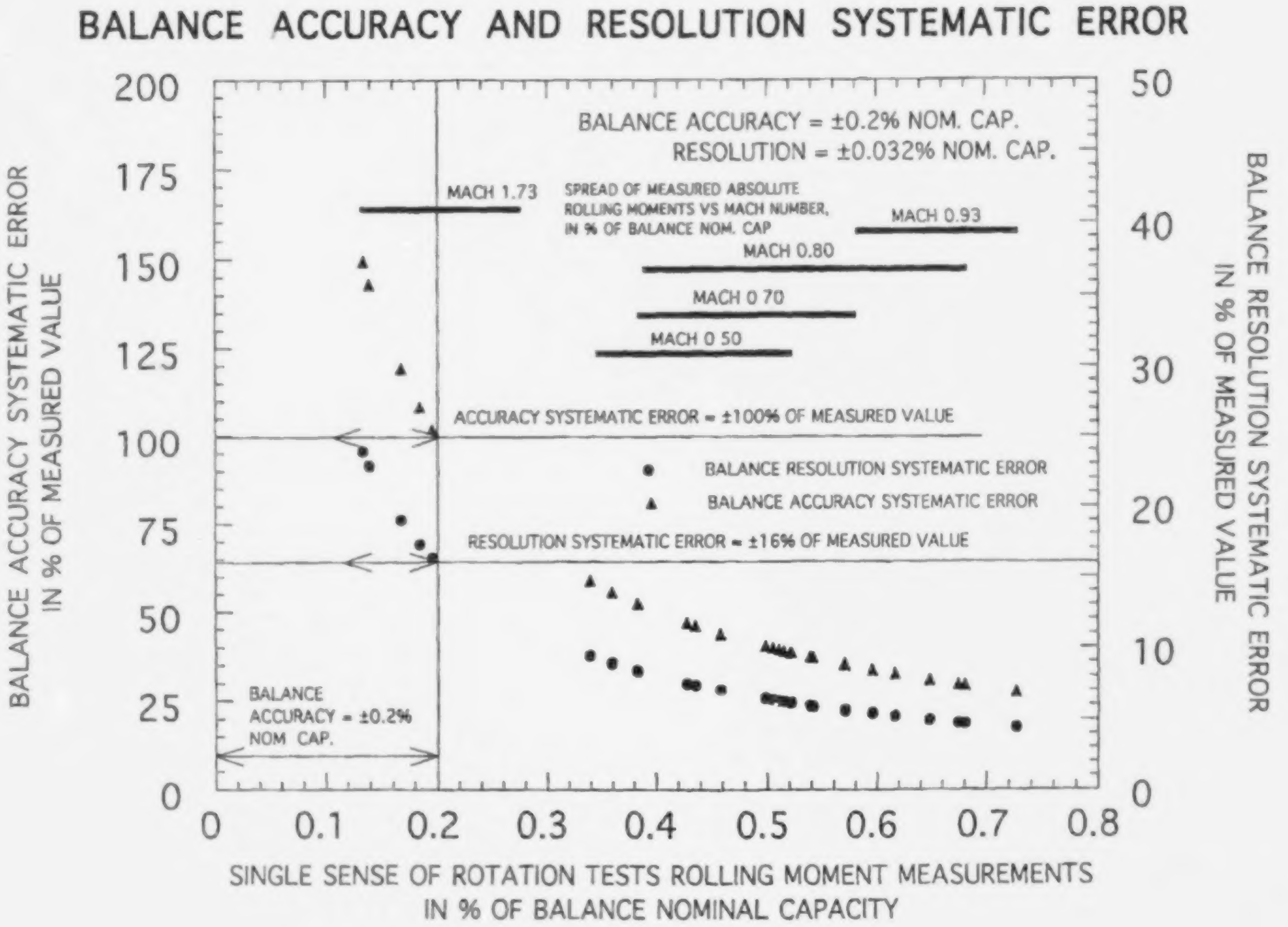

FIGURE D4 - Characterization of rolling moment measurements from spin tests made in single sense of rotation

Demonstration of Measurement Errors Calculation Methodology

n = 3 or 4 etc... ≡ number of repeated wind tunnel tests to investigate interval limits relative to a specific level of confidence.

X_1 , - - X_k measured data for angle of attack: *alpha₁* , - - *alphaₖ*

$X_{1,1}$ - - $X_{1,4}$ measured data for angle of attack: *alpha₁* and n=1 to 4

σ^2 = VAR (X_i) while assuming a constant value for each particular variable at specific Mach number (2.0, 2.5, 3.0 etc...) and model spin rate. It means that the methodology is an evaluator of the run-to-run repeatability while it is assumed that test conditions stay constant during a single test run, although it is expected that test conditions could vary from run-to-run

$$S^2=\sum_{1}^{n}\frac{(X_{1,i}-\overline{X_1})^2}{n-1} \text{ estimator of } \sigma^2 \text{ where } \overline{X_j}=\sum_{i=1}^{n}\frac{X_{j,i}}{n} \quad \text{where } j = 1,2\ldots k$$

$$\mu_i = \text{idealized value of } X_j = \lim_{n\to\infty}\left(\sum_{i=1}^{n}\frac{X_{j,i}}{n}\right)$$

$$\frac{X_j-\mu_j}{\sigma} \quad \text{obey the normal law } N(0\ ,\ 1)$$

$$\sum_{1}^{n}\frac{(X_{1,i}-\overline{X}_1)^2}{\sigma^2}=\left(\frac{n-1}{\sigma^2}\right)S^2 \quad \text{obey } \chi^2_{n-1} \quad \text{theorem}$$

then:

$$\frac{\dfrac{X_j-\mu_j}{\sigma}}{\sqrt[2]{\dfrac{S^2(n-1)}{(n-1)\sigma^2}}}=\frac{X_j-\mu_j}{S} \quad \text{obey law } t(n-1)$$

$$P\left[-a \le \frac{X_j-\mu_j}{S} \le a\right] = P\left[-aS \le X_j-\mu_j \le aS\right] =$$

$$= P\left[-aS-X_j \le -\mu_j \le aS-X_j\right] = P\left[X_j-aS \le \mu_j \le X_j+aS\right]$$

where: $a = t\left(1 - \alpha/2\ ;\ n-1\right)$

$$P\left[X_j-t\left(1 - \alpha/2\ ;\ n-1\right)S \le \mu_j \le X_j+t\left(1 - \alpha/2\ ;\ n-1\right)S\right] \ge \left(1 - \alpha\right)$$

$\alpha = 0.05$

$1 - \alpha = 0.95$

$1 - \frac{\alpha}{2} = 0.975$

$n - 1 = 2$ or 3 etc... $\equiv \nu$

Law for percentiles of the " t " distribution gives:

t(0.975, 2) =	4.303	t(0.90, 2) =	1.886
t(0.975, 3) =	3.182	t(0.90, 3) =	1.638
t(0.975, 4) =	2.776	t(0.90, 4) =	1.533
t(0.975, 6) =	2.447	t(0.90, 6) =	1.440
t(0.975, 9) =	2.262	t(0.90, 9) =	1.383

The following equation:

$$\boxed{\mu_j = X_j +- t\ (\ 0.975\ ,\ \nu\ )\ S}$$

applies **for a confidence level of 95.0%** and where there are 2.5% chances that the true experimental value that should have been measured would be lower than the defined low interval limit, and 2.5% chances that it would be higher than the upper interval limit.

Because for all aerodynamic coefficient tests at least 2 runs were normally made instead of a single individual run, it was worthwhile to determine the 95.0% confidence interval limits to be used for the prediction of future average values calculated from multiple test data results. In these cases where the data results of K observations (or K wind tunnel test runs) were averaged it would be possible to adapt the interval limits of Tables D-I to D-V as follows:

$$\frac{X_j-\mu_j}{\sigma} \quad \text{becomes} \quad \frac{\overline{X}_j-\mu_j}{\frac{\sigma}{\sqrt{K}}} \quad \text{where} \quad \overline{X_j}=\sum_{i=1}^{K}\frac{X_{j,i}}{K}$$

$$\frac{\dfrac{\overline{X}_j-\mu_j}{\frac{\sigma}{\sqrt{K}}}}{\sqrt[2]{\dfrac{S^2(n-1)}{(n-1)\sigma^2}}} = \sqrt{K}\,\frac{(\overline{X}_j-\mu_j)}{S}$$

$$P\left[X_j-aS \le \mu_j \le X_j+aS\right] \quad \text{becomes} \quad P\left[\overline{X}_j-a\frac{S}{\sqrt{K}} \le \mu_j \le \overline{X}_j+a\frac{S}{\sqrt{K}}\right]$$

$$\boxed{\mu_j = \overline{X}_j +- \, t\,(\,0.975\,,\,\nu\,)\,\frac{S}{\sqrt{K}}}$$

This means that the values identified as $\mu_j = \overline{X_j} \pm$ and $\frac{t(0.975\ ,\ n\text{-}1)S}{\overline{X_j}}$ in the Tables mentioned above and corresponding to the single run case could be multiplied by the factors specified below in the case where the average of multiple runs would be calculated:

K number of multiple test runs	Multiple factor to transform single run test interval limits into multiple runs test interval limits
2	0.7071
3	0.5774
4	0.5000
5	0.4472
6	0.4082

Since these factors are less than unit, statistical theory suggest that results based on calculated averages from multiple test run provide more precise results than single run test, which was to be expected anyway. The table indicates that to double the precision of data results, test run must be repeated 4 times.

TABLE D-I
Aerodynamic Coefficient Tests Error
(Mach 1.16, PD/2V = 0.185, 31,000 RPM)

RUN NUMBER	MACH NUMBER	CNA	CMA	XCP0	CA0
R2960 2150.110	1.1561	2.384	8.363	-3.51	0.472
R2961 2150.110-1	1.1569	2.636	9.173	-3.48	0.471
R2962 2150.110-2	1.1562	2.642	9.181	-3.47	0.469
R2971 2160.110	1.1558	2.518	8.625	-3.42	0.470

TOTAL ERROR

$\overline{X}_j =$	1.1563	2.5450 =0.0888 at 2 deg angle of attack	8.836 =0.2372 w/r BRC at 2 deg angle of attack	-3.47	0.471
$S^2 =$	2.167-7	1.4781-2	.1669	1.400-3	1.667-2
$S =$	4.655-4	1.2157-1	.4086	3.742-2	1.291-3
$\mu_j = \overline{X}_j \pm$	±1.481-3	±.3868	±1.300	±0.1191	±4.108-3
$\frac{t(0.975\ ,\ 3)S}{\overline{X}_j}$	±0.13%	±15.20%	±14.72%	±3.43%	±0.87%

SYSTEMATIC ERROR

	Balance accuracy in % of nom. cap. = A	±0.1%	±0.1% w/r BRC	N/A	±0.2%
QA= 51.54 N QA·d = 2.0893 N·m	Balance component force	4.577 N	0.4956 N•m		24.25 N
	Percentage balance nom. cap. = B	±1.03%	±4.165%	N/A	±11.02%
	systematic error = A•100/B	±9.72%	±2.401%		±1.82%

TABLE D-II
Aerodynamic Coefficient Tests Error
(Mach 1.27, PD/2V = 0.200, 36,000 RPM)

RUN NUMBER	MACH NUMBER	CNA	CMA	XCP0	CA0
R2935 2211.125	1.2714	2.494	8.482	-3.40	0.441
R2936 2211.125-1	1.2716	2.544	8.744	-3.44	0.440
R2937 2211.125-2	1.2714	2.673	9.119	-3.41	0.440
R2952 2106.125-2	1.2724	2.442	8.741	-3.54	0.449
R2954 2106.125-4	1.2710	2.631	9.328	-3.55	0.446

TOTAL ERROR

$\overline{X}_j =$	1.2716	2.557 =0.0893 at 2 deg angle of attack	8.883 =0.2359 w/r BRC at 2 deg angle of attack	-3.47	0.443
$S^2 =$	2.680-7	9.074-3	.1135	5.170-3	1.670-5
$S =$	5.177-4	9.526-2	.3569	7.1903-2	4.087-3
$\mu_j = \overline{X}_j \pm$	±1.437-3	±.2644	±0.9352	±0.1996	±1.134-2
$\frac{t(0.975\ ,\ 4)S}{\overline{X}_j}$	**±0.11%**	**±10.34%**	**±10.53%**	**±5.76%**	**±2.56%**

SYSTEMATIC ERROR

	Balance accuracy in % of nom. cap. = A	±0.1%	±0.1% w/r BRC	N/A	±0.2%
QA= 53.546 N QA•d = 2.1708 N•m	Balance component force	4.779 N	0.5121 N•m		23.73 N
	Percentage balance nom. cap. = B	±1.074%	±4.303%	N/A	±10.79%
	systematic error = A•100/B	±9.31%	±2.32%		±1.85%

TABLE D-III
Aerodynamic Coefficient Tests Error
(Mach1.27, PD/2V = 0.220, 39,500 RPM)

RUN NUMBER	MACH NUMBER	CNA	CMA	XCP0	CA0
R2938 2226.125	1.2728	2.705	9.413	-3.47	0.438
R2955 2091.125	1.2714	2.587	8.958	-3.46	0.442
R2956 2091.125-1	1.2714	2.422	8.535	-3.52	0.443
R2957 2091.125-2	1.2723	2.513	8.824	-3.51	0.445

TOTAL ERROR

$\overline{X}_j =$	1.2720	2.5568 =0.0892 at 2 deg angle of attack	8.9325 =0.2402 w/r BRC at 2 deg angle of attack	-3.49	0.442
$S^2 =$	4.825-7	1.432-2	.1338	8.667-4	8.667-6
$S =$	6.946-4	1.197-1	.3657	2.944-2	2.944-3
$\mu_j = \overline{X}_j \pm$	±2.210-3	±.3808	±1.164	±9.368-2	±9.368-3
$\frac{t(0.975\ ,\ 3)S}{\overline{X}_j}$	**±0.17%**	**±14.89%**	**±13.03%**	**±2.68%**	**±2.12%**

SYSTEMATIC ERROR

	Balance accuracy in % of nom. cap. = A	±0.1%	±0.1% w/r BRC	N/A	±0.2%
QA= 53.222 N QA•d = 2.1576 N•m	Balance component force	4.747 N	0.5183 N•m	N/A	23.52 N
	Percentage balance nom. cap. = B	±1.067%	±4.355%		±10.69%
	systematic error = A•100/B	±9.37%	±2.30%		±1.87%

TABLE D-IV

Aerodynamic Coefficient Tests Error

(Mach 2.95, PD/2V = 0.107, 31,000 RPM)

RUN NUMBER	MACH NUMBER	CNA	CMA	XCP0	CA0
R2885 2187.300-1	2.9539	3.310	9.372	-2.83	0.202
R2894 2157.300	2.9528	3.260	9.259	-2.84	0.214
R2895 2157.300-1	2.9530	3.328	9.341	-2.61	0.211
R2908 2187.300-4	2.9512	3.379	9.476	-2.80	0.213

TOTAL ERROR

$\overline{X}_j =$	2.9527	3.319 =0.1159 at 2 deg angle of attack	9.362 =0.2339 w/r BRC at 2 deg angle of attack	-2.770	0.210
$S^2 =$	1.270-6	2.414-3	0.00805	1.167-2	3.000-5
$S =$	1.127-3	4.914-2	0.08971	1.080-1	5.477-3
$\mu_j = \overline{X}_j \pm$	±3.586-3	±.1563	±0.2855	±0.3437	±1.743-2
$\frac{t(0.975\ ,\ 3)S}{\overline{X}_j}$	**±0.12%**	**±4.71%**	**±3.05%**	**±12.41%**	**±8.30%**

SYSTEMATIC ERROR

	Balance accuracy in % of nom. cap. = A	±0.1%	±0.1% w/r BRC	N/A	±0.2%
QA= 23.0665 N QA•d = 0.9351 N•m	Balance component force	2.673 N	0.2187 N•m		4.844 N
	Percentage balance nom. cap. = B	±0.601%	±1.838%	N/A	±2.202%
	systematic error = A•100/B	±16.65%	±5.44%		±9.08%

TABLE D-V

Spin Damping Coefficient Tests Error

Run numbers used to calculate spin damping coefficient corrected for balance roll element offset	Corrected **CLPC** for balance rolling element offset, **MACH 1.16 PD/2V = 0.185**	Run numbers used to calculate spin damping coefficient corrected for balance roll element offset	Corrected **CLPC** for balance rolling element offset **MACH 1.27 PD/2V = 0.200**	Run numbers used to calculate spin damping coefficient corrected for balance roll element offset	Corrected **CLPC** for balance rolling element offset **MACH 1.27 PD/2V = 0.220**
R2971 (R) R2960 (L)	-0.0195	R2935 (R) R2952 (L)	-0.0190	R2938 (R) R2957 (L)	-0.0190
R2971 (R) R2962 (L)	-0.0213	R2936 (R) R2952 (L)	-0.0193	R2938 (R) R2956 (L)	-0.0190
R2971 (R) R2961 (L)	-0.0207	R2937 (R) R2954 (L)	-0.0188	R2938 (R) R2955 (L)	-0.0185

TOTAL ERROR

$\overline{X_j}$ = **CRMC =**	-0.0205 **-0.00379**	$\overline{X_j}$ = **CRMC =**	-0.0190 **-0.00380**	$\overline{X_j}$ = **CRMC =**	-0.0188 **-0.00414**
$S^2 =$	8.400-7	$S^2 =$	6.333-8	$S^2 =$	8.333-8
S =	9.165-4	S =	2.517-4	S =	2.887-4
$\mu_j = \overline{X_j} \pm$	±3.944-3	$\mu_j = \overline{X_j} \pm$	±1.083-3	$\mu_j = \overline{X_j} \pm$	±1.2422-3
$\frac{t(0.975\ ,\ 2)S}{\overline{X_j}}$	**±19.24%**	$\frac{t(0.975\ ,\ 2)S}{.\ \overline{X_j}}$	**±5.69%**	$\frac{t(0.975\ ,\ 2)S}{\overline{X_j}}$	**±6.60%**

SYSTEMATIC ERROR

QA= 51.54 N	QA•d = 2.0893 N•m	QA= 53.55 N	QA•d = 2.1708 N•m	QA= 53.22 N	QA•d = 2.1576 N•m
Balance accuracy in % of nominal capacity = A	±0.2%	**Balance accuracy in % of nominal capacity = A**	±0.2%	**Balance accuracy in % of nominal capacity = A**	±0.2%
Balance component force	0.00792 N•m	**Balance component force**	0.00825 N•m	**Balance component force**	0.00892 N•m
Percentage of balance nom. capacity = **B**	±0.4660%	Percentage of balance nom. capacity = **B**	±0.4852%	Percentage of balance nom. capacity = **B**	±0.5249%
systematic error = **A•100/B**	±42.9%	systematic error = **A•100/B**	±41.2%	systematic error = **A•100/B**	±38.1%

UNCLASSIFIED

INTERNAL DISTRIBUTION

DREV TN 2001-116

1 – Director General
6 – Document Library
1 – M. Boivin
1 – R. Bélanger
1 – G. Dumas
1 – A. Dupuis
1 – É. Fournier
1 – F. Lesage

EXTERNAL DISTRIBUTION

DREV TN 2001-116

1 – DRDKIM
1 – DRDKIM (unbound copy)

UNCLASSIFIED

SECURITY CLASSIFICATION OF FORM
(Highest classification of Title, Abstract, Keywords)

DOCUMENT CONTROL DATA

1. ORIGINATOR (name and address)

Defence Research Establishment Valcartier (DREV)

2. SECURITY CLASSIFICATION
(Including special warning terms if applicable)

UNCLASSIFIED

3. TITLE (Its classification should be indicated by the appropriate abbreviation (S, C, R or U)

WIND TUNNEL TESTS WITH A SPINNING MODEL OF A
5-CALIBRE ARMY-NAVY SPINNER AT MACH 0.5 TO 3.0

4 AUTHORS (Last name, first name, middle initial. If military, show rank, e.g. Doe, Maj. John E.)

Girard, Bertrand and Drouin, Gédéon

5. DATE OF PUBLICATION (month and year)

6a. NO. OF PAGES

241

6b. NO. OF REFERENCES

77

7. DESCRIPTIVE NOTES (the category of the document, e.g. technical report, technical note or memorandum. Give the inclusive dates when a specific reporting period is covered.)

Memorandum

8. SPONSORING ACTIVITY (name and address)

DREV

9a. PROJECT OR GRANT NO. (Please specify whether project or grant)

2na13 Flight mechanics of munitions

9b. CONTRACT NO.

10a. ORIGINATOR'S DOCUMENT NUMBER

DREV-TM-

10b. OTHER DOCUMENT NOS

N/A

11. DOCUMENT AVAILABILITY (any limitations on further dissemination of the document, other than those imposed by security classification)

☒ Unlimited distribution
☐ Contractors in approved countries (specify)
☐ Canadian contractors (with need-to-know)
☐ Government (with need-to-know)
☐ Defense departments
☐ Other (please specify)

12. DOCUMENT ANNOUNCEMENT (any limitation to the bibliographic announcement of this document. This will normally correspond to the Documen Availability (11). However, where further distribution (beyond the audience specified in 11) is possible, a wider announcement audience may be selected.)

Full unlimited announcement

UNCLASSIFIED

SECURITY CLASSIFICATION OF FORM
(Highest classification of Title, Abstract, Keywords)

#516137

CA011574

UNCLASSIFIED

SECURITY CLASSIFICATION OF FORM
(Highest classification of Title, Abstract, Keywords)

13. ABSTRACT (a brief and factual summary of the document. It may also appear elsewhere in the body of the document itself. It is highly desirabl the abstract of classified documents be unclassified. Each paragraph of the abstract shall begin with an indication of the security classification information in the paragraph (unless the document itself is unclassified) represented as (S), (C), (R), or (U) It is not necessary to include here abs in both official languages unless the text is bilingual).

Most of shells and bullets that are fired from a gun barrel have to be gyroscopically stabilized during flight by a high spin rate (axial) and this must be made in conjunction with a proper ratio of their axial and lateral inertia moments. For the wind tunnel tests related to spin stabilized projectiles, it is very desirable to be able to spin the model which makes possible to evaluate the aerodynamic effects induced by the spinning motion as the Magnus forces and moments. the spin/roll damping and also to study the influence of the spin rate on other aerodynamic coefficients (lift, drag, pitching moment, etc...) When considering the relatively small size of the test section. an electrical motor was used for the spin rig. It is a departure from the more current air turbine state-of-the-art but has proven to be efficient with the DREV facility. This memorandum describes wind tunnel tests made in the DREV 0.6 m x 0.6 m trisonic wind tunnel with a spinning model of an ARMY-NAVY SPINNER 5-calibre. This is a standard model configuration used to qualify and normalize wind tunnel test results. These tests were primordially intended to measure the spin damping and the Magnus force and also the influence of the spin rate on other standard aerodynamic coefficients, in order to evaluate the results that can be obtained with a spin rig apparatus and its controller developed at DREV. All the necessary details are included to enable a pursuit of subsequent experiments. Results then obtained compare well with data from literature for similar models tested in aeroballistic range facilities. These wind tunnel tests have increased the knowledge on experimental aerodynamics technics for spinning projectiles with a flat base.

14. KEYWORDS, DESCRIPTORS or IDENTIFIERS (technically meaningful terms or short phrases that characterize a document and could be hel cataloguing the document. They should be selected so that no security classification is required Identifiers, such as equipment model desigr trade name, military project code name, geographic location may also be included. If possible keywords should be selected from a pub thesaurus, e.g. Thesaurus of Engineering and Scientific Terms (TEST) and that thesaurus-identified. If it is not possible to select indexing terms are Unclassified, the classification of each should be indicated as with the title.)

AERODYNAMICS
ARMOR PIERCING AMMUNITION
ARTILLERY SHELLS
WIND TUNNEL MODELS
ANTITANK AMMUNITION
SUBCALIBER PROJECTILES
WARHEADS
PROJECTILES
MACH 0 5 TO 3 0
KINETIC ENERGY PROJECTILE
SUPERSONIC
AERODYNAMIC COEFFICIENTS
BODIES OF REVOLUTION
DRAG
AERODYNAMIC CONFIGURATIONS
SUPERSONIC WIND TUNNELS
LAMINAR BOUNDARY LAYER
TURBULENT BOUNDARY LAYER
BOUNDARY LAYER CONTROL
SPIN STABILIZED AMMUNITION
TRAINING AMMUNITION
SPIN STABILIZATION
MAGNUS EFFECT
FLUID DYNAMICS
STATIC PRESSURE
GUNNERY
GUNS (ORDNANCE)
WIND TUNNELS
CYLINDRICAL BODIES
LIFTING BODIES
SLENDER BODIES
AERODYNAMICS FORCES
AERODYNAMIC DRAG
AERODYNAMIC LOADS
BLOW DOWN
TEST FACILITIES
BLUNT BODIES
AFTERBODIES
FLOW SEPARATION
PITOT TUBES
BOUNDARY LAYER FLOW
FLUID FLOW
FLIGHT SIMULATORS
SUBSONIC WIND TUNNELS
TRANSONIC WIND TUNNELS
MODEL TESTS
ABSOLUTE PRESSURE
BASE PRESSURE
DYNAMIC PRESSURE
DIFFERENTIAL PRESSURE
GAS LAWS
PRESSURE MEASUREMENT
STATISTICAL ANALYSIS
TURBULENT FLOW
NONUNIFORM FLOW
FLIGHT CHARACTERISTIC
AEROBALLISTICS
BOUNDARY LAYER
VELOCITY PROFILING
BASE FLOW
VELOCITY
WIND TUNNEL NOZZLES
ELECTRIC MOTORS
DC MOTORS
FRACTIONAL HORSEPOWER-
-MOTORS

(Thesaurus of Engineering and Scientific Terms. Engineering Joint Council March 1969)

UNCLASSIFIED

SECURITY CLASSIFICATION OF FORM
(Highest classification of Title, Abstract, Keywords)